Ulm University
Medical Faculty

Characterization of the molecular mechanisms underlying the pathophysiological differentiation of small airway epithelial cells in Chronic Obstructive Pulmonary Disease (COPD)

Dissertation
submitted to obtain the doctoral degree of Human Biology
of the Medical Faculty of Ulm University

Julia Anna Gindele
Tettnang, Germany

2020

Active Dean:	Prof. Dr. Thomas Wirth
1st Reviewer:	PD Dr. Jürgen Schymeinsky
2nd Reviewer:	Prof. Dr. Manfred Frick
3rd Reviewer:	Prof. Dr. Wolfgang Kummer
Day of Graduation:	21. May 2021

Index

List of abbreviations

Ac Tub	Acetylated tubulin
ADAM	A disintegrin and metalloproteinase
AHR	Aryl hydrocarbon receptor
AKT	Protein kinase B
ALI	Air-liquid interface
AMP	Antimicrobial peptide
ASL	Airway surface liquid
AUC	Area under the curve
CAT	COPD Assessment Test
CLDN	Claudin
CO	Carbon monoxide
CO_2	Carbon dioxide
COPD	Chronic Obstructive Pulmonary Disease
CS	Cigarette smoke
CSE	Cigarette smoke etract
Ct	Cycle threshold
CYP2F1	Cytochrome P450 Family 2 Subfamily F Member 1
DAB	3'Diaminobenzidine
DMSO	Dimethyl sulfoxide
DNAI1	Dynein axonemal intermediate chain 1
DUOX	Dual oxidase
Dvl	Dishevelled
EGF	Epidermal growth factor
EGFR	Epidermal growth factor receptor
EMT	Epithelial-mesenchymal transition
ERK	Extracellular signal-regulated kinase
FEV1	Forced expiratory volume in one second
FOXJ1	Forkhead Box J1
FVC	Forced vital capacity
G-CSF	Granulocyte colony-stimulating factor
GOLD	Global initiative for COPD
Grb-2	Growth factor receptor-bound protein 2
GSK	Glycogen synthase kinase-3
H&E	Hematoxylin & eosin
H2S	Hydrogen sulfide
HB-EGF	Heparin-binding EGF-like growth factor
HC	Healthy control
HCN	Hydrogen cyanide
HER	Human epidermal growth factor receptor
IHC	Immunohistochemistry
IL-8	Interleukin-8
IPA	Ingenuity Pathway Analysis
ISO	International Organization for Standardization
IVL	Involucrin
JAK	Janus kinase
JAM	Junctional adhesion molecule

KRT	Cytokeratin
LABA	Long-acting β-adrenoreceptor agonists
LAMA	Long-acting muscarinic receptor antagonist
LDH	Lactate dehydrogenase
log	Logarithm
M	Molar
MEK	Mitogen-activated protein kinase kinase
mMRC	Modified British Medical Research Council questionnaire
MSD	Meso Scale Discovery
MUC5AC	Mucin 5 AC
N2	Nitrogen
NaCl	Sodium Chloride
NGS	Next generation sequencing
NOX	NADPH oxidase
Nrf2	Nuclear factor erythroid 2-related factor 2
Nrx	Nucleoredoxin
ns	Not significant
O2	Oxygen
P.R.I.T.	Professionelle In-Vitro Technologien
p63	Tumor protein (Trp)-63
PAH	Polycyclic aromatic hydrocarbon
p70S6K	Ribosomal protein S6 kinase beta-1 (S6K1)
PAS	Periodic acid schiff
PBS	Phosphate-buffered saline
PDE4	Phosphodiesterase 4
PI3K	Phosphatidylinositol-3-kinase
PIP3	Phosphatidylinositol (3,4,5)-triphosphate
POLR2A	RNA Polymerase II Subunit A
ROC	Receiver operating characteristic
ROS	Reactive oxygen species
RT-PCR	Reverse Transcription Polymerase Chain Reaction
SABA	Short-acting β-adrenoreceptor agonists
SAEC	Small airway epithelial cells
SAMA	Short-acting muscarinic receptor antagonist
SCGB1A1	Secretoglobin Family 1A Member 1/Uteroglobin
SEM	Standard error of the mean
SFN	Stratifin
SLPI	Secretory leukoprotease inhibitor
SOS	Guanine nucleotide exchange protein
STAT	Signal Transducers and Activators of Transcription
TEER	Transepithelial electrical resistance
TGFα	Transforming growth factor beta
TKI	Tyrosine kinase inhibitor
TSNA	Tobacco-specific nitrosamines
WHO	World Health Organization
WNT	Wingless/integrase-1
ZO	Zonula occludens

Preliminary Remark

Parts of this thesis have been previously published:

Gindele, J.A., Kiechle, T., Benediktus, K. et al. Intermittent exposure to whole cigarette smoke alters the differentiation of primary small airway epithelial cells in the air-liquid interface culture. Sci Rep 10, 6257 (2020). https://doi.org/10.1038/s41598-020-63345-5

1 Introduction

1.1 Chronic Obstructive Pulmonary Disease (COPD)

1.1.1 Prevalence of COPD

Chronic obstructive pulmonary disease (COPD) is a severe lung disease with cigarette smoking being the primary risk factor (Laniado-Laborin, 2009; Lozano et al., 2012; Yoshida and Tuder, 2007). By 2030, COPD is predicted to become the third leading cause of death worldwide (Mathers and Loncar, 2006). The prevalence of COPD increases with smoking and age. The risk for people over 65 years of age is five-fold increased compared to patients under 40 (Raherison and Girodet, 2009). Smoking burden is usually measured in pack-years, i.e. the average number of cigarette packs smoked per day multiplied with the duration of smoking in years. For instance, 20 pack-years can mean ten years smoking two packs per day or 20 years smoking one pack per day. Recent studies suggest that smoking duration is a better indicator of estimated COPD risk than the composite index of pack years (Bhatt et al., 2018). Severe COPD patients die about six years earlier, in addition to the almost four years they have lost from smoking (Shavelle et al., 2009). Overall life expectancy is reduced about ten years compared to non-smokers.

1.1.2 Pathological alterations in the airways of COPD patients

The disease features three pathological disorders, chronic bronchitis, small airways disease and emphysema, which can exist separately or in combination (Thorley and Tetley, 2007). Chronic bronchitis was described as “the presence of chronic cough and recurrent increases in bronchial secretions sufficient to cause expectoration. The secretions are present on most days for a minimum of three months a year, for at least two successive years, and cannot be attributed to other pulmonary or cardiac causes” (Siafakas et al., 1995). These symptoms are ascribed to goblet cell hyperplasia in the bronchial epithelium, reduced mucociliary clearance and hence, increased susceptibility to infections (Kim and Criner, 2013; Rennard, 2003).

Narrowing and destruction of small airways is an important hallmark of COPD. Smoking induces epithelial injury, which triggers a pathophysiological response leading to tissue remodeling (Perotin et al., 2014; Puchelle et al., 2006). The pathological changes of the small airway epithelium in COPD include: goblet cell metaplasia (Lumsden et al., 1984; Polosukhin et al., 2017; Saetta et al., 2000), reduced cilia function (Hessel et al., 2014; Lam et al., 2013; Rennard, 2003; Yaghi and Dolovich, 2016; Yaghi et al., 2012), reduced club cell numbers (Lomas et al., 2008; Lumsden et al., 1984; Park et al., 2013), basal membrane thickening (Gohy et al., 2015; Hogg et al., 1968), epithelial barrier dysfunction (Aghapour et al., 2018; Heijink et al., 2014) and squamous metaplasia (Araya et al., 2007; Polosukhin et al., 2011; Polosukhin et al., 2017; Rigden et al., 2016). Moreover, small airway inflammation was reported to be associated with disease severity (Hogg et al., 2004; Hogg et al., 1968; Lams et al., 1998; Saetta et al., 1998). Consequently, the small airways are the

principal site of increased airway resistance in COPD leading to severe airflow limitation (Hogg et al., 1968).

Emphysema occurs in the alveoli, where gas exchange takes place. Porth described this pathophysiology as ”a loss of lung elasticity and abnormal enlargement of the air spaces distal to the terminal bronchioles, with destruction of the alveolar walls and capillary beds” (Porth, 2011). The reduction of functional alveoli and the insufficient gas exchange results in one typical symptom that COPD patients often suffer from: shortness of breath. Dyspnoea (= shortness of breath), cough and sputum production further lead to reduced mobility and fatigue. Acute symptom worsenings, so-called exacerbations, are mainly triggered by bacterial or viral infections and often lead to hospitalization of the patient (Bafadhel et al., 2011).

1.1.3 Grading of the disease severity of COPD patients

Airflow limitation of COPD patients is assessed spirometrically by measuring the forced expiratory volume in one second (FEV_1) and the forced vital capacity (FVC). A ratio of $FEV_1/FVC < 0.70$ (after bronchodilation treatment) is the spirometric criterion of airflow limitation. FEV_1 is severely diminished in obstructive lung diseases. The global initiative for COPD (GOLD) grouped COPD patients therefore according to their FEV_1 values relative to expected FEV_1 values of healthy individuals of the same age, gender, body size and ethnicity: GOLD 1 ≥ 80 %, GOLD 2 50-79 %, GOLD 3 30-49 %, GOLD 4 < 30 %. As a further advancement of the simple spirometric grading system, the GOLD initiative implemented the "ABCD" assessment tool. In addition to the spirometric grade, patients are examined for their symptoms and risk of exacerbations using questionnaires (mMRC = modified British Medical Research Council questionnaire, CAT = COPD Assessment Test) and assigned to groups A-D, where A corresponds to mild symptoms and D to severe symptoms with exacerbations leading to hospitalization. The “ABCD” assessment tool therefore also considers the negative influence of exacerbations on the course of the disease. (Global Initiative for Chronic Obstructive Pulmonary Disease, 2020; Vogelmeier et al., 2017)

1.1.4 Treatment options for COPD

According to the World Health Organization (WHO) in 2017, COPD is a not curable, progressive disease. Smoking cessation is still the only proven way to reduce the underlying processes leading to COPD. However, available treatments relieve symptoms, help to improve quality of life and reduce the risk of death. Bronchodilators are inhaled drugs that open constricted airways and facilitate breathing. One class of bronchodilators are β_2-adrenoreceptor agonists. Short-acting β_2-adrenoreceptor agonists (SABA) such as salbutamol relief acute bronchoconstriction and long-acting β_2-adrenoreceptor agonists (LABA), such as salmeterol, formoterol and olodaterol, help to prevent symptoms. Another

class of bronchodilators are anticholinergics. They competitively inhibit binding of the neurotransmitter acetylcholine and therefore prevent constriction of the airways. Muscarinic acetylcholine receptor antagonists can be divided in short- and long-acting classes (LAMA = long-acting muscarinic receptor antagonists, and SAMA = short-acting muscarinic receptor antagonists). It is assumed that anticholinergic drugs also reduce excessive mucus secretion. According to GOLD, the use of LABAs and LAMAs in combination is recommended for COPD patients with persistent symptoms. In clinical studies, it was shown that combination therapy has synergistic effects and improves "lung function, lung hyperinflation, exercise tolerance, exacerbation frequency and quality of life". (Malerba et al., 2019; Mirza et al., 2018; Montuschi and Ciabattoni, 2015)

Apart from bronchodilators, COPD patients are often treated with corticosteroids such as prednisone. Steroids are intended to reduce inflammation and help relieve irritation and swelling of the airways, although their positive effects are controversial (Barnes, 2010). Corticosteroids also have negative effects as they increase the risk of infections and pneumonia (Suissa et al., 2013). In advanced stages of COPD, oxygen therapy may be necessary to ensure sufficient oxygenation of the blood. (Vogelmeier et al., 2017)

1.2 Morphology and function of the human airway epithelium

1.2.1 Architecture of the human airway epithelium

The lung epithelium can be anatomically divided into large airways (2^0 to 2^5 branches) and small airways (2^6 to 2^{23} branches). The bronchi branch out into bronchioles and terminal bronchioles, and gradually the epithelium changes from a pseudostratified to a simple cuboid epithelium (Fig. 1). After 2^{23} branches, the airway epithelium merges with the alveolar epithelium, with alveolar type I and type II cells. (Crystal et al., 2008; Wright, 1984)

Conducting airway epithelial cells are categorized into three main classes: basal, secretory and ciliated cells. (Spina, 1998). The large airways comprise mainly basal cells, ciliated cells and secretory goblet cells, whereas the small airways exhibit a thinner epithelium consisting of basal, ciliated and secretory club cells (Fig.1).

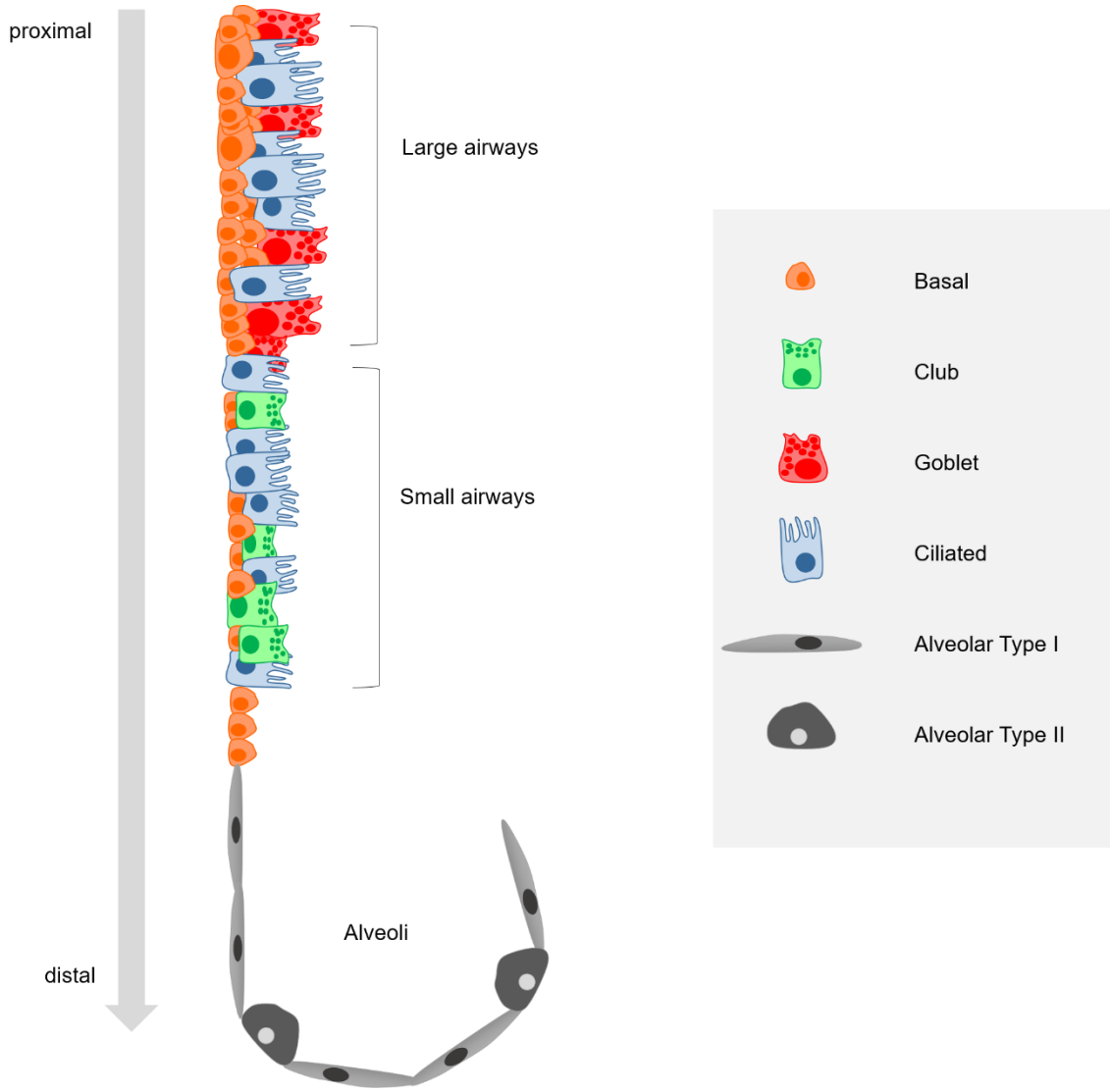

Figure 1: Schematic representation of the human airway epithelium and the different cell types present in each region.

1.2.2 Cell types of the human airway epithelium and its role in COPD

1.2.2.1 Basal cells

Basal cells are attached to the basement membrane and characteristically express cytokeratin 5 (KRT5) (Evans et al., 2001). They act like progenitor cells, which self-renew and give rise to other differentiated cell types, such as club, goblet and ciliated cells (Hong et al., 2004; Rock et al., 2010). With their stem cell like properties, basal cells are present throughout the conducting epithelium. However, the number of basal cells decreases with airway size. Epithelial thickness is directly correlated to the number of basal cells. Hence, less basal cells are found in the epithelium lining the small airways. (Evans and Plopper, 1988; Knight and Holgate, 2003)

Basal cells play an important role in tissue homeostasis. Therefore, an alteration of their function can contribute to the initiation and progression of airway diseases. Excessive proliferation leads to basal cell hyperplasia and changes in basal cell fate might induce goblet cell hyperplasia or squamous metaplasia (Rock et al., 2010). A schematic representation of healthy and COPD small airways is depicted in Fig. 2.

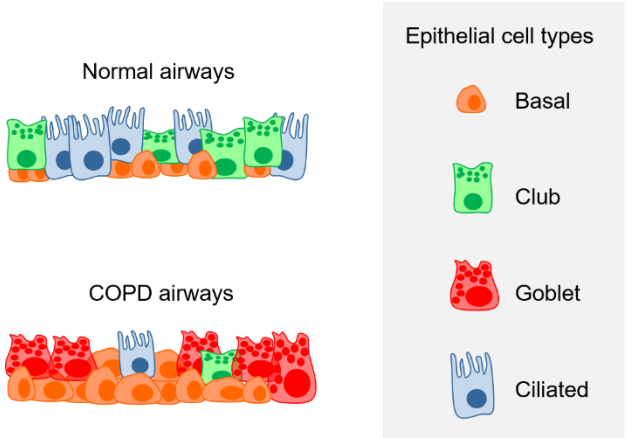

Figure 2: Schematic representation of the human small airway epithelium of healthy individuals and chronic obstructive pulmonary disease (COPD) patients. The healthy small airway epithelium is composed of differentiated cell types, such as secretory club cells and ciliated cells; and basal cells, which serve as a progenitor cell type. Aberrant remodeling of the airway epithelium in COPD patients lead to basal cell hyperplasia and metaplasia of mucus-producing goblet cells. Club and ciliated cells are severely reduced.

1.2.2.2 Club cells

Club cells are characterized by electron-dense granules (Fig. 3) and are mainly located in the small airways (Knight and Holgate, 2003; Zuo et al., 2018). Different studies indicate that club cells act as progenitors for ciliated and goblet cells (Hong et al., 2001; Knight and Holgate, 2003).

Club cells play a key role in host defense by metabolizing and eliminating potentially noxious compounds (Zuo et al., 2018). They secrete bronchiolar surfactant, specific antiproteases, such as secretory leukocyte protease inhibitor (SLPI), and p450 mono-oxygenases (De Water et al., 1986). Their primary secretory product is uteroglobin (SCGB1A1, Secretoglobin Family 1A Member 1) (Knight and Holgate, 2003; Zuo et al., 2018).

Laucho-Contreras et al. revealed reduced levels of SCGB1A1 in smokers and COPD patients and showed a correlation of SCGB1A1 with COPD severity. SCGB1A1 deficient mice are more susceptible to cigarette smoke (CS) induced injury and exhibit emphysema, airway remodeling, inflammation and Mucin-5AC (MUC5AC) overexpression. Therefore, the authors suggest a protective role for SCGB1A1 in the pathogenesis of COPD (Laucho-Contreras et al., 2015).

1.2.2.3 Goblet cells

Goblet cells are mucus producing cells mainly located in the upper airways that contain electron-lucent acidic-mucin granules (Fig. 3) (Jeffery, 1983). They secrete mucins, mainly Mucin-5AC (MUC5AC), to the apical side of the epithelium to trap inhaled particles and pathogens (Fahy and Dickey, 2010). In a healthy state, mucus secretion and clearance is balanced. However, in airway diseases such as COPD goblet cell hyperplasia and metaplasia can occur, resulting in excessive mucus production that obstructs the airways (Lumsden et al., 1984). An extreme form of that is air trapping, which is a critical feature seen in severe COPD patients (Morenz et al., 2012).

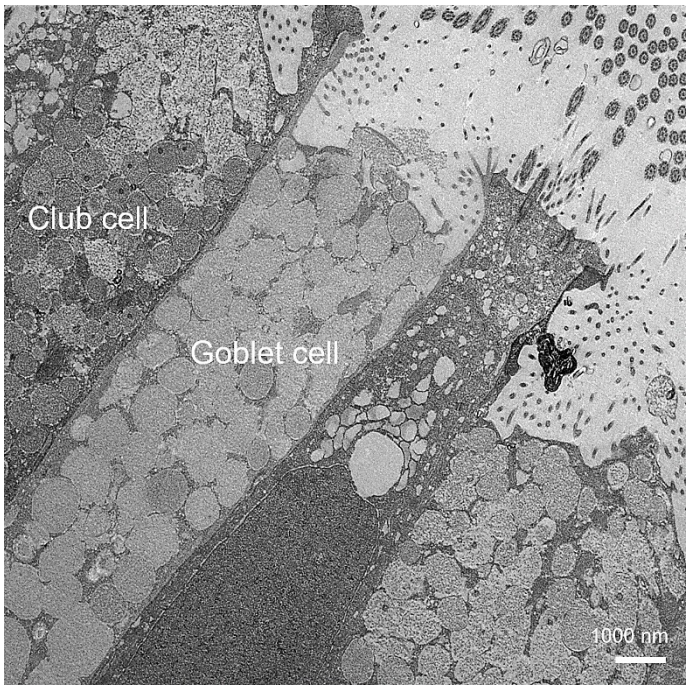

Figure 3: Transmission electron microscopic image of a small airway epithelial cell (SAEC) air-liquid interface (ALI) culture with electron-dense club cells and electron-lucent goblet cells.

1.2.2.4 Ciliated cells

Ciliated cells are terminally differentiated cells and feature up to 300 cilia per cell, which are located on the luminal side of the cell (Fig. 4). Motile cilia consist of structural proteins, such as dyneins, and motor proteins, which enable motility (Whitsett, 2018). A major transcription factor for cilia assembly is Forkhead box J1 (FOXJ1) (Yu et al., 2008). Directed cilia beating is critical for mucociliary clearance of the airways (compare section 1.2.3.2) (Knight and Holgate, 2003). A large number of mitochondria provide the required energy (Harkema et al., 1991).

Figure 4: Scanning electron microscopic image of a small airway epithelial cell (SAEC) air-liquid interface (ALI) culture with a ciliated surface.

1.2.3 Host defense against inhaled agents

1.2.3.1 Defense mechanisms of the airway epithelium

The airway epithelium is exposed to environmental agents, such as pathogens, allergens or particles, through the air we breathe. An intact barrier is therefore highly important for tissue homeostasis. Three main mechanisms are essential to maintain barrier integrity: mucociliary clearance to remove inhaled particles, intercellular junctional complexes, which regulate paracellular permeability and secreted antimicrobial products, which kill intruding pathogens. (Ganesan et al., 2013)

1.2.3.2 Mucociliary clearance

Effective removal of invading particles and pathogens from the airways requires mucus secretion and coordinated beating of cilia. Mucus captures inhaled agents and directed cilia movements are necessary to transport them upwards, where they can be swallowed or expectorated. (Kilburn, 1968)
Goblet cells and submucosal glands secrete mucus, which consists of more than 200 proteins. Mucins make up most of the mucus. These polymeric O-linked glycoproteins build the organizing framework of the airway's mucus gel. (Rose et al., 2001; Thornton et al., 2008)

The most prevalent mucins in the human airways are MUC5AC (Mucin 5 AC), the major mucin from goblet cells, and MUC5B (Mucin 5B), which is mainly released by submucosal glands (Hovenberg et al., 1996; Rose and Voynow, 2006; Wickstrom et al., 1998). Rapid mucin secretion by goblet cells is important during homeostasis. However, hyperplasia of goblet cells, as occurs in asthma and COPD, leads to pathological mucus overproduction (Rogers, 2003).
The airway surface liquid (ASL) consists of an upper viscoelastic layer of mucins, which is required for particle retention and transport, and a lower periciliary layer containing cell surface tethered mucins and other molecules such as glycolipids. The less viscous lower layer allows coordinated cilia beating. Hydration of the ASL is regulated via ion transport across the apical plasma membrane, i.e. chloride and sodium channels. (Ganesan et al., 2013; Randell and Boucher, 2006; Sheehan et al., 2006)
Viscosity of mucus plays an important role for the clearance efficiency. Highly viscous mucus cannot be cleared by cilia, which leads to an accumulation of inhaled particles causing airway obstruction and infections. (Ganesan et al., 2013; Knowles and Boucher, 2002; Puchelle et al., 1995; Randell and Boucher, 2006; Sethi, 2000)

In addition to proper mucus composition, coordinated cilia beating is crucial for effective mucociliary clearance. Therefore, impaired cilia function and the decline in ciliated cells also plays a role in the reduced clearance of particles and pathogens in COPD airways. (Liu and Di, 2012; Yaghi et al., 2012).

1.2.3.3 Airway epithelial junctions

To prevent inhaled pathogens and particles penetrating the epithelium, intercellular junctional complexes are essential. The airway epithelium exhibits two major types of intercellular junctions located on the apicolateral membranes: adherens junctions and tight junctions (compare Fig. 5) (Pohl et al., 2009). Adherens junctions are central for the initiation, maturation and maintenance of cell-cell contacts. The major transmembrane proteins of adherens junctions are cadherins, such as E-cadherin. Together with intracellular catenin family members including p120-catenin, β-catenin and α-catenin, they form junctional complexes (Hartsock and Nelson, 2008).
Tight junctions regulate the paracellular permeability of ions and solutes across the epithelium and prevent intramembrane diffusion of apical and basolateral membrane components (Shin et al., 2006). Occludin and claudins are the two types of transmembrane proteins that form tight junctions. In addition to that, cytoplasmic zonula occludens (ZO) proteins connect tight junctions to the actin-cytoskeleton and the adherens junctions. (Hartsock and Nelson, 2008)

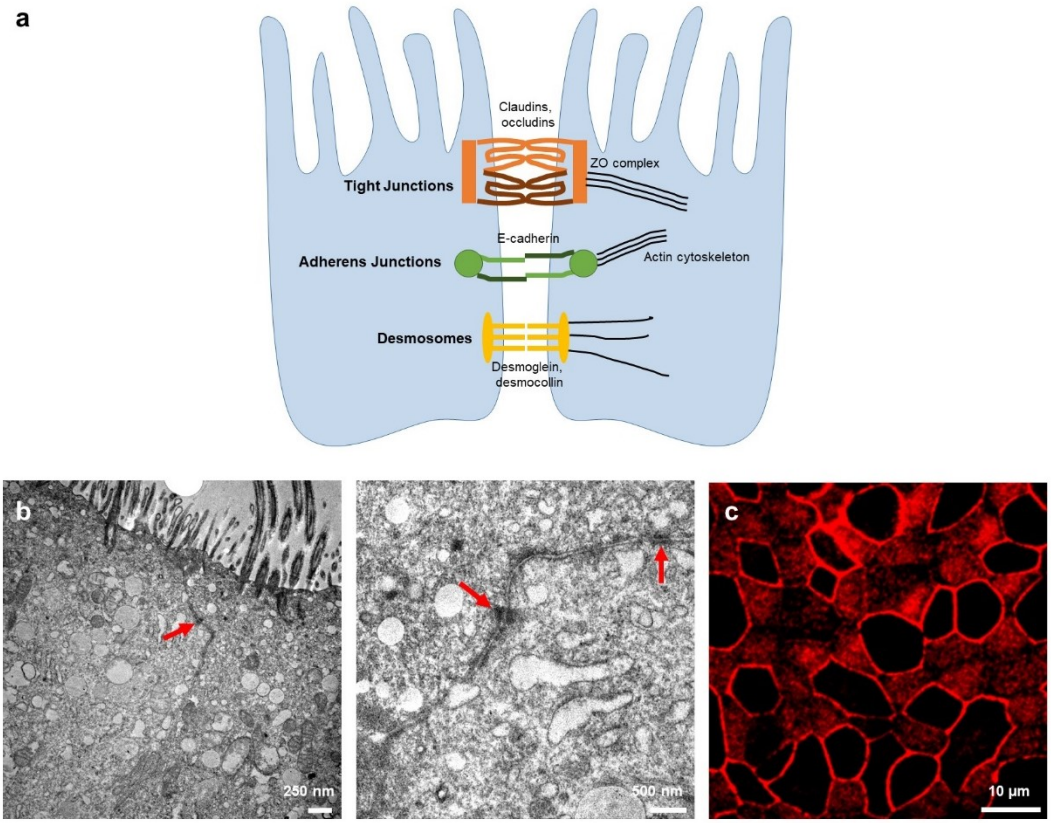

Figure 5: Airway epithelial junctions. (a) Schematic representation of intercellular junctions between epithelial cells. (b) Transmission electron microscopic images of small airway epithelial cell (SAEC) air-liquid interface (ALI) cultures. Red arrows indicate cell-cell junctions. (c) Immunofluorescent staining of a SAEC ALI culture stained for the tight junction protein zonula occludens (ZO-1).

Occludin is a ~ 65-kDa protein and features four putative membrane-spanning segments with two extracellular loops (Furuse et al., 1993). The first extracellular domain regulates paracellular permeability, whereas the second loop interacts with claudins and other junctional adhesion molecules (JAMs) (Nusrat et al., 2005).

The claudin family comprises at least 24 members. These 20–27-kDa tetraspan proteins with two extracellular loops are structurally similar to occludin, although no sequence similarities exist (Furuse et al., 1998; Van Itallie and Anderson, 2006). Claudins play a key role in paracellular permeability (Gunzel and Yu, 2013). In mammalian airways, Claudin-1, -2, -3, -4, -5, -7, -10, and -18 were reported to be expressed (Coyne et al., 2003; Kaarteenaho-Wiik and Soini, 2009; Moldvay et al., 2007; Niimi et al., 2001). Conceptually, claudins can be divided into barrier- (e.g. Claudin-11, -18) and pore-forming (e.g. Claudin-2, 7, 10) claudins (Amasheh et al., 2002; Gunzel et al., 2009; Gunzel and Yu, 2013; Koval, 2013; Soini, 2011). In this context, pore means that the paracellular permeability for molecules of a certain size or a certain charge (or both) is increased, whereas the epithelial barrier integrity against macromolecules is maintained (Gunzel and Yu, 2013). The epithelial barrier in COPD patients is dysfunctional, which leads to an impaired defense against intruding pathogens, resulting in an increased susceptibility to infections (Aghapour et al., 2018; Heijink et al., 2014).

1.2.3.4 Secreted factors contributing to epithelial defense

The airway epithelium secretes a variety of enzymes, protease inhibitors, oxidants, and antimicrobial peptides to combat inhaled pathogens (Ganesan et al., 2013).
Lysozyme kills certain Gram-positive and to a lesser extent Gram-negative bacteria (Ibrahim et al., 2002). Protease inhibitors, such as secretory leukoprotease inhibitor (SLPI), neutralize the effects of proteases expressed by invading pathogens (Ganesan et al., 2013). Nitric oxide (NO) and hydrogen peroxide are oxidants produced by the airway epithelium via NO synthases and dual oxidases (DUOX) and contribute to the clearance of viral and bacterial infections. Defensins are important antimicrobial peptides (AMPs), which are effective against multiple bacteria and viruses (Ganz, 2003). Furthermore, airway epithelial cells secrete cytokines and chemokines, such as granulocyte colony-stimulating factor (G-CSF) and interleukin (IL)-8, and therefore activate and regulate immune responses (Gern et al., 2000). Deficiencies of antimicrobial factors, such as SLPI and lysozyme, in COPD airways is linked to the frequency of exacerbations (Janoff, 1985; Lomas, 2016; Parameswaran et al., 2011; Saetta et al., 1997; Stockley, 2001).

1.3 The role of cigarette smoke in airway diseases

1.3.1 Composition of cigarette smoke

Cigarette smoke is estimated to consist of more than 7000 chemical substances, either bound to aerosol particles or free in the gas phase (Rodgman and Perfetti, 2008). Many of these compounds are known or suspected to be toxic, carcinogenic, and addictive (International Agency for Research on Cancer, 2004; U.S. Department of Health and Human Services et al., 2010). The following substances are included in the gas phase of cigarette smoke: nitrogen (N_2), oxygen (O_2), carbon dioxide (CO_2), carbon monoxide (CO), acetaldehyde, methane, hydrogen cyanide (HCN), nitric acid, acetone, acrolein, ammonia, methanol, hydrogen sulfide (H_2S), hydrocarbons, gas phase nitrosamines, and carbonyl compounds (Borgerding and Klus, 2005; Rodgman and Perfetti, 2008). Whereas carboxylic acids, phenols, water, humectants, nicotine, terpenoids, paraffin waxes, tobacco-specific nitrosamines (TSNAs), polycyclic aromatic hydrocarbons (PAHs), and catechols are found in the particulate phase (Borgerding and Klus, 2005; Rodgman and Perfetti, 2008). The concentrations of these chemicals can vary between the mainstream smoke (released from the cigarette butt when puffing) and the side-stream smoke (released when the burning cigarette smolders) (Perfetti et al., 1998).

1.3.2 Standardization of smoking profiles

By inhaling cigarette smoke, toxic and carcinogenic chemicals are adsorbed throughout the respiratory tract, from the mouth to the upper and lower airways to the alveoli. The individual

smoking profile varies a lot, depending on daytime, stress-level and the time since last nicotine consumption. Puff numbers and volume is different for each cigarette consumed by a single smoker. Therefore, the amount and concentration of chemicals reaching the smoker's airways is highly variable. Due to this high variability, it is impossible to reproduce the exact dose of chemical substances in the human lung with a cigarette machine-smoking method. However, there are standardized protocols to generate cigarette smoke *in vitro* to ensure consistent and comparable conditions. According to the International Organization for Standardization (ISO) the standard puff volume is 35 ml with two-second puff duration, one-minute puff frequency, and butt length defined as either 23 mm for nonfilter cigarettes or the length of the filter overwrap paper plus 3 mm (ISO 3308:2012) (International Organization for Standardization, 2012).

1.3.3 Cigarette smoke-induced oxidative stress

Previous studies in human smokers as well as *in vitro* and *in vivo* models have shown that acute exposure to cigarette smoke induces oxidative stress (Aoshiba et al., 2003; Cavarra et al., 2001; Guatura et al., 2000; Kharitonov et al., 1995; Morrison et al., 1999; Munakata et al., 2018). Due to the oxygen-rich environment, its large surface area and blood supply, the lungs are susceptible to injuries mediated by reactive oxygen species (ROS) (Rahman, 2005). The presence of ROS is directly related to the oxidation of proteins, DNA and lipids, which can either directly injure the lung or trigger a variety of cellular reactions by forming secondary metabolic reactive species. Therefore, ROS can alter extracellular matrix (ECM) remodeling, stimulate mucus secretion, inactivate anti-proteases, induce apoptosis, and modulate cell proliferation (Fig. 6) (Rahman, 2005; Rahman and MacNee, 1996, 1999). Furthermore, oxidants enhance pro-inflammatory pathways through neutrophil attraction and cytokine production (Bowler et al., 2004; MacNee, 2005). The chemokine interleukin-8 (IL-8) plays a critical role in the initiation and progression of inflammation after smoke exposure (Perng et al., 2013). Excessive neutrophil recruitment may trigger tissue damage and chronic inflammation (Jasper et al., 2019). Previous studies suggest that the pathogenesis in COPD is the result of an imbalance of proteases and anti-proteases, leading to emphysema (Janoff, 1985; Lomas, 2016; Saetta et al., 1997; Stockley, 2001).

Figure 6: Cigarette smoke mediates oxidative stress via free radicals and reactive oxygen species (ROS) and induces oxidative injuries in the lungs, such as oxidation of proteins, lipids and DNA, extracellular matrix (ECM) remodeling, imbalance of proteases and antiproteases, apoptosis, cell proliferation, mucus hypersecretion and lung inflammation.

1.3.4 Cigarette smoke-induced changes of the respiratory epithelium

A range of epithelial alterations follows cigarette smoke-induced epithelial injury (Dye and Adler, 1994). It is assumed that one of the first cells affected by CS are basal cells (Shaykhiev and Crystal, 2014a, b). Abnormal proliferation leads to basal cell hyperplasia (Crystal, 2014; Rock et al., 2010). The impaired differentiation capacity of basal cells result in a loss of ciliated cells (Auerbach et al., 1961). Furthermore, cilia length is reduced upon CS exposure (Leopold et al., 2009). Basal cell fate is shifted towards mucus-producing goblet cells, which accumulate and induce mucus overproduction (Lumsden et al., 1984; Saetta et al., 2000). In addition to alterations in cell type composition, the epithelium acquires a flat, squamous phenotype, a process called squamous metaplasia (Peters et al., 1993). Besides differential changes, important cell-cell junctions are lost and the epithelium becomes “leaky” (Kennedy et al., 1984; Shaykhiev et al., 2011).

Causal conclusions have been drawn between smoking and various respiratory diseases. In addition to lung cancer and COPD, the following disorders were reported: acute respiratory illnesses including pneumonia, impaired lung growth in children, early onset of lung

function decline, respiratory symptoms, such as coughing, phlegm, wheezing, and dyspnea. (Office of the Surgeon General and Office on Smoking Health, 2004)

1.4 Epidermal growth factor receptor (EGFR) and its role in COPD

1.4.1 EGFR types and signaling pathway

The Human Epidermal Growth Factor Receptor (HER) family consists of four cell surface receptors: HER1 (also known as EGFR or ErbB1), HER2 (ErbB2), HER3 (ErbB3) and HER4 (ErbB4). They exhibit a cysteine-rich extracellular ligand-binding domain, a single-pass α-helix transmembrane domain and a C-terminal signaling domain (Zhang et al., 2007). Apart from HER3, all HER family members feature a cytoplasmic tyrosine kinase domain. Ligand binding to the receptor induces either homodimerization (same receptor types) or heterodimerization (different EGF receptor types) (Graus-Porta et al., 1997; Lemmon, 2009). This leads to receptor autophosphorylation and cytoplasmic protein binding, activating four main downstream effectors: the MEK/ERK (MAPK kinase/extracellular signal-regulated kinase) pathway, the PI3K/AKT (phosphatidyl-inositol-3-kinase/protein kinase B) pathway, the JAK/STAT (Janus kinase/signal transducer and activator of transcription) pathway or the mTOR (mammalian target of rapamycin) pathway (Jorissen et al., 2003).

EGFR signaling pathways regulate a number of different cell functions. The actual outcome of receptor activation depends on "ligand choice and binding affinity, receptor homo- and/or heterodimerisation, extracellular ligand release and physical segregation of ligands and receptors, accessibility and abundance of intracellular and cell surface antagonists, speed and capacity for receptor recycling, and choice of downstream signaling pathway and subsequent gene regulation" (Vallath et al., 2014). After receptor activation through ligand binding, EGF receptors are rapidly internalized (Avraham and Yarden, 2011).

1.4.2 EGFR ligands

At least 13 extracellular ligands are reported to activate EGFR signaling (Yarden and Sliwkowski, 2001). The following ligands are known to bind to HER1: epidermal growth factor (EGF), Heparin-binding EGF-like growth factor (HB-EGF), Epigen, Epiregulin, Amphiregulin, β-cellulin and transforming growth factor α (TGF-α). So far, no ligands for HER2 have been identified. HER3 is supposed to be activated by Neuregulins 1-3.
HB-EGF, Epiregulin, β-cellulin and Neuregulins (1-5) are ligands for the HER4 receptor. (Vallath et al., 2014)

All EGFR ligands are membrane-bound proteins that need to be cleaved to become biologically active (Higashiyama et al., 2008). Key regulators of EGFR ligand release are ADAMs (disintegrin metalloproteases), such as ADAM10, which is central for the

ectodomain shedding of EGF and β-cellulin, or ADAM17, a major sheddase of epiregulin, TGF-α, amphiregulin, and HB-EGF (Sahin et al., 2004).

Depending on which ligand binds to the receptor, a different response is evoked. This is due to conformational changes of the ligand-receptor complexes (Wilson et al., 2009).

1.4.3 EGFR signaling in airway homeostasis and tissue repair

EGFRs are expressed on the basolateral membrane of basal cells, whereas the EGF family ligands are shed from the apical side of differentiated cells of the epithelium. Due to the physical distance of receptor and ligand, activation of EGFR signaling is prevented. Ligand-receptor binding can only occur if the epithelial barrier is disrupted, i.e. in case of airway epithelial injury. Subsequently, signaling pathways that induce proliferation are activated to reconstitute barrier integrity. (Shaykhiev et al., 2013; Vallath et al., 2014; Vermeer et al., 2003)
Brechbuhl et al. demonstrated that EGFR signaling is necessary for mouse basal cell proliferation and normal epithelial repair *in vivo* and *in vitro* (Brechbuhl et al., 2014).

In the absence of functional EGFR (HER1, ErbB1), lung development in mice is severely compromised, leading to impaired lung branching morphogenesis (Miettinen et al., 1997). HER2 and HER3 have been shown to play a role in human lung development *in vitro* (Patel et al., 2000). In addition, HER4 has been shown to regulate surfactant synthesis and proliferation in adult rat pulmonary epithelial cells and fetal rat lungs (Liu et al., 2009; Zscheppang et al., 2011). Therefore, EGF receptor signaling is assumed to play a key role in lung development and homeostasis (Fig. 7).

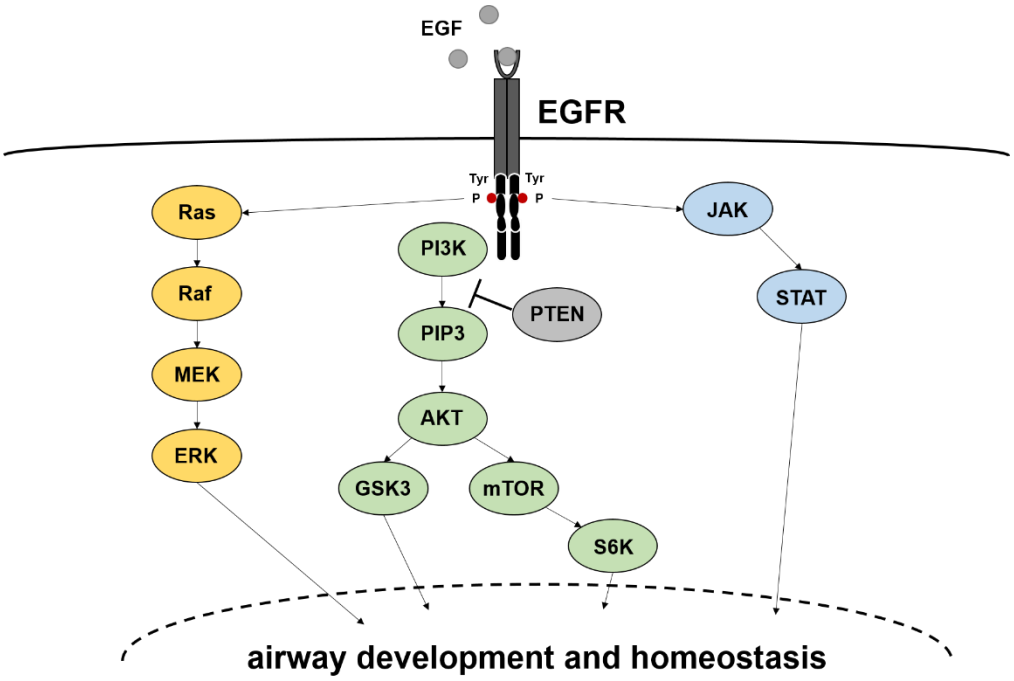

Figure 7: Schematic representation of epidermal growth factor receptor (EGFR) signal transduction. Epidermal growth factor (EGF) binds to EGFR and induces receptor dimerization and autophosphorylation (P) of tyrosine (Tyr) residues. This activates multiple pathways, such as the MEK/ERK (MAPK kinase/extracellular signal-regulated kinase), PI3K (phosphatidylinositol-3-kinase) and JAK/STAT (Janus kinase/signal transducer and activator of transcription) signaling pathway. Together these pathways regulate lung development and homeostasis. AKT: protein kinase B; GSK3: glycogen synthase kinase 3; mTOR: mammalian target of rapamycin, S6K: Ribosomal protein S6 kinase beta-1 (also known as p70S6K).

1.4.4 EGFR signaling in COPD

Goblet cell metaplasia and excessive mucus secretion are critical hallmarks of COPD, which are triggered by aberrant EGFR signaling. Long-term smokers exhibit increased levels of HER3 expression in the bronchial epithelium, which correlates with an increase in MUC5AC expression (O'Donnell et al., 2004). Furthermore, HER1-3 mRNA was elevated in COPD patients compared to non-COPD smokers (Anagnostis et al., 2013). It has been shown that HER4 is elevated in smokers compared to non-smokers and is even more pronounced in COPD patients compared to non-COPD smokers. A finding that is inversely correlated to FEV_1, indicating a link between HER4 receptor expression and COPD severity (Anagnostis et al., 2013).

Shaykhiev et al. revealed an elevated *EGF* mRNA expression in the airway epithelium of smokers. Expression was highest in ciliated cells compared to secretory, basal and intermediate cell types. In agreement to this, cigarette smoke extract (CSE) exposure induced EGF protein secretion to the apical side of the epithelium *in vitro*. (Shaykhiev et al., 2013)

Basal cell hyperplasia and squamous metaplasia are also characteristic for COPD. Previous studies demonstrated that EGF induces squamous metaplasia in primary bronchial air-liquid interface (ALI) cultures, suggesting that aberrant EGFR signaling triggers these pathologic

effects (Shaykhiev et al., 2013). Besides COPD, aberrant EGFR signaling plays an important role in multiple lung cancers, often associated with gene mutations in the *EGFR* (*HER1*) gene (Lynch et al., 2004).

1.4.5 Targeting EGFR signaling

Several therapeutic approaches have been developed to prevent aberrant EGFR signaling. There are two main strategies to target the EGFR signaling pathway: inhibiting the tyrosine kinase activity of EGFR using small molecules and blocking ligand-receptor binding using monoclonal antibodies. Small molecule tyrosine kinase inhibitors (TKIs), such as erlotinib, gefitinib, lapatinib, HKI-272 and BIBW-2948, prevent EGFR autophosphorylation and therefore inhibit downstream signaling. (Vallath et al., 2014)
Gefitinib was shown to be efficacious in patients suffering from pulmonary adenocarcinoma (Mok et al., 2009). The use of TKIs has also been investigated for the treatment of COPD patients. The therapeutic benefit of BIBW 2948 in COPD patients was assessed in a clinical study. BIBW 2948 did not show a significant decrease in mucus production and was furthermore poorly tolerated by COPD patients (Woodruff et al., 2010). It is assumed that higher doses may be more effective but may also induce severe adverse events (Woodruff et al., 2010).
Cetuximab and trastuzumab are examples for EGFR-blocking monoclonal antibodies that prevent the binding of endogenous ligands and thereby attenuate downstream pathway activation (Vallath et al., 2014). The efficacy of cetuximab for the treatment of non-small-cell lung cancer appears to be comparable to currently available chemotherapeutic agents or EGFR TKIs (Hanna et al., 2006).

1.5 Modelling epithelial changes of COPD in vitro

1.5.1 Need for airway epithelial *in vitro* models

To study COPD-relevant mechanisms and investigate potential therapeutic targets appropriate models are pivotal. Animal models with rodents have contributed a lot to the understanding of important mechanisms in respiratory research. However, the lung architecture, cellular composition or molecular processes in humans differ significantly from rodents; therefore, murine or rat models are not sufficient for the investigation of human airway diseases (Boers et al., 1999; Churg et al., 2011; Irvin and Bates, 2003). Furthermore, animal models are called into question by ethical evaluations. The principles for animal welfare, the “Three R’s” – Replacement, Reduction and Refinement, require alternative *in vitro* methods (Flecknell, 2002). The complexity of the available *in vitro* models and their relevance for mimicking the human situation varies greatly. The starting material, i.e. the source of cells, plays an important role. Some models are based on cell lines (section 1.5.2), whereas others use primary cells (section 1.5.3) as a source. The cultivation method is

another important aspect. Epithelial cells can be cultivated submerged (two dimensions) or physiologically in a three-dimensional model under air-liquid interface conditions.

1.5.2 Airway epithelial cell lines

Immortalized cell lines (such as 16HBE, BEAS-2B, PBEC) or tumor cell lines (such as NCI-H292, Calu-3) are easy to handle and can be cultured either submerged or on Transwell inserts under air-liquid interface (ALI) conditions with air exposure on the apical side and culture medium on the basolateral side of the membrane; a culture method closely resembling physiological conditions in the airways (Azzopardi et al., 2015; Broekman et al., 2016; Ghio et al., 2013; Hao et al., 2012; Heijink et al., 2016a; Heijink et al., 2016b; Jang et al., 2014; Kreft et al., 2015; Randall et al., 2013; Shaykhiev et al., 2011; Taylor et al., 2016; Vinhas et al., 2011). For some applications, these cell lines may be suitable; however, they do not succeed in forming a highly differentiated epithelium. Wang et al. immortalized and characterized a normal human small airway epithelial basal cell line (hSABCi-NS1.1), which is capable to differentiate into specialized cell types and may be useful to mimic disease-relevant processes in the small airways (Wang et al., 2019).

1.5.3 Primary airway epithelial *in vitro* models

Besides cell lines, primary cells can be used to model the airway epithelium. Grown at ALI, primary epithelial cells differentiate within four weeks into a pseudostratified epithelium and reflect organ-specific features such as apical-to-basal polarization, ciliary development, mucus production or barrier function (Fig. 8). These cultures most closely resemble that of *in vivo* airway epithelia (Pezzulo et al., 2011). Primary cells can be isolated from explanted human tissue, obtained commercially as frozen stocks, or purchased fully differentiated, ready-to-use, such as EpiAirway (MatTec, Ashland, MA, USA) or MucilAir (Epithelix, Geneva, Switzerland).

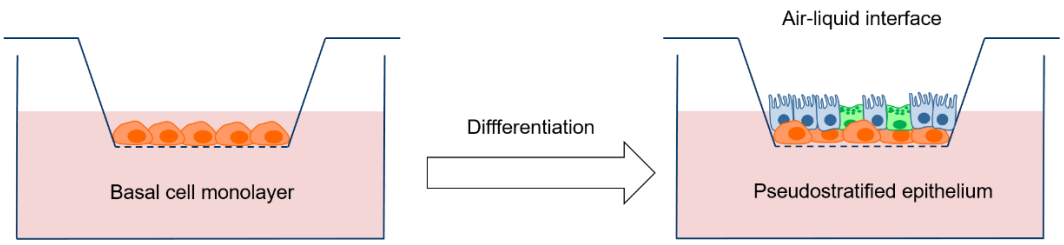

Figure 8: Primary small airway epithelial basal cells (orange) differentiate within four weeks under air-liquid interface (ALI) conditions to a pseudostratified epithelium with differentiated cell types, such as secretory club (green) and ciliated cells (blue).

1.5.4 Induction of COPD-relevant phenotypes in airway epithelial *in vitro* models

In principle, there are two ways to study the pathogenesis of COPD in the airway epithelium *in vitro*. The first option is to isolate primary epithelial cells from COPD patients that already have disease-relevant characteristics and investigate the differences in comparison to cells from healthy donors. The second option is to treat healthy cells with certain substances to induce a COPD-like phenotype.

Soluble substances are mostly administered via the cell culture medium. Shaykhiev et al. showed for instance that EGF shifts human airway basal cells towards abnormal, squamous and epithelial-mesenchymal transition (EMT)-like phenotypes, resembling the morphology seen in smokers and COPD patients (Shaykhiev et al., 2013)

For volatile compounds, such as cigarette smoke, more complex exposure techniques are required, which will be introduced in closer detail. To understand the underlying mechanisms, previous *in vitro* studies have mainly used cigarette smoke extract (CSE) to mimic smoke-induced effects. CSE is generated by introducing cigarette smoke into a liquid medium and therefore contains only soluble components of cigarette smoke. To investigate the effects of whole cigarette smoke, including particulate and gaseous phase, exposure devices, such as the Vitrocell® 24/48 exposure system (VITROCELL Systems, Waldkirch) or the Professional In-Vitro Technologies (P.R.I.T.) Expo Cube (Fraunhofer Institute for Toxicology and Experimental Medicine, Hannover), are required. A major advantage of these exposure set-ups is that the cells can be exposed from the apical side, which reflects a physiological administration. In case of the P.R.I.T. Expo Cube, the medium is not exposed to cigarette smoke, which prevents soluble components from affecting the cells basolateral.

1.6 Aim of the thesis

An important hallmark of COPD is the pathologic remodeling of the small airways, leading to airway obstruction, mucus hypersecretion, reduced ciliary function and loss of barrier integrity (Singh, 2017). The pathophysiological mechanisms underlying small airway disease in COPD are not yet covered by any therapeutic approach. Research in this field is therefore of great benefit to the patient population. The aim of this thesis was to investigate the molecular processes underlying the pathophysiological remodeling of small airway epithelial cells in COPD. Therefore, a novel *in vitro* model had to be established that mimics the small airway epithelium. Its translatability to the human situation *in vivo* was an important aspect that had to be demonstrated.

COPD-relevant alterations of the small airway epithelium had to be induced *in vitro* in order to investigate the underlying mechanisms. Smoking is the major causative factor to develop COPD (Laniado-Laborin, 2009; Lozano et al., 2012; Yoshida and Tuder, 2007); hence, CS exposure may be an important trigger for pathological alterations. In the present dissertation, primary human material isolated from the small airways was used to elucidate the role of the small airway epithelium in the pathogenesis of COPD. Investigating the effects of CS on

SAEC provides an important basis to assess new therapeutic targets in smoke-associated diseases. Previous *in vitro* studies focused mostly on cells from the upper airways and *in vivo* models are challenged by inter-species differences regarding lung architecture, cellular composition or molecular processes.
The ability to translate with confidence the data from any model to potential efficacy in the clinical disease is important in drug discovery. Therefore, both the newly established SAEC ALI model and the CS exposure model had to be thoroughly evaluated with respect to their suitability to mimic human small airways in health and disease (COPD) and to reflect CS-induced changes in human smokers.

The newly established *in vitro* models were used to investigate specific COPD-relevant mechanisms, such as the EGFR signaling pathway or effects associated with oxidative stress. Various substances modulating these mechanisms were examined for their suitability to prevent CS-induced effects in order to find therapeutic approaches for the treatment of smoking-related diseases such as COPD.

2 Material and Methods

2.1 Human small airway model

Human small airway epithelial cells (SAEC, CC-2547, Lonza, Basel, Switzerland) of three healthy donors and three COPD patients (compare Tab. 1) were used for the experiments in this dissertation. As stated by Lonza, the cells were isolated from donated human tissue after obtaining permission for their use in research applications by informed consent or legal authorization. Established ethical practices of the donation and transplantation organizations in the US (American Association of Tissue Banks, Association of Organ Procurement Organizations, Eye Bank Association of America) are followed at Lonza.

Table 1: Donor information of small airway epithelial cells (SAEC) purchased from Lonza. Cells from n=3 healthy controls (HC) and n=3 patients with chronic obstructive pulmonary disease (COPD) were used for the experiments in this dissertation.

	Age (years)	Sex	Race	Smoking
HC-1	67	Female	Caucasian	No
HC-2	42	Female	Hispanic	No
HC-3	38	Male	Caucasian	No
COPD-1	57	Female	Caucasian	Yes
COPD-2	51	Female	Caucasian	Yes
COPD-3	62	Female	Black	Yes

After thawing, approximately one million cells were seeded into a T175 cell culture flask with 50 ml pre-warmed PneumaCult-Ex Plus medium (Stemcell Technologies, Vancouver, Canada). On the following day, the medium was exchanged, to remove residuals from the cryoprotectant cocktail. On the fourth day after seeding, the cells were sufficiently confluent (max. 80 %) to be harvested for seeding into Transwell inserts. The Transwells (#3460, Corning Life Sciences B.V., Amsterdam, the Netherlands) were coated with 300 µl rat tail collagen type 1 solution (Corning Life Sciences B.V., Amsterdam, the Netherlands, 30 µg/ml in phosphate buffered saline) for 45 minutes at 37 °C. Collagen solution was aspirated and Transwell inserts were washed with phosphate buffered saline (PBS). The basolateral compartments of the Transwells were filled with 1.5 ml PneumaCult-Ex Plus medium. Dissociation of SAEC was performed using the Animal Component-Free Cell Dissociation Kit (Stemcell Technologies, Vancouver, Canada) according to the manufacturer's instructions. Subsequently, 100.000 cells per insert were seeded in 300 µl of PneumaCult-Ex Plus medium on the Transwell membrane. On the following day, apical and basolateral media was exchanged using PneumaCult-Ex Plus medium. On day three after seeding into Transwell inserts, cells were fully confluent. The apical and basolateral medium was removed and 1.5 ml Pneumacult-ALI-S medium (Stemcell Technologies, Vancouver,

Canada) was added basolateral. The apical compartment was washed with PBS to remove residual growth factors of the expansion medium. Afterwards, cells were maintained in air-liquid interface (day 0) to allow differentiation into pseudostratified epithelial cultures. Medium exchanges were performed three times a week. The cells were fully differentiated 28 days after air-lift.

2.2 Smoke exposure

2.2.1 Cigarette smoke extract

Mainstream smoke of five 3R4F reference cigarettes (University of Kentucky, Lexington, KY, USA) was bubbled through 50 ml PBS using a water-jet vacuum pump. The obtained extract was considered as 100 % CSE. To ensure standardization between experiments, CSE was sterile-filtered through a 0.2 µm Minisart® syringe filter (Sartorius Stedim Biotech, Goettingen, Germany), aliquoted and stored at -80 °C. For usage, CSE was thawed and diluted with cell culture medium to the final concentration.

2.2.2 Whole cigarette smoke

SAECs were exposed to whole cigarette smoke of 3R4F reference cigarettes (University of Kentucky, Lexington, KY, USA) using an automated cigarette smoking machine (In-Expose smoking robot, Scireq Montreal, QC, Canada) and the P.R.I.T. (Professional In-Vitro Technologies) ExpoCube in the experimental setup developed by Fraunhofer Institute for Toxicology and Experimental Medicine (Fig. 9 and 10).

Four cigarettes were smoked in parallel in compliance to ISO 3308, drawing every 15 seconds a puff from the sequentially smoked cigarettes (9 puffs per cigarette). The smoke was diluted with ambient air (dilution rate: 0.5 l/min). The cells were exposed to CS three times a week during the differentiation phase (28 days) beginning on day 0 (= day of air-lift). Cells were cultured on 12-well plates, with the upper four wells exposed to smoke and the lower four wells exposed to air. All wells were uniformly exposed to CS due to computational fluid dynamics-optimized geometry of the flow paths. Ritter et al., (Fraunhofer Institute for Toxicology and Experimental Medicine) previously tested and described this in detail (Ritter et al., 2018; Ritter and Knebel, 2014). Readouts were performed 24 hours post last exposure.

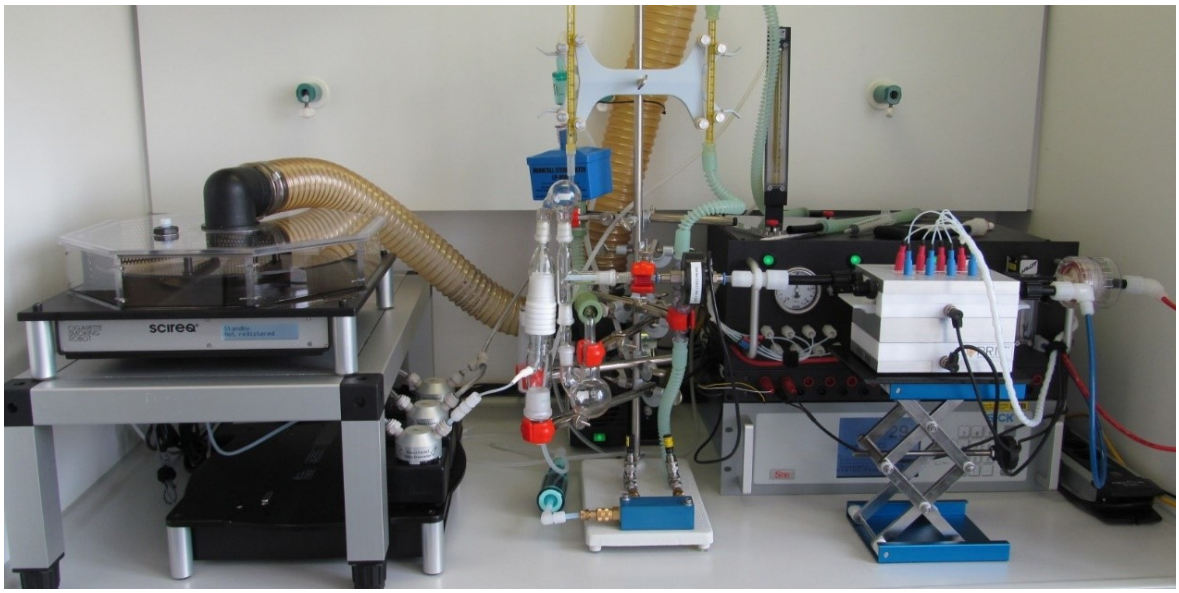

Figure 9: Setup for whole cigarette smoke exposure of ALI cultures. From left to right: Automated cigarette smoking machine (Scireq Montreal, QC, Canada), custom-made dilution system with adaptation to whole native cigarette smoke and relevant dilution rates, P.R.I.T ExpoCube for exposure of ALI cell cultures with P.R.I.T. Control Unit (Fraunhofer Institute for Toxicology and Experimental Medicine). ALI = air-liquid interface, P.R.I.T. = Professional In-Vitro Technologies.

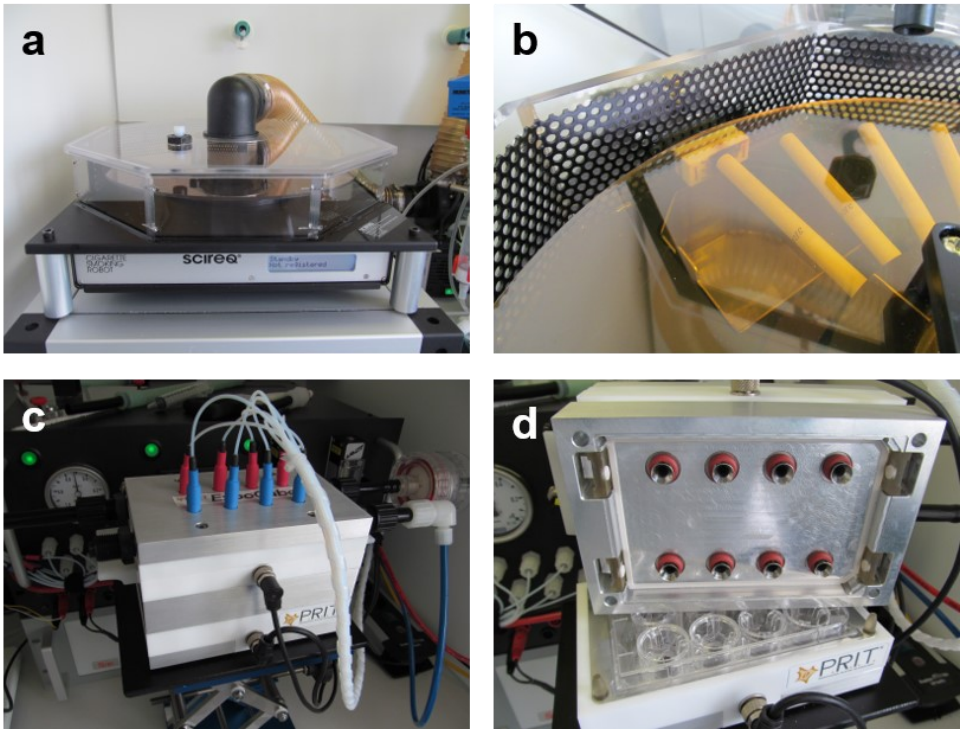

Figure 10: Close-up images of smoke exposure device. (a) Automated cigarette smoking machine (Scireq Montreal, QC, Canada) with (b) combustion chamber and smoke carousel. (c) P.R.I.T ExpoCube for exposure of ALI cultures with exposure flow inlets for air (blue) and smoke (red) exposure. (d) Opened P.R.I.T. Expo Cube with 12-well Transwell inserts and exposure outlets. P.R.I.T. = Professional In-Vitro Technologies, ALI = air-liquid interface.

2.3 Compound Treatment

SAEC ALI cultures were exposed to a number of substances via the basolateral medium (compare Tab. 2). Medium containing compounds was refreshed three times a week. In case of multiple treatments (e.g. compound + CS), compounds were pre-incubated for one hour.

Table 2: Compounds used to treat small airway epithelial cell (SAEC) air-liquid interface (ALI) cultures in different experimental settings.

Compound	Concentration	Supplier
Cigarette smoke extract (CSE)	0.5 %	Self-made (see 2.2.1)
N-acetyl-cysteine (NAC), A9165	15 mM	Sigma-Aldrich, St. Louis, MO, USA
Trolox, 238813	10 µM	Sigma-Aldrich, St. Louis, MO, USA
Protein kinase D (PKD) inhibitor, kb-NB142-70, SML0525	1 µM	Sigma-Aldrich, St. Louis, MO, USA
Epidermal growth factor receptor (EGFR) tyrosine kinase inhibitor, Gefitinib, ab142052 (EXBX0080)	3 µM	abcam, Cambrige, UK
recombinant human epidermal growth factor (EGF) protein, 236-EG	0,8 nM	R&D Systems Minneapolis, USA
recombinant human TGFβ protein, 240-B	5 ng/ml	R&D Systems Minneapolis, USA
Olodaterol	1 µM	Resynthesized at Boehringer Ingelheim
Roflumilast	100 nM	Resynthesized at Boehringer Ingelheim
Aryl hydrocarbon receptor (AHR) antagonist, CH-223191	500 nM	Sigma-Aldrich, St. Louis, MO, USA

2.4 Functional analysis

2.4.1 Transepithelial electrical resistance (TEER)

Epithelial barrier integrity was monitored by measuring transepithelial electrical resistance (TEER) using an EVOM2 epithelial volt-ohmmeter (World precision Instruments, Sarasota, FL, USA) according to the manufacturer's instructions. To perform the TEER measurement, 300 µl PBS were added to the apical compartment of the insert. The long stem of the electrode was inserted through the gap of the Transwell to be in contact with the basolateral medium and the short stem of the electrode was placed above the apical surface to be in contact with the apical PBS. The measured resistance was multiplied by the surface area of the epithelium (1.12 cm^2) to obtain TEER (Ω*cm^2).

2.4.2 Cilia beat measurement

The detailed description of this method has previously been published:

Gindele, J.A., Kiechle, T., Benediktus, K. et al. Intermittent exposure to whole cigarette smoke alters the differentiation of primary small airway epithelial cells in the air-liquid interface culture. Sci Rep 10, 6257 (2020). https://doi.org/10.1038/s41598-020-63345-5

An excerpt of the mentioned publication can be found below.

A variety of methods are used to obtain quantitative data from beating cilia, these range from manual or automated (Meste et al., 2015; Smith et al., 2012) tracking of cilia in video sequences to very sophisticated solutions with optical coherence tomography (Jing et al., 2017).

Repeated observations of vital cell cultures on air-liquid interfaces limit the options for data acquisition. We chose to use video-microscopy. Unfortunately, the ciliary beat frequency cannot be directly extracted from the image space. Manual tracking is a time consuming task, fully automated processes would ease this workload, but there appear to be challenges in the ability to incorporate intensity, resolution and focal changes. What we are interested in is the beat frequency, and this is in time domain (Norina et al., 1998). However, in a video of beating cilia, the time domain is not directly accessible. To circumvent this, we use image stacks of 2D+time, 512 images with a size of 512 *512 pixels. If the microscopic images describe the transversal planes, then sagittal and coronal planes nicely present the intensity modulated signal caused by beating cilia.

The disadvantage is that an image in a sagittal or coronal plane still has time and spatial information (Fig. 11a). A power spectrum generated from such an image would be difficult to interpret, however, an image from a single line of size 1 pixel by 512 pixels, simplifies the analysis. A line profile of this image with intensity changes caused by a beating cilia would also allow simple counting of swings per time as shown in Figure 11b (39 beats in 512 frames at 100 fps result in beat frequency of 7.62 Hz) or could be sent to any other Fourier analysis tool.

We implemented a fully automated version using imaging processing tools, including the Discrete Fourier Transformation, for the characterization of a ciliary beating pattern and frequency in an air-liquid interface cell culture. The corresponding time track is taken for all the pixels in the x-y (spatial) domain. The signal is multiplied by a Gaussian window function before the fast Fourier transformation is calculated. The resulting power spectrum is searched for the most relevant frequency and the result is mapped back onto x-y-coordinates (Fig. 11c).

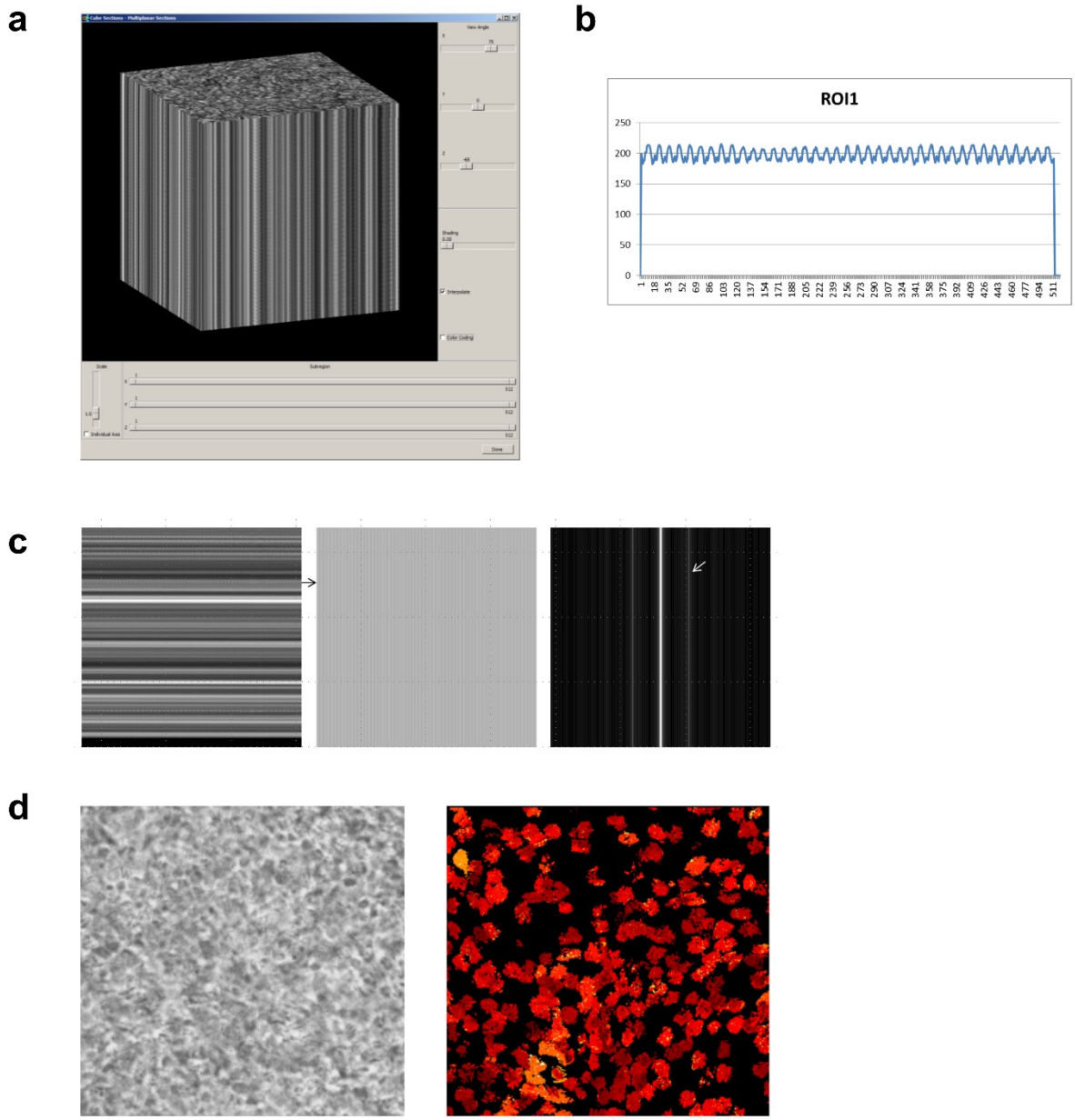

Figure 11: Quantitative cilia beat measurement. (a) 2D+t stack of a small airway epithelial cell (SAEC) culture at air liquid interface (ALI). (b) Intensity changes over time taken from a single line of voxels of a 2D+t stack. (c) Image of 1D+time (left), single line image (middle, stretched to 512 by 512 pixels) and the corresponding fast Fourier transform (right) where the significant frequency can be seen. (d) One image out of the image stack (left) and the frequency image (right). (Gindele et al., 2020)

The results for all pixels are represented using a false-color lookup table (LUT), in this example a temperature LUT, i.e. the faster the hotter (Fig. 11d). A histogram of frequencies [Hz] found for the field of view is displayed as an overlay. The mean frequency, area covered by moving cilia, and histogram of frequencies present in the experiment are stored on file. The analysis of an image stack takes approximately one minute. Time could be further

reduced by optimizing code for reading and rotating volume, using parallelization and minimizing stack size if required.

Typical beat frequencies are in the range of 5 Hz to 15 Hz. Analyzing beating cilia with a minimum of 50 frames per second would theoretically be sufficient, but we prefer to use a camera running at 100 frames per second (acA 1300-200µm, black and white, USB-3.0, Basler AG, 22926 Ahrensburg, Germany). A stack size of the power of two is not mandatory but often used in the field of medical imaging and is often preferred when using Fourier transformations with image processing tools. Applications for image capture and analysis are developed using a commercially available machine vision software toolbox (Halcon 13.0.2, MVTec Software GmbH, Munich). Visualization of image stack was done with Analyze (AnalyzeDirect, Inc. Overland Park, KS, USA).

2.5 Morphologic analysis

2.5.1 Light microscopy

SAEC ALI cultures were visually assessed using an EVOS FL microscope (AMF6000, Life technologies, Oregon, OR, USA).

2.5.2 Histology

Cells, growing on Transwell membranes (pore size of 0.4 µM), were fixed in 4 % paraformaldehyde over night and embedded in paraffin. After sectioning (section slice thickness approximately 3-4 µm), slides were deparaffinized and hematoxylin and eosin (H&E) or Alcianblue periodic acid Schiff (PAS) stainings were performed according to standard procedures. Images were acquired with an AxioCam MR3 (Zeiss, Oberkochen, Germany) using the 20x objective of an Axio Imager Z1 (Zeiss, Oberkochen, Germany).

2.5.3 Epithelial Thickness

Epithelial thickness was measured at several sites of formalin-fixed, paraffin-embedded tissue sections from SAEC ALI cultures. Subsequently, the median epithelial thickness was calculated for further comparison.

2.5.4 Transmission Electron Microscopy

SAEC ALI cultures were fixed in 2.5 % glutaraldehyde with 1 % tannin in 0.05 M sodium cacodylate buffer (pH 7.4) for 90 minutes. Subsequently, the samples were rinsed three times for ten minutes with wash buffer (0.1 M sodium cacodylate buffer with 400 mg sodium chloride (NaCl) per 100 ml, pH 7.4). Then the membranes were placed in 1 % osmium tetroxide fixing solution (according to Dalton) for one hour, followed by three more washing steps. Dehydration of the tissue followed a series of alcohol washes. Therefore, the samples were incubated in 30 % isopropanol (2x 15 min), 50 % isopropanol (15 min), 70 % isopropanol (15 min), 90 % isopropanol (15 min) and 100 % isopropanol (15 min and 30 min). The specimen were then rinsed with a mixture of the embedding resin Epon and isopropanol (1+1), Epon and isopropanol (2+1) and Epon and isopropanol (4+1) for 30 minutes each. Afterwards, the samples were placed in 100 % Epon for one hour, the solution was renewed and the fixed cultures were incubated over night. After another six hours incubation, the wells were filled with the epoxy resin Epon and the samples were polymerized at 60 °C for 48 hours. Blocks were then sawn out. Excessive material around the area of interest was removed with a trimming device (Leica EM TXP, Leica Microsystems, Wetzlar, Germany). Ultra-thin sectioning (approximately 60 nm) was performed by ultramicrotomy (Ultramicrotome Artos 3D, Leica Microsystems, Wetzlar, Germany). Specimen were analyzed using a transmission electron microscope (transmission electron microscope EM912, Zeiss, Oberkochen, Germany).

2.5.5 Scanning Electron Microscopy

Fully differentiated ALI cultures were fixed with 2.5 % glutaraldehyde/1 % tannin (primary fixation) and osmium tetroxide (secondary fixation) as described in section 2.5.4. The samples were then rinsed with distilled water (2x 5 min) followed by a series of alcohol washes in order to dehydrate the tissue. Samples were washed with 30 % ethanol (2x 15 min), 50 % ethanol (15 min), 70 % ethanol (15 min), 90 % ethanol (15 min), and 100 % ethanol (30 min and 1 hour). Fixed ALI cultures were then subjected to critical point drying (Critical Point Dryer 030, Balzers Instruments, Balzers, Liechtenstein). Therefore, the samples were placed in the pre-cooled chamber filled with ethanol, in which water was exchanged for liquid CO_2 in ten cycles of five minutes each. Afterwards, the chamber was heated above the critical point of CO_2 (31.1 °C, 74.04 bar) and held for 20 minutes. The pressure was then slowly reduced to atmospheric level. Subsequently, the samples were coated with 40 nm gold using a sputtercoater (SCD 500 EVN, Balzers Instruments, Balzers, Liechtenstein). The probes were analyzed using a scanning electron microscope (Supra 55VP, Zeiss, Oberkochen, Germany).

2.6 Protein analysis

2.6.1 Preparation of a single cell suspension from SAEC ALI cultures

The detailed description of this method has previously been published:

Gindele, J.A., Kiechle, T., Benediktus, K. et al. Intermittent exposure to whole cigarette smoke alters the differentiation of primary small airway epithelial cells in the air-liquid interface culture. Sci Rep 10, 6257 (2020). https://doi.org/10.1038/s41598-020-63345-5

An excerpt of the mentioned publication can be found below.

Fully differentiated SAEC ALI cultures growing on 12 well Transwells inserts were dissociated enzymatically and mechanically. Cells were incubated with 300 µl Accumax solution (Sigma-Aldrich, St. Louis, MO, USA) for 15 minutes at room temperature. Apical liquid containing already dissociated cells was transferred to a tube and 300 µl fresh Accumax solution were added into the Transwell insert for another 15 minutes. By clapping the plate gently, cells dissociated from the membrane. Transwell membrane was washed with Accumax solution several times until cell layer was completely dissociated. Cells were transferred into a gentleMACS C Tube and were gently dissociated by the gentleMACS Dissociator (Miltenyi Biotec, Bergisch Gladbach, Germany) using programme m_lung_01. The suspension was centrifuged and resuspended in 0.04 % Bovine Serum Albumin in Hank's Balanced Salt Solution. This step was repeated several times to obtain a single cell suspension. Large aggregates were removed by passing the suspension through 30 µm cell strainers. Cell concentration, viability and number of aggregates were determined using a NucleoCounter NC-200 (ChemoMetec, Allerod, Denmark).

2.6.2 Flow cytometry

Single cell suspensions of SAEC ALI cultures were fixed in 4 % paraformaldehyde for 20 minutes at room temperature. Cells were washed twice using Perm/Wash Buffer (BD Biosciences, San Jose, CA, USA) and blocked to prevent non-specific binding using Human BD Fc Block (BD Biosciences, San Jose, CA, USA). Cells were stained in Perm/Wash Buffer for one hour at room temperature. Anti-human antibodies used for staining are listed in Tab. 3. Flow cytometry was performed using a BD LSRFortessa X-20 cytometer equipped with DIVA-software (BD Biosciences, San Jose, CA, USA).

Table 3: Antibodies used for flow cytometry analysis of small airway epithelial cell (SAEC) air-liquid interface (ALI) cultures

Antigen	Antibody
Cytokeratin 5 (KRT5)	Rabbit monoclonal Anti-Cytokeratin 5 antibody, clone EP1601Y, ab193895 (Abcam, Cambrige, UK)
Mucin 5 AC (MUC5AC)	mouse monoclonal Anti-MUC5AC antibody, clone 45M1, NBP2-32732AF405 (Novus Biologicals, Centennial, CO, USA)
Uteroglobin (SCGB1A1)	rat monoclonal Anti-SCGB1A1 antibody, Clone #394324, MAB4218 (R&D; Minneapolis, MN, USA)
Secondary antibody	Mouse monoclonal Anti-Rat IgG1 secondary antibody, PE, Clone R1-12D10, 12-4812-82 (eBioscience, San Diego, CA, USA)

2.6.3 Immunohistochemistry

For immunohistochemical (IHC) investigation, paraffin-embedded tissue slices were subjected to heat induced antigen retrieval in citrate buffer (pH 6.0, H.I.E.R, BioLegend San Diego, CA, USA) for 30 minutes. Antibodies used for immunofluorescence or chromogenic antigen detection are listed in Tab. 4.

After staining, tissues slides were mounted either with ProLong™ Diamond Antifade Mountant (Thermo Fisher Scientific, Waltham, MA, USA) or with Entellan® new (Merck KGaA, Darmstadt, Germany). For immunofluorescence samples, stained slides were stored at 4 °C in the dark and images were taken using the Zeiss Laser Scanning Microscope 710 or an AxioImager M2 (both Carl Zeiss, Oberkochen, Germany) in case of chromogenic IHC.

Table 4: Antibodies used for immunohistochemistry (IHC) of small airway epithelial cell (SAEC) air-liquid interface (ALI) cultures

Antigen	**Antibody**
Cytokeratin 5 (KRT5)	rabbit monoclonal Anti-Cytokeratin 5 antibody, clone EP1601Y, ab193895 (Abcam, Cambrige, UK)
Mucin 5 AC (MUC5AC)	mouse monoclonal Anti-MUC5AC antibody, clone 45M1, NBP2-32732AF488 (Novus Biologicals, Centennial, CO, USA)
Uteroglobin (SCGB1A1)	rat monoclonal Anti-SCGB1A1 antibody, Clone #394324, MAB4218 (R&D; Minneapolis, MN, USA)
Acetylated Tubulin (Ac. Tub.)	Mouse monoclonal Anti-Acetylated Tubulin antibody, clone 6-11B-1 (Sigma-Aldrich, St. Louis, MO, USA)
Secondary antibody	secondary Goat anti-Rat IgG (H+L) Cross-Adsorbed Antibody, Alexa Fluor 568, A-11077 (Life Technologies, Oregon, OR, USA)
Claudin 10 (CLDN10)	Rabbit polyclonal Anti-Claudin 10 antibody, ab52234 (Abcam, Cambrige, UK)

2.6.4 Image Analysis

IHC staining of Claudin-10 was analyzed in a semi-quantitative way using automated image analysis as described previously (Gindele et al., 2020).
Formalin-fixed paraffin embedded slices from ALI cultures stained for Claudin-10 (ab52234, Rabbit polyclonal to Claudin-10, Abcam, Cambridge, MA, USA) were scanned with an Axio Scan.Z1 scanner (Carl Zeiss Microscopy GmbH, Jena, Germany) using a 20x objective (0.22 µM/px) in bright field illumination. Semi-quantitative image analysis was performed with the Halo 3.0 software using the CytoNuclear 1.6 module (Indicalabs, Corales, NM, USA). In preparation for the automated analysis, regions with damaged tissue sections or insufficiently stained cells were manually excluded. For automated analysis, a random forest tissue classifier was trained to recognize the cellular layer of the epithelial sections to limit the following analysis to this region and exclude the supporting material and background. Subsequently, the CytoNuclear module was applied within this region. As first step, the channels of nuclear (hematoxylin) and IHC stain (3'Diaminobenzidine (DAB) signal of Claudin-10) were unmixed using color deconvolution. Cell segmentation used the nuclear stain and empirical parameters on size and shape of the cells. Positive cells were identified using a manually optimized threshold value on the DAB channel, within the segmented region of a cell. The generated readout per ALI culture section was the number of positive cells n per analyzed area of the cell layer A, i.e. n/A.

2.6.5 Multiplex immunoassays

Multiplex immunoassay kits from Meso Scale Discovery (MSD, Gaithersburg, MD, USA) were used to quantify Interleukin-8 (IL-8, high-abundance V-PLEX) in cell culture medium of SAEC ALI cultures and to determine phospho-EGFR (Tyr1173) and total EGFR in whole cell lysates of SAEC ALI cultures (Phospho(Tyr1173)/Total EGFR Whole Cell Lysate Kit). Downstream signaling pathways were analyzed using MSD phosphoprotein assays: AKT signaling Panel (phospho-p70S6K (Thr421/Ser424), phospho-GSK-3β (Ser9), phospho-Akt (Ser473)), phospho-STAT panel (phosho-STAT3 (Tyr705), phospho-STAT4 (Tyr693), phospho-STAT5a,b (Tyr694)) and the ERK-STAT3 cascade (phospho-STAT3 (Tyr705), phospho-ERK1/2 (Thr202/Tyr204; Thr185/Tyr187), phospho-MEK1/2 (Ser217/221)). Assays were performed according to manufacturer's instructions.

2.6.6 Lactate Dehydrogenase (LDH) Assay

Cytotoxicity was assessed based on the measurement of lactate dehydrogenase (LDH) activity released from the cytosol of damaged cells into the supernatant. LDH release was analyzed using the Cytotoxicity Detection Kit (cat #11644793001 Roche, Indianapolis, USA) according to manufacturer instructions. Optical density (OD) was measured with a spectrophotometer at 490 nm (Spectramax M5e; Molecular Devices, San José, USA).

2.7 Gene expression analysis

2.7.1 Nucleic Acid Purification

Cells were lysed by adding 350 µl Buffer RLT Plus (Qiagen, Hilden, Germany) to the apical compartment of the Transwells. RLT lysates were stored at -20 °C until continuation of RNA purification. RNA was isolated using the MagMAX™-96 Total RNA Isolation Kit (Thermo Fisher Scientific, Waltham, MA, USA) according to the manufacturer's instructions. Briefly, a guanidinium thiocyanate-based solution was used to disrupt the samples. Thereby, cell membranes were solubilized and nucleases were inactivated (Chirgwin et al., 1979; Chomczynski and Sacchi, 1987). Magnetic beads with a nucleic acid binding surface were added to the homogenized samples. Washing removed cell debris, protein, and other contaminants from the magnetically captured nucleic acids. A DNase treatment removed residual DNA from the samples. Purified RNA was eluted in 50 µl nuclease-free water.
RNA concentration was determined using a NanoDrop 8000 sprectrophotometer (Thermo Fisher Scientific, Waltham, MA, USA), by measuring absorption at 260 nm.

2.7.2 Reverse Transcription

Isolated RNA was reverse transcribed into cDNA using the High-Capacity cDNA Reverse Transcription Kit (Applied Biosystems, Darmstadt, Germany) with a thermal cycler (Eppendorf, Hamburg, Germany) according to manufacturer's instructions.

2.7.3 Real-Time PCR (qPCR)

Quantitative gene expression analysis was performed using TaqMan Assay-on-Demand kits with TaqMan Fast Advanced Mastermix and ViiA 7 real-time cycler (all Applied Biosystems, Darmstadt, Germany) according to manufacturer's instructions. The following genes were analyzed: *KRT5* (Hs00361185_m1), *MUC5AC* (Hs01365616_m1), *SCGB1A1* (Hs00171092_m1), *FOXJ1* (HS00230964_m1), *KRT14* (Hs00265033_m1) and *POLR2A* (Hs00172187_m1). Relative expression of RNAs was determined by the comparative Ct method. Expression values were normalized to the control RNA (*POLR2A*).

2.7.4 RT^2 profiler PCR array

To analyze the expression of 84 genes related to oxidative stress the RT^2 Profiler PCR Array (384-Well [4 x 96] Format), Human Oxidative Stress, Cat. no. 330231 PAHS-065ZA (Qiagen, Hilden, Germany) was used according to the manufacturer's instructions.
In order to evaluate the expression of 84 key genes encoding proteins that form impermeable barriers between epithelial cells to regulate polarity, proliferation, and differentiation the RT^2 Profiler PCR Array (384-Well [4 x 96] Format), Human Tight Junctions, Cat. no. 330231 PAHS-143ZA (Qiagen, Hilden, Germany), was used.

Data analysis was performed according to the RT^2 Profiler PCR Array Data Analysis Webportal (https://dataanalysis.sabiosciences.com/pcr/arrayanalysis.php).

Explanation of terminology:
"Fold-change ($2^{-\Delta\Delta CT}$) is the normalized gene expression ($2^{-\Delta CT}$) in the Test Sample divided the normalized gene expression ($2^{-\Delta CT}$) in the Control Sample.
Fold-Regulation represents fold-change results in a biologically meaningful way. Fold-change values greater than one indicate a positive- or an up-regulation, and the fold-regulation is equal to the fold-change. Fold-change values less than one indicate a negative or down-regulation, and the fold-regulation is the negative inverse of the fold-change." (Qiagen, Hilden, Germany)

2.7.5 Next generation sequencing and detection of differentially expressed genes

2.7.5.1 RNA extraction, Illumina library preparation and sequencing

RNA extraction, Illumina library preparation and sequencing was performed as previously described (Sollner et al., 2017). Comparative analysis was done using the limma R-package (Ritchie et al., 2015) by applying the following linear model:

```
anno.sub <- data.frame(group=pre.design$group,donorID=pre.design$donorID)

dmat <- model.matrix(~0+group+donorID,data=anno.sub)
```

Benjamini-Hochberg correction was used to adjust for multiple testing. Expression data has been deposited to Gene Expression Omnibus (https://www.ncbi.nlm.nih.gov/geo/; accession no. GSE135188). The previously published data set GSE11784 (Tilley et al., 2011) was used for comparative analysis. (Gindele et al., 2020)

2.7.5.2 Hierarchical clustering

Hierarchical clustering was performed with TIBCO Spotfire Analyst 7.11.1 LTS HF-013. As clustering method, UPGM with correlation as distance measure was used for both columns and rows, respectively. Expression values were normalized to a per transcript range between 0 and 1 prior to clustering. (Gindele et al., 2020)

2.7.5.3 *Classification*

The Random Forest classifier offered by WEKA Workbench 3.8.3 (Weka, University of Waikato, New Zealand) with parameters -P 100 -I 100 -num-slots 1 -K 10 -M 1.0 -V 0.001 -S 1 was used for classifying samples and generating ROC curves and confusion matrices. Classification was performed on expression values normalized to a per transcript range between 0 and 1. The WEKA CorrelationAttributeEval attribute evaluator (Weka, University of Waikato, New Zealand) with standard parameters and WEKA Ranker as search method with standard parameters was used for ranking features according to their classification power. (Gindele et al., 2020)

2.7.5.4 *Network generation*

Ingenuity Pathway Analysis (IPA; Qiagen) version 48207413 was used to perform all network related analyses. Molecules associated with “Xenobiotic Metabolism Signaling” were compiled, using the “Pathways and Tox Lists” related search tool, and gathered in one pathway view. Subsequently, molecules were overlaid with SAEC ALI (GSE135188) and small airway epithelial brushes (GSE11784) expression data representing significantly deregulated transcripts in one or the other experiment. Molecules, which did not show deregulation in either experiment, were removed. The “Connect” tool was used to introduce

relationships as reported within the IPA knowledge base among the remaining transcripts. Orphans and smaller graphs (less than four nodes) were removed in order to focus on the largest interconnected graph. To focus on specific transcripts and increase readability, a number of hubs were removed from the graph. Finally, either SAEC ALI or small airway epithelial brushes expression values were laid over the resulting network and transcripts representing selected biological processes according to the IPA knowledge base were highlighted. (Gindele et al., 2020)

2.8 Statistics

All data are represented as mean ± SEM of three donors (n=3), unless indicated otherwise. The statistical tests used are indicated in the corresponding figure legend.
Gaussian distribution was assumed for all groups (for assessment of the normality assumption for data of figures 19, 21-23, 40, 42-45 and 47 see Supplementary Information). One- or two-tailed Student's t-tests were used to compare two conditions. Paired tests were used where the data from each donor formed independent pairs. Data analysis was performed using GraphPad Prism 8.0 (Graph Pad Software Inc., San Diego, CA, US). Significance values are marked as * $p < 0.05$, ** $p < 0.01$, *** $p < 0.001$.
Statistical testing used for RNA sequencing analysis is described in section 2.7.5.

Statistical assessment for Figure 19 was conducted as follows:

Each of the investigated parameter was analyzed separately. The data was analyzed with a mixed effect model. In detail it was assumed that

$$x_{i,j} = \mu + \beta_j + z_i + \varepsilon_{i,j},$$

where ...

- $x_{i,j}$ denotes the observed value of the sample from donor i under treatment j.
- β_j denotes the effect of treatment j.
- $\varepsilon_{i,j}$ is the normally distributed residual error with mean 0 and stand. dev. σ_{Residual}.
- z_i denotes the normally distributed random effect of donor i with mean 0 and stand. dev. $\sigma_{\text{Intercept}}$. This quantity accounts for fact that samples from the same donor received all treatments (repeated measurement).

In order to receive a unique solution one β_j must be set to 0. The value of the corresponding treatment coincides with intercept μ.
The degrees of freedom were calculated with the method between/within. The degrees of freedom are divided into a between and within donor part. If an effect varies within subject the within subject degrees of freedom are assigned otherwise the between subject degrees of freedom are assigned.
The factor treatment was tested with an F-test.
Differences between selected treatments and 95% confidence intervals were computed. The hypothesis no difference was tested against the two-side alternative using a model-based t-test.

Results and original data were visualized.
If for a parameter no variation was attributed to the random donor effect, the parameter is still kept in the model, as the model reflects the design of the study. This procedure affects the calculation of the degrees of freedom and leads to smaller degrees of freedom and more conservative p-values.
The F-test assess an overall effect of the treatments on the parameter.
In order to account for multiplicity (2 parameters are investigated), a Bonferroni correction should be applied. The p-values should be compared to the significance level α^{*}=0.05⁄2≈0.025.
The experiments are based on samples from three healthy donors. The results are of an exploratory nature and should be used for the generation of hypotheses that have to be tested in an additional (larger) study.
All treatments were applied to samples of each donor. Each donor serves as its own control.
The forest plots show the point estimate for difference between the compared treatments with 95% confidence intervals. Exclusion of the null from the confidence interval corresponds to a p-value less than 0.05.
The statistical evaluation was prepared using the software package SAS Version 9.4 (SAS Institute Inc., Cary, North Carolina, USA).

Statistical assessment for Figures 21-23 was conducted as follows:

Each of the investigated parameter was analyzed separately. The data was analyzed with a mixed effect model. In detail it was assumed that

$$x_{i,j} = \mu + \beta_j + z_i + \varepsilon_{i,j},$$

where ...

- $x_{i,j}$ denotes the observed value of the sample from donor i under treatment j.
- β_j denotes the effect of treatment j.
- $\varepsilon_{i,j}$ is the normally distributed residual error with mean 0 and stand. dev. σ_{Residual}.
- z_i denotes the normally distributed random effect of donor i with mean 0 and stand. dev. $\sigma_{\text{Intercept}}$. This quantity accounts for fact that samples from the same donor received all treatments (repeated measurement).

In order to receive a unique solution one β_j must be set to 0. The value of the corresponding treatment coincides with intercept μ.
The degrees of freedom were calculated with the method *between/within*. The degrees of freedom are divided into a between and within donor part. If an effect varies within subject the within subject degrees of freedom are assigned otherwise the between subject degrees of freedom are assigned.
The factor treatment was tested with an *F*-test.
Differences between selected treatments and 95% confidence intervals were computed. The hypothesis no difference was tested against the two-side alternative using a model-based t-test. Results and original data were visualized.

For some parameters, no variation was attributed to the random donor effect. However, the parameter is kept in the model, as the model reflects the design of the study. This procedure affects the calculation of the degrees of freedom and leads to smaller degrees of freedom and more conservative p-values.
The F-test assess an overall effect of the treatments on the parameter.
In order to account for multiplicity (8 parameters are investigated; 1 parameter is measured with two kits) a Bonferroni correction should be applied. The p-values should be compared to the significance level $\alpha^* = 0.05/9 \approx 0.00555$.
The experiments are based on samples from three donors. The results are of an exploratory nature and should be used for the generation of hypotheses that have to be tested in an additional (larger) study.
All treatments were applied to samples of each donor. Each donor serves as its own control. pSTAT3 was measured with two different kits, the obtained results (comparison of the different treatments) are comparable.
The forest plots show the point estimate for difference between the compared treatments with 95% confidence intervals. Exclusion of the null from the confidence interval corresponds to a p-value less than 0.05.
The statistical evaluation was prepared using the software package SAS Version 9.4 (SAS Institute Inc., Cary, North Carolina, USA).

Statistical assessment of Figure 40 was conducted as follows:

Each of the investigated parameter was analyzed separately. The data was analyzed with a mixed effect model. In detail it was assumed that

$$x_{i,j,k} = \mu + \beta_j + z_i + \varepsilon_{i,j,k},$$

where ...

- $x_{i,j,k}$ denotes the observed value of the sample from donor i under treatment j in experiment k. (Average of the two determinations generated in one experiment.)
- β_j denotes the effect of treatment j.
- $\varepsilon_{i,j,k}$ is the normally distributed residual error with mean 0 and stand. dev. $\sigma_{\text{Residual, } j}$.
- z_i denotes the normally distributed random effect of donor i with mean 0 and stand. dev. $\sigma_{\text{Intercept}}$. This quantity accounts for the fact that samples from the same donor received all treatments and were measured in several experiments (repeated measurement).

In order to receive a unique solution one β_j must be set to 0. The value of the corresponding treatment coincides with the intercept μ.
The degrees of freedom (DF) were calculated with the containment method:
"DF"="#Observations"-"#Treatments"-"#Donors"+1.
The factor treatment was tested with an *F*-test.
Differences between selected treatments and 95% confidence intervals were computed. The hypothesis no difference was tested against the two-side alternative using a model-based t-test.

Results and original data were visualized.
If for a parameter no variation was attributed to the random donor effect, the parameter is still kept in the model, as the model reflects the design of the study. This procedure affects the calculation of the degrees of freedom and leads to smaller degrees of freedom and more conservative p-values.
The experiments are based on samples from three healthy donors. The results are of an exploratory nature and should be used for the generation of hypotheses that have to be tested in an additional (larger) study.
All treatments were applied to samples of each donor. Each donor serves as its own control.
The forest plots show the point estimate for difference between the compared treatments with 95% confidence intervals. Exclusion of the null from the confidence interval corresponds to a p-value less than 0.05.
The statistical evaluation was prepared using the software package SAS Version 9.4 (SAS Institute Inc., Cary, North Carolina, USA).

Statistical assessment of Figure 42-45 and 47 was conducted as follows:

Each of the investigated parameter was analyzed separately. The data was analyzed with a mixed effect model. In detail it was assumed that

$$x_{i,j} = \mu + \beta_j + z_i + \varepsilon_{i,j},$$

where ...

- $x_{i,j}$ denotes the observed value of the sample from donor i under treatment j.
- β_j denotes the effect of treatment j.
- $\varepsilon_{i,j}$ is the normally distributed residual error with mean 0 and stand. deviation
    - $\sigma_{\text{Residual, CS}}$, (treatment j involved CS) or $\sigma_{\text{Residual, Air}}$ (treatment j involved Air). (Figure 42-45)
    - σ_{Residual} (Figure 47)
- z_i denotes the normally distributed random effect of donor i with mean 0 and stand. dev. $\sigma_{\text{Intercept}}$. This quantity accounts for the fact that samples from the same donor received all treatments (repeated measurement).

In order to receive a unique solution one β_j must be set to 0. The value of the corresponding treatment coincides with the intercept μ.
The degrees of freedom (DF) were calculated with the containment method:
"DF"="#Observations"-"#Treatments"-"#Donors"+1.
The factor treatment was tested with an F-test.
Differences between selected treatments and 95% confidence intervals were computed. The hypothesis no difference was tested against the two-side alternative using a model-based t-test.
Results and original data were visualized.
If for a parameter no variation was attributed to the random donor effect, the parameter is still kept in the model, as the model reflects the design of the study. This procedure affects

the calculation of the degrees of freedom and leads to smaller degrees of freedom and more conservative p-values.
The experiments are based on samples from three healthy donors. The results are of an exploratory nature and should be used for the generation of hypotheses that have to be tested in an additional (larger) study.
All treatments were applied to samples of each donor. Each donor serves as its own control.
The forest plots show the point estimate for difference between the compared treatments with 95% confidence intervals. Exclusion of the null from the confidence interval corresponds to a p-value less than 0.05.
The statistical evaluation was prepared using the software package SAS Version 9.4 (SAS Institute Inc., Cary, North Carolina, USA).

Longitudinal data from the long-term CS exposure experiment (section 3.4.2) was analyzed as previously published:

Gindele, J.A., Kiechle, T., Benediktus, K. et al. Intermittent exposure to whole cigarette smoke alters the differentiation of primary small airway epithelial cells in the air-liquid interface culture. Sci Rep 10, 6257 (2020). https://doi.org/10.1038/s41598-020-63345-5

An excerpt of the mentioned publication can be found below.

Instead of modelling the longitudinal data, the analyses were performed with adjusted areas under the curve (AUC) or the logarithmized (log) adjusted AUC. The adjusted AUC was obtained by dividing the AUC by the length of the considered time interval. Each of the endpoints was analyzed separately. The data was analyzed with a repeated measurement model, as both treatments (CS/Air) were applied to cells of each donor. Compound symmetry was assumed as underlying covariance structure in order to account for the repeated measurement within a donor. The fixed factors status of the cells (HC/COPD), treatment (CS/Air) and the interaction of status of the cells and treatment were included in the model. The degrees of freedom were calculated by dividing the residual degrees of freedom into between-subject and within-subject portions. If a fixed effect changed within any subject, the within-subject degrees of freedom were assigned to the considered fixed effect (cell status, treatment, interaction effect). Otherwise, the between-subject degrees of freedom were used. The applied repeated measurement model assumes that the errors follow a normal distribution.

Using linear combinations of the parameter estimates obtained from the repeated measurement model, it was tested whether treatment with CS compared to Air had an impact on the considered endpoint. This analysis was performed separately for each status of cells (HC/COPD). Depending on the expected change of the endpoint under the treatment with smoke, the following hypotheses were tested:

$\mathcal{H}_{0,\text{HC, Lower}}: \mu_{\text{HC, CS}} - \mu_{\text{HC, Air}} \geq 0$ vs. $\mathcal{H}_{1,\text{Lower}}: \mu_{\text{HC, CS}} - \mu_{\text{HC, Air}} < 0$ and
$\mathcal{H}_{0,\text{COPD, Lower}}: \mu_{\text{COPD, CS}} - \mu_{\text{COPD, Air}} \geq 0$ vs. $\mathcal{H}_{1,\text{Lower}}: \mu_{\text{COPD, CS}} - \mu_{\text{COPDC, Air}} < 0$, where $\mu_{i,j}$ denotes the mean value of the investigated endpoint under treatment j for the status of cells i.

For the following endpoints the above stated hypotheses were tested as a decrease was assumed when cells were treated with smoke: Logarithmized AUC of Area covered by active cilia, AUC of Cilia beat frequency, logarithmized AUC of TEER, AUC of KRT5 mRNA (Ct), AUC of KRT14 mRNA (Ct), AUC of MUC5AC mRNA (Ct).

$\mathcal{H}_{0,\text{ HC, Upper}}: \mu_{\text{HC, CS}} - \mu_{\text{HC, Air}} \leq 0$ vs. $\mathcal{H}_{1,\text{ HC, Upper}}: \mu_{\text{HC, CS}} - \mu_{\text{HC, Air}} > 0$ and
$\mathcal{H}_{0,\text{ COPD, Upper}}: \mu_{\text{COPD, CS}} - \mu_{\text{COPD, Air}} \leq 0$ vs. $\mathcal{H}_{1,\text{ COPD, Upper}}: \mu_{\text{COPD, CS}} - \mu_{\text{COPD, Air}} > 0$.

For the following endpoints, the above stated hypotheses were tested as an increase was assumed when cells were treated with smoke: Claudin-10 protein expression, AUC of SCGB1A1 mRNA (Ct), AUC of FOXJ1 mRNA (Ct).
All tests are t-test like tests based on the linear combinations of the parameter estimates from the repeated measurement model and were performed post-hoc. The p-values were not adjusted for multiplicity induced by the number of tested endpoints and hypotheses and the selection of the finally applied statistical model.
The statistical evaluation was prepared using the software package SAS Version 9.4 (SAS Institute Inc., Cary, North Carolina, USA).

3 Results

3.1 Establishment of a small airway epithelial cell model

Small airway disease plays a major role in the pathogenesis of COPD. Previous *in vitro* studies have mostly focused on the upper airways, and the translation from murine *in vivo* models to the human disease is challenged by substantial inter-species differences. In this study, a novel *in vitro* model system was established to investigate the remodeling of the small airway epithelium that is associated with COPD. In order to characterize the new SAEC ALI model, the cultures were examined according to the following aspects:

- Cellular anatomy, assessed by immunohistochemistry and electron microscopy
- Formation of an epithelial barrier, evaluated by resistance measurements (TEER)
- Ciliary function, analyzed by video-microscopy
- Transcriptomic profile, examined by RNA sequencing

The morphology of SAEC cultures was investigated by H&E staining, which showed a pseudostratified epithelium (Fig. 12a). To assess the cellular composition, the cultures were stained for the major small airway cell types: $KRT5^+$ basal cells, $SCGB1A1^+$ club cells and Ac. $Tub.^+$ ciliated cells. All of which were detected in SAEC ALI tissue slices (Fig. 12a). An intermediate cell population of $SCGB1A1^+/MUC5AC^+$ double positive secretory cells and a few $SCGB1A1^-/MUC5AC^+$ goblet cells were detected in the healthy ALI cultures, although $MUC5AC^+$ goblet cells are normally absent in the human small airways (Burgel et al., 2011).
To examine the epithelial barrier formation, TEER measurements were performed. Fully differentiated healthy ALI cultures obtained values between 400–600 $\Omega*cm^2$, indicating a functional epithelial barrier (Fig 12b).
To evaluate the cellular architecture of the ALI cultures, an electron microscopic analysis was conducted. Transmission electron microscopy confirmed the pseudostratified structure of the ALI culture and revealed the 9 + 2 arrangement of microtubules typical for motile cilia (Fig. 13).

This thesis deals with the remodeling of the small airway epithelium in COPD, therefore cells originated from COPD patients also served as starting material for ALI cultures to investigate whether COPD-like features are conserved.
Histological analyses of COPD-derived cultures revealed a less ciliated epithelium with more secretory cell types (Fig. 12a). These findings were further validated by means of electron microscopy (Fig. 14). COPD-derived ALI cultures exhibited a less pseudostratified columnar epithelium, and were flatter compared to healthy cultures (Fig. 14a). In addition, an increase in the number of secretory cells filled with electron-lucent mucus granules and an accumulation of cuboidal basal cells was observed. Analysis of the epithelial surface by scanning electron microscopy revealed a less ciliated epithelium (Fig. 14b). Instead, patches of cilia formed sporadically on the surface.

Barrier integrity, analyzed by means of TEER measurements, was not significantly different from healthy cultures (Fig. 12b).

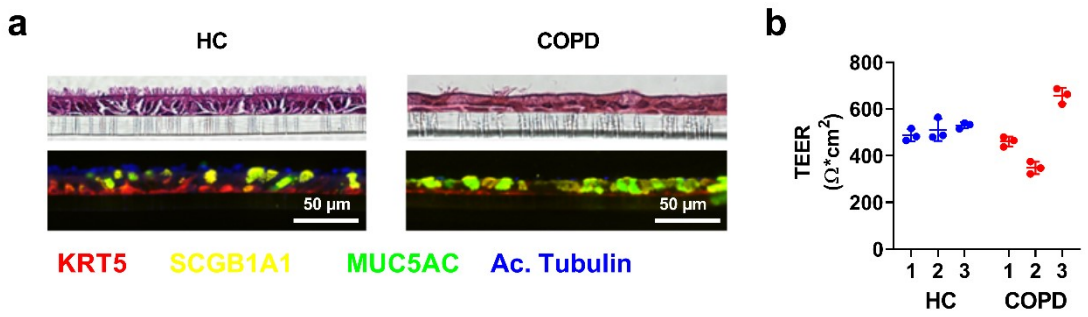

Figure 12: Morphology and barrier integrity of small airway epithelial cell (SAEC) cultures derived from chronic obstructive pulmonary disease (COPD) patients and healthy controls (HC). (a) Morphological assessment of formalin-fixed paraffin-embedded tissue slices from fully differentiated air-liquid interface (ALI) cultures. Representative hematoxylin and eosin (H&E) stainings and immunohistochemical stainings for cytokeratin 5 (KRT5), uteroglobin (SCGB1A1), Mucin 5 AC (MUC5AC) and acetylated tubulin (Ac. Tubulin). (b) Transepithelial electrical resistance (TEER) measurements of healthy and COPD-derived cultures (n=3) on day 28 after air-lift. Data is represented as mean ± SEM. (Gindele et al., 2020)

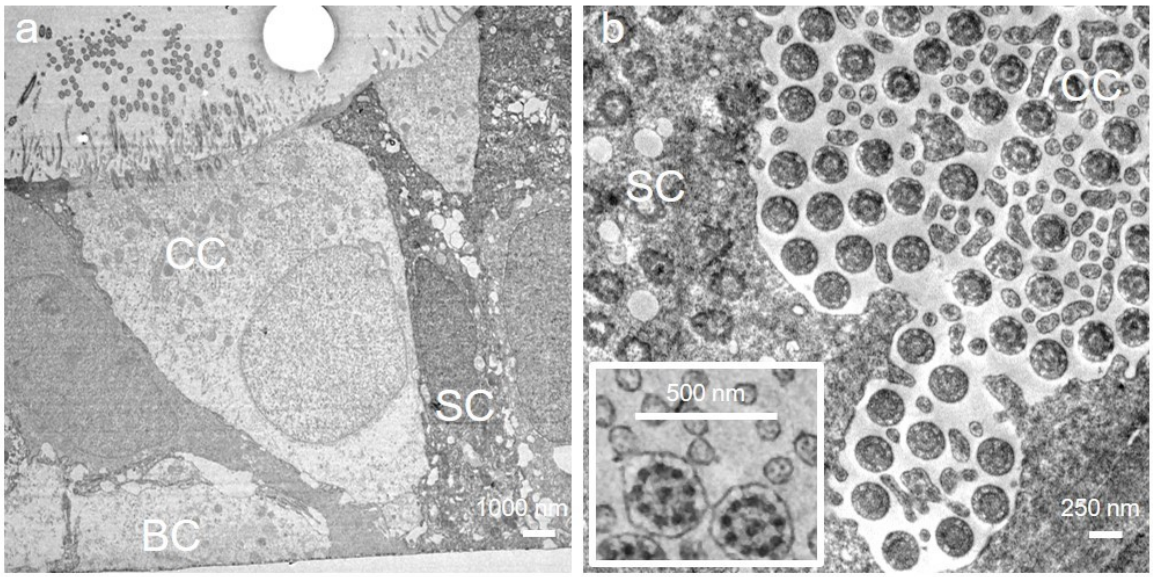

Figure 13: Representative transmission electron microscopic (TEM) images from fully differentiated healthy small airway epithelial cell (SAEC) cultures. (a) Cross section of pseudostratified epithelium with basal (BC), secretory club (SC) and ciliated cells (CS). (b) Longitudinal section of the epithelial surface showing cilia. Magnified box in the lower left shows the 9 + 2 arrangement of microtubules typical for motile cilia.

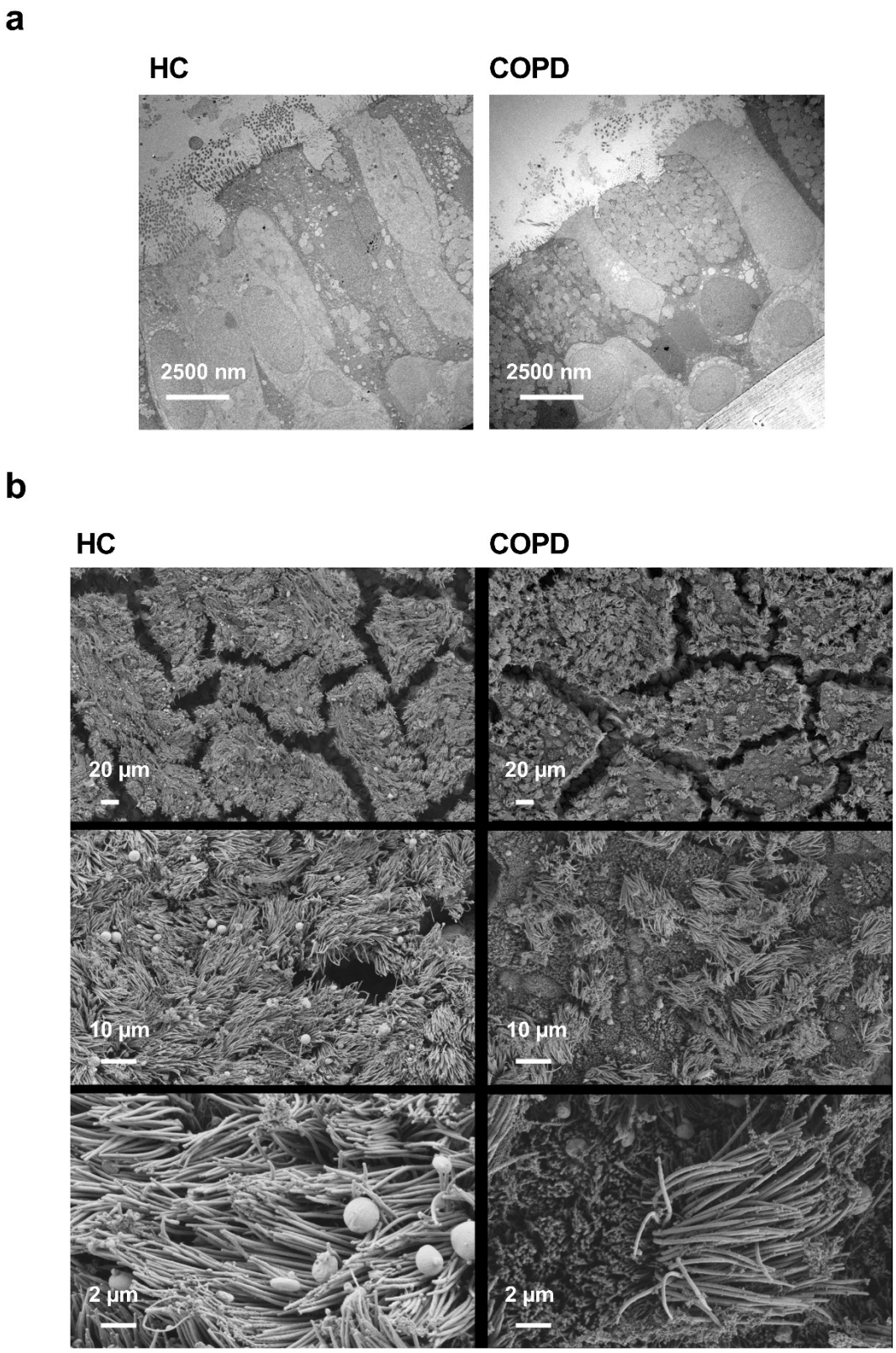

Figure 14: Electron microscopic images of small airway epithelial cell (SAEC) air-liquid interface (ALI) cultures derived from healthy controls (HC) or chronic obstructive pulmonary disease (COPD) donors. (a) Representative transmission electron microscopic (TEM) images of healthy and COPD-derived fully differentiated SAEC ALI cultures. (b) Representative scanning electron microscopic (SEM) images of healthy and COPD-derived fully differentiated SAEC ALI cultures.

To investigate whether the observed reduced number of ciliated cells is associated with a reduced area of beating cilia, the cilia function was examined by video microscopy. The analysis revealed a clear trend towards a reduced area covered by actively beating cilia in COPD cultures. However, due to the high donor variability, the observed difference is not significant. Cilia beat frequency seemed not to be changed (Fig. 15). In this context, it may be noted that the cilia beat analysis is a composite readout and is influenced by other factors such as the epithelial thickness and the viscosity of the mucus.

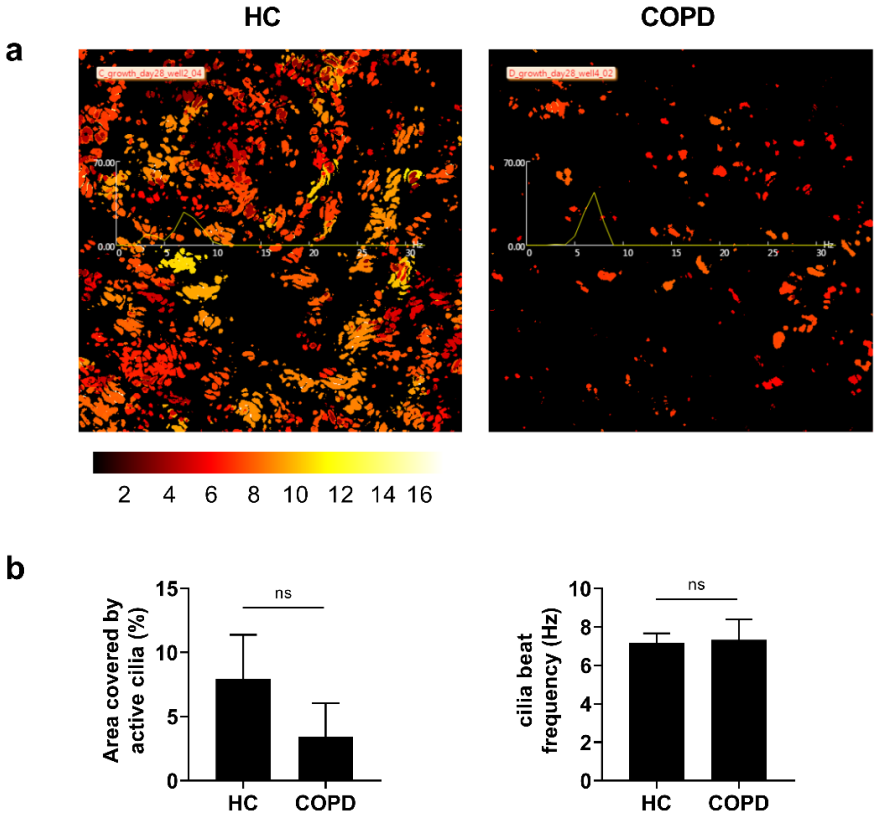

Figure 15: Cilia beat measurement of fully differentiated small airway epithelial cell (SAEC) ALI cultures from healthy controls (HC) and chronic obstructive pulmonary disease (COPD) donors. (a) Representative false-color look-up table. Each pixel represents the beat frequency (Hz) of the cilia covering that area. (b) Calculated area covered by active cilia and cilia beat frequency. Data is represented as mean ± SEM. Significance was assessed using one-tailed unpaired t-test. p value < 0.05; ** for p value < 0.01; *** for p value < 0.001.

To further characterize the differences between ALI cultures obtained from healthy non-smokers and COPD smokers, a comprehensive gene expression analysis was performed by means of Next Generation Sequencing (NGS). Therefore, cells from three healthy and three COPD donors were used to generate fully differentiated ALI cultures after four weeks of differentiation. Differential gene expression analysis revealed 248 transcripts that were significantly changed between healthy and COPD-derived ALI cultures. Hierarchical clustering highlighted the different mRNA signatures (Fig. 16a). To find out whether these differentially expressed genes actually reflect the transcriptional deregulation seen in COPD

patients *in vivo*, the COPD ALI signature was used as a classifier to distinguish between human small airway samples collected from healthy non-smokers and COPD smokers. Therefore, the signature was used as a feature vector in a random forest classification analysis. The signature's power to separate the respective samples was assessed by determining the ROC (receiver operating characteristic) curves (Fig. 16b).

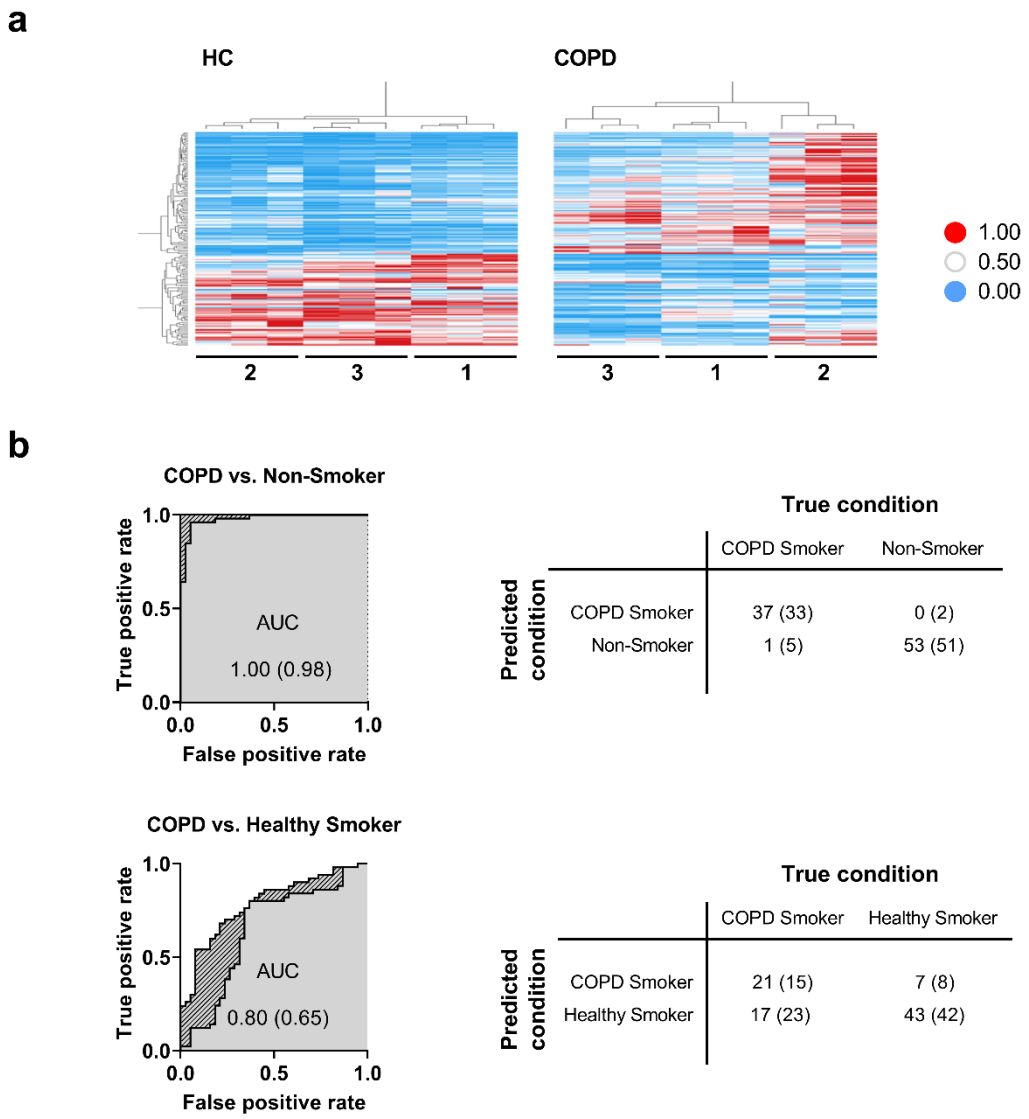

Figure 16: Gene expression profiles of small airway epithelial cell (SAEC) air-liquid interface (ALI) cultures derived from chronic obstructive pulmonary disease (COPD) patients and healthy controls (HC). (a) Heatmap representation of unbiased cluster analysis of 170 transcripts exhibiting a q value < 0.05 in comparing HC versus COPD. Absolute expression values were normalized to a range from 0 to 1. Numbers represent samples from same subjects (donor 1 – 3 for HC and COPD, respectively). (b) ROC curves (receiver operating characteristic curve) and confusion matrices to characterize the classification power of the *in vitro* ALI COPD signature (predicted condition) towards a published data set from epithelial brushes of patients with COPD and healthy controls (true condition). A random forest classifier with 50-fold cross validation was used to classify COPD (n=38) vs. Non-Smoker (n=53) and COPD (n=38) vs. Healthy Smoker (n=50). SAECs from an independent cohort utilizing the ALI COPD signature as feature vector. Dashed regions indicate AUCs observed for the full signature, grey regions AUCs upon removal of the ten highest correlating transcripts. Numbers in parentheses represent values obtained for the reduced signature. (Gindele et al., 2020)

Classification of samples from healthy non-smokers and COPD smokers yielded an AUC of 1.0, indicating an almost perfect separation of the samples based on the COPD ALI signature. In order to rule out that the high classification power was only attributed to very few well-separating transcripts but rather to a large proportion of the signature, the best correlating transcripts were identified. Subsequently, ten transcripts with the highest correlation were removed from the signature and the classification was repeated, yielding an AUC of 0.98. This indicates a strong relationship between the transcriptional changes within the ALI culture *in vitro* and small airway samples *in vivo*, independently of the top ten classifying transcripts. Hence, the COPD ALI culture reflects transcriptional differences that are relevant *in vivo* and allows a good prediction of the health status (healthy vs. COPD).
In order to determine whether the signature obtained from COPD-derived ALI cultures reflects a COPD-specific deregulation and to a lesser extent a smoke-induced deregulation, a classification analysis was carried out using the COPD ALI signature to distinguish healthy smokers from COPD smokers. This classification yielded an AUC of 0.8. After removal of the ten highest correlating transcripts, this value drops to 0.65. Even if the classification power is lower in this case, it still indicates a considerable overlap of COPD-related transcriptional changes in the ALI culture with the changes observed in the human small airway epithelial samples.

3.2 Cigarette smoke extract-induced effects on epithelial remodeling

To assess the role of CS induced remodeling of the airway epithelium in COPD, SAEC were treated with cigarette smoke extract (CSE) during the differentiation process (28 days beginning on the day of air-lift).

To identify the appropriate concentration of CSE, a titration experiment was performed. Cultures exposed to 2.5 % and 5.0 % CSE detached from the membrane and lysed, which was observed microscopically (Fig. 17a). SAEC ALI cultures treated with 0.5 % CSE upon differentiation exhibited a pseudostratified epithelium with a morphology comparable to control cultures; all main cell types were found to be expressed (Fig 17a-c). This concentration was used for further experiments, since cells differentiated normally.
TEER measurements were carried out to assess barrier integrity of cultures exposed to 0.5 % CSE during differentiation. Analysis revealed a significant reduction in TEER upon CSE treatment from (696 ± 110) Ω *cm^2 to (476 ± 51) Ω*cm^2 (Fig. 17d).
Exposure to 0.5 % CSE did not have an effect on ciliary beating (area covered by active cilia and cilia beat frequency; data not shown), indicating that the basolateral CSE treatment did not impair the differentiation of ciliated cells.

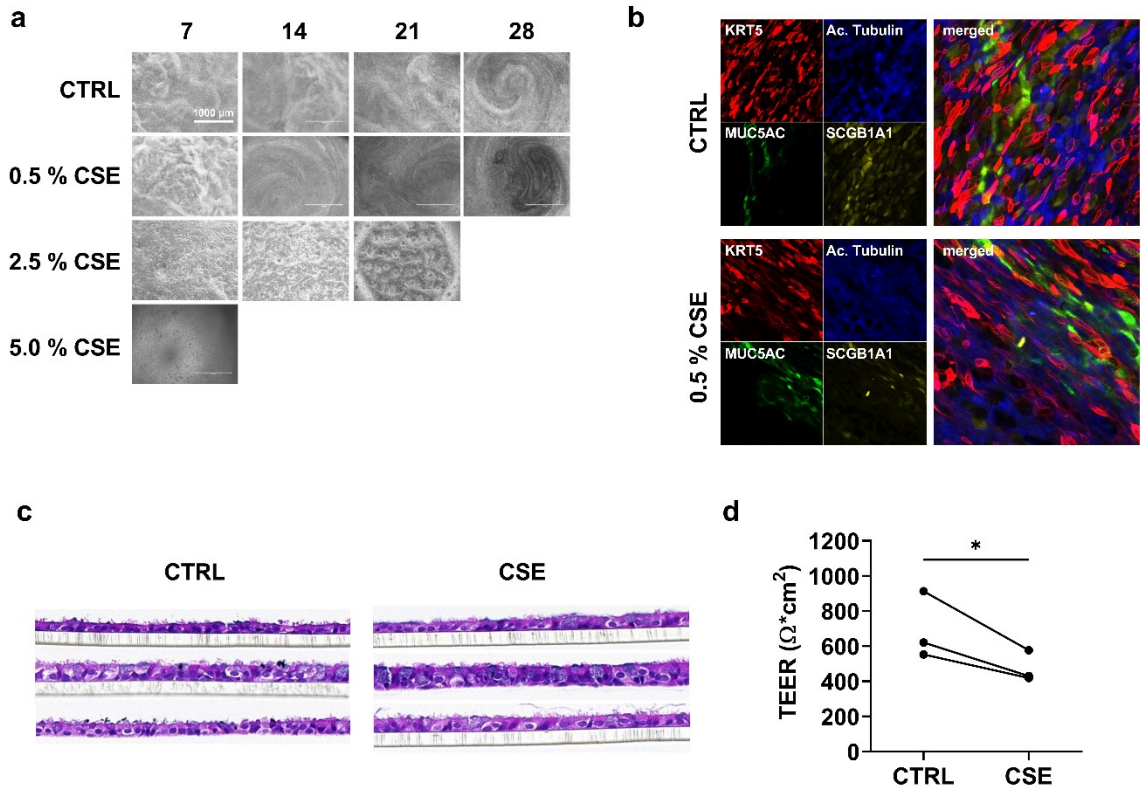

Figure 17: Effect of cigarette smoke extract (CSE) on small airway epithelial cell (SAEC) air-liquid interface (ALI) cultures. (a) Representative microscopic images of ALI cultures exposed to different concentrations of CSE during differentiation (day 7, 14, 21, 28). Cultures treated with 2.5 % and 5.0 % CSE died during differentiation (indicated by missing images). (b) Image stacks of immunofluorescent stainings of inserts exposed to either 0.5 % CSE or phosphate buffered saline (PBS) as control. KRT5 = Cytokeratin 5, MUC5AC = Mucin 5 AC, SCGB1A1 = Uteroglobin, Ac. Tubulin = Acetylated tubulin. (c) Representative images of hematoxylin & eosin (H&E) stainings of SAEC ALI cultures (n=3) exposed to either 0.5 % CSE or PBS as control. (d) Transepithelial electrical resistance (TEER) measurement of SAEC ALI cultures exposed to 0.5 % CSE or PBS as control (CTRL) for 28 days post air-lift. n=3 healthy donors. Significance was assessed using one-tailed paired t-test. p value < 0.05; ** for p value < 0.01; *** for p value < 0.001.

3.3 Role of EGF signaling in epithelial remodeling in COPD

Aberrant EGF receptor signaling is associated with COPD characteristics such as goblet cell hyperplasia and squamous metaplasia (Anagnostis et al., 2013; Shaykhiev et al., 2013). To model these COPD-relevant phenotypic alterations, SAEC ALI cultures were exposed to different concentrations of EGF during the differentiation process (28 days beginning on the day of air-lift). Of note, EGF is an important component of the SAEC medium and enables normal differentiation. The addition of extra EGF is intended to mimic the increased EGF concentration in COPD airways (Shaykhiev et al., 2013).
The aim was to investigate which aspects of epithelial remodeling in COPD are inducible by EGF in the SAEC model and whether they can be blocked.

In order to evaluate the morphology of the EGF-treated ALI cultures, cells were assessed microscopically. Evaluation revealed a concentration-dependent darkening of the cultures,

indicating increasing thickness (Fig. 18a). This finding was validated by histological analysis of formalin-fixed paraffin-embedded tissue slices of the SAEC ALI cultures on day 28 (Fig. 18b). The Alcianblue Periodic Acid Schiff (PAS) staining also showed a concentration-dependent increase in secretory cells, which were characterized by a dark blue staining and large vacuole-like structures, and a concentration-dependent increase in basal cells (Fig. 18b). Cultures exposed to 1 ng/ml EGF showed moderate effects, so that this concentration was used in further experiments.

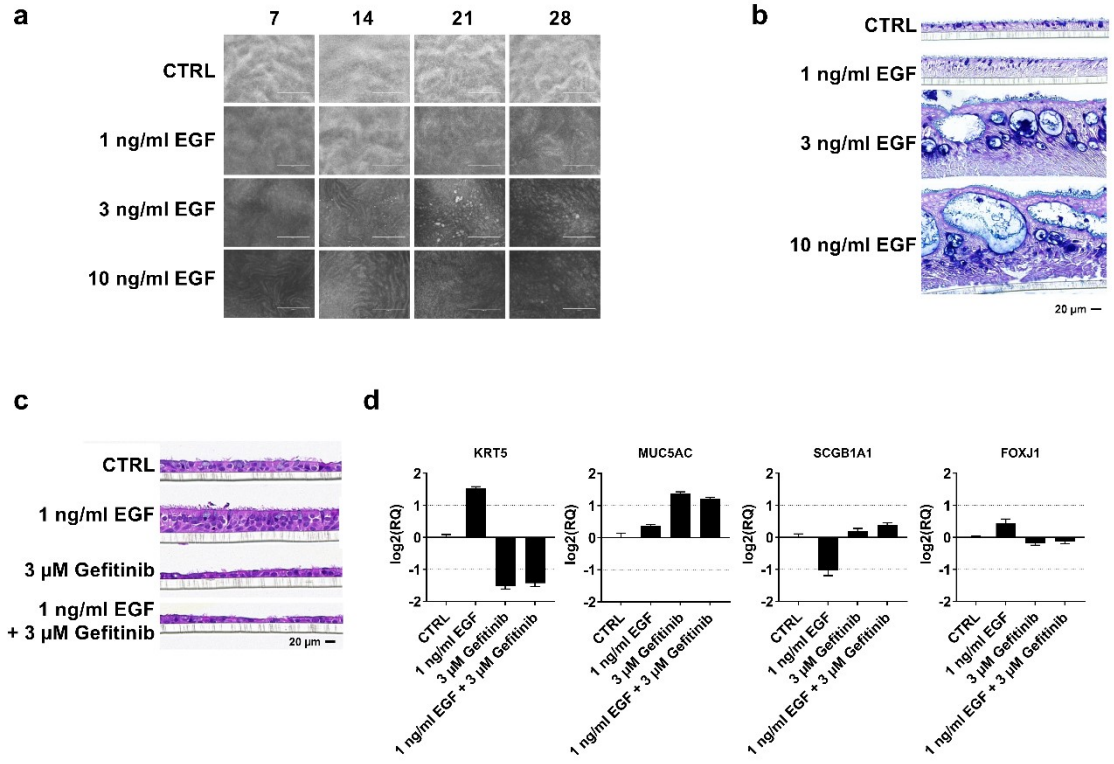

Figure 18: Effect of epidermal growth factor (EGF) on small airway epithelial cell (SAEC) air-liquid interface (ALI) cultures. (a) Microscopic images of SAEC ALI cultures treated with different concentrations of EGF during differentiation. Representative images of day 7, 14, 21 and 28 of one healthy donor (n=1) are depicted. (b) Histological assessment of SAEC ALI cultures treated with different concentrations of EGF during differentiation. Alcianblue-Periodic Acid Schiff (PAS) stainings of formalin-fixed paraffin-embedded tissue slices of day 28 (n=1). (c) Histological assessment of SAEC ALI cultures treated with either EGF, the EGF receptor inhibitor gefitinib, or a combination of both during the differentiation process. Hematoxylin & eosin (H&E) stainings of formalin-fixed paraffin-embedded tissue slices of day 28 (n=1). (d) Gene expression analysis of cell marker genes on day 28 upon treatment with either EGF, the EGFR inhibitor gefitinib, or a combination of both during the differentiation process. *KRT5* = cytokeratin 5, *MUC5AC* = Mucin 5 AC, *SCGB1A1* = uteroglobin, *FOXJ1* = forkhead box protein J1.

In order to block the EGF-induced effects, the tyrosine kinase inhibitor gefitinib was added to the basolateral medium during differentiation. Both epithelial thickening and transcriptional deregulation were investigated to assess whether gefitinib is able to block EGF-induced effects on SAEC ALI cultures. Histological evaluation exhibited a reduction in epithelial thickness upon gefitinib treatment (Fig 18c). Gene expression analysis by qPCR

demonstrated the increase in *KRT5*$^{+}$ basal cells upon EGF treatment, which was reversed by the inhibitor (Fig. 18d). Unexpectedly, gefitinib did not rescue the cells from the increase in *MUC5AC* expression at transcriptional level. However, EGFR inhibition contributed positively to the regulation of *SCGB1A1*$^{+}$ club cells. The expression of the ciliated cell marker *FOXJ1* seemed to be hardly affected by either EGF or the inhibitor.

To investigate a possible interplay between the elevated EGF concentrations found in the airway epithelium of smokers (Shaykhiev et al., 2013) and the exposure to CS that might induce COPD-relevant characteristics, SAEC were treated with a combination of both, CSE and EGF during differentiation.

Interestingly, ALI cultures exposed to both 0.5 % CSE and 1 ng/ml EGF showed a significant increase in epithelial thickness compared to CSE or EGF alone (Fig. 19a and b; p value for synergy = 0.05697). To address the question whether EGFR signaling mediates these remodeling processes, cultures were treated with the EGFR inhibitor gefitinib. Inhibition of EGFR signaling prevented thickening of the epithelium (Fig. 19a and b). The hyperplasia of basal and secretory cells through the combination of EGF and CSE was corroborated by transmission electron microscopic analysis (Fig 19c-3) and was prevented by gefitinib (Fig 19c-4). Analysis of the epithelial surface by means of scanning electron microscopy revealed an increase of mucus covering the cilia when treated with EGF and CSE (Fig. 19d-3). Gefitinib prevented this mucus overproduction (Fig. 19d-4). EGFR inhibition in control cultures adversely affected basal cell differentiation, resulting in a rather thinner and less differentiated epithelium (Fig. 19b-d).

Taken together, these findings corroborate the hypothesis that CSE enhances EGFR signaling and that this effect may be blocked by EGFR inhibition. To investigate the underlying molecular mechanisms, phosphorylation of EGFR (pEGFR) was analyzed in a short-term experiment. Five minutes after stimulation of fully differentiated SAEC ALI cultures with either 1 ng/ml EGF, 0.5 % CSE, 3 µM gefitinib, or any combination of the three, pEGFR was measured. Although not significant, EGF treatment showed a trend towards induced receptor phosphorylation (Fig. 19e). However, the combination of CSE and EGF did not increase pEGFR induction. Gefitinib significantly reduced EGFR phosphorylation in all cases, indicating pathway inhibition.

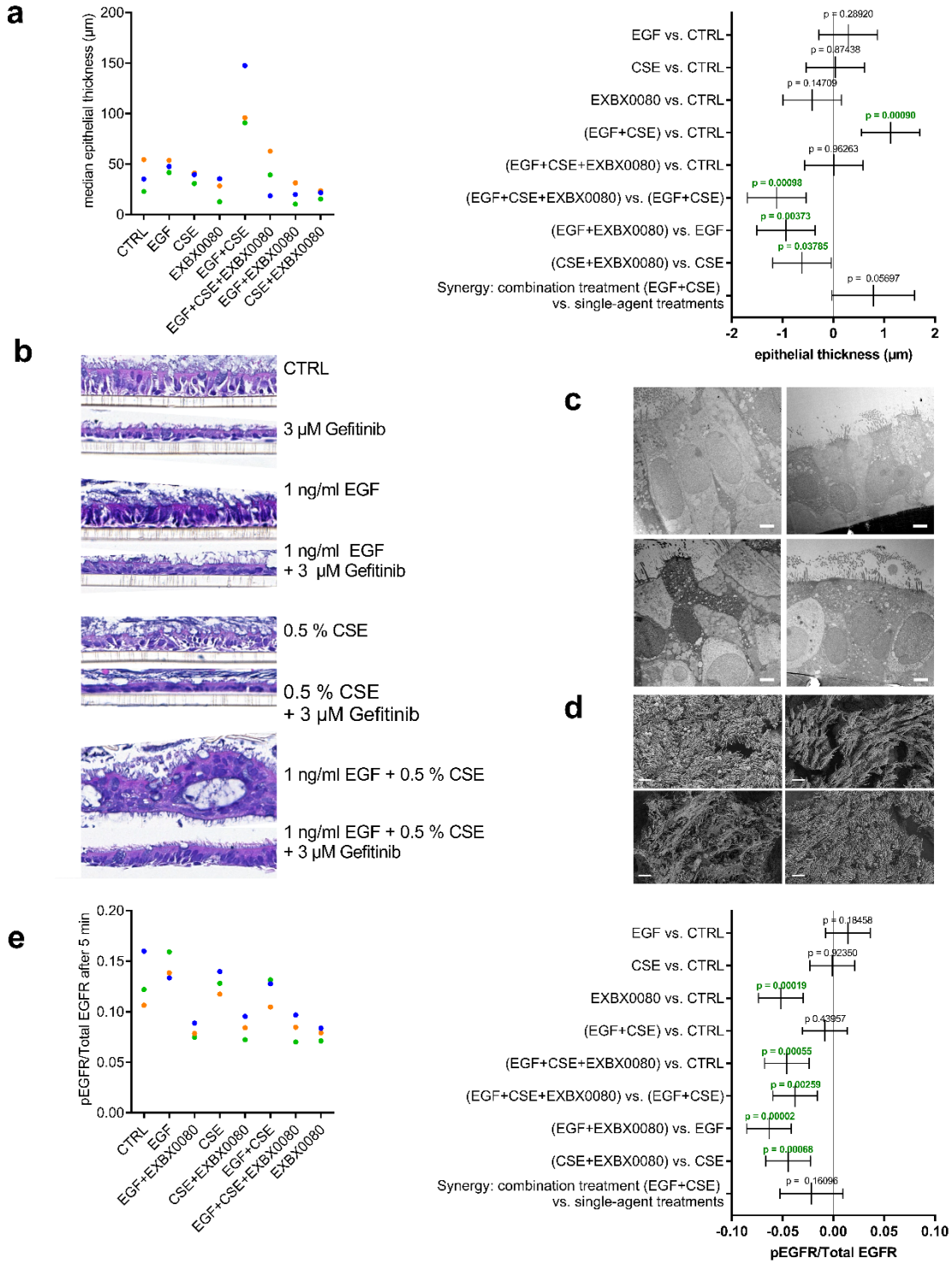

Figure 19: Effect of epidermal growth factor (EGF) and cigarette smoke extract (CSE) on small airway epithelial cell (SAEC) air-liquid interface (ALI) cultures. (a) Histological assessment of ALI cultures exposed to either EGF, CSE, gefitinib (EXBX0080) or any combination of the three during differentiation. Quantitative analysis of epithelial thickness (n=3). The data was analyzed with a mixed effect model. The forest plots show the point estimate for difference between the compared treatments with 95% confidence intervals. Exclusion of the null from the confidence interval corresponds to a p-value < 0.05 (highlighted in green). (b) Representative hematoxylin & eosin (H&E) stainings of one healthy donor on day 28 are depicted. (c) Representative transmission electron microscopic images of cultures exposed to (1) dimethyl sulfoxide (DMSO) control, (2) gefitinib (EXBX0080), (3) EGF + CSE, (4) EGF + CSE + gefitinib during differentiation.

d) Representative scanning electron microscopic images of cultures exposed to (1) DMSO control, (2) gefitinib (EXBX0080), (3) EGF + CSE, (4) EGF + CSE + gefitinib during differentiation. (e) Evaluation of EGFR phosphorylation of fully differentiated ALI cultures five minutes after stimulation with either EGF, CSE, gefitinib (EXBX0080) or any combination of the three. Data is represented as the relative amount of pEGFR compared to total EGFR, n=3. The data was analyzed with a mixed effect model. The forest plots show the point estimate for difference between the compared treatments with 95% confidence intervals. Exclusion of the null from the confidence interval corresponds to a p-value < 0.05.

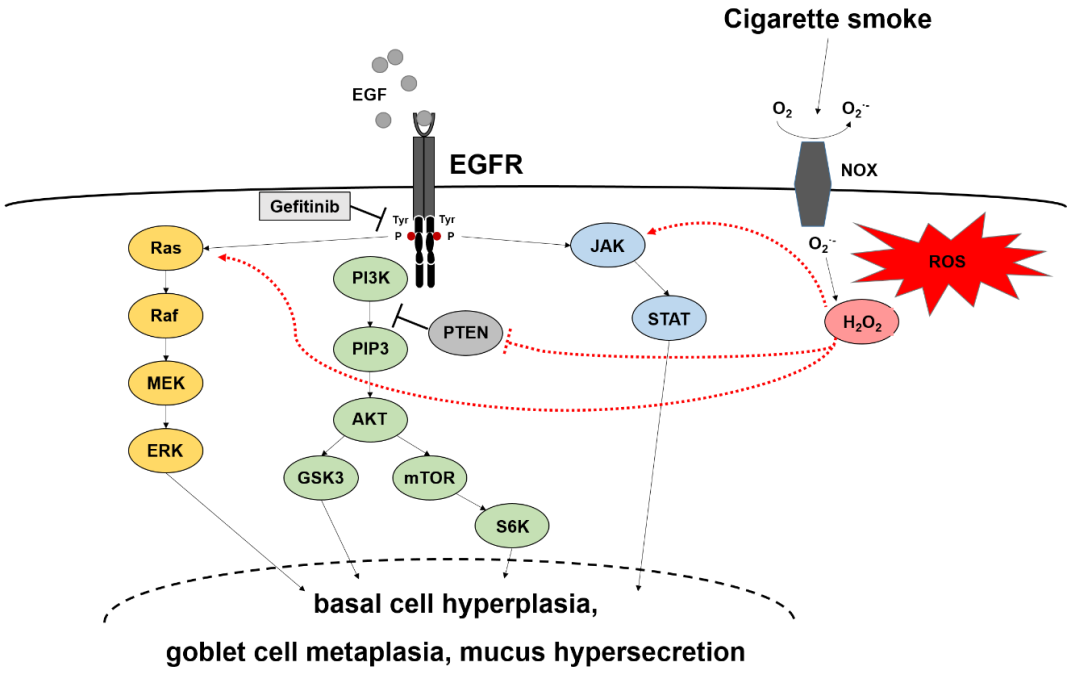

Figure 20: Schematic of the possible interaction between epidermal growth factor receptor (EGFR) signaling and cigarette smoke (CS) induced reactive oxygen species (ROS). Epidermal growth factor (EGF) binds to EGFR and induces receptor dimerization and autophosphorylation (P) of tyrosine (Tyr) residues. This activates multiple pathways, such as the MEK/ERK (MAPK kinase/extracellular signal-regulated kinase), PI3K (phosphatidylinositol-3-kinase) and JAK/STAT (Janus kinase/signal transducer and activator of transcription) signaling pathway. CS-induced oxidative stress induces ROS production via NADPH oxidase (NOX). Hydrogen peroxide (H_2O_2) induces oxidation of phosphatase and tensin homolog (PTEN) and therefore promote AKT signaling. Furthermore, H_2O_2 activates Ras/MEK signaling through complex formation of SHC-Grb2-SOS with the EGFR. JAK-STAT pathway is activated by intracellular H_2O_2. Aberrant EGFR signaling results in basal cell hyperplasia, goblet cell metaplasia and mucus hypersecretion. Grb-2, growth factor receptor-bound protein 2; SOS, guanine nucleotide exchange protein; PIP3: phosphatidylinositol (3,4,5)-triphosphate; AKT: protein kinase B; GSK3: glycogen synthase kinase 3; mTOR: mammalian target of rapamycin, S6K: Ribosomal protein S6 kinase beta-1 (also known as p70S6K).

To investigate how CSE interacts with the EGFR signaling pathways (Fig. 20), the phosphorylation of downstream mediators was analyzed. Downstream phosphoprotein targets include pMEK1/2, pERK1/2, pSTAT3, pSTAT4, pSTAT5, pAKT, p-p70S6K and pGSK-3β. The combination of EGF and CSE led to a significant increase in p-p70S6K and pGSK-3β compared to EGF or CSE alone (Fig. 21, p value for synergy (p-p70SGK) = 0.00259; p value for synergy (pGSK-3β) = 0.00127). EGFR inhibition by gefitinib prevented this effect. The ERK/STAT3 cascade and other STATs were not altered significantly (Fig. 22 and Fig. 23). This may indicate that CSE enhances the EGFR signal transduction via the GSK3β and p70S6K pathways.

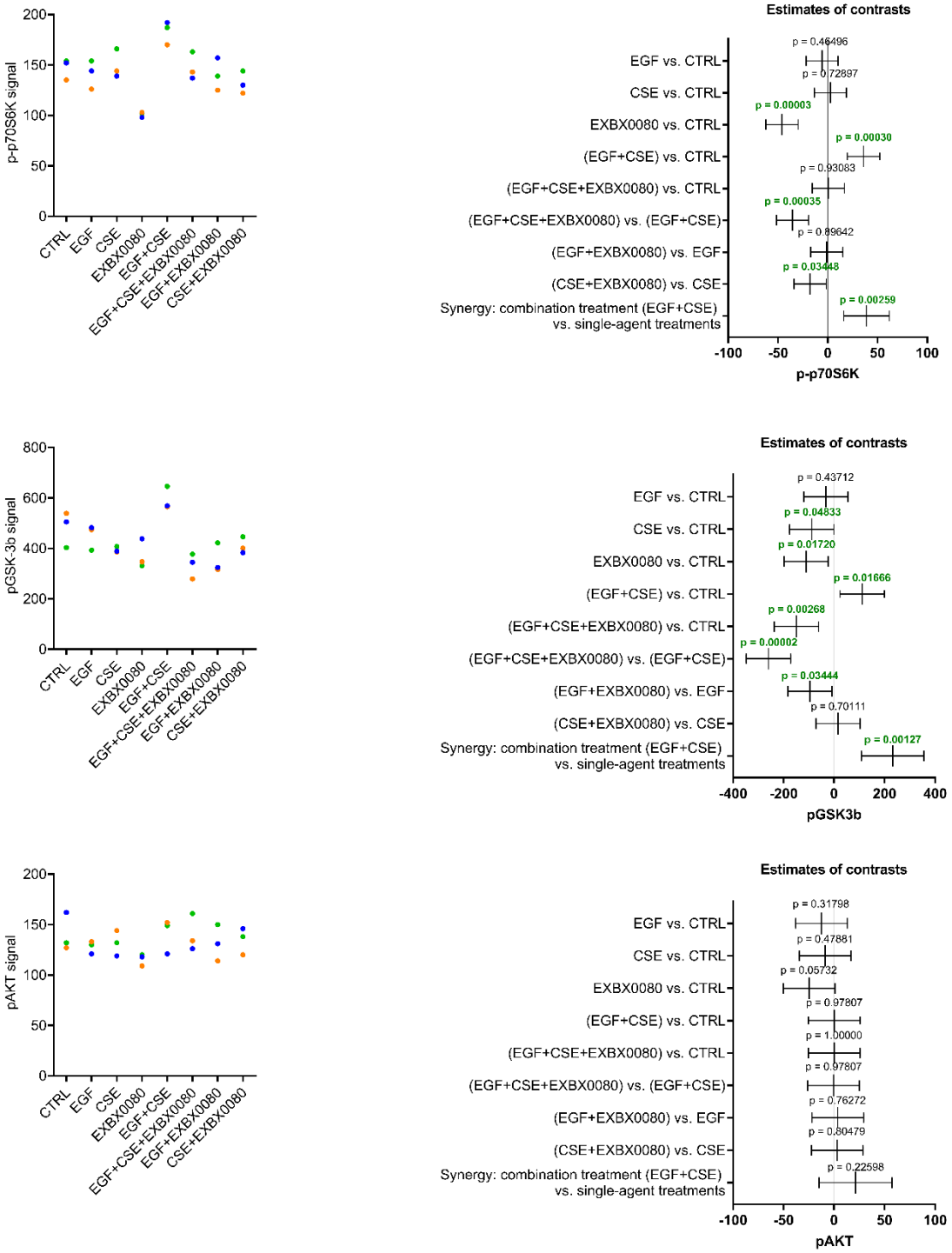

Figure 21: Analysis of downstream signaling pathways of EGFR. Fully differentiated small airway epithelial cell (SAEC) air-liquid interface (ALI) cultures were exposed to epidermal growth factor (EGF), cigarette smoke extract (CSE), gefitinib (EXBX0080) or any combination of the three. After 20 minutes, cells were lysed, and phosphorylation of specific downstream modulators was assessed (n=3). The data was analyzed with a mixed effect model. The forest plots show the point estimate for difference between the compared treatments with 95% confidence intervals. Exclusion of the null from the confidence interval corresponds to a p-value < 0.05 (highlighted in green). p70s6K: Ribosomal protein S6 kinase beta-1; GSK-3b: glycogen synthase kinase 3b; AKT: protein kinase B.

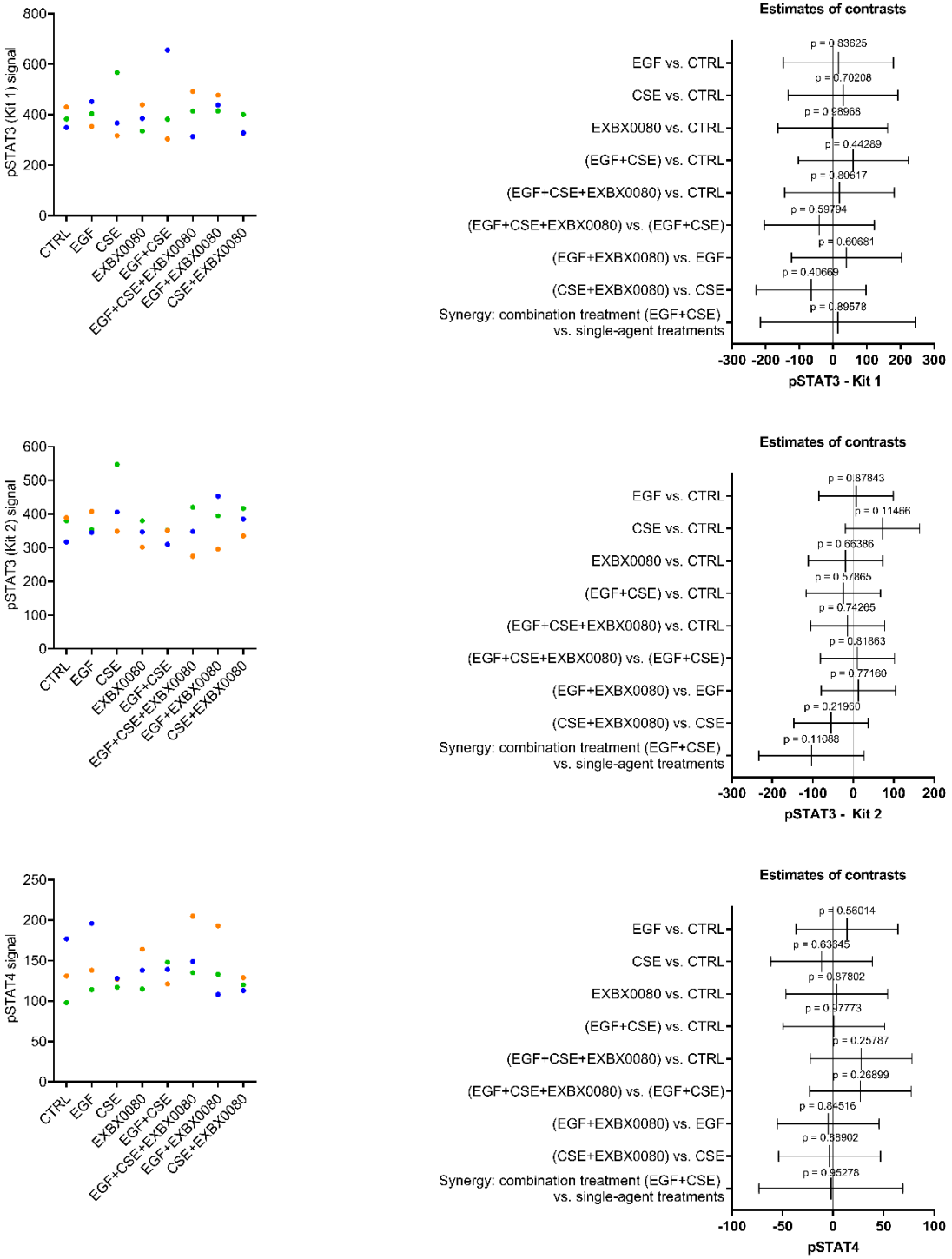

Figure 22: Analysis of downstream signaling pathways of EGFR. Fully differentiated small airway epithelial cell (SAEC) air-liquid interface (ALI) cultures were exposed to epidermal growth factor (EGF), cigarette smoke extract (CSE), gefitinib (EXBX0080) or any combination of the three. After 20 minutes, cells were lysed, and phosphorylation of specific downstream modulators was assessed (n=3). The data was analyzed with a mixed effect model. The forest plots show the point estimate for difference between the compared treatments with 95% confidence intervals. Exclusion of the null from the confidence interval corresponds to a p-value < 0.05. STAT: signal transducer and activator of transcription.

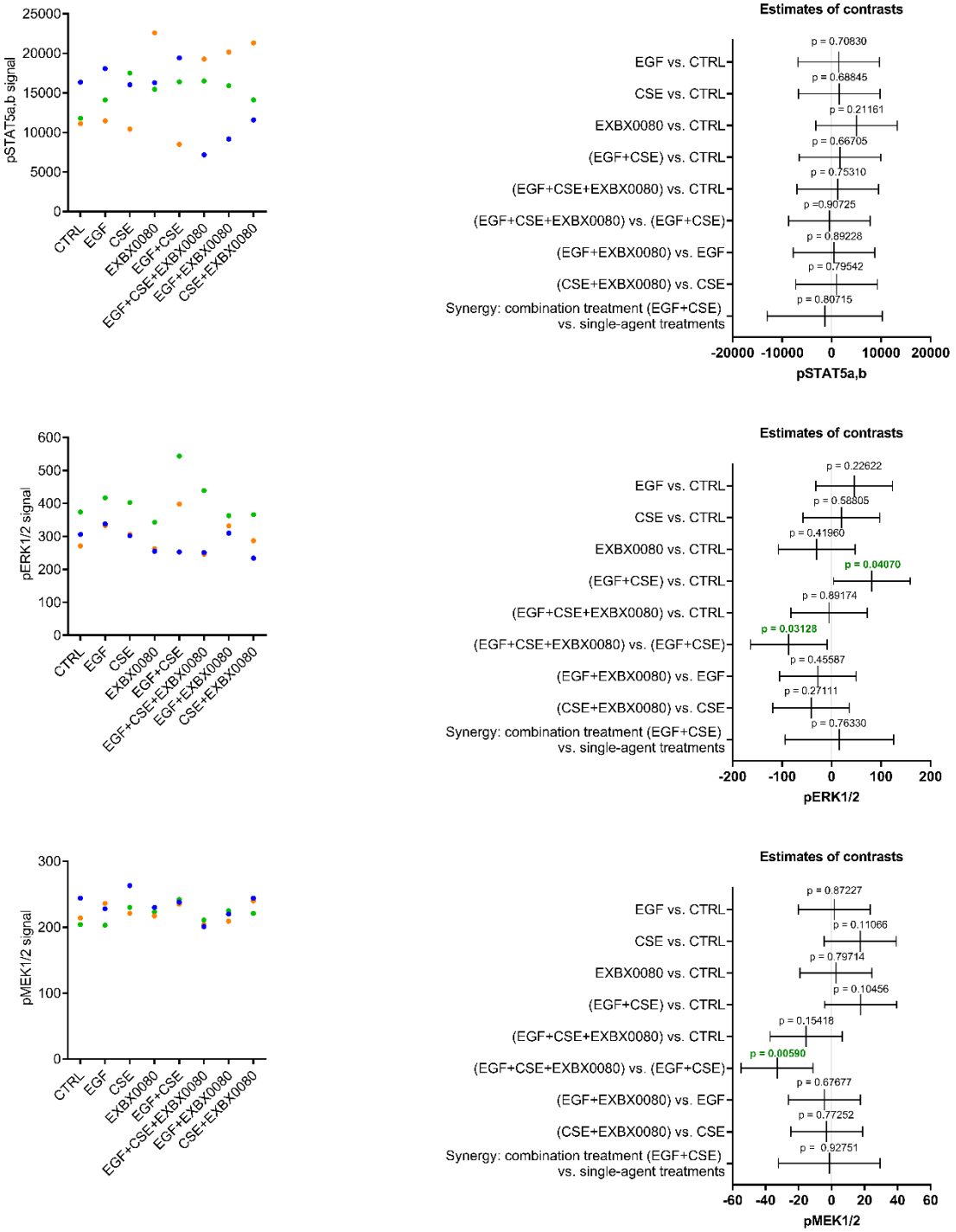

Figure 23: Analysis of downstream signaling pathways of EGFR. Fully differentiated small airway epithelial cell (SAEC) air-liquid interface (ALI) cultures were exposed to epidermal growth factor (EGF), cigarette smoke extract (CSE), gefitinib (EXBX0080) or any combination of the three. After 20 minutes, cells were lysed, and phosphorylation of specific downstream modulators was assessed (n=3). The data was analyzed with a mixed effect model. The forest plots show the point estimate for difference between the compared treatments with 95% confidence intervals. Exclusion of the null from the confidence interval corresponds to a p-value < 0.05 (highlighted in green). STAT: signal transducer and activator of transcription; ERK: extracellular-signal regulated kinase; MEK: mitogen-activated protein kinase kinase (MAPK kinase).

Phosphorylation of AKT was not significantly increased after treatment with EGF and CSE (Fig. 21). This led to the hypothesis that ROS-induced Wingless/integrase-1 (WNT) signaling might be responsible for the increase in pGSK3β (Fig. 24). Further experiments are required to confirm this hypothesis and to elucidate activation of p70S6K (see section 4.4).

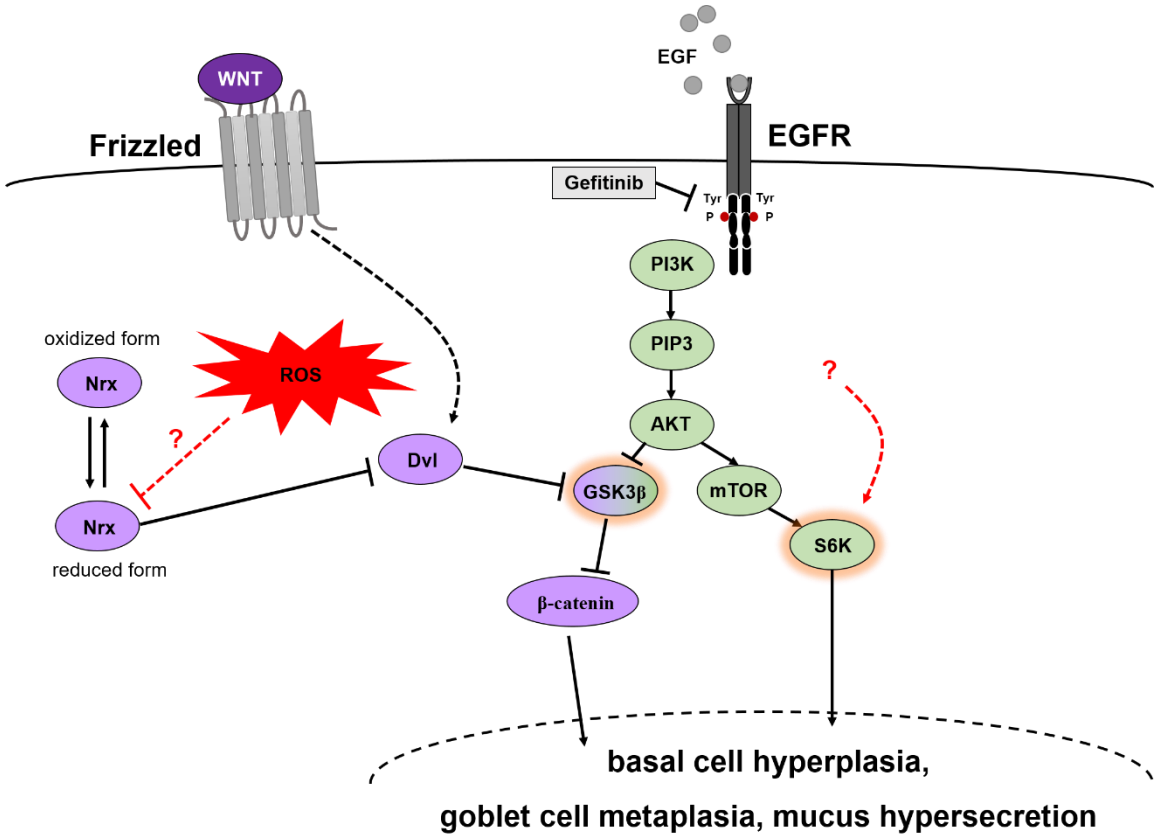

Figure 24: Schematic of the hypothesized interaction between epidermal growth factor receptor (EGFR) signaling and cigarette smoke (CS) induced reactive oxygen species (ROS). Epidermal growth factor (EGF) binds to EGFR and induces receptor dimerization and autophosphorylation (P) of tyrosine (Tyr) residues. This activates the PI3K (phosphatidylinositol-3-kinase) signaling pathway. Intracellular ROS interacts with Wingless/integrase-1 (WNT) pathway by inhibiting the redox-sensitive association of nucleoredoxin (NRX) with dishevelled (Dvl). This induces inhibition of GSK3β by phosphorylation. Therefore, phosphorylation of β-catenin is prevented and it can translocate into the nucleus, where it regulates transcription. PIP3: phosphatidylinositol (3,4,5)-triphosphate; AKT: protein kinase B; GSK3: glycogen synthase kinase 3; mTOR: mammalian target of rapamycin, S6K: Ribosomal protein S6 kinase beta-1 (also known as p70S6K).

3.4 Cigarette smoke induced effects on epithelial remodeling

3.4.1 Defined exposure of ALI cultures with whole cigarette smoke

To achieve a more disease-related *in vitro* setup, the SAEC ALI cultures were treated with whole cigarette smoke (CS) from the air-exposed apical side either during differentiation (starting with the air-lift) or fully differentiated. This modification of the model format is of

advantage since CSE comprises only soluble ingredients of cigarette smoke, but many components are volatile and therefore not represented in the liquid extract. Besides, CSE is administered via the basolateral medium to the basal side of the epithelium.

To allow constant smoke composition, well-defined research cigarettes (3R4F, University of Kentucky, Lexington, KY, USA) were used. A standardized and controlled smoking profile (compare section 1.3.2) is important to ensure reproducible conditions during CS exposure, i.e. uniform exposure to toxins. This was achieved using the P.R.I.T. (Professional In-Vitro Technologies) ExpoCube in the experimental setup developed by Fraunhofer Institute for Toxicology and Experimental Medicine. Particle concentration and carbon monoxide (CO) were monitored during CS exposure to confirm consistent conditions. A typical diagram of smoke monitoring is shown in Fig. 25. Both parameters increase over time. Puffs were drawn directly from the cigarette (active smoking). Therefore, the cigarette served as a filter itself. As the exposure time progressed, the cigarette length became shorter and shorter. Hence, the filtering property decreased. Consequently, the particle concentration increased with later puffs.

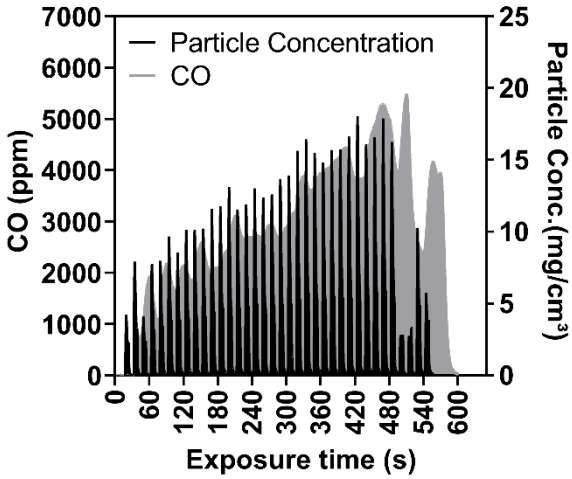

Figure 25: Cigarette smoke exposure of air-liquid interface (ALI) cultures. Monitoring of particle concentration (black) and carbon monoxide (CO; grey) during exposure to four 3R4F cigarettes. Representative data of one exposure cycle is shown.

In order to find an appropriate concentration of CS that induces disease-relevant features without showing cytotoxic effects, a titration experiment was conducted. On four consecutive days, fully differentiated SAEC ALI cultures were exposed to smoke from different amounts of research cigarettes (3R4F, University of Kentucky, Lexington, KY, USA) per day. After the exposure to eight cigarettes a day, the Lactate Dehydrogenase (LDH) release increased significantly (HC: $p = 0.03$; COPD: $p < 0.0001$; two-way ANOVA with Sidak's test) and the cultures were leaky, indicating a cytotoxic concentration of CS (Fig. 26). When exposed to four cigarettes a day, LDH release was similar to control and the epithelium exhibited a normal morphology (data not shown). To further investigate, whether

this is a suitable CS concentration for further experiments, SAEC ALI cultures were exposed to CS from four cigarettes a day during differentiation (three exposure cycles per week, Fig. 27).

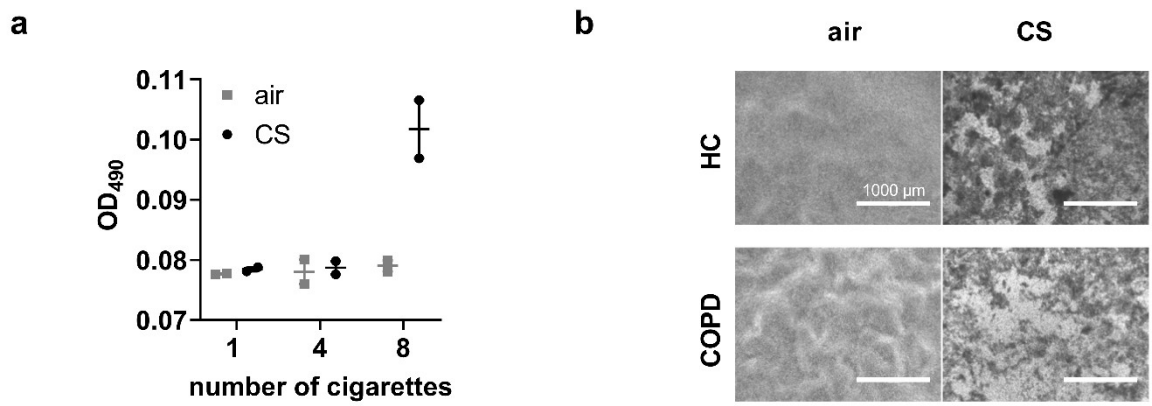

Figure 26: Titration of cigarette smoke (CS) exposure. Fully differentiated small airway epithelial cell (SAEC) air-liquid interface (ALI) cultures were exposed to either one, four or eight cigarettes per day on four consecutive days with a dilution rate of 0.5 l/min. (a) Lactate Dehydrogenase (LDH) release in CS- and air-exposed ALI cultures from one healthy control and one COPD donor. Optical density (OD) at 490 nm indicate LDH release in cell culture supernatants. n=2, data is represented as mean ± SEM. (b) Top view of ALI cultures from one healthy control (HC) and one COPD donor exposed to either eight cigarettes per day or air as control.

Regarding toxicity tests, four cigarettes per exposure cycle were defined as the daily concentration for further CS exposure experiments (compare Fig 26-27).

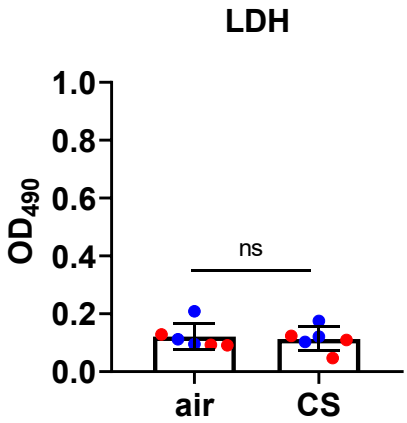

Figure 27: Lactate Dehydrogenase (LDH) release in cigarette smoke (CS) and air-exposed air-liquid interface (ALI) cultures. OD_{490} measurements indicate LDH release in small airway epithelial cell (SAEC) culture supernatants on day 28 after air-lift. Blue dots represent cultures from healthy individuals (n=3) and red dots represent cultures from chronic obstructive pulmonary disease (COPD) patients. (Gindele et al., 2020)

To reflect CS-induced changes in the small airways, two CS exposure models were established: a long-term model to investigate the effects of CS on SAEC differentiation and a short-term model to investigate acute effects of CS on fully differentiated ALI cultures (four days). Both models will be discussed in more detail in the following chapters.

3.4.2 Effect of cigarette smoke exposure on epithelial remodeling

3.4.2.1 Remark on published data

The data in section 3.4.2 has previously been published:

Gindele, J.A., Kiechle, T., Benediktus, K. et al. Intermittent exposure to whole cigarette smoke alters the differentiation of primary small airway epithelial cells in the air-liquid interface culture. Sci Rep 10, 6257 (2020). https://doi.org/10.1038/s41598-020-63345-5

3.4.2.2 Experimental setup of CS exposure during SAEC differentiation

As previously described in section 3.2 aberrant basal cell differentiation plays an important role in COPD (Rock et al., 2010; Shaykhiev and Crystal, 2014a). To investigate important mechanisms underlying the pathogenesis of small airway disease in COPD, SAEC from three healthy non-smokers and three COPD-smokers were exposed to whole CS during differentiation (four weeks, starting with the air-lift).

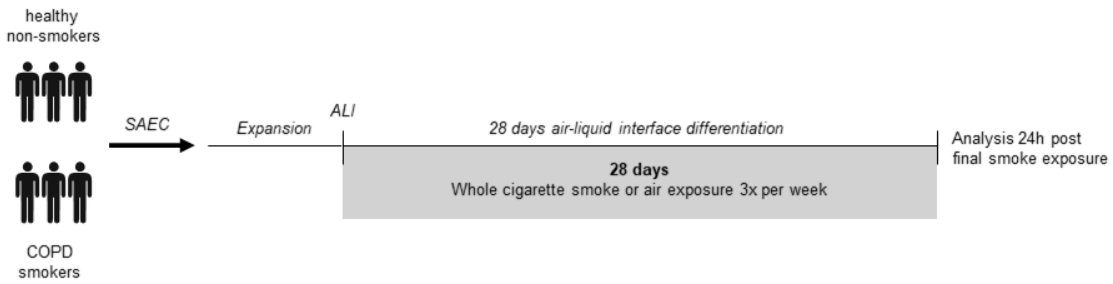

Figure 28: Experimental setup of cigarette smoke exposure during differentiation. Small airway epithelial cells (SAEC) of three healthy non-smokers and three chronic obstructive pulmonary disease (COPD) smokers were cultivated until fully differentiated at the air-liquid interface (ALI). During the differentiation process (starting with the air-lift) cultures were exposed to whole cigarette smoke of four cigarettes a day three times a week. Readouts were performed throughout differentiation or 24 hours after the last smoke exposure.

Various analyses, including functional (sections 3.4.2.3 and 3.4.2.6) and morphologic assessments (sections 3.4.2.3 to 3.4.2.6), evaluation of specific markers at protein and transcriptional level (sections 3.4.2.3 to 3.4.2.6), as well as a detailed RNA sequencing analysis (sections 3.4.2.3 to 3.4.2.7) with translatability evaluation (section 3.4.2.8), were conducted throughout differentiation or 24 hours after the final smoke exposure (Fig. 28). This allowed the investigation of important pathophysiological mechanisms, such as the loss of barrier function, squamous differentiation, goblet cell metaplasia, loss of club and ciliated cells and the induction of specific pathways upon smoking. In particular, the RNA sequencing analysis was of crucial importance for all parameters mentioned, as it revealed the deregulation of important genes and signaling pathways in response to CS.

3.4.2.3 CS exposure impairs epithelial barrier integrity

The epithelial barrier is an important defense mechanism against inhaled pathogens (Ganesan et al., 2013). To investigate the effect of CS on epithelial integrity, SAEC were exposed to whole cigarette smoke during differentiation and TEER was regularly monitored.

Upon CS treatment, transepithelial electrical resistance (TEER) was decreased. To quantify this effect, the area under the curve (AUC) was calculated and standardized in terms of time. The adjusted AUC dropped in the healthy ALI cultures from (535 ± 91) $\Omega*cm^2$ in air controls to (354 ± 36) $\Omega*cm^2$ ($p = 0.010$) upon CS exposure, and in the COPD ALI cultures from (500 ± 143) $\Omega*cm^2$ to (337 ± 50) $\Omega*cm^2$ ($p = 0.017$), respectively (Fig 29a). The decline in TEER indicates a more permeable epithelium. To elucidate the underlying molecular mechanisms, gene expression of junctional protein transcripts was analyzed. Some of the genes, which were deregulated upon CS exposure, are associated with cell adhesion, permeability and tight junction regulation. *JAM3*, *CLDN11* and *CLDN18* were down regulated after 28 days of intermittent CS treatment. *CLDN7* and *CLDN10* were up regulated in both healthy and COPD cultures (Fig. 29b). The expression of claudin-10, which was strongly up regulated on RNA level, was confirmed on protein level by means of immunohistochemistry (Fig. 29c). Other claudins, which were described to play a role in the human lung, such as claudin-1, -3, -4, and -5 (Schlingmann et al., 2015), were not significantly deregulated (data not shown). An extended panel with key genes encoding for proteins associated with the regulation of tight junctions is shown in Tab. 7 (see supplementary information).

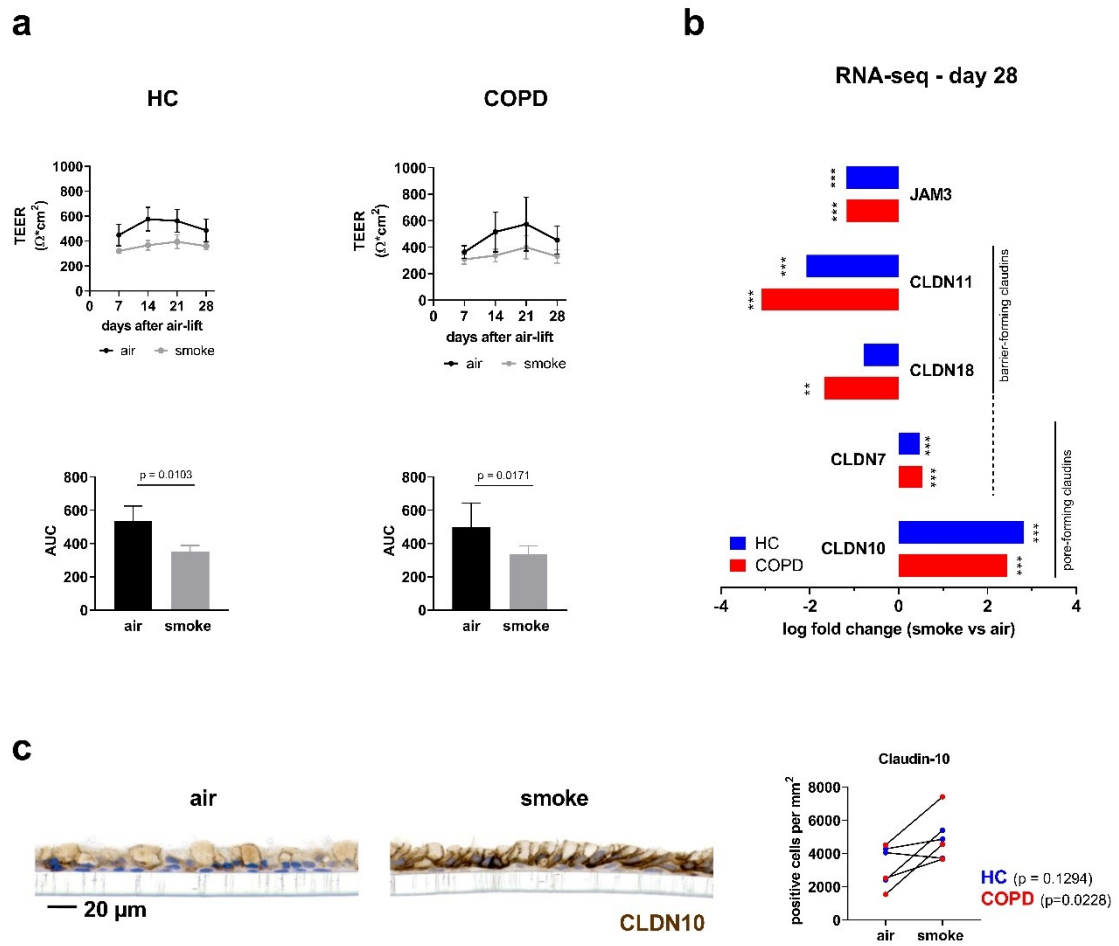

Figure 29: Cigarette smoke exposure impairs epithelial barrier integrity. (a) Transepithelial electrical resistance (TEER) of healthy (HC) and chronic obstructive pulmonary disease (COPD)-derived cultures (n=3) during differentiation upon smoke or air treatment, respectively. Upper graphs show TEER values over time, lower graphs represent adjusted area under the curve (AUC). Data are represented as mean ± SEM; p values are based on the analysis of the log AUC values with a repeated measurement model. (b) Gene expression analysis by RNA sequencing exhibit deregulation of junctional genes upon smoke treatment. Data are represented as log fold changes. Significance of deregulation is indicated as * for q value < 0.05; ** for q value < 0.01; *** for q value < 0.001, n=3 donors for HC and COPD. *JAM3* = junctional adhesion molecule C, *CLDN11* = Claudin 11, *CLDN18* = Claudin 18, *CLDN7* = Claudin 7, *CLDN10* = Claudin 10. (c) Immunohistochemical staining for Claudin 10 (CLDN10) on formalin-fixed paraffin-embedded tissue slices from SAEC cultures intermittently exposed to smoke or air for control. Figure shows representative images of one healthy donor and semi-quantitative assessment by image analysis. SAEC = small airway epithelial cells. (Gindele et al., 2020)

3.4.2.4 CS exposure induces squamous differentiation

Squamous metaplasia is a critical hallmark of COPD (Rigden et al., 2016). To evaluate, whether intermittent CS exposure induces squamous differentiation in SAEC ALI cultures, the expression of different squamous cell markers were analyzed. Cytokeratin 5 and 14 (*KRT5*, *KRT14*) mRNA expression was measured by means of qPCR. Delta Ct (cycle threshold) values correspond to the difference between Ct of the gene of interest and Ct of the reference sequence, *POLR2A* (RNA Polymerase II Subunit A). Upon differentiation, ΔCt

of *KRT5* and *KRT14* increased until reaching a plateau (day 14 after air-lift). This indicates that RNA expression of these genes decreased during the normal differentiation process (Fig. 30).

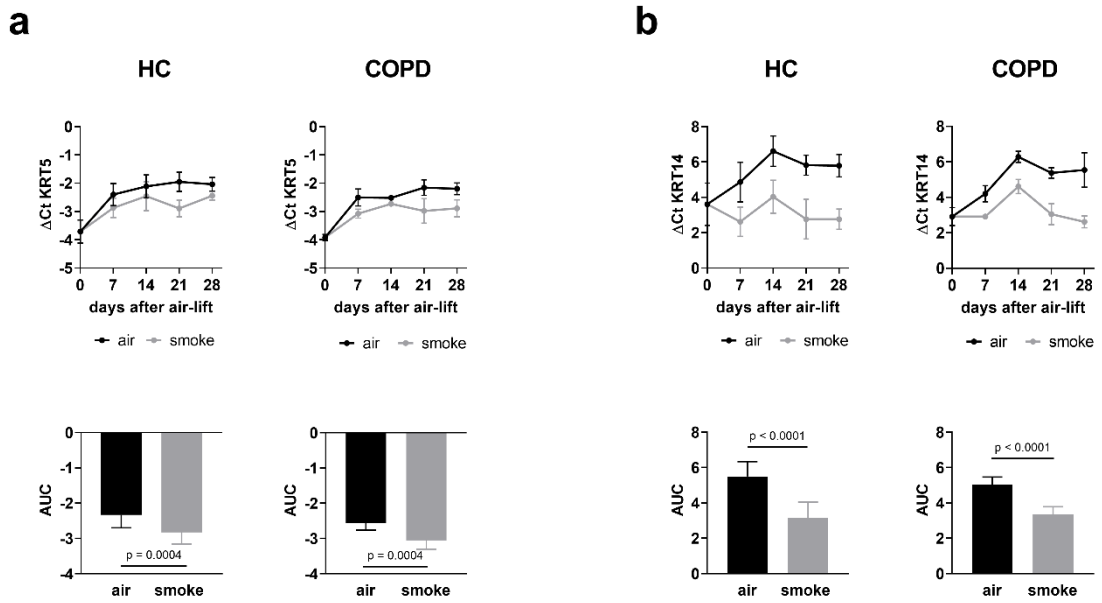

Figure 30: Cigarette smoke alters the expression of basal cell markers and induces squamous differentiation. (a) Quantitative Reverse Transcription Polymerase Chain Reaction (RT-PCR) analysis of the basal cell marker cytokeratin 5 (*KRT5*) and (b) the squamous cell marker cytokeratin 14 (*KRT14*). Gene expression analysis of healthy (HC) and chronic obstructive pulmonary disease (COPD) cultures was performed on day 7, 14, 21 and 28 with intermittent exposure to smoke or air for control. Upper graphs show ΔCt values over time, lower graphs represent adjusted area under the curve (AUC). Data are represented as mean ± SEM, n=3 donors for HC and COPD; p values are based on the analysis of the AUC values with a repeated measurement model. (Gindele et al., 2020)

Cultures of healthy non-smokers and COPD smokers had a similar course of *KRT5* and *KRT14* expression. CS exposure induced a reduction of ΔCt, indicating an up-regulation of *KRT5* and *KRT14* mRNA expression in healthy as well as in COPD ALI cultures. For quantification, the AUC was calculated and standardized in terms of time span, which showed a significant deregulation. Expression of other genes associated with squamous differentiation, such as Cytokeratin 6A (*KRT6A*), Cytokeratin 13 (*KRT13*), and Stratifin (*SFN*) were analyzed by means of RNA sequencing. Gene expression of these markers was up-regulated upon CS exposure, indicated by a positive fold-change (Fig. 31a). In order to validate these findings at protein level, formalin-fixed paraffin-embedded ALI culture slices were stained exemplarily for KRT5. The semi-quantitative evaluation suggested an increase in KRT5 protein expression at CS exposure during differentiation (Fig 31b).

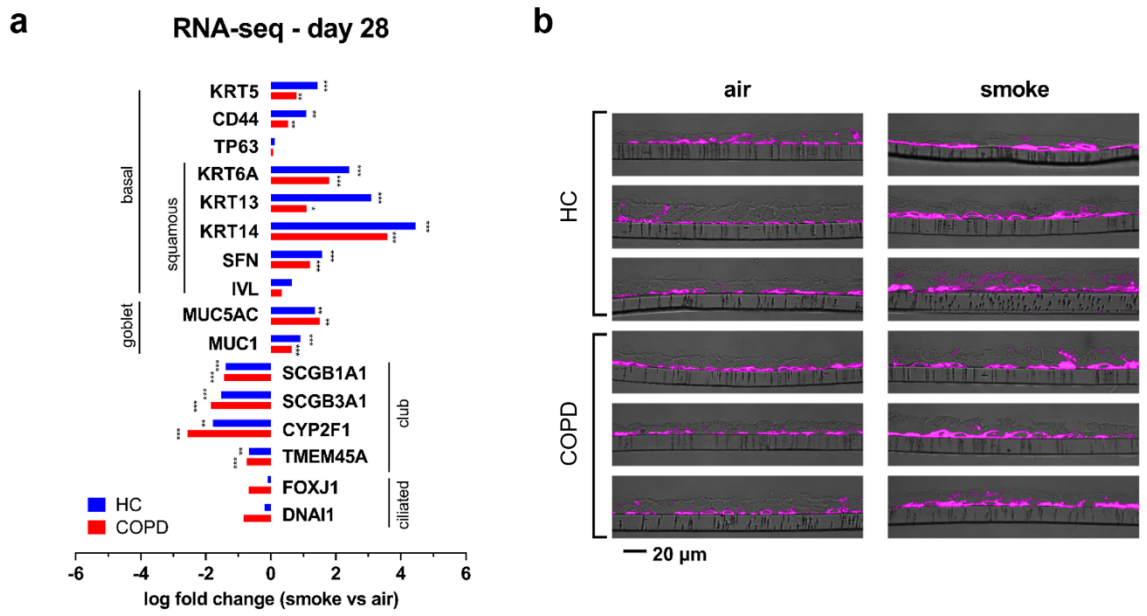

Figure 31: Cigarette smoke exposure alters small airway differentiation (a) Gene expression analysis by next generation sequencing (NGS) revealed RNA expression of genes related to aspects of airway epithelial differentiation. Data are represented as log fold changes. Significance of deregulation is indicated as * for q value < 0.05; ** for q value < 0.01; *** for q value < 0.001, n=3 donors for healthy control (HC) and chronic obstructive pulmonary disease (COPD). Cytokeratin 5 (*KRT5*), CD44 (*CD44*), tumor protein p63 (*TP63*), Cytokeratin 6A (*KRT6A*), Cytokeratin 13 (*KRT13*), Cytokeratin 14 (*KRT14*), Stratifin (*SFN*), Involucrin (*IVL*), Mucin 5 AC (*MUC5AC*), Mucin 1 (*MUC1*), Uteroglobin (*SCGB1A1*), Secretoglobin family 3A member 1 (*SCGB3A1*), Cytochrome P450 2F1 (*CYP2F1*), Transmembrane protein 45A (*TMEM45A*), Forkhead box protein J1 (*FOXJ1*) and Dynein intermediate chain 1 (*DNAI1*). (b) Immunohistochemical staining for cytokeratin 5 (KRT5) on formalin-fixed paraffin-embedded tissue slices from SAEC cultures intermittently exposed to smoke or air for control. Figure shows representative images of three healthy and three COPD cultures on day 28. (Gindele et al., 2020)

Other cell type-specific genes (goblet, club, and ciliated cell markers) were also deregulated upon CS exposure in SAEC ALI cultures (Fig. 31a). These were further discussed in the following sections (see 3.4.2.5 and 3.4.2.6).

3.4.2.5 CS exposure alters the differentiation of secretory cells

To elucidate, whether CS exposure shifts basal cell fate towards a secretory phenotype *in vitro*, ALI cultures were exposed to whole CS during differentiation and secretory cell markers were analyzed at RNA and protein level. Goblet cell hyperplasia and mucus overproduction are characteristic for COPD airways and have been demonstrated to be linked to smoking (Lumsden et al., 1984; Saetta et al., 2000).

The goblet cell marker *MUC5AC* and the club cell marker *SCGB1A1* were evaluated by qPCR analysis on day 7, 14, 21 and 28 after air-lift (Fig. 32). Delta Ct values of *MUC5AC* did not change remarkably in air-exposed ALI cultures during differentiation. However, ΔCt of *SCGB1A1* decreased over time, indicating an increased *SCGB1A1* mRNA expression upon normal differentiation. SAEC cultures, which were exposed to CS, showed a tendency

towards increased *MUC5AC* mRNA levels (reduced ΔCt values) and reduced *SCGB1A1* mRNA levels (increased ΔCt values).

RNA sequencing analysis of SAEC ALI cultures on day 28 revealed a significant up-regulation of goblet cell associated genes, such as *MUC5AC* and Mucin 1 (*MUC1*), and a significant down-regulation of club cell associated genes, such as Uteroglobin (*SCGB1A1*), Secretoglobin family 3A member 1 (*SCGB3A1*), Cytochrome P450 2F1 (*CYP2F1*) and Transmembrane protein 45A (*TMEM45A*) (Fig. 31a). Thus, the sequencing confirmed the previous qPCR data.

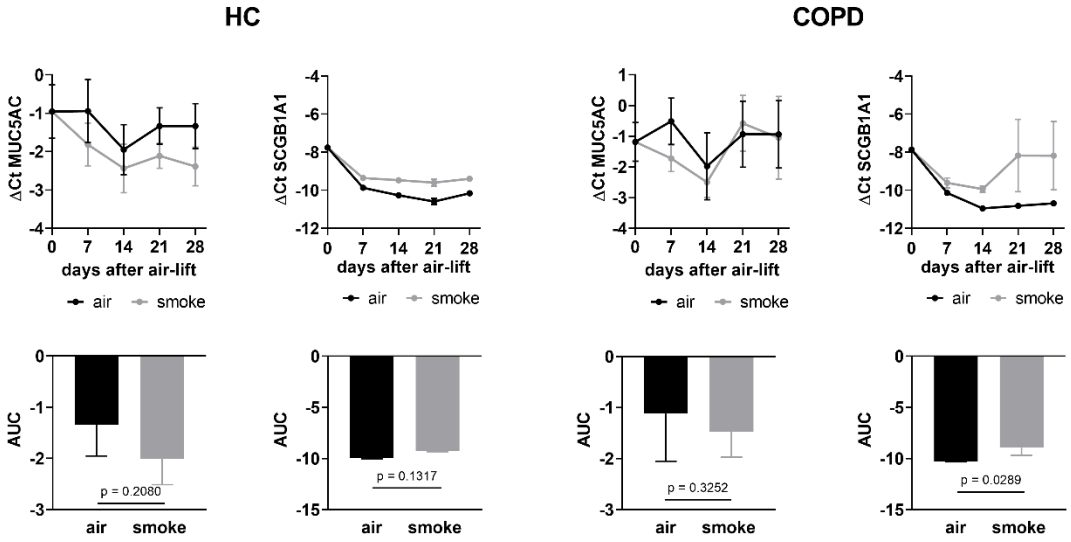

Figure 32: Cigarette smoke alters the differentiation of secretory cells. Quantitative Reverse Transcription Polymerase Chain Reaction (RT-PCR) analysis of the goblet cell marker Mucin 5AC (MUC5AC) and the club cell marker uteroglobin (SCGB1A1). Gene expression analysis of healthy (HC) and chronic obstructive pulmonary disease (COPD) cultures was performed on day 7, 14, 21 and 28 with intermittent exposure to smoke or air for control. Upper graphs show ΔCt values over time, lower graphs represent adjusted area under the curve (AUC). Data are represented as mean ± SEM, n=3 donors for HC and COPD; p values are based on the analysis of the AUC values with a repeated measurement model. (Gindele et al., 2020)

To further investigate the increase in goblet cells and the reduction in club cells at protein level, formalin-fixed paraffin-embedded slices from SAEC ALI cultures were subjected to immunohistochemical evaluation. Cultures were stained for MUC5AC and SCGB1A1 (Fig. 33). Semi-quantitative assessment indicated an increase in $MUC5AC^{+}$ cells and a decrease in $MUC5AC^{-}/SCGB1A1^{+}$ cells.

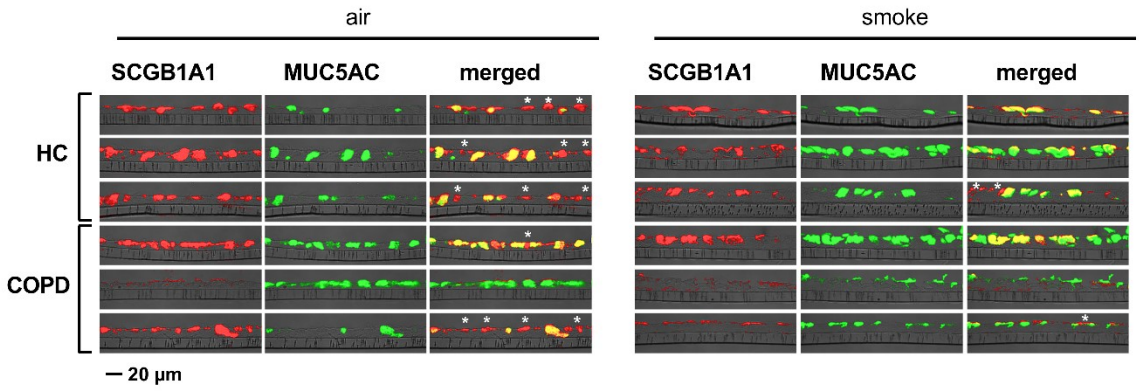

Figure 33: Cigarette smoke exposure stimulates the differentiation of MUC5AC^{+} goblet cells and reduces SCGB1A1^{+} club cells. Immunohistochemical staining for uteroglobin (SCGB1A1) and Mucin 5 AC (MUC5AC) on formalin-fixed paraffin-embedded tissue slices from SAEC cultures intermittently exposed to smoke or air for control. Figure shows representative images of three healthy and three chronic obstructive pulmonary disease (COPD) cultures on day 28. SCGB1A1 single positive cells are marked by an asterix in the merged images. (Gindele et al., 2020)

Quantification of protein markers, i.e. the abundance of MUC5AC^{+}/SCGB1A1^{-}, MUC5AC^{+}/SCGB1A1^{+}, MUC5AC^{-}/SCGB1A1^{+} cells, was realized by flow cytometry (Fig. 34). Although not significant, it confirmed the trend from the previous analyses.

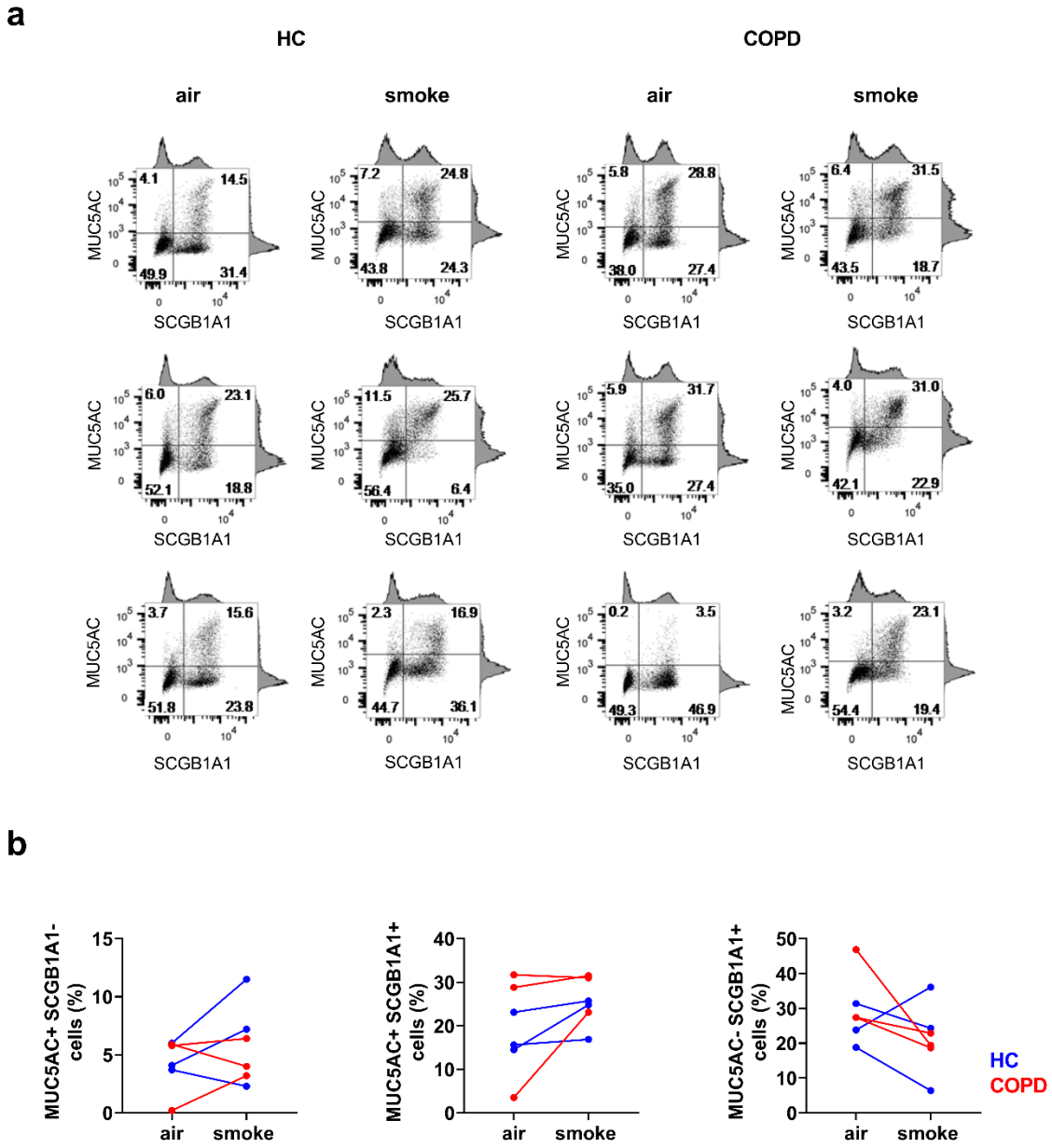

Figure 34: Flow cytometry analysis of single cell suspensions of small airway epithelial cell (SAEC) air-liquid interface (ALI) cultures stained for Mucin 5AC (MUC5AC) and uteroglobin (SCGB1A1). $MUC5AC^{+}/SCGB1A1^{-}$ single positive, $MUC5AC^{+}/SCGB1A1^{+}$ double positive and $MUC5AC^{-}/SCGB1A1^{+}$ single positive cells on day 28 upon air-lift with intermittent exposure to smoke or air for control. (a) Scatterplots with histograms of three healthy controls (HC) and three chronic obstructive pulmonary disease (COPD) cultures double stained for MUC5AC and SCGB1A1 are depicted. (b) Quantitative analysis of the flow cytometry analyses in (a). Values from healthy cultures are depicted in blue; values from COPD-derived cultures are depicted in red. (Gindele et al., 2020)

3.4.2.6 CS exposure impairs the development of ciliated cells

Functional cilia beating is vital to ensure mucociliary clearance, which is an important defense mechanism of the airways (Kilburn, 1968). A diminishing number of ciliated cells characterizes COPD airways and is directly correlated with smoking (Auerbach et al., 1961; Hessel et al., 2014; Lam et al., 2013; Rennard, 2003; Yaghi and Dolovich, 2016; Yaghi et al., 2012). To investigate, whether this aberrant differentiation can be modelled *in vitro*, SAEC ALI cultures were exposed to whole CS during differentiation (28 days, starting with the air-lift).
Cilia function was monitored weekly using a video-microscopic approach of quantitative cilia beat measurement (Fig. 35). Area covered with actively beating cilia increased over time upon normal differentiation. A similar course was seen for the cilia beat frequency, indicating the normal differentiation of ciliated cells. Cigarette smoke exposure led to a reduced area of beating cilia and a reduced beat frequency (Fig. 35a, b). This applied to cultures from healthy non-smokers as well as cultures from COPD smokers.

To assess whether the reduced cilia function was associated with a reduced ciliated cell differentiation and reduced ciliogenesis, gene expression of *FOXJ1* was analyzed using qPCR (Fig. 35c). Delta Ct values of the transcription factor *FOXJ1* decreased during normal differentiation, indicating the development of ciliated cells. In CS-exposed cultures, a delay of this progression was observed. The AUC was calculated to compare the course of the two treatments, resulting in a p value of 0.1609 in healthy non-smokers and a p value of 0.0490 in COPD smokers.
RNA sequencing analysis on day 28 showed no significant deregulation of ciliated cell associated genes, such as *FOXJ1* or Dynein intermediate chain 1 (*DNAI1*) (Fig. 31a).

To investigate whether the abundance of ciliated cells was reduced upon CS exposure, formalin-fixed paraffin-embedded ALI culture slices were subjected to immunohistochemical evaluation using an antibody against acetylated tubulin (Fig. 35d). CS-exposed cultures exhibited a reduced number of acetylated tubulin-positive cells compared to air controls.

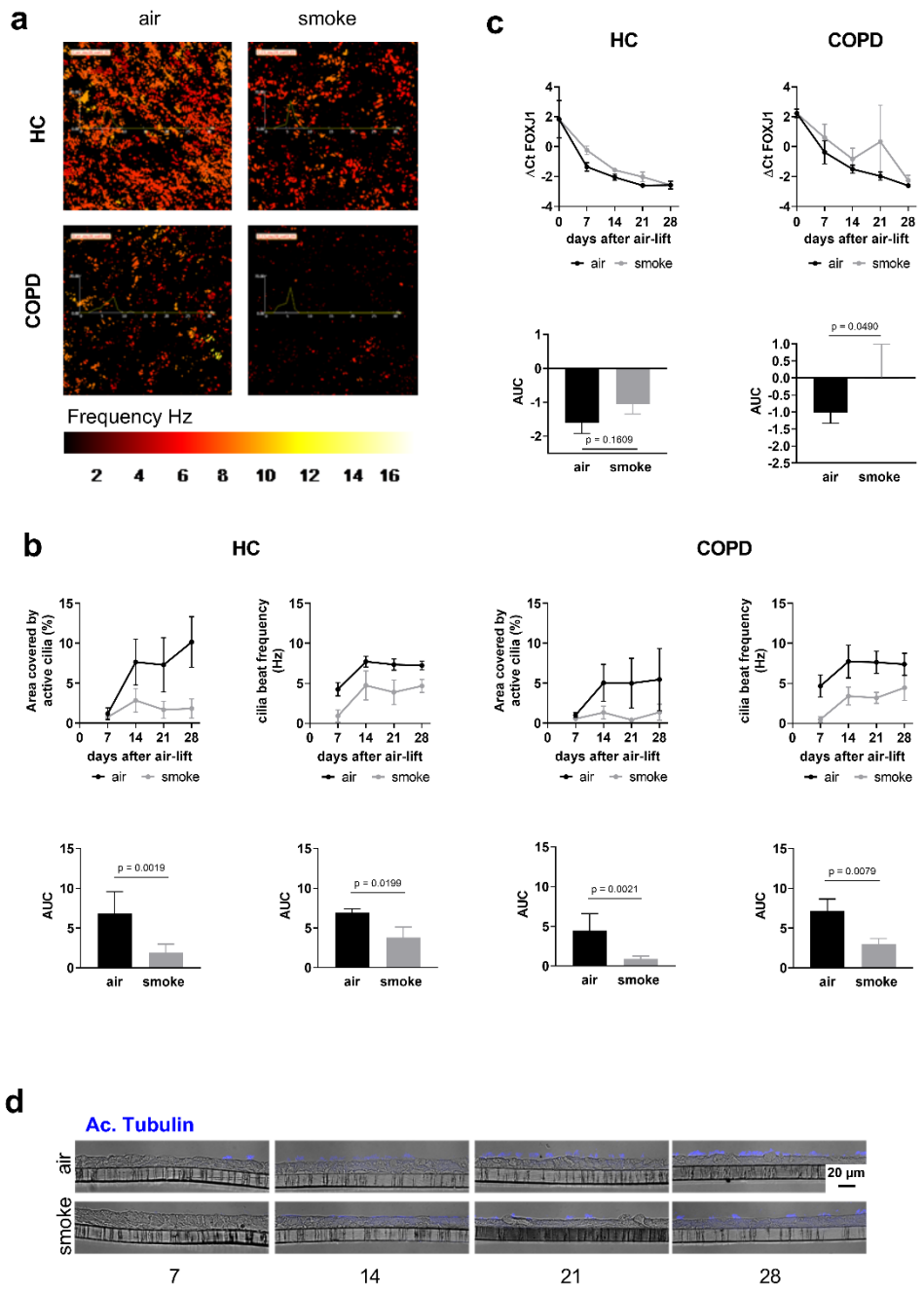

Figure 35: Cigarette smoke (CS) exposure impairs the development and physiology of ciliated cells. (a) Representative images of functional cilia beat measurement on day 28 upon air-lift of one donor with chronic obstructive pulmonary disease (COPD) and one healthy control (HC), after the exposure with CS during the differentiation process (smoke) and air treatment for control. The area covered with beating ciliated cells is visualized by false color staining and the cilia beat frequency is translated to the color code shown at the temperature lookup table at the bottom. (b) Quantification of the area covered by active cilia and the cilia beat frequencies at days 0, 7, 14, 21 and 28 upon air-lift. Adjusted area under the curve (AUC) was calculated to compare the development and changes over time. Data are presented as mean ± SEM. n=3 donors with COPD and 3 healthy controls (HC); p values are based on the analysis of the AUC values with a repeated measurement model. (c) Upper panel: Quantitative Reverse Transcription Polymerase Chain Reaction (RT-PCR) analysis of the ciliated cell marker Forkhead Box J1 (*FOXJ1)* from the same cultures. Lower panel: Adjusted area under the curve (AUC) was calculated to compare the changes of mRNA expression over time. Data are presented as mean ± SEM; p values are based on the analysis of the AUC values with a repeated measurement model. (d) Immunohistochemical staining of ALI sections of day 7, 14, 21 and 28 for acetylated tubulin. Representative images of one healthy donor. (Gindele et al., 2020)

3.4.2.7 Common response to CS in healthy and COPD-derived cultures

To investigate whether COPD-derived SAEC ALI cultures respond differently to CS exposure than healthy cultures a comparative analysis was conducted. SAEC cultures from healthy non-smokers and COPD smokers showed similar responses to CS with regard to barrier integrity and basal cell fate (compare sections 3.4.2.3 to 3.4.2.6, statistical comparison not shown). To evaluate whether their transcriptomic profile in response to CS is different, data from the RNA sequencing analysis were compared. CS modulated the expression of 2442 genes in cultures originated from healthy non-smokers and 3249 genes in COPD-derived cultures. In this context, 1945 genes were regulated in both healthy and COPD cultures. The fact that all but one of the 1945 overlapping transcripts were regulated in the same way suggests that the main stimulus for the altered gene expression in this study was CS and not the disease status of the donors, i.e. COPD vs. healthy.

Taken together, healthy and COPD-derived cultures showed common responses to CS exposure during SAEC differentiation.

3.4.2.8 Translatability assessment

To evaluate, how consistent the newly established CS-exposure model reflects mechanisms in the human body, a translatability assessment was carried out. Therefore, the CS-induced transcriptional changes of the healthy ALI cultures were compared with a published data set (Tilley et al., 2011) of small airway epithelial brushes from healthy smokers and non-smokers (GSE11784) to assess the overlap of deregulated genes. The normalized gene expression data (range from 0 to 1) from small airway epithelial brushes and ALI cultures were combined and filtered for those transcripts that were significantly deregulated in both comparisons: a) smoked ALI cultures versus air controls and b) small airway epithelial brushes from healthy smokers versus small airway epithelial brushes from non-smokers. Subsequently an unsupervised, hierarchical clustering was performed using correlation as distance measure on the combined and filtered data-set (Fig. 36a). This approach allowed different clusters to be separated according to their commonalities. Two distinct clusters representing the *in vitro* samples from CS and air-treated ALI cultures were separated. It is noteworthy that most samples originated from small airway epithelial brushes from smokers clustered with the smoked ALI cultures, while samples originated from small airway epithelial brushes from non-smokers clustered with the ALI air controls. This unbiased approach (which focuses only on transcripts that have been significantly deregulated, but does not filter for the common directionality of deregulation) suggests that CS alters overlapping molecular pathways *in vitro* and in the human lung.

To quantify the extent to which the smoked ALI culture resembles the small airway epithelium of smokers, a correlation analysis was performed (Fig. 36b). More than 86 % of the genes that were significantly deregulated in the CS-exposed ALI cultures and the small airway epithelial brushes of healthy smokers showed a consistent direction of deregulation (Fig. 36c).

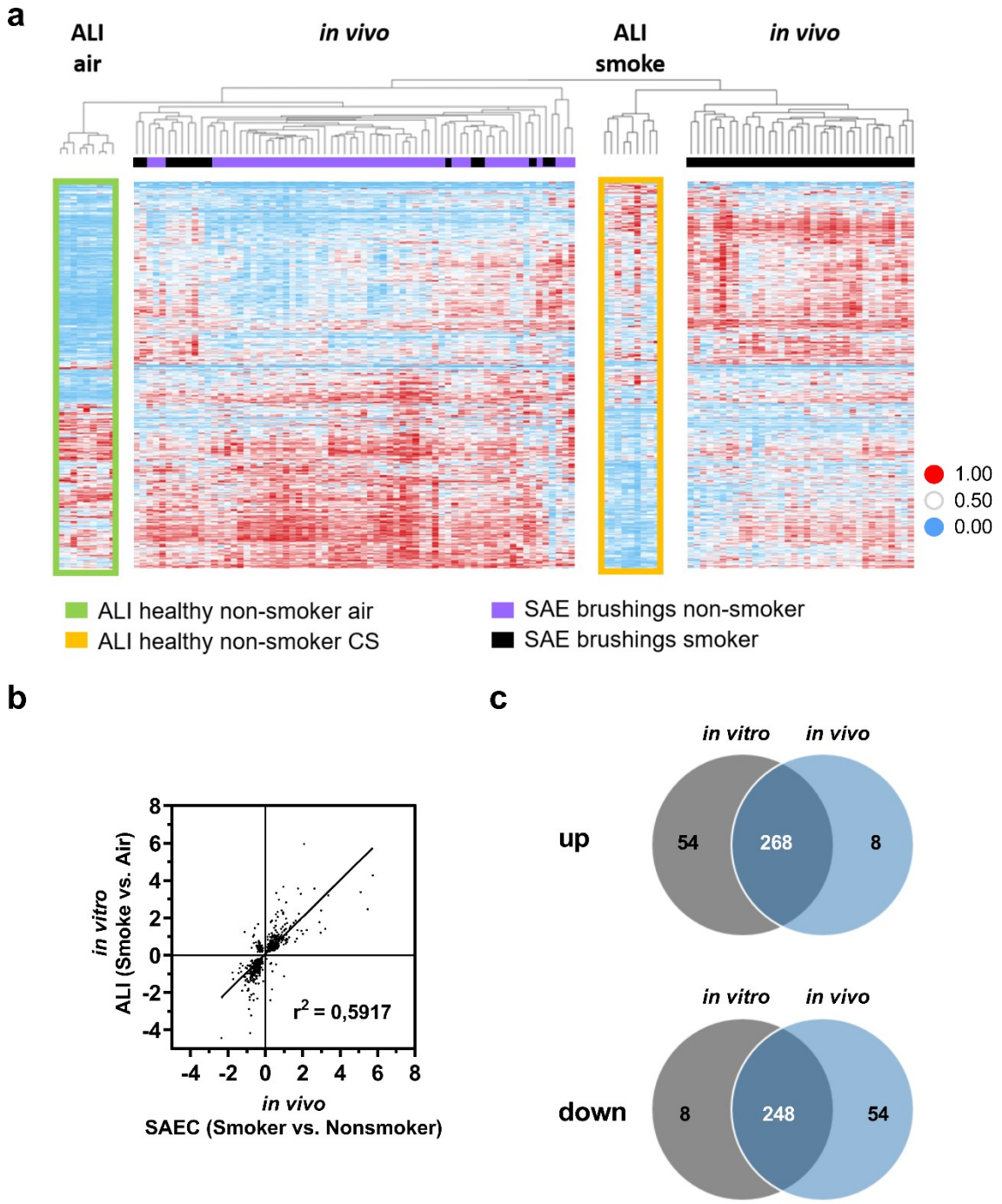

Figure 36: Comparison of transcriptional data from air-liquid interface (ALI) experiments with *in vivo* small airway epithelium supports the translational value of the *in vitro* assay. (a) Heatmap representing transcripts that are significantly deregulated in small airway epithelial cell (SAEC) ALI cultures (*in vitro* model, GSE135188) as well as in SAEC from human smokers (*in vivo* data from small airway epithelial (SAE) brushes, GSE11784) (adjusted p value < 0.05). Data have been independently normalized to a range between 0 and 1 on transcript level. Data sets have been joined and the resulting data set has been clustered. The gaps have been introduced into the map to visualize data representing different experiments. (b) Scatter plot of log ratios of the above mentioned transcripts represents the CS vs. air in ALI and smoker vs. non-smoker SAEC comparisons. (c) Venn diagram exhibiting the overlap within the above mentioned comparisons. Intersection represents transcripts deregulated in the same direction. (Gindele et al., 2020)

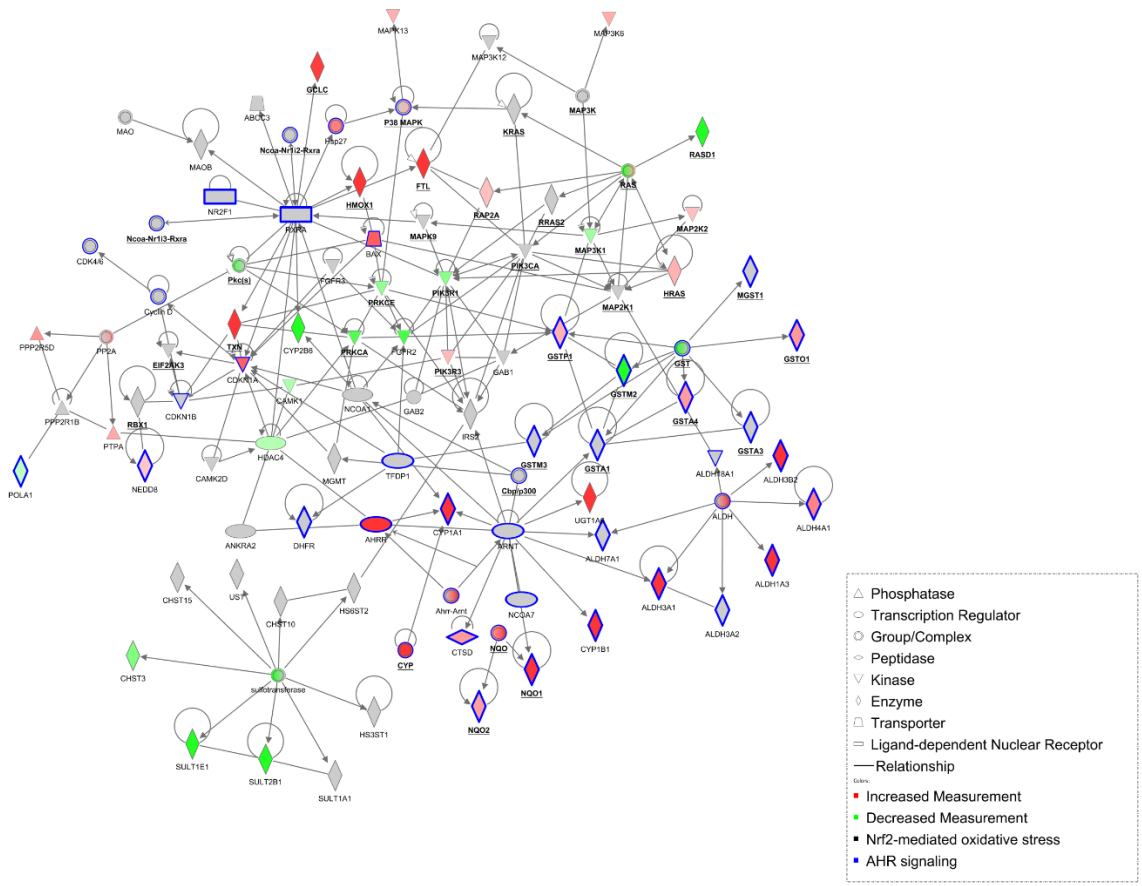

Figure 37: Cigarette smoke induces xenobiotic metabolism in the small airway epithelial cell (SAEC) air-liquid interface (ALI) culture as well as in smoking individuals. Network representation focusing on related transcripts (according to Ingenuity Pathway Analysis (IPA)) that are annotated as being involved in xenobiotic metabolism and are either deregulated in SAEC ALI cultures (*in vitro* model, GSE135188) or in SAEC from human smokers (*in vivo* data from epithelial brushes, GSE11784). Coloring indicates the deregulation in SAEC ALI cultures (red color = up-regulation; green = down-regulation; grey = deregulation in SAEC from human smokers only). Bold and underlined transcripts are associated with Nrf2-mediated oxidative stress; transcripts associated with AHR signaling are highlighted in blue. Network diagram was generated using the Ingenuity Pathway Analysis software. (Deregulation in SAEC from human smokers shown in Fig. 43.) (Gindele et al., 2020)

A pathway analysis was carried out to elucidate common smoke-induced mechanisms that are altered in CS-exposed *in vitro* ALI cultures and small airway epithelial brushes from smokers. To enable the identification of pathways that were altered in both data sets, the significantly deregulated transcripts with the same direction of change were combined. A core analysis with this set of transcripts was performed using Ingenuity Pathways Analysis (IPA). A considerable number of top scoring canonical pathways were categorized to "xenobiotic metabolism" (compare supplementary information, Tab. 8). Therefore, all transcripts reported to be associated with xenobiotic metabolism were extracted and used to create a combined network representing the *in vivo* and *in vitro* data (Fig, 37). Key deregulated canonical pathways associated with the network and consistent with *in vivo* data include Nuclear factor erythroid 2–related factor 2 (NRF2)-mediated oxidative stress, xenobiotic metabolism and aryl hydrocarbon (AHR) signaling (Figure 37 and Tab. 5).

Table 5: Common Cigarette Smoke (CS) Response Genes among *in vitro* and *in vivo* small airway epithelial cells (SAEC). Expression of Nuclear Erythroid 2-Related Factor 2 (Nrf2)-mediated oxidative stress response, Aryl Hydrocarbon Receptor (AHR) signaling and xenobiotic metabolism genes in healthy CS-exposed *in vitro* air-liquid interface (ALI) cultures and *in vivo* SAEC from human smokers. Transcripts as well deregulated in SAEC ALI cultures (GSE135188) as in SAEC from human smokers (GSE11784) are listed. Red color indicates up-regulation; green indicates down-regulation; bold font indicates statistically significant deregulation (q value < 0.05). Association to pathways were performed according to Ingenuity Pathways Analysis. (Gindele et al., 2020)

Pathway	Gene	*in vitro* ALI (Smoke vs. Air) Log FC	*in vivo* SAEC (Smoker vs. Nonsmoker) Log FC
Nrf2-mediated oxidative stress response	*EIF2AK3*	0,108	**0,312**
	FGFR2	**-0,786**	**-0,387**
	FGFR3	-0,403	**-0,565**
	FTL	**2,194**	**0,568**
	GAB1	**-0,332**	**-0,268**
	GAB2	-0,211	**-0,167**
	GCLC	**1,005**	**0,817**
	GSTA1	-0,197	**1,258**
	GSTA3	-0,736	**0,459**
	GSTA4	**0,510**	**0,299**
	GSTM2	**-1,136**	-0,314
	GSTM3	**0,683**	**0,724**
	GSTO1	**0,529**	0,073
	GSTP1	**0,388**	0,187
	HMOX1	**1,418**	-0,072
	HRAS	**0,400**	0,009
	IRS2	-0,266	**-0,554**
	KRAS	**0,235**	**0,286**
	MAP2K1	0,132	**-0,174**
	MAP2K2	**0,329**	0,104
	MAP3K1	**-0,398**	**-0,316**
	MAPK9	0,030	**-0,193**
	MGST1	**0,458**	**0,369**
	NQO1	**1,872**	**1,839**
	NQO2	**0,494**	-0,159
	PIK3CA	-0,063	**-0,277**
	PIK3R1	**-0,495**	-0,132
	PIK3R3	**0,352**	0,182
	PRKCA	**-0,733**	**-0,566**
	PRKCE	**-0,466**	**-0,274**
	RAP2A	**0,324**	0,224
	RASD1	**-1,424**	-0,161
	RBX1	0,129	**-0,195**
	RRAS2	**-0,213**	**-0,248**
	TXN	**1,336**	**0,546**
AHR signaling	*AHRR*	**3,662**	**0,969**
	ALDH18A1	**0,282**	**0,174**
	ALDH1A3	**1,840**	**0,564**
	ALDH3A1	**1,762**	**2,896**
	ALDH3A2	0,096	**0,293**
	ALDH3B2	**1,049**	-0,391
	ALDH4A1	**0,630**	0,073
	ALDH7A1	**-0,219**	**-0,331**
	ARNT	-0,120	**-0,218**
	BAX	**0,837**	-0,027
	CDKN1A	**0,817**	-0,003
	CDKN1B	-0,058	**-0,204**
	CTSD	**0,509**	0,294
	CYP1A1	**5,938**	**2,071**
	CYP1B1	**4,270**	**5,748**
	DHFR	-0,052	**-0,373**
	EIF2AK3	0,108	**0,312**
	FGFR2	**-0,786**	**-0,387**
	FGFR3	-0,403	**-0,565**
	FTL	**2,194**	**0,568**
	GAB1	**-0,332**	**-0,268**
	GAB2	-0,211	**-0,167**
	GCLC	**1,005**	**0,817**
	GSTA1	-0,197	**1,258**
	GSTA3	-0,736	**0,459**
	GSTA4	**0,510**	**0,299**
	GSTM2	**-1,136**	-0,314
	GSTM3	**0,683**	**0,724**
	GSTO1	**0,529**	0,073
	GSTP1	**0,388**	0,187
	HMOX1	**1,418**	-0,072
	HRAS	**0,400**	0,009
	IRS2	-0,266	**-0,554**
	KRAS	**0,235**	**0,286**
	MAP2K1	0,132	**-0,174**
	MAP2K2	**0,329**	0,104
	MAP3K1	**-0,398**	**-0,316**
	MAPK9	0,030	**-0,193**
	MGST1	**0,458**	**0,369**
	NCOA7	**-0,505**	**-0,422**
	NEDD8	**0,284**	0,057
	NQO1	**1,872**	**1,839**
	NQO2	**0,494**	-0,159
	NR2F1	-0,073	**0,594**
	PIK3CA	-0,063	**-0,277**
	PIK3R1	**-0,495**	-0,132
	PIK3R3	**0,352**	0,182
xenobiotic metabolism	*POLA1*	**-0,277**	-0,238
	PRKCA	**-0,733**	**-0,566**
	PRKCE	**-0,466**	**-0,274**
	RAP2A	**0,324**	0,224
	RASD1	**-1,424**	-0,161
	RBX1	0,129	**-0,195**
	RRAS2	**-0,213**	**-0,248**
	RXRA	-0,008	**-0,235**
	TFDP1	-0,033	**-0,327**
	TXN	**1,336**	**0,546**
	ABCC3	**0,310**	**1,419**
	AHRR	**3,662**	**0,969**
	ALDH18A1	**0,282**	**0,174**
	ALDH1A3	**1,840**	**0,564**
	ALDH3A1	**1,762**	**2,896**
	ALDH3A2	0,096	**0,293**
	ALDH3B2	**1,049**	-0,391
	ALDH4A1	**0,630**	0,073
	ALDH7A1	**-0,219**	**-0,331**
	ANKRA2	0,083	**-0,209**
	ARNT	-0,120	**-0,218**
	CAMK1	**-0,366**	-0,078
	CAMK2D	**-0,343**	**-0,419**
	CHST10	**-0,639**	**-0,575**
	CHST15	0,005	**0,807**
	CHST3	**-0,545**	**-0,421**
	CYP1A1	**5,938**	**2,071**
	CYP1B1	**4,270**	**5,748**
	CYP2B6	**-2,384**	-0,044
	EIF2AK3	0,108	**0,312**
	FGFR2	**-0,786**	**-0,387**
	FGFR3	-0,403	**-0,565**
	FTL	**2,194**	**0,568**
	GAB1		**-0,268**
	GAB2		**-0,167**
	GCLC	**1,005**	**0,817**
	GSTA1	-0,197	**1,258**
	GSTA3	-0,736	**0,459**
	GSTA4	**0,510**	**0,299**
	GSTM2	**-1,136**	-0,314
	GSTM3	**0,683**	**0,724**
	GSTO1	**0,529**	0,073
	GSTP1	**0,388**	0,187
	HDAC4	**-0,314**	**-0,577**
	HMOX1	**1,418**	-0,072
	HRAS	**0,400**	0,009
	HS3ST1	0,259	**-0,331**
	HS6ST2	**0,316**	**0,925**
	IRS2	-0,266	**-0,554**
	KRAS	**0,235**	**0,286**
	MAOB	-0,268	**-1,252**
	MAP2K1	0,132	**-0,174**
	MAP2K2	**0,329**	0,104
	MAP3K1	**-0,398**	**-0,316**
	MAP3K12	**-0,506**	**-0,382**
	MAP3K6	**0,421**	0,031
	MAPK13	**0,408**	0,24
	MAPK9	0,030	**-0,193**
	MGMT	-0,085	**-0,29**
	MGST1	**0,458**	**0,369**
	NCOA1	**-0,213**	**-0,226**
	NQO1	**1,872**	**1,839**
	NQO2	**0,494**	-0,159
	PIK3CA	-0,063	**-0,277**
	PIK3R1	**-0,495**	-0,132
	PIK3R3	**0,352**	0,182
	PPP2R1B	0,127	**-0,44**
	PPP2R5D	**0,542**	0,114
	PRKCA	**-0,733**	**-0,566**
	PRKCE	**-0,466**	**-0,274**
	PPP2R4	**0,438**	0,196
	RAP2A	**0,324**	0,224
	RASD1	**-1,424**	-0,161
	RBX1	0,129	**-0,195**
	RRAS2	**-0,213**	**-0,248**
	RXRA	-0,008	**-0,235**
	SULT1A1	-0,258	**0,368**
	SULT1E1	**-1,383**	-0,193
	SULT2B1	**-1,793**	-0,311
	TXN	**1,336**	**0,546**
	UGT1A6	**1,213**	**0**
	UST	-0,161	**-0,529**

3.4.3 Acute effects of CS on the small airway epithelium

To investigate the acute effects of CS on SAEC, fully differentiated ALI cultures were exposed to whole CS on four consecutive days (Fig. 38). In contrast to the previous setup, this model does not investigate the effects on the developing epithelium but the acute response to cigarette smoke in a mature setting. The aim was to assess, whether acute exposure to whole CS alters the epithelium in terms of barrier integrity and cell type composition and whether it induces oxidative stress and inflammatory processes.

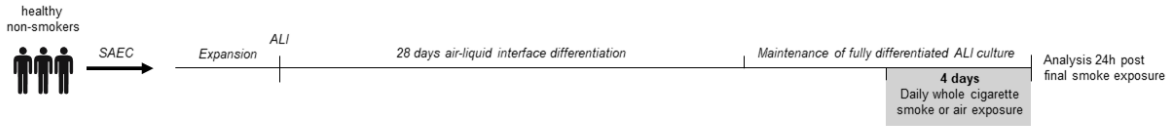

Figure 38: Experimental setup of acute cigarette smoke exposure. Small airway epithelial cells (SAEC) of three healthy non-smokers were cultivated until fully differentiated. On four consecutive days, cultures were exposed to whole cigarette smoke of four cigarettes a day. Readouts were performed 24 h after last smoke exposure.

Smoking has been demonstrated to damage the epithelial barrier (Kennedy et al., 1984; Shaykhiev et al., 2011). In the models described above with exposure of CSE and CS during differentiation, detrimental effects on barrier integrity were also observed. Therefore, TEER measurements were conducted after acute CS exposure of fully differentiated cultures for four days. Resistance was significantly reduced in CS-exposed cultures compared to air controls (Fig. 39a). A transcriptomic analysis of tight junction-associated genes was performed to investigate the underlying mechanisms leading to reduced barrier integrity. Junctional adhesion molecule (*JAM*) 2 and 3 were down-regulated upon CS exposure (Fig. 39b). In contrast, Casein Kinase 2 β (*CSNK2B*), claudin-10 (*CLDN10*) and claudin-3 (*CLDN3*) were up-regulated.

Ciliary function was not significantly affected by acute CS exposure, which was video-microscopically monitored (data not shown). Histological evaluation of formalin-fixed paraffin-embedded tissue slices showed no morphological differences after four days of intermittent CS exposure (data not shown). On transcriptional level, deregulation of marker genes was detected. Upon CS exposure, *KRT5*, *SCGB1A1*, and *FOXJ1* mRNA were decreased, whereas *MUC5AC* was increased (Fig. 40).

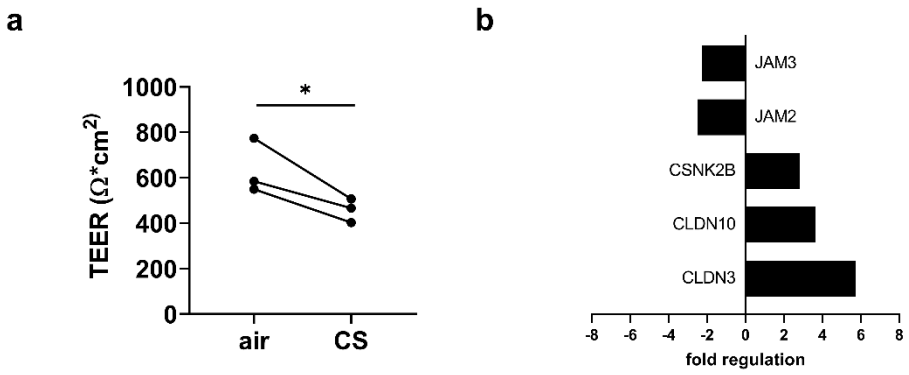

Figure 39: Assessment of barrier integrity after four days of cigarettes smoke (CS) exposure. (a) Transepithelial electrical resistance (TEER) measurements of either CS or air exposed cultures 24 h post last exposure. n=3 healthy controls. Statistical significance was assessed using paired one-tailed t-test. * for p value < 0.05; ** for p value < 0.01; *** for p value < 0.001. (b) Gene expression analysis of genes associated with tight junctions, using the RT2 profiler PCR array. Fold regulation of deregulated genes after four days of CS exposure compared to air controls. n=1 healthy control. *JAM* = junctional adhesion molecule, *CLDN* = claudin, *CSNK2B* = Casein Kinase 2 β.

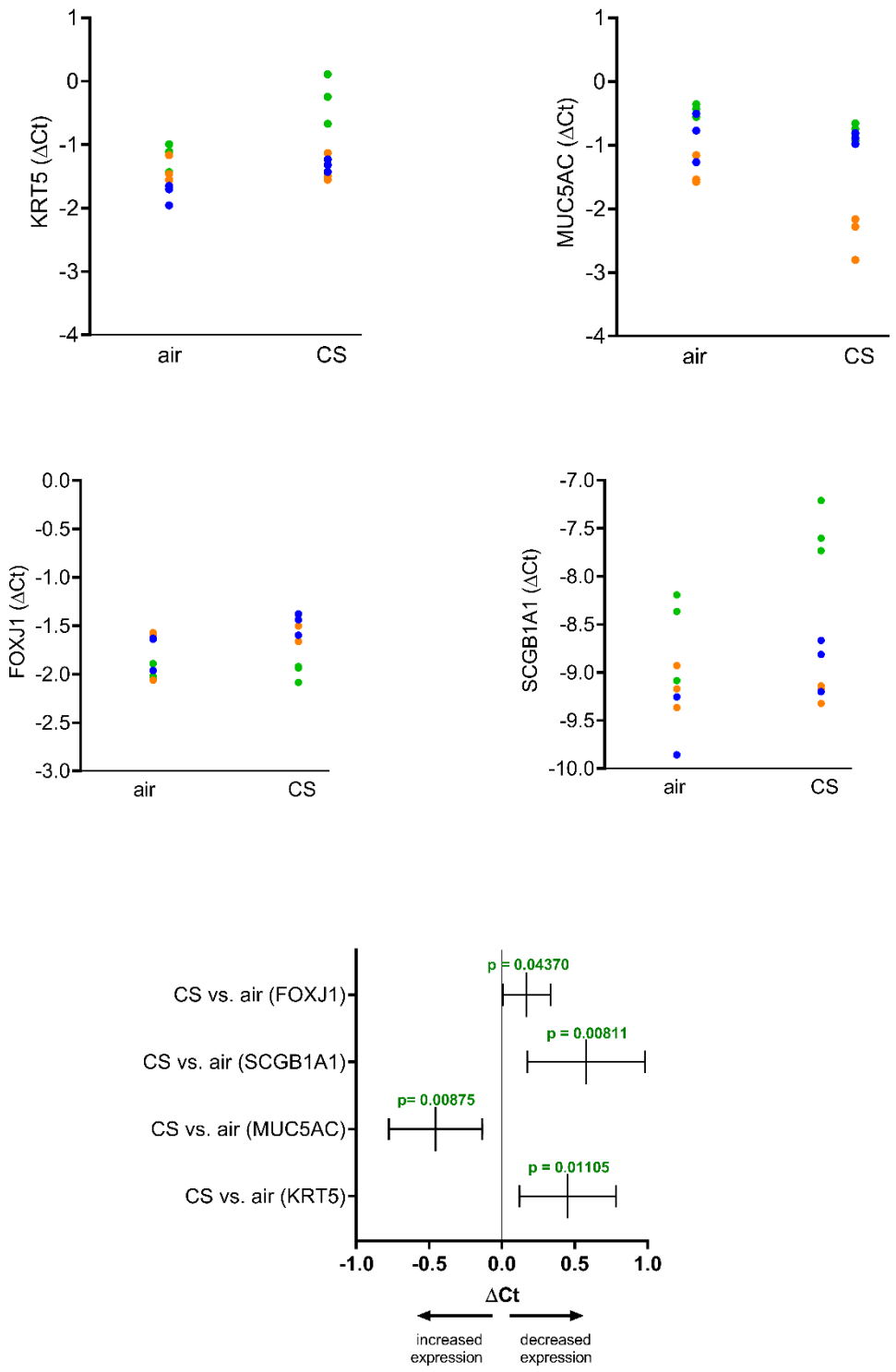

Figure 40: Gene expression analysis after cigarette smoke (CS) exposure. Small airway epithelial cell (SAEC) air-liquid interface (ALI) cultures from healthy donors (n=3) were exposed to whole CS on four consecutive days. Cells were lysed 24 hours post last exposure and Reverse Transcription Polymerase Chain Reaction (RT-PCR) analysis was performed. The data was analyzed with a mixed effect model. The forest plots show the point estimate for difference between the compared treatments with 95% confidence intervals. Exclusion of the null from the confidence interval corresponds to a p-value < 0.05 (highlighted in green). *KRT5* = Cytokeratin 5, *MUC5AC* = Mucin 5 AC, *SCGB1A1* = uteroglobin, *FOXJ1* = forkhead box protein J1.

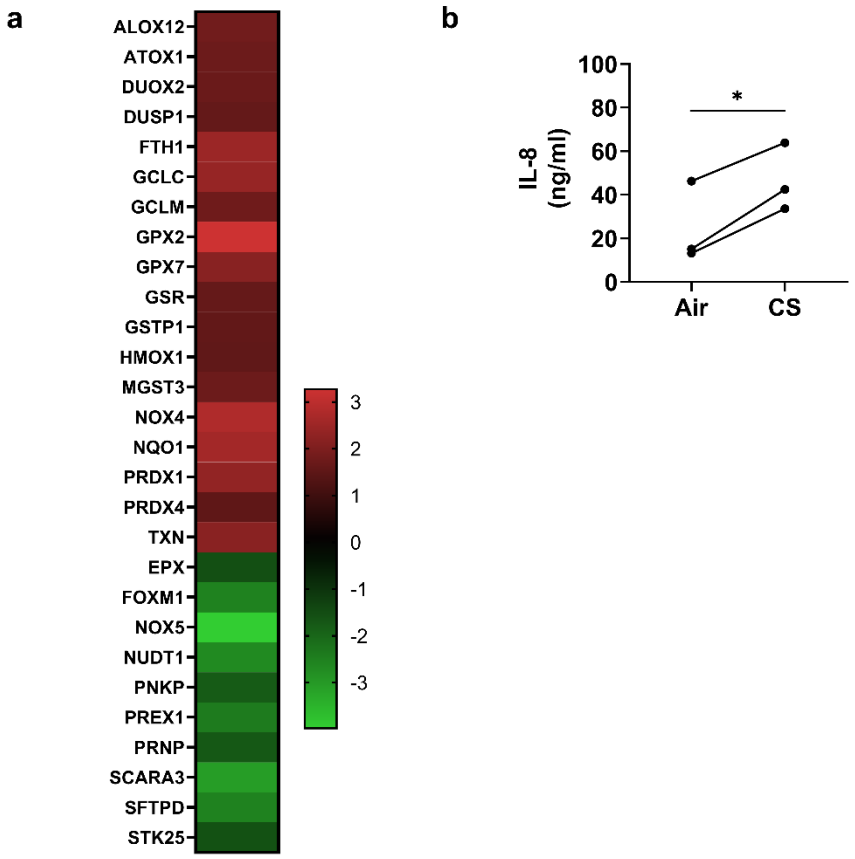

Figure 41: Cigarette smoke (CS) exposure induced oxidative stress response. (a) Gene expression analysis of transcripts, which are associated with oxidative stress using the RT2 profiler PCR array. Fold regulation of deregulated genes after four days of CS exposure compared to air controls. n=1 healthy control. (b) Interleukin-8 (IL-8) secretion of small airway epithelial cell (SAEC) air-liquid interface (ALI) cultures after four days of CS exposure compared to air controls (n=3). Significance was assessed using paired two-tailed t-test. * for p value < 0.05; ** for p value < 0.01; *** for p value < 0.001.

Previous studies have shown that acute exposure to cigarette smoke induces oxidative stress (Aoshiba et al., 2003; Cavarra et al., 2001; Guatura et al., 2000; Kharitonov et al., 1995; Morrison et al., 1999; Munakata et al., 2018). Accumulation of reactive oxygen species (ROS) can lead to chronic inflammation (Hussain et al., 2016). To assess whether these effects are induced in the newly established model of acute CS exposure, transcripts of genes, which are associated with oxidative stress were analyzed. Furthermore, the chemotactic and inflammatory cytokine interleukin-8 (IL-8) was measured in the supernatant (Baggiolini and Clark-Lewis, 1992). Gene expression analysis revealed a number of deregulated genes linked to oxidative stress (Fig. 41a) and CS exposure induced a significant increase in IL-8 secretion (Fig. 41b).

Transcriptional changes upon acute CS exposure were further analyzed by single cell RNA sequencing (data not shown).

3.5 Modulation of CS-induced effects on small airway epithelium

3.5.1 Modulation of CS-induced effects on SAEC differentiation

Olodaterol and roflumilast are approved drugs for the treatment of COPD (Gibb and Yang, 2013; Giembycz and Field, 2010). To assess whether these compounds also have beneficial effects on small airway remodeling, SAEC ALI cultures were intermittently exposed to CS in the presence or absence of 1 µM olodaterol, 100 nm roflumilast or a combination of both during the differentiation process.

Barrier integrity was shown to be reduced upon CS exposure (compare section 3.4.3). Neither olodaterol nor roflumilast nor a combination of both succeeded in preventing the reduction of TEER after 28 days of CS exposure (Fig. 42). Instead, compound treatment even seemed to result in a reduction of TEER (Fig. 42, air comparisons).

In order to assess whether the substances have an anti-inflammatory effect, IL-8 secretion was analyzed on day 28. IL-8 was significantly increased in CS-exposed cultures compared to air controls (Fig. 43). Compound treatment did not lead to a reduction in IL-8 release.

In section 3.4.2.6, it was shown that CS exposure impairs ciliary function. To investigate whether olodaterol or roflumilast can prevent the defective development of ciliated cells, cilia function was measured using video-microscopy. Area covered by actively beating cilia and cilia frequency were calculated. Neither olodaterol nor roflumilast nor a combination of both improved ciliary function by day 28 (Fig. 44-45). Taken together, treating SAEC ALI cultures with olodaterol and roflumilast did not prevent the CS-induced decline in barrier integrity and ciliary function, and the induction of inflammatory responses.

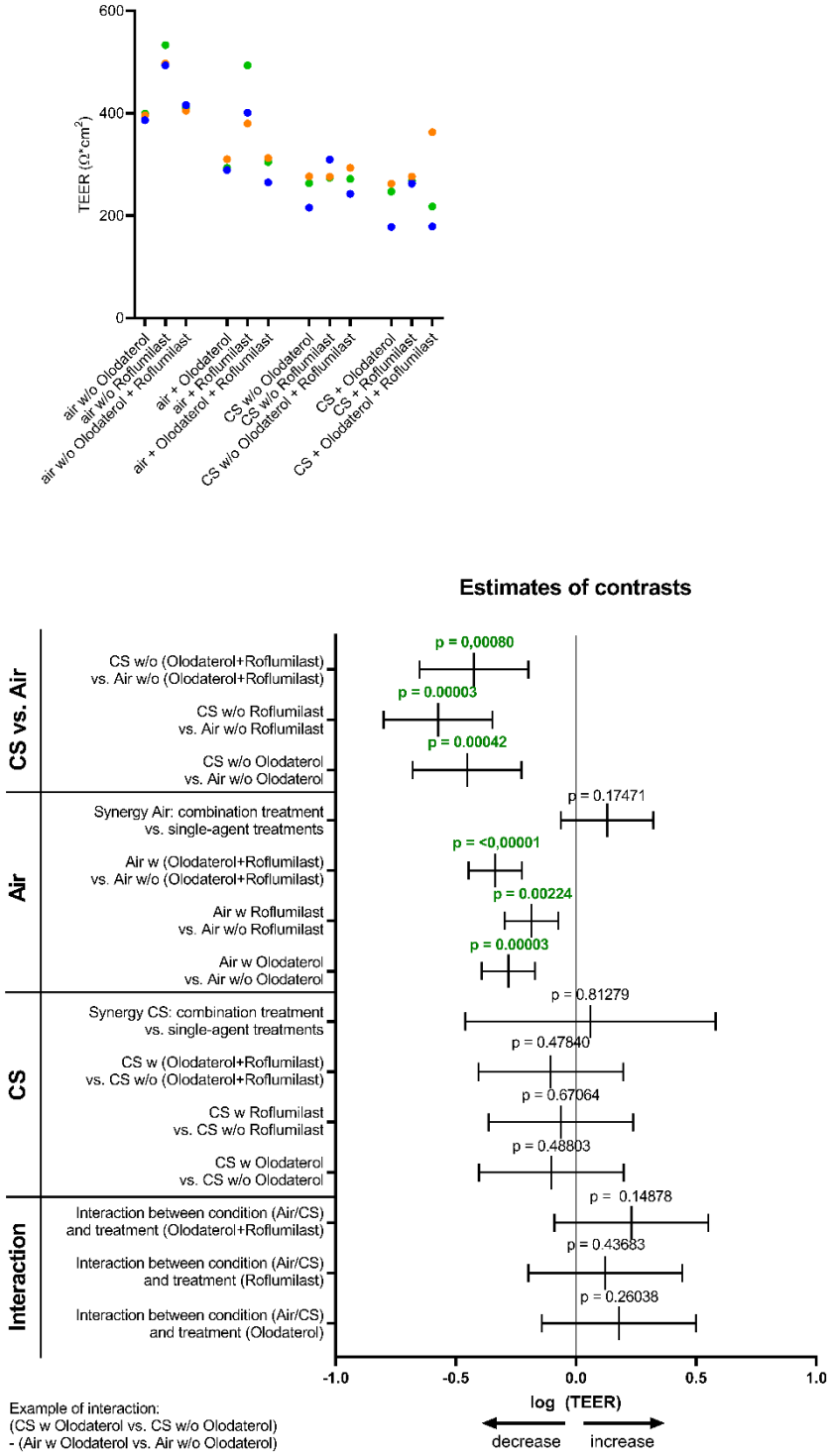

Figure 42: Modulation of cigarette smoke (CS)-induced effects with either 1 µM Olodaterol, 100 nM Roflumilast, or a combination of both. Transepithelial electrical resistance (TEER) measurements after 28 days of intermittent exposure to CS or air as control with or without compound treatment. Experiments were conducted with n=3 healthy donors. The data was analyzed with a mixed effect model. The forest plots show the point estimate for difference between the compared treatments with 95% confidence intervals. Exclusion of the null from the confidence interval corresponds to a p-value < 0.05 (highlighted in green). w = with; w/o = without.

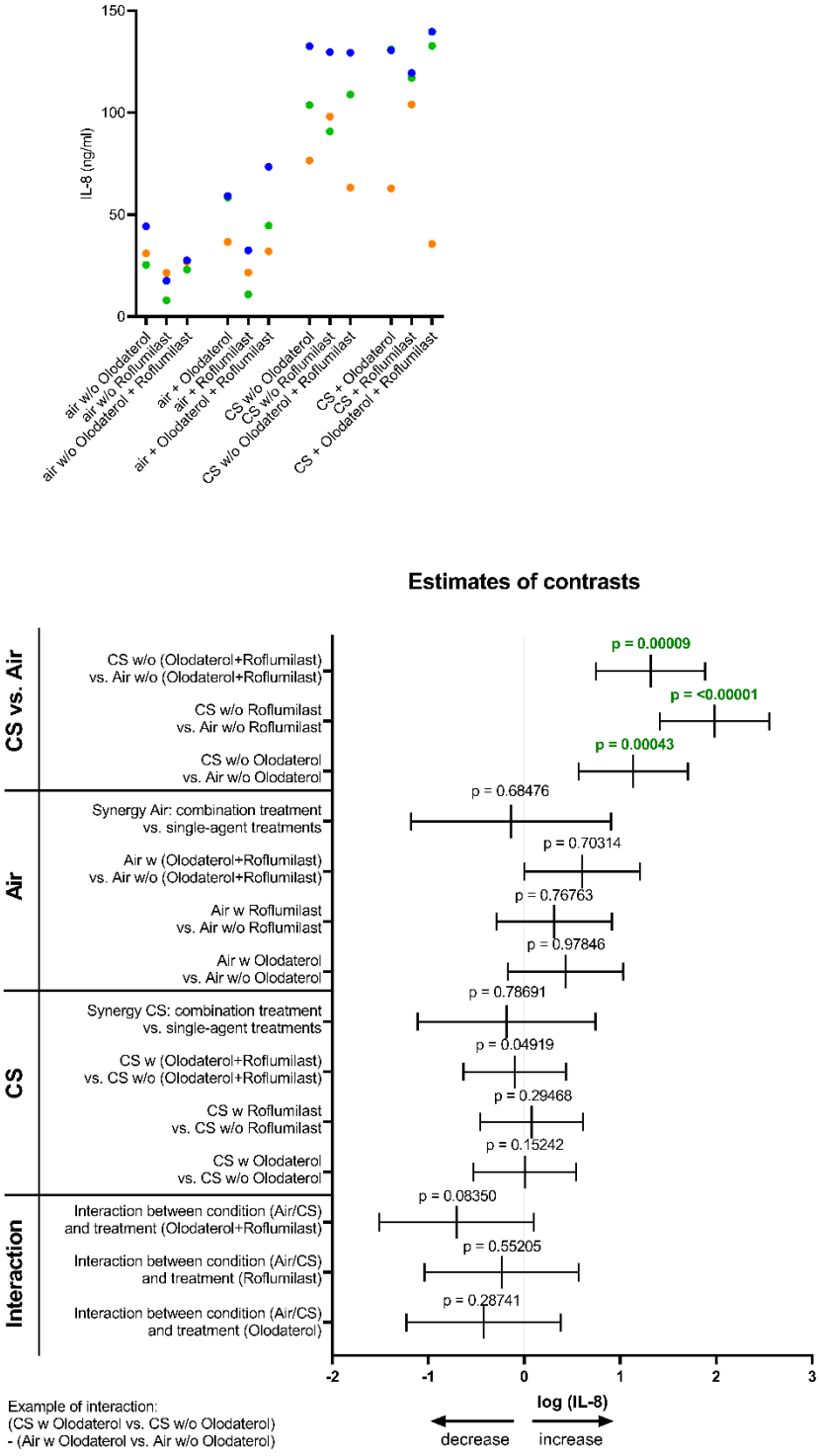

Figure 43: Modulation of cigarette smoke (CS)-induced effects with either 1 µM Olodaterol, 100 nM Roflumilast, or a combination of both. Interleukin-8 (IL-8) concentration in basolateral medium measured on day 28 after intermittent exposure to CS or air as control with or without compound treatment. Experiments were conducted with n=3 healthy donors. The data was analyzed with a mixed effect model. The forest plots show the point estimate for difference between the compared treatments with 95% confidence intervals. Exclusion of the null from the confidence interval corresponds to a p-value < 0.05 (highlighted in green). w = with; w/o = without.

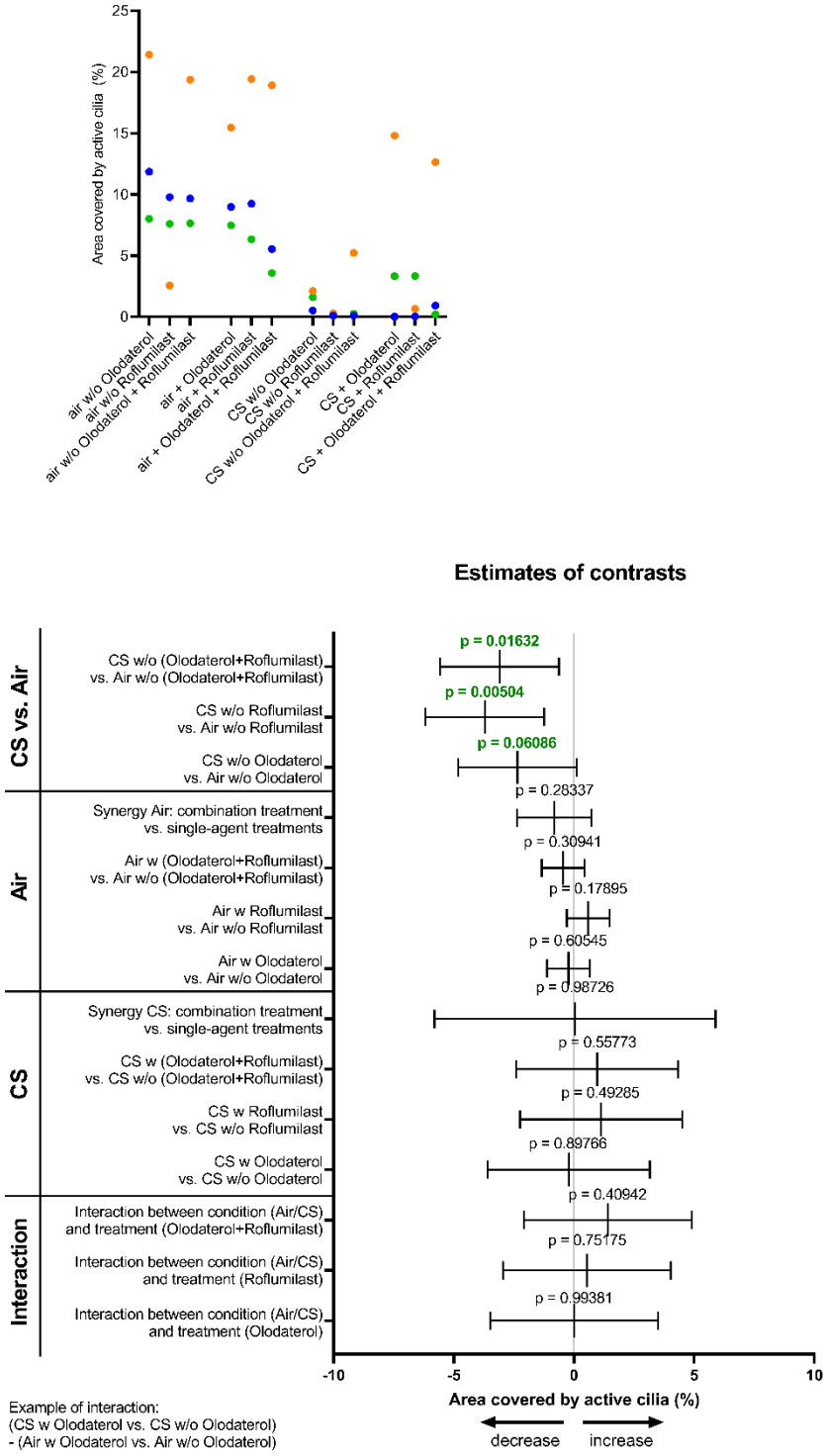

Figure 44: Modulation of cigarette smoke (CS)-induced effects with either 1 µM Olodaterol, 100 nM Roflumilast, or a combination of both. Functional cilia beat measurement on day 28 after intermittent exposure to CS or air as control with or without compound treatment. Area covered by actively beating cilia was analyzed by means of video-microscopy. Experiments were conducted with n=3 healthy donors. The data was analyzed with a mixed effect model. The forest plots show the point estimate for difference between the compared treatments with 95% confidence intervals. Exclusion of the null from the confidence interval corresponds to a p-value < 0.05 (highlighted in green). w = with; w/o = without.

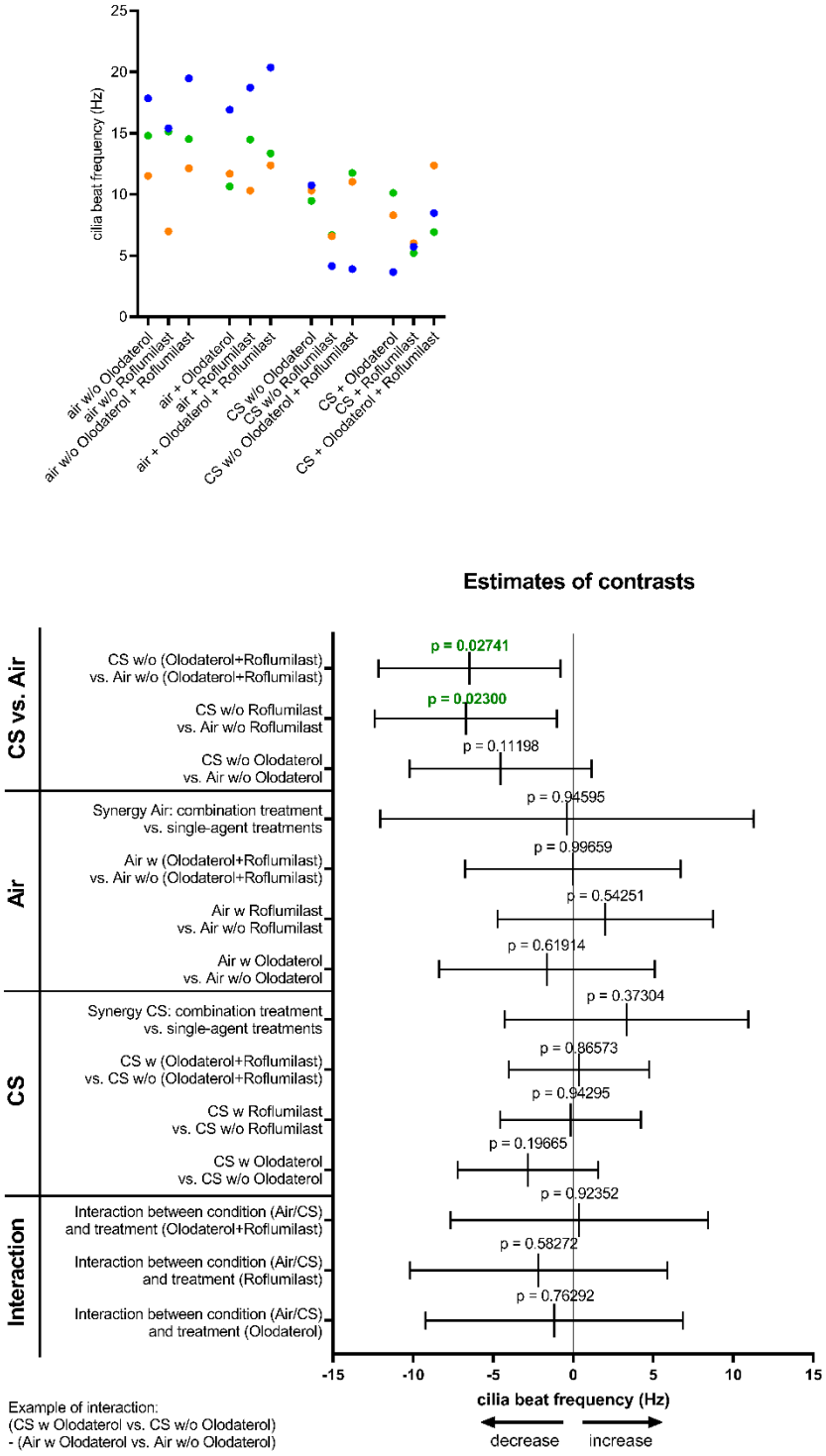

Figure 45: Modulation of cigarette smoke (CS)-induced effects with either 1 µM Olodaterol, 100 nM Roflumilast, or a combination of both. Functional cilia beat measurement on day 28 after intermittent exposure to CS or air as control with or without compound treatment. Cilia beat frequency was analyzed by means of video-microscopy. Experiments were conducted with n=3 healthy donors. The data was analyzed with a mixed effect model. The forest plots show the point estimate for difference between the compared treatments with 95% confidence intervals. Exclusion of the null from the confidence interval corresponds to a p-value < 0.05 (highlighted in green). w = with; w/o = without.

3.5.2 Modulation of acute effects of CS on SAEC

Acute CS exposure adversely affects TEER in SAEC ALI cultures (compare section 3.4.3). Previously, several compounds have been described to restore barrier integrity (compare Tab. 6). To test their efficacy in the acute CS exposure model, fully differentiated SAEC were treated with these compounds followed by CS exposure on four consecutive days. TEER was measured 24 hours after the last exposure.

Table 6: Treatment options to restore barrier integrity after cigarette smoke (CS)-induced injury.

Compound	Target/Function	Conc.	Reported Effects	Reference
N-acetyl-cysteine (NAC)	ROS scavenger (PDK1, Akt)	15 mM	Regulates claudin-18 expression; Protects intestinal barrier function under LPS challenge	(Lee et al., 2020; Lee and Kang, 2019)
Trolox	ROS scavenger	10 µM	Reduces oxidative stress and increases TEER	(Messier et al., 2013; Vergauwen et al., 2015)
PKD inhibitor (kb-NB142-70)	PKD3	1 µM	Increases TEER and CLDN1 expression upon calcium depletion	(Gan et al., 2014)
EGF	EGFR	0,8 nM	Increases TEER and ZO-1 expression upon CS exposure	(Xiao et al., 2011)
Gefitinib	EGFR inhibitor	3 µM	No positive effects on TEER reported	
TGFβ	TGFβ receptor	5 ng/ml	Increases ZO-1 and ZO-2 expression and prevents TEER reduction upon CS exposure	(Schamberger et al., 2014)
Olodaterol	anti-inflammatory	1 µM	Increases TEER upon RSV infection	(Singhera et al., 2017)
Roflumilast	cAMP	100 nM	Prevents E-cadherin and ZO-1 downregulation upon CS exposure	(Milara et al., 2015; Milara et al., 2013; Milara et al., 2014)
AHR antagonist (CH-223191)	AHR	500 nM	inhibits tryptophan metabolite-derived indoxyl sulfate-induced endothelial hyperpermeability	(Assefa et al., 2019)

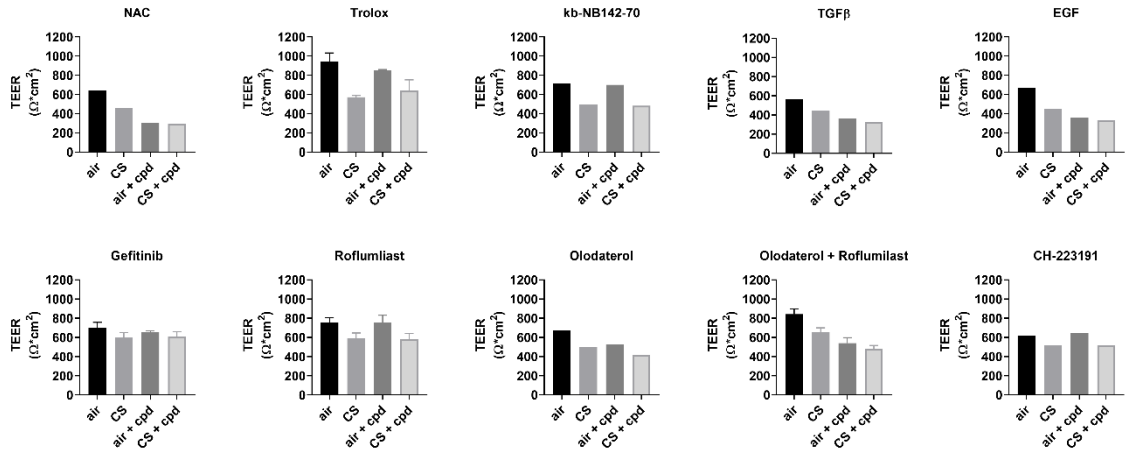

Figure 46: Transepithelial electrical resistance (TEER) measurements of small airway epithelial cell (SAEC) air-liquid interface (ALI) cultures. Fully differentiated SAEC cultures were exposed to either cigarette smoke (CS) or air in the presence or absence of different compounds (cpd) on four consecutive days. Analysis was performed 24 hours after the last CS exposure. Experiments were performed with n=1 or n=3 healthy donors, data is represented as mean or mean ± SEM, respectively. NAC = N-acetyl cysteine; kb-NB142-70 = protein kinase D (PKD) inhibitor; TGFβ = transforming growth factor beta; EGF = epidermal growth factor; CH-223191 = aryl hydrocarbon receptor (AHR) antagonist.

In this initial study, the data suggest that none of the tested substances succeeded in preventing the decrease in barrier integrity (Fig. 46).

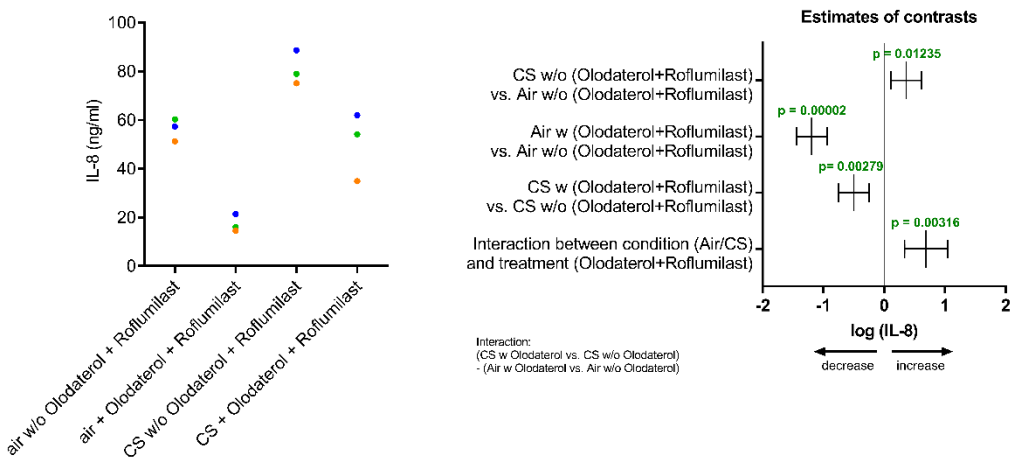

Figure 47: Interleukin-8 (IL-8) secretion of SAEC ALI cultures treated with a combination of 1 µM Olodaterol and 100 nm Roflumilast and CS exposure for four days (n=3 healthy donors). The data was analyzed with a mixed effect model. The forest plots show the point estimate for difference between the compared treatments with 95% confidence intervals. Exclusion of the null from the confidence interval corresponds to a p-value < 0.05 (highlighted in green). w = with; w/o = without.

IL-8 secretion was significantly increased upon acute CS exposure (compare section 3.4.3). A combination of Olodaterol and Roflumilast reduced the level of IL-8 in the basolateral medium of CS-exposed cultures as well as in the air controls (Fig. 47).

4 Discussion

4.1 Cultivation of small airway epithelium in vitro

The small airways are strongly affected in COPD (Higham et al., 2019; Hogg et al., 1968). However, there is still no effective therapy for COPD patients that prevents disease progression and targets the pathologic remodeling and aberrant repair processes in the small airway epithelium (Singh, 2017). Hence, there is a high unmet medical need and a demand to investigate the underlying pathophysiological mechanisms leading to aberrant basal cell differentiation in the small airways. At present, most *in vitro* models of COPD use tracheal or bronchial epithelial cells. However, the small airway epithelium is more relevant for COPD. For this purpose, a novel *in vitro* system was developed that models the human small airways. The newly established protocol allows cultivation of human SAEC *in vitro*, which enables the investigation of site-specific processes in the small airways. This clearly distinguishes it from previous *in vitro* models that focus mainly on the bronchial epithelium.

The current study demonstrated that ALI cultures from human SAEC exhibit a two-layered pseudostratified epithelium closely resembling the human small airway *in vivo*. This is a remarkable achievement, as previous *in vitro* models lacked the necessary translatability to the *in vivo* situation. The new protocol enables SAEC from non-smokers and COPD smokers to be cultured *in vitro* with the latter showing some conserved pathological characteristics. COPD-derived ALI cultures exhibit a less ciliated, more secretory epithelium with a distinct gene signature. A classification analysis using the gene signature of healthy and COPD-derived ALI cultures with *in vivo* samples of small airway epithelial brushes revealed a high classification power and thus a high predictability of the health status. The fact that disease-specific properties are conserved in the basal cells of the small airways was demonstrated for the first time. So far, this was only shown for bronchial epithelial cultures (Comer et al., 2013; Gohy et al., 2015; Milara et al., 2013; Pierrou et al., 2007).

A limiting factor of experiments with primary cells is the availability of donors. At the initiation of the studies, no more than three different COPD donors were available. Unfortunately, no information was provided on the disease severity of the respective patients. Hence, heterogeneity of donors was challenging. Nevertheless, the detailed characterization of the SAEC ALI cultures revealed a robust signature that clearly distinguishes ALI cultures from healthy non-smokers and COPD smokers. A potential solution for the limitation of primary cells could be the use of a recently published immortalized small airway basal cell line or the use of induced pluripotent stem cell derived cultures (Schruf et al., 2020; Wang et al., 2019).

Taken together, the newly established SAEC culture model shares key characteristics seen in human airways *in vivo*, such as a pseudostratified morphology comprising basal, club, goblet and ciliated cells, a tight epithelial barrier, functional ciliary beating and a distinct gene signature. This provides an important basis for epithelial research in the future. Of note, with the developed *in vitro* system it is possible to investigate the remodeling of the epithelium selectively. It is well known that other cell populations, including leukocytes,

fibroblasts, endothelial cells etc. play an essential role in the pathology of COPD. For further studies the here developed SAEC model may be a good starting point for the establishment of co-culture systems to investigate the role of cellular crosstalk on epithelial remodeling.

4.2 Induction of COPD-relevant phenotypes in SAEC cultures

4.2.1 Cigarette smoke extract (CSE) and EGF induce COPD-relevant phenotypes

Cigarette smoke is the major risk factor to develop COPD (Laniado-Laborin, 2009; Lozano et al., 2012; Yoshida and Tuder, 2007). Differentiation of SAEC under CSE treatment resulted in a reduction of TEER, indicating an impaired epithelial barrier formation. This reflects the reduced barrier function and increased susceptibility to infections seen in COPD patients (Aghapour et al., 2018; Heijink et al., 2014; Jafarinejad et al., 2017; Leung et al., 2017; Yi et al., 2018). Although CSE contains only soluble components of CS, the model was successful in inducing this COPD-relevant phenotype, a finding that is in accordance with a previous study investigating the effect of CSE on bronchial epithelial cells (Schamberger et al., 2015).

As described in section 1.4.4, aberrant EGFR signaling plays a decisive role in the pathology of COPD. EGF induced a concentration-dependent thickening of the epithelium and an increase in secretory cells in SAEC ALI cultures. This is consistent with aberrant basal cell differentiation and goblet cell metaplasia, which are key features of COPD airways (Lumsden et al., 1984; Polosukhin et al., 2017; Saetta et al., 2000; Shaykhiev and Crystal, 2014a). EGFR inhibition by gefitinib prevented the effects.

EGF is elevated in the airway epithelium of smokers compared to non-smokers (Shaykhiev et al., 2013). To investigate possible interactions between the increased EGF concentration and smoke exposure, SAEC were treated with a combination of both, CSE and EGF. Interestingly, the combined treatment induced epithelial thickening in a way that exceeded the calculated additive effect of EGF and CSE ($p=0.05697$). The selective EGFR inhibitor gefitinib was able to prevent both epithelial thickening and hyperplasia of secretory cells, indicating that these effects might be triggered by EGFR signaling. Expression of pEGFR tended to be increased after stimulation with EGF for 5 minutes, which is consistent with previous studies (Shaykhiev et al., 2013). The combination of EGF and CSE did not lead to an increase in pEGFR, suggesting a CSE-induced amplification of EGFR signaling by downstream regulators. Possibly, CSE interacts with the EGF-EGFR-axis via NADPH oxidase (NOX)-mediated reactive oxygen species (ROS) signaling pathways (Weng et al., 2018). The combined treatment of EGF and CSE enhanced signal transduction downstream of PI3K/AKT, and gefitinib prevented the increase in pGSK3 and p-p70S6K. This is to some extent consistent with previous studies on lung cancer cells, which showed that EGF induces phosphorylation of downstream targets after 20 minutes, which could be moderately inhibited by 3 µM gefitinib (Gao et al., 2007). Other downstream modulators, such as MEK, ERK or STATs, were not significantly increased after EGF/CSE treatment in our

experimental setting. These results indicate that CSE-induced oxidative stress might boost EGFR via the GSK3 and p70S6K pathways (Fig. 24). Of note, phosphorylation of AKT was not significantly increased leading to the hypothesis that ROS-induced Wingless/integrase-1 (WNT) signaling might be responsible for the increase in pGSK3. Previous studies suggested that NOX1 modulates the WNT pathway by inhibiting the redox-sensitive association of nucleoredoxin (NRX) with dishevelled (Dvl) (Coant et al., 2010; Funato et al., 2006). It remains to be investigated whether this triggers the translocation of β-catenin into the cell nucleus, which was previously associated with epithelial-to-mesenchymal transition (EMT) and cancer (Lee et al., 2010; Paul et al., 2013; Zou et al., 2013). The whole study is based on samples from three healthy donors. The results are of an exploratory nature and should be used for the generation of hypotheses that have to be tested in an additional (larger) study.

Nevertheless, the findings suggest a therapeutic benefit of EGFR inhibitors in COPD airways by reducing airway obstruction and mucus hypersecretion. However, EGFR signaling plays a central role in normal tissue homeostasis (Shaykhiev et al., 2013; Vallath et al., 2014; Vermeer et al., 2003). Inhibition of this vital pathway in a healthy setting might be detrimental in terms of normal differentiation and repair. Gefitinib treatment in control cultures resulted in a rather thinner, less differentiated epithelium, indicating the adverse impact of rigorous EGFR inhibition. The use of EGFR inhibitors in the treatment of COPD therefore remains a challenge and needs further refinement to enable tissue homeostasis while preventing excessive signaling that induces pathological features. So far, targeting the EGFR pathway has only been shown to be clinically beneficial in the treatment of lung cancer. However, the potential of EGFR antagonism has not yet been fully explored.

4.2.2 Whole cigarette smoke induces COPD-relevant epithelial remodeling

4.2.2.1 Cigarette smoke alters small airway epithelial differentiation

The previously described CSE model comprises only soluble components of CS. Volatile substances get lost during CSE preparation. Hence, CSE does not sufficiently represent the complexity of cigarette smoke. Furthermore, basolateral administration does not reflect physiological exposure of CS. To optimize these limitations, another *in vitro* model was established, which allows exposure to whole CS. With the Professional In-Vitro Technologies (P.R.I.T.) Expo Cube (Fraunhofer Institute for Toxicology and Experimental Medicine, Hannover), cells can be exposed to CS from the apical side of the epithelium. This allows CS administration in a physiological way.

Aberrant basal cell differentiation is a key driver in the pathogenesis of COPD (Rock et al., 2010; Shaykhiev and Crystal, 2014a). To understand the impact of CS on the differentiation of SAEC basal cells, ALI cultures derived from three healthy non-smokers and three COPD smokers were intermittently exposed to whole CS during the differentiation process. Several genes associated with basal and squamous metaplasia were increased in SAEC ALI cultures after 28 days of intermittent CS exposure, namely *KRT5, KRT6A, KRT13, KRT14* and *SFN.*

These findings are in accordance with previous publications investigating histological and transcriptional alterations in COPD basal cells. They suggest basal cells to be the first cell population affected by CS, resulting in an altered differentiation and therefore an aberrant architecture of the small airway epithelium (Auerbach et al., 1961; Ghosh et al., 2017). Basal cell hyperplasia and squamous metaplasia play a major role in the development of airway obstruction in COPD (Hogg et al., 1968) and increase the risk of developing squamous cell carcinoma (Barnes and Adcock, 2011; de Torres et al., 2011; Papi et al., 2004). The bronchial epithelium of COPD patients shows more squamous metaplasia compared to healthy smokers (Rigden et al., 2016). Taken together, the established *in vitro* CS model allows the study of the molecular mechanisms underlying the early effects of CS on basal cell proliferation.

The model was also capable of reproducing further pathophysiological changes: Goblet cell markers, such as *MUC5AC*, were increased upon CS treatment, whereas club cell markers (*SCGB1A1*, *CYP2F1*) were reduced. Furthermore, a downward trend of $MUC5AC^{-}$ /$SCGB1A1^{+}$ cells was observed on protein level. There is evidence that smoking induces changes in the abundance of secretory cell populations, leading to goblet cell hyperplasia and a loss of club cells (Lumsden et al., 1984; Rokicki et al., 2016). Previous studies suggested that the hyperplasia of goblet cells found in COPD patients is associated with current smoking (Kim et al., 2015; Saetta et al., 2000). Small airway differentiation in smokers and COPD patients appears to be altered towards a more proximal phenotype (Burgel et al., 2011; Cosio et al., 1980); an effect recently described as smoking-dependent distal-to-proximal repatterning (Yang et al., 2017). Goblet cells were present in the small airway epithelium of smokers, where they are normally absent (Saetta et al., 2000). Furthermore, in the airways of smokers and COPD patients, a reduced number of club cells is present, indicating lower uteroglobin (SCGB1A1) serum levels that correlate with a decrease in FEV1 (Forced Expiratory Volume in 1 Second) and disease progression (Ghosh et al., 2017; Lomas et al., 2008; Lumsden et al., 1984; Park et al., 2013). Other smoking models using CSE have not seen a reduction in the number of club cells (Schamberger et al., 2015). There is evidence that apical exposure of ALI cultures to whole CS better reflects physiological administration and thus better represents the pathophysiological processes induced by smoking. Hence, the model may be helpful to investigate the molecular mechanisms that lead to an altered differentiation of basal cells in COPD patients (Knabe et al., 2015; Laucho-Contreras et al., 2015; Park et al., 2013; Rokicki et al., 2016; Shijubo et al., 1997).

CS exposure during SAEC differentiation led to an impaired development of ciliated cells, resulting in reduced ciliary function. This reflects the pathophysiological decline of ciliated cells in COPD airways (Hessel et al., 2014; Lam et al., 2013; Rennard, 2003; Yaghi and Dolovich, 2016; Yaghi et al., 2012), Mucociliary clearance in COPD patients is often insufficient, leading to severe exacerbations due to bacterial or viral infections (Leung et al., 2017; Randell and Boucher, 2006). These findings are also in line with a study investigating the effect of CSE on human bronchial epithelial cells (Schamberger et al., 2015).

CS affected the epithelial barrier formation in SAEC ALI cultures, measured by a decrease in TEER. This smoke-induced TEER reduction was also seen in exposure models with CSE (compare section 3.2) (Schamberger et al., 2014) and mimics the reduced airway epithelial barrier function in COPD airways. A hallmark that is linked to an increased susceptibility to viral and bacterial infections (Aghapour et al., 2018; Heijink et al., 2014; Jafarinejad et al., 2017; Leung et al., 2017; Yi et al., 2018). The functional impairment of barrier integrity may be related to the deregulation of several genes associated with cell-cell contact, permeability and tight junctions. Claudins are important tight junctions proteins and play a key role in paracellular permeability (Gunzel and Yu, 2013). Some claudin family members were seen to be deregulated upon CS exposure. Claudin-11 and -18, which are barrier-forming claudins that help to maintain barrier integrity, were down-regulated in CS-exposed ALI cultures (Gunzel and Yu, 2013; Koval, 2013; Soini, 2011). Claudin-18 deficiency has also been reported in association with airway epithelial barrier dysfunction and asthma (Sweerus et al., 2017). The pore-forming claudin-10 was up-regulated upon CS exposure, a finding that was also validated at protein level (Gunzel et al., 2009; Koval, 2013). A previous study showed increased claudin-10 and claudin-7 expression in smokers and COPD smokers in a transcriptomic approach (Shaykhiev et al., 2011). JAM family members are involved in tight junction formation (Zhao et al., 2016). *JAM3* was decreased in CS-exposed cultures and was shown to be also reduced in COPD airways (Shaykhiev et al., 2011). In conclusion, several genes associated with the regulation of epithelial barrier function were deregulated in CS-exposed ALI cultures, which may be related to the pathogenesis of COPD.
To assess the extent to which the established CS *in vitro* model reflects smoking-induced effects on the epithelium of the small airways in living humans, a comparative transcriptomic analysis of SAEC ALI cultures and human small airway epithelial brushes was performed. Remarkably, SAEC ALI cultures exposed to CS showed a gene expression pattern that overlaps with epithelial samples from healthy smokers. When combining both data sets and performing a hierarchical clustering of overlapping deregulated transcripts, one would expect similar patterns, but not that the *in vivo* data and the *in vitro* data form separate clusters. It is noteworthy that smoked SAEC ALI cultures clustered with samples from smokers, while air-treated SAEC ALI cultures clustered with healthy control samples. In this approach, we did not include mechanisms that were only altered *in vitro* and not *in vivo* or vice versa, but we focused on processes that were modulated in both situations. The results underline the existence of common processes showing a corresponding deregulation, i.e. a similar up- or down-regulation *in vitro* and *in vivo*. This suggests that the CS-exposed SAEC ALI culture is a valuable *in vitro* method to investigate smoke-induced effects on epithelial differentiation. Furthermore, a performed single cell RNA sequencing analysis that was performed with suspension from smoked SAEC ALI cultures will lead to a more detailed understanding on the cell specific mechanisms and underlying molecular pathways that are triggered by CS.

The model does not allow distinguishing between ALI cultures derived from healthy controls and cultures derived from COPD patients, since CS is the main driver of differential expression. The dissection of potential differences between CS-exposed healthy and CS-exposed COPD-derived ALI cultures would require a much higher number of donors. This

is a clear limitation of the complex experimental *in vitro* setup. Nevertheless, COPD-derived ALI cultures may be extremely helpful in testing whether potential therapeutic concepts also work in a diseased setting.

Pathway analysis revealed the top deregulated canonical pathways in CS-exposed ALI cultures, including Nuclear factor erythroid 2–related factor 2 (NRF2)-mediated oxidative stress, xenobiotic metabolism and aryl hydrocarbon receptor (AHR) signaling, all of which were associated with smoking (Guerrina et al., 2018; Huang et al., 2005; Nebert et al., 2000; Yun et al., 2017). Smoking is known to induce reactive oxygen species that activate the Nrf2 signaling pathway (Huang et al., 2005; Sajadimajd and Khazaei, 2018). CS covers a range of toxic chemicals including polycyclic aromatic hydrocarbons (PAHs), such as benzo[a]pyrene, which activates the AHR signaling pathway and induces the expression of several metabolic enzymes, including *CYP1A1*, *CYP1A2* and *CYP1B1* (Miller and Ramos, 2001; Nebert et al., 2000; Stedman, 1968). The model reflects these CS-induced pathways in a manner closely related to the *in vivo* situation and offers new possibilities for the investigation of new therapeutic targets that address the response to oxidative stress and xenobiotic metabolism. Inconsistencies with the *in vivo* data were strongly associated with lipid metabolism (e.g. cholesterol biosynthesis).

The results of this in-depth characterization of smoke-exposed ALI cultures show that CS exposure specifically alters the small airway epithelium by affecting basal cell differentiation. Important signaling pathways are deregulated in the same way as in the small airways of human smokers. Taken together, the model mimics critical pathophysiological and molecular effects described in the small airways of smokers *in vitro*, which could lead to new essential therapeutic approaches to restore impaired epithelial repair mechanisms in a smoke-induced chronic disease like COPD.

4.2.2.2 Cigarette smoke induces acute responses in the small airway epithelium

It was previously shown that epithelial barrier function is impaired by CS exposure (compare section 3.2 and section 3.4.2.3). To assess whether this is also true in an acute experimental setting, SAEC were exposed to whole CS on four consecutive days. Resistance measurements revealed a drop in TEER, indicating reduced barrier integrity. A transcriptome analysis was conducted to evaluate regulation of genes coding for tight junction proteins. This analysis was based on the data of a single donor and requires further confirmatory testing. Nevertheless, the results provide first evidence for a possible smoke-induced regulation of junctional genes. *JAM2* and *JAM3* were down-regulated after four days of intermittent CS exposure. *JAM2* was also found to be downregulated in lung tumor tissue, which was associated with a decrease in tight junctions and the occurrence of metastases (Zhao et al., 2016). *JAM3* was already described to be down-regulated upon CS exposure during differentiation (compare section 3.4.2.3) and was shown to be reduced in COPD airways (Shaykhiev et al., 2011). Casein kinase II subunit beta (*CSNK2B*) mRNA expression was increased upon CS treatment. Casein kinase II was reported to be a critical regulator of epithelial homeostasis. It was shown to be up-regulated in chronic intestinal inflammation

and was associated with barrier defects seen in inflammatory bowels disease (Koch et al., 2013). In contrast to a previously published transcriptome analysis of small airway samples from human non-smokers and smokers, claudin-3 was increased upon CS exposure in the current model (Shaykhiev et al., 2011). Expression of the pore-forming claudin-10 was increased, which is consistent with previous analyses (compare section 3.4.2.3) (Shaykhiev et al., 2011).
Already after four days of CS exposure, a deregulation of cell markers was visible. The expression of MUC5AC was increased whereas the expression of SCGB1A1 and FOXJ1 was decreased. These findings are consistent with the early development of goblet cell hyperplasia and the loss of club and ciliated cells found in COPD airways (Hessel et al., 2014; Lumsden et al., 1984; Park et al., 2013; Polosukhin et al., 2017; Saetta et al., 2000).

CS exposure is known to induce oxidative stress (Aoshiba et al., 2003; Cavarra et al., 2001; Guatura et al., 2000; Kharitonov et al., 1995; Morrison et al., 1999; Munakata et al., 2018). Several genes associated with oxidative stress were deregulated upon acute CS exposure in the newly established *in vitro* model. Among those, dual oxidase 2 (*DUOX2*), which was reported to be upregulated in the airway epithelium of smokers compared non-smokers, was increased after four days of intermittent CS exposure (Nagai et al., 2008). Increased mRNA levels were also measured for Glutathione peroxidase 2 (*GPX2*), which was previously shown to be smoke-inducible (Singh et al., 2006). One of the genes discriminating smokers from non-smokers identified in bronchial epithelium was NAD(P)H dehydrogenase quinone 1 (*NQO1*) (Shahdoust et al., 2013), which was also increased after acute CS exposure in SAEC ALI cultures.

Oxidative stress is often accompanied by inflammation (Hussain et al., 2016). IL-8 secretion was increased upon CS exposure, indicating activation of the innate immune system, a finding that is consistent with studies in human bronchial epithelial cells (Mio et al., 1997).
The newly established acute CS exposure model reflects many smoke-induced epithelial changes also seen in human airways. To further analyze transcriptional effects of acute CS exposure, a single cell RNA sequencing was performed. The data set will be published separately (manuscript in preparation).

4.3 Modulation of cigarette smoke-induced effects on the small airway epithelium

To investigate whether approved drugs for COPD can prevent SAEC from CS-induced remodeling, olodaterol and roflumilast were tested in the novel *in vitro* model. Neither olodaterol nor roflumilast nor a combination of both succeeded in preventing the impaired barrier formation after 28 days of CS exposure. Furthermore, the drugs failed to improve ciliary function by day 28. No anti-inflammatory effect was observed with either olodaterol or roflumilast or a combination of both. These findings are in contrast to previous studies, showing that olodaterol improves barrier integrity in bronchial ALI cultures after virus infection and suggesting anti-inflammatory effects (Singhera et al., 2017; Wollin and Pieper,

2010). Considering that the type of injury is different (CS vs. virus), the evoked pathways may also be different, which could be the reason why olodaterol shows different effects. Furthermore, the primary target for LABAs is the smooth muscle (and not the epithelium) and this is a reasonable explanation for lack of effect (Blair, 2019).
Aside from olodaterol, the anti-inflammatory phosphodiesterase-4 (PDE4) inhibitor roflumilast was reported to improve ciliary function after smoke exposure (Milara et al., 2012; Schmid et al., 2015).
The fact that the drugs could not modulate the smoke-induced effects on SAEC differentiation does not mean that they have no beneficial effects on the epithelium in the human system. The *in vitro* setup only covers epithelial aspects. However, the interaction between epithelium and immune cells, such as the crosstalk with macrophages or neutrophils, could be of great importance for full effectiveness. This could be investigated in co-culture experiments in the future.
In the acute exposure model, the combination of olodaterol and roflumilast reduced IL-8 secretion, indicating a reduction in neutrophil recruitment. This is in line with a previous study, showing that olodaterol attenuates the neutrophilic cell count in the bronchoalveolar lavage fluid in mice after CS exposure on four consecutive days (Wex et al., 2015).

CS exposure compromised the barrier integrity of fully differentiated SAEC ALI cultures. A number of compounds reported to have positive effects on TEER and tight junctions were tested to prevent the CS-induced impairment. One approach was the administration of ROS-scavengers, such as NAC and trolox, to protect the epithelium from oxidative injury. Although they are known to reduce oxidative stress and improve barrier function (Lee et al., 2020; Lee and Kang, 2019; Messier et al., 2013; Vergauwen et al., 2015), they could not prevent the smoke-induced reduction of TEER in the ALI cultures. To validate, whether ROS-scavengers can protect SAEC ALI cultures from CS-induced reduction in TEER, more substances need to be tested. Possibly, the interaction with other cell types, such as immune cells or fibroblasts, would be necessary to reflect the action of ROS scavengers in the human airways.

None of the other substances tested improved TEER in SAEC ALI cultures after four days of CS exposure. This could indicate that the smoke-induced injury is either too harmful to the epithelium or that the concentration of the substances used was not sufficient, or that interaction with other cell types besides the epithelium is necessary to achieve protective effects. It is also conceivable that another mechanism is responsible for the CS-mediated TEER reduction, which is not covered by the tested substances. Further experiments are required to clarify this question.

4.4 Conclusions and perspectives

Investigating the pathophysiological mechanisms of small airway disease in COPD in an *in vitro* model with common characteristics and pathways is of great importance to address the unmet medical need for treatment of aberrant remodeling and repair in the small airway

epithelium of COPD patients. The established SAEC ALI culture provides an essential basis for further research, since it reflects functional, morphological and transcriptional features of human airways *in vivo*. It allows the cultivation of cells derived from healthy individuals as well as cells from COPD donors; with the latter having some conserved characteristics. COPD-derived SAEC ALI cultures may be extremely helpful to test whether potential therapeutic concepts work also in a diseased setting.

The present study investigated the impact of CS on the pathological alteration of the small airway epithelium in COPD. Disease-relevant characteristics, such as the decline in barrier function, were induced by treating SAEC ALI cultures with liquid CSE.
The role of EGFR signaling was investigated in closer detail, since has been demonstrated to be involved in the pathogenesis of COPD (Vallath et al., 2014). Our findings suggest that CSE-mediated oxidative stress enhances EGFR signaling via downstream modulators, leading to basal cell hyperplasia and goblet cell metaplasia. EGFR inhibition by gefitinib was sufficient to prevent these pathological effects. It would be of great interest to investigate whether whole CS can induce the same effects on EGFR signaling, since exposure to whole CS reflects physiological administration of smoke into the airways. Treatment with whole CS might trigger more reactive oxygen species and might activate the pathway more strongly. This remains to be investigated in future experiments using the newly established *in vitro* smoke model. Furthermore, the gefitinib concentration used in the experimental setting might be reduced in order to minimize harmful side effects and off-target effects. Taken together, the acquired data serve as a basis to further investigate the hypothesized signaling pathway downstream of EGFR. Future experiments should also clarify temporal aspects of intracellular signaling. The investigation of downstream targets in the smoked ALI model could reveal potential new therapeutic approaches.

CS altered basal cell differentiation in SAEC ALI cultures in a way that resembles the pathological remodeling in COPD. Impaired barrier function, squamous differentiation, goblet cell hyperplasia and a loss of club and ciliated cells are disease-relevant features that were induced by CS exposure *in vitro*. The detailed RNA sequencing analysis contributed significantly to the confirmation of all mentioned parameters on a transcriptional level and revealed deregulated pathways, such as Nrf2-mediated oxidative stress, xenobiotic metabolism and AHR signaling, which are associated with smoking (Guerrina et al., 2018; Huang et al., 2005; Nebert et al., 2000; Yun et al., 2017).
Acute responses to CS exposure in fully differentiated SAEC included a reduced barrier integrity, deregulation of marker genes indicating a remodeling of the epithelium towards a more mucus producing phenotype and the induction of oxidative stress and inflammatory processes.

An important aspect of this work was to investigate whether CS-induced effects on the small airway epithelium can be prevented by treatment with substances, which have been described to modulate COPD-related mechanisms. The drugs olodaterol and roflumilast, which are approved for COPD, failed to prevent the negative effects of cigarette smoke on basal cell differentiation including reduced barrier function, impaired development of cilia, and inflammation. Other compounds known to improve barrier integrity were not effective in

preventing TEER reduction after acute CS exposure. Further research is needed to assess how CS-induced remodeling of the small airway epithelium can be prevented.

Another important objective of this thesis was to evaluate the translatability of the new model. Drug discovery begins with simplified models such as biochemical assays followed by more complex i*n vitro* and *in vivo* models. Many drug substances fail in clinical trials due to low efficacy or adverse events that could not be predicted in laboratory models. Translatability assessment revealed a great overlap between the *in vitro* CS model and human small airways *in vivo*. Hence, the model is a valuable tool to investigate COPD-relevant mechanisms *in vitro*, find new therapeutic targets and test potential drug candidates. A limiting factor is the availability of SAEC donors and the limited throughput that can be achieved with CS exposure in the 12-well format. Nevertheless, the SAEC smoke model can be extremely useful for future drug development.

In the future, the model could be used to assess the effects of long-term CS exposure on fully differentiated ALI cultures. Furthermore, CS exposure of co-culture models with epithelial cells, fibroblasts and macrophages may elucidate the role of cellular crosstalk in response to CS.

5 Summary

A characteristic feature of Chronic Obstructive Pulmonary Disease (COPD) is the pathological and progressive remodeling of the small airway epithelium, for which there is currently no effective therapy. To investigate the underlying pathophysiological mechanisms a novel *in vitro* model was established that allows the cultivation of primary human small airway epithelial cells (SAEC) at the air-liquid interface (ALI). To show, whether the established SAEC ALI culture reflects the human situation *in vivo,* functional, morphological and transcriptional features were assessed by measuring transepithelial electrical resistance (TEER) and ciliary beating, evaluating histological and electron microscopic images and performing a detailed RNA sequencing analysis. The new protocol allows the cultivation of cells from healthy individuals and cells from COPD donors, the latter showing some conserved characteristics, such as a less ciliated and more secretory epithelium. A classification analysis based on the gene signature of healthy and COPD-derived ALI cultures with *in vivo* samples of small airway epithelial brushes showed a high classification power and thus a high predictability of health status. Our data demonstrate that disease-specific properties are conserved in COPD-derived small airway basal cells.

To model disease-relevant changes in the small airways, SAEC ALI cultures were exposed to different COPD-related stimuli. The basolateral administration of liquid cigarette smoke extract (CSE) during SAEC differentiation resulted in a reduction in TEER, indicating an impaired epithelial barrier formation, which is characteristic for COPD airways. Furthermore, our findings suggest that CSE-mediated oxidative stress enhances epidermal growth factor receptor (EGFR) signaling via downstream modulators, leading to the induction of COPD-relevant features, such as basal cell hyperplasia and goblet cell metaplasia. This was evaluated by histological and electron microscopic analysis as well as the detection of specific proteins. EGFR inhibition by the tyrosine kinase inhibitor (TKI) gefitinib was sufficient to prevent the pathological effects. These results suggest a therapeutic benefit of EGFR inhibitors in COPD by reducing airway obstruction and mucus hypersecretion. However, therapeutic inhibition of EGFR signal transduction remains a challenge, as it requires a balanced approach to enable normal tissue homeostasis while preventing excessive signaling that causes pathological features.

To model the pathological alterations of the small airway epithelium in a more physiological setting, SAEC ALI cultures were exposed to whole cigarette smoke (CS). In contrast to liquid CSE, whole CS contains not only soluble but also volatile components of smoke. CS exposure during SAEC differentiation led to a number of pathological changes, such as impaired barrier function, squamous differentiation, goblet cell hyperplasia and a reduction of club and ciliated cells. These aspects were analyzed by means of TEER measurements, histological assessments, flow cytometry, cilia beat measurements and transcriptional evaluations including a detailed RNA sequencing analysis. Pathway analysis revealed the deregulation of important pathways associated with smoking, such as nuclear factor erythroid 2–related factor 2 (Nrf2)-mediated oxidative stress, xenobiotic metabolism and aryl hydrocarbon receptor (AHR) signaling.

The CS-induced remodeling of the small airway epithelium *in vitro* closely resembles the epithelium of smokers *in vivo*. This was evaluated by comparative transcriptomic analysis of SAEC ALI cultures and human small airway epithelial brushes.

To investigate acute effects of CS on the small airway epithelium, SAEC ALI cultures were exposed to CS on four consecutive days. The response to acute CS exposure included a decline in barrier integrity, a shift of cellular markers on RNA level indicating a remodeling towards Mucin 5 AC (MUC5AC) positive cells, and the induction of oxidative stress and inflammatory processes. This was shown by analysis of TEER, transcriptional evaluation of cell markers, analysis of transcripts associated with tight junctions and oxidative stress, and measurement of secreted interleukin-8 (IL-8). The newly established model of acute CS exposure reflects many smoke-induced epithelial changes that can also be observed in the human airways. In addition, a comprehensive single cell RNA sequencing was performed, which will be published separately.

An important aim of this work was to investigate whether CS-induced changes of the small airway epithelium can be prevented pharmacologically. Therefore, two drugs approved for the treatment of COPD, olodaterol and roflumilast, were tested for their efficacy in preventing CS-mediated SAEC remodeling. Neither olodaterol nor roflumilast or a combination of both drugs was able to prevent the CS-induced decrease in barrier integrity, improve ciliary function or show leukocyte-independent anti-inflammatory effects. The interaction with immune cells, which is missing in the present model, could be of great importance for full efficacy.

Furthermore, multiple substances, which were described to have beneficial effects on tight junctions, were tested. Among those were reactive oxygen species (ROS) scavengers, such as N-acetyl cysteine (NAC) and trolox. However, none of the tested compounds could prevent the reduction of TEER after CS exposure.

Taken together, important aspects of the pathological remodeling of the small airway epithelium could be modeled *in vitro*. The novel SAEC ALI model reflects CS-induced processes and may help to identify and test new therapeutic approaches to restore the impaired epithelial repair mechanisms in COPD.

6 References

Aghapour, M., Raee, P., Moghaddam, S.J., Hiemstra, P.S., and Heijink, I.H. (2018). Airway Epithelial Barrier Dysfunction in Chronic Obstructive Pulmonary Disease: Role of Cigarette Smoke Exposure. American journal of respiratory cell and molecular biology *58*, 157-169.

Amasheh, S., Meiri, N., Gitter, A.H., Schoneberg, T., Mankertz, J., Schulzke, J.D., and Fromm, M. (2002). Claudin-2 expression induces cation-selective channels in tight junctions of epithelial cells. Journal of cell science *115*, 4969-4976.

Anagnostis, A., Neofytou, E., Soulitzis, N., Kampas, D., Drositis, I., Dermitzaki, D., Tzanakis, N., Schiza, S., Siafakas, N.M., and Tzortzaki, E.G. (2013). Molecular profiling of EGFR family in chronic obstructive pulmonary disease: correlation with airway obstruction. European journal of clinical investigation *43*, 1299-1306.

Aoshiba, K., Koinuma, M., Yokohori, N., and Nagai, A. (2003). Immunohistochemical evaluation of oxidative stress in murine lungs after cigarette smoke exposure. Inhalation toxicology *15*, 1029-1038.

Araya, J., Cambier, S., Markovics, J.A., Wolters, P., Jablons, D., Hill, A., Finkbeiner, W., Jones, K., Broaddus, V.C., Sheppard, D.*, et al.* (2007). Squamous metaplasia amplifies pathologic epithelial-mesenchymal interactions in COPD patients. The Journal of clinical investigation *117*, 3551-3562.

Assefa, E., Yan, Q., Gezahegn, S., Mahamane Salissou, M., He, S., Wu, N., Zuo, X., and Ying, C.-J. (2019). Role of Resveratrol on Indoxyl Sulfate-Induced Endothelial Hyperpermeability via Aryl Hydrocarbon Receptor (AHR)/Src-Dependent Pathway. Oxidative medicine and cellular longevity *2019*, 1-15.

Auerbach, O., Stout, A.P., Hammond, E.C., and Garfinkel, L. (1961). Changes in bronchial epithelium in relation to cigarette smoking and in relation to lung cancer. The New England journal of medicine *265*, 253-267.

Avraham, R., and Yarden, Y. (2011). Feedback regulation of EGFR signalling: decision making by early and delayed loops. Nature reviews Molecular cell biology *12*, 104-117.

Azzopardi, D., Haswell, L.E., Foss-Smith, G., Hewitt, K., Asquith, N., Corke, S., and Phillips, G. (2015). Evaluation of an air-liquid interface cell culture model for studies on the inflammatory and cytotoxic responses to tobacco smoke aerosols. Toxicology in vitro : an international journal published in association with BIBRA *29*, 1720-1728.

Bafadhel, M., McKenna, S., Terry, S., Mistry, V., Reid, C., Haldar, P., McCormick, M., Haldar, K., Kebadze, T., Duvoix, A.*, et al.* (2011). Acute exacerbations of chronic obstructive pulmonary disease: identification of biologic clusters and their biomarkers. American journal of respiratory and critical care medicine *184*, 662-671.

Baggiolini, M., and Clark-Lewis, I. (1992). Interleukin-8, a chemotactic and inflammatory cytokine. FEBS letters *307*, 97-101.

Barnes, P.J. (2010). Inhaled corticosteroids in COPD: a controversy. Respiration; international review of thoracic diseases *80*, 89-95.

Barnes, P.J., and Adcock, I.M. (2011). Chronic obstructive pulmonary disease and lung cancer: a lethal association. American journal of respiratory and critical care medicine *184*, 866-867.

Bhatt, S.P., Kim, Y.I., Harrington, K.F., Hokanson, J.E., Lutz, S.M., Cho, M.H., DeMeo, D.L., Wells, J.M., Make, B.J., Rennard, S.I., *et al.* (2018). Smoking duration alone provides stronger risk estimates of chronic obstructive pulmonary disease than pack-years. Thorax *73*, 414-421.

Blair, H.A. (2019). Tiotropium/Olodaterol: A Review in COPD. Drugs *79*, 997-1008.

Boers, J.E., Ambergen, A.W., and Thunnissen, F.B. (1999). Number and proliferation of clara cells in normal human airway epithelium. American journal of respiratory and critical care medicine *159*, 1585-1591.

Borgerding, M., and Klus, H. (2005). Analysis of complex mixtures--cigarette smoke. Experimental and toxicologic pathology : official journal of the Gesellschaft fur Toxikologische Pathologie *57 Suppl 1*, 43-73.

Bowler, R.P., Barnes, P.J., and Crapo, J.D. (2004). The role of oxidative stress in chronic obstructive pulmonary disease. Copd *1*, 255-277.

Brechbuhl, H.M., Li, B., Smith, R.W., and Reynolds, S.D. (2014). Epidermal growth factor receptor activity is necessary for mouse basal cell proliferation. American journal of physiology Lung cellular and molecular physiology *307*, L800-810.

Broekman, W., Amatngalim, G.D., de Mooij-Eijk, Y., Oostendorp, J., Roelofs, H., Taube, C., Stolk, J., and Hiemstra, P.S. (2016). TNF-alpha and IL-1beta-activated human mesenchymal stromal cells increase airway epithelial wound healing in vitro via activation of the epidermal growth factor receptor. Respiratory research *17*, 3.

Burgel, P.R., Bourdin, A., Chanez, P., Chabot, F., Chaouat, A., Chinet, T., de Blic, J., Devillier, P., Deschildre, A., Didier, A., *et al.* (2011). Update on the roles of distal airways in COPD. European respiratory review : an official journal of the European Respiratory Society *20*, 7-22.

Cavarra, E., Lucattelli, M., Gambelli, F., Bartalesi, B., Fineschi, S., Szarka, A., Giannerini, F., Martorana, P.A., and Lungarella, G. (2001). Human SLPI inactivation after cigarette smoke exposure in a new in vivo model of pulmonary oxidative stress. American journal of physiology Lung cellular and molecular physiology *281*, L412-417.

Chirgwin, J.M., Przybyla, A.E., MacDonald, R.J., and Rutter, W.J. (1979). Isolation of biologically active ribonucleic acid from sources enriched in ribonuclease. Biochemistry *18*, 5294-5299.

Chomczynski, P., and Sacchi, N. (1987). Single-step method of RNA isolation by acid guanidinium thiocyanate-phenol-chloroform extraction. Analytical biochemistry *162*, 156-159.

Churg, A., Sin, D.D., and Wright, J.L. (2011). Everything prevents emphysema: are animal models of cigarette smoke-induced chronic obstructive pulmonary disease any use? American journal of respiratory cell and molecular biology *45*, 1111-1115.

Coant, N., Ben Mkaddem, S., Pedruzzi, E., Guichard, C., Tréton, X., Ducroc, R., Freund, J.N., Cazals-Hatem, D., Bouhnik, Y., Woerther, P.L., *et al.* (2010). NADPH oxidase 1 modulates WNT and NOTCH1 signaling to control the fate of proliferative progenitor cells in the colon. Molecular and cellular biology *30*, 2636-2650.

Comer, D.M., Kidney, J.C., Ennis, M., and Elborn, J.S. (2013). Airway epithelial cell apoptosis and inflammation in COPD, smokers and nonsmokers. European Respiratory Journal *41*, 1058-1067.

Cosio, M.G., Hale, K.A., and Niewoehner, D.E. (1980). Morphologic and morphometric effects of prolonged cigarette smoking on the small airways. The American review of respiratory disease *122*, 265-221.

Coyne, C.B., Gambling, T.M., Boucher, R.C., Carson, J.L., and Johnson, L.G. (2003). Role of claudin interactions in airway tight junctional permeability. American journal of physiology Lung cellular and molecular physiology *285*, L1166-1178.

Crystal, R.G. (2014). Airway basal cells. The "smoking gun" of chronic obstructive pulmonary disease. American journal of respiratory and critical care medicine *190*, 1355-1362.

Crystal, R.G., Randell, S.H., Engelhardt, J.F., Voynow, J., and Sunday, M.E. (2008). Airway epithelial cells: current concepts and challenges. Proceedings of the American Thoracic Society *5*, 772-777.

de Torres, J.P., Marin, J.M., Casanova, C., Cote, C., Carrizo, S., Cordoba-Lanus, E., Baz-Davila, R., Zulueta, J.J., Aguirre-Jaime, A., Saetta, M., *et al.* (2011). Lung cancer in patients with chronic obstructive pulmonary disease-- incidence and predicting factors. American journal of respiratory and critical care medicine *184*, 913-919.

De Water, R., Willems, L.N., Van Muijen, G.N., Franken, C., Fransen, J.A., Dijkman, J.H., and Kramps, J.A. (1986). Ultrastructural localization of bronchial antileukoprotease in central and peripheral human airways by a gold-labeling technique using monoclonal antibodies. The American review of respiratory disease *133*, 882-890.

Dye, J.A., and Adler, K.B. (1994). Effects of cigarette smoke on epithelial cells of the respiratory tract. Thorax *49*, 825-834.

Evans, M.J., and Plopper, C.G. (1988). The role of basal cells in adhesion of columnar epithelium to airway basement membrane. The American review of respiratory disease *138*, 481-483.

Evans, M.J., Van Winkle, L.S., Fanucchi, M.V., and Plopper, C.G. (2001). Cellular and molecular characteristics of basal cells in airway epithelium. Experimental lung research *27*, 401-415.

Fahy, J.V., and Dickey, B.F. (2010). Airway mucus function and dysfunction. The New England journal of medicine *363*, 2233-2247.

Flecknell, P. (2002). Replacement, reduction and refinement. Altex *19*, 73-78.

Funato, Y., Michiue, T., Asashima, M., and Miki, H. (2006). The thioredoxin-related redox-regulating protein nucleoredoxin inhibits Wnt-beta-catenin signalling through dishevelled. Nature cell biology *8*, 501-508.

Furuse, M., Fujita, K., Hiiragi, T., Fujimoto, K., and Tsukita, S. (1998). Claudin-1 and -2: novel integral membrane proteins localizing at tight junctions with no sequence similarity to occludin. The Journal of cell biology *141*, 1539-1550.

Furuse, M., Hirase, T., Itoh, M., Nagafuchi, A., Yonemura, S., Tsukita, S., and Tsukita, S. (1993). Occludin: a novel integral membrane protein localizing at tight junctions. The Journal of cell biology *123*, 1777-1788.

Gan, H., Wang, G., Hao, Q., Wang, Q.J., and Tang, H. (2014). Protein kinase D promotes airway epithelial barrier dysfunction and permeability through down-regulation of claudin-1. The Journal of biological chemistry *289*, 20489.

Ganesan, S., Comstock, A.T., and Sajjan, U.S. (2013). Barrier function of airway tract epithelium. Tissue barriers *1*, e24997.

Ganz, T. (2003). Defensins: antimicrobial peptides of innate immunity. Nature reviews Immunology *3*, 710-720.

Gao, Q., Bautista, A., and Allauzen, S. (2007). Downstream EGFR protein phosphorylation and Gefitinib inhibition in non-small cell lung cancer cells detected with the multiplexed phosphoprotein Assay. Cancer research *67*, 2824-2824.

Gern, J.E., Vrtis, R., Grindle, K.A., Swenson, C., and Busse, W.W. (2000). Relationship of upper and lower airway cytokines to outcome of experimental rhinovirus infection. American journal of respiratory and critical care medicine *162*, 2226-2231.

Ghio, A.J., Dailey, L.A., Soukup, J.M., Stonehuerner, J., Richards, J.H., and Devlin, R.B. (2013). Growth of human bronchial epithelial cells at an air-liquid interface alters the response to particle exposure. Particle and fibre toxicology *10*, 25.

Ghosh, M., Miller, Y.E., Nakachi, I., Kwon, J.B., Baron, A.E., Brantley, A.E., Merrick, D.T., Franklin, W.A., Keith, R.L., and Vandivier, R.W. (2017). Exhaustion of Airway Basal Progenitor Cells in Early and Established COPD. American journal of respiratory and critical care medicine *197*, 885-896.

Gibb, A., and Yang, L.P. (2013). Olodaterol: first global approval. Drugs *73*, 1841-1846.

Giembycz, M.A., and Field, S.K. (2010). Roflumilast: first phosphodiesterase 4 inhibitor approved for treatment of COPD. Drug design, development and therapy *4*, 147-158.

Gindele, J.A., Kiechle, T., Benediktus, K., Birk, G., Brendel, M., Heinemann, F., Wohnhaas, C.T., LeBlanc, M., Zhang, H., Strulovici-Barel, Y.*, et al.* (2020). Intermittent exposure to whole cigarette smoke alters the differentiation of primary small airway epithelial cells in the air-liquid interface culture. Scientific reports *10*, 6257.

Global Initiative for Chronic Obstructive Pulmonary Disease, I. (2020). Global Strategy for the Diagnosis, Management, and Prevention of Chronic Obstructive Pulmonary Disease (2020 Report) (https://goldcopd.org/gold-reports/).

Gohy, S.T., Hupin, C., Fregimilicka, C., Detry, B.R., Bouzin, C., Gaide Chevronay, H., Lecocq, M., Weynand, B., Ladjemi, M.Z., Pierreux, C.E., *et al.* (2015). Imprinting of the COPD airway epithelium for dedifferentiation and mesenchymal transition. The European respiratory journal *45*, 1258-1272.

Graus-Porta, D., Beerli, R.R., Daly, J.M., and Hynes, N.E. (1997). ErbB-2, the preferred heterodimerization partner of all ErbB receptors, is a mediator of lateral signaling. The EMBO journal *16*, 1647-1655.

Guatura, S.B., Martinez, J.A., Santos Bueno, P.C., and Santos, M.L. (2000). Increased exhalation of hydrogen peroxide in healthy subjects following cigarette consumption. Sao Paulo medical journal = Revista paulista de medicina *118*, 93-98.

Guerrina, N., Traboulsi, H., Eidelman, D.H., and Baglole, C.J. (2018). The Aryl Hydrocarbon Receptor and the Maintenance of Lung Health. International journal of molecular sciences *19*.

Gunzel, D., Stuiver, M., Kausalya, P.J., Haisch, L., Krug, S.M., Rosenthal, R., Meij, I.C., Hunziker, W., Fromm, M., and Muller, D. (2009). Claudin-10 exists in six alternatively spliced isoforms that exhibit distinct localization and function. Journal of cell science *122*, 1507-1517.

Gunzel, D., and Yu, A.S. (2013). Claudins and the modulation of tight junction permeability. Physiological reviews *93*, 525-569.

Hanna, N., Lilenbaum, R., Ansari, R., Lynch, T., Govindan, R., Janne, P.A., and Bonomi, P. (2006). Phase II trial of cetuximab in patients with previously treated non-small-cell lung cancer. Journal of clinical oncology : official journal of the American Society of Clinical Oncology *24*, 5253-5258.

Hao, Y., Kuang, Z., Walling, B.E., Bhatia, S., Sivaguru, M., Chen, Y., Gaskins, H.R., and Lau, G.W. (2012). Pseudomonas aeruginosa pyocyanin causes airway goblet cell hyperplasia and metaplasia and mucus hypersecretion by inactivating the transcriptional factor FoxA2. Cellular microbiology *14*, 401-415.

Harkema, J., Mariassy, A., George, J.S., Hyde, D., and Plopper, C. (1991). Epithelial cells of the conducting airways: a species comparison. Lung biology in health and disease *55*, 3-39.

Hartsock, A., and Nelson, W.J. (2008). Adherens and tight junctions: structure, function and connections to the actin cytoskeleton. Biochimica et biophysica acta *1778*, 660-669.

Heijink, I.H., de Bruin, H.G., Dennebos, R., Jonker, M.R., Noordhoek, J.A., Brandsma, C.A., van den Berge, M., and Postma, D.S. (2016a). Cigarette smoke-induced epithelial expression of WNT-5B: implications for COPD. The European respiratory journal *48*, 504-515.

Heijink, I.H., Jonker, M.R., de Vries, M., van Oosterhout, A.J., Telenga, E., Ten Hacken, N.H., Postma, D.S., and van den Berge, M. (2016b). Budesonide and fluticasone propionate differentially affect the airway epithelial barrier. Respiratory research *17*, 2.

Heijink, I.H., Noordhoek, J.A., Timens, W., van Oosterhout, A.J., and Postma, D.S. (2014). Abnormalities in airway epithelial junction formation in chronic obstructive pulmonary disease. American journal of respiratory and critical care medicine *189*, 1439-1442.

Hessel, J., Heldrich, J., Fuller, J., Staudt, M.R., Radisch, S., Hollmann, C., Harvey, B.G., Kaner, R.J., Salit, J., Yee-Levin, J.*, et al.* (2014). Intraflagellar transport gene expression associated with short cilia in smoking and COPD. PLoS One *9*, e85453.

Higashiyama, S., Iwabuki, H., Morimoto, C., Hieda, M., Inoue, H., and Matsushita, N. (2008). Membrane-anchored growth factors, the epidermal growth factor family: beyond receptor ligands. Cancer science *99*, 214-220.

Higham, A., Quinn, A.M., Cancado, J.E.D., and Singh, D. (2019). The pathology of small airways disease in COPD: historical aspects and future directions. Respiratory research *20*, 49.

Hogg, J.C., Chu, F., Utokaparch, S., Woods, R., Elliott, W.M., Buzatu, L., Cherniack, R.M., Rogers, R.M., Sciurba, F.C., Coxson, H.O.*, et al.* (2004). The nature of small-airway obstruction in chronic obstructive pulmonary disease. The New England journal of medicine *350*, 2645-2653.

Hogg, J.C., Macklem, P.T., and Thurlbeck, W.M. (1968). Site and nature of airway obstruction in chronic obstructive lung disease. The New England journal of medicine *278*, 1355-1360.

Hong, K.U., Reynolds, S.D., Giangreco, A., Hurley, C.M., and Stripp, B.R. (2001). Clara cell secretory protein-expressing cells of the airway neuroepithelial body microenvironment include a label-retaining subset and are critical for epithelial renewal after progenitor cell depletion. American journal of respiratory cell and molecular biology *24*, 671-681.

Hong, K.U., Reynolds, S.D., Watkins, S., Fuchs, E., and Stripp, B.R. (2004). Basal cells are a multipotent progenitor capable of renewing the bronchial epithelium. The American journal of pathology *164*, 577-588.

Hovenberg, H.W., Davies, J.R., and Carlstedt, I. (1996). Different mucins are produced by the surface epithelium and the submucosa in human trachea: identification of MUC5AC as a major mucin from the goblet cells. The Biochemical journal *318 (Pt 1)*, 319-324.

Huang, M.F., Lin, W.L., and Ma, Y.C. (2005). A study of reactive oxygen species in mainstream of cigarette. Indoor air *15*, 135-140.

Hussain, T., Tan, B., Yin, Y., Blachier, F., Tossou, M.C., and Rahu, N. (2016). Oxidative Stress and Inflammation: What Polyphenols Can Do for Us? Oxidative medicine and cellular longevity *2016*, 7432797.

Ibrahim, H.R., Aoki, T., and Pellegrini, A. (2002). Strategies for new antimicrobial proteins and peptides: lysozyme and aprotinin as model molecules. Current pharmaceutical design *8*, 671-693.

International Agency for Research on Cancer (2004). Tobacco smoke and involuntary smoking. IARC monographs on the evaluation of carcinogenic risks to humans *83*, 1-1438.

International Organization for Standardization (2012). Routine analytical cigarette-smoking machine - Definitions and standard conditions (ISO 3308:2012).

Irvin, C.G., and Bates, J.H. (2003). Measuring the lung function in the mouse: the challenge of size. Respiratory research *4*, 4.

Jafarinejad, H., Moghoofei, M., Mostafaei, S., Salimian, J., Azimzadeh Jamalkandi, S., and Ahmadi, A. (2017). Worldwide prevalence of viral infection in AECOPD patients: A meta-analysis. Microbial pathogenesis *113*, 190-196.

Jang, J.H., Bruse, S., Liu, Y., Duffy, V., Zhang, C., Oyamada, N., Randell, S., Matsumoto, A., Thompson, D.C., Lin, Y.*, et al.* (2014). Aldehyde dehydrogenase 3A1 protects airway epithelial cells from cigarette smoke-induced DNA damage and cytotoxicity. Free radical biology & medicine *68*, 80-86.

Janoff, A. (1985). Elastases and emphysema. Current assessment of the protease-antiprotease hypothesis. The American review of respiratory disease *132*, 417-433.

Jasper, A.E., McIver, W.J., Sapey, E., and Walton, G.M. (2019). Understanding the role of neutrophils in chronic inflammatory airway disease. F1000Research *8*.

Jeffery, P.K. (1983). Morphologic features of airway surface epithelial cells and glands. The American review of respiratory disease *128*, S14-20.

Jing, J.C., Chen, J.J., Chou, L., Wong, B.J.F., and Chen, Z. (2017). Visualization and Detection of Ciliary Beating Pattern and Frequency in the Upper Airway using Phase Resolved Doppler Optical Coherence Tomography. Scientific reports *7*, 8522.

Jorissen, R.N., Walker, F., Pouliot, N., Garrett, T.P., Ward, C.W., and Burgess, A.W. (2003). Epidermal growth factor receptor: mechanisms of activation and signalling. Experimental cell research *284*, 31-53.

Kaarteenaho-Wiik, R., and Soini, Y. (2009). Claudin-1, -2, -3, -4, -5, and -7 in usual interstitial pneumonia and sarcoidosis. The journal of histochemistry and cytochemistry : official journal of the Histochemistry Society *57*, 187-195.

Kennedy, S.M., Elwood, R.K., Wiggs, B.J., Pare, P.D., and Hogg, J.C. (1984). Increased airway mucosal permeability of smokers. Relationship to airway reactivity. The American review of respiratory disease *129*, 143-148.

Kharitonov, S.A., Robbins, R.A., Yates, D., Keatings, V., and Barnes, P.J. (1995). Acute and chronic effects of cigarette smoking on exhaled nitric oxide. American journal of respiratory and critical care medicine *152*, 609-612.

Kilburn, K.H. (1968). A hypothesis for pulmonary clearance and its implications. The American review of respiratory disease *98*, 449-463.

Kim, V., and Criner, G.J. (2013). Chronic bronchitis and chronic obstructive pulmonary disease. American journal of respiratory and critical care medicine *187*, 228-237.

Kim, V., Oros, M., Durra, H., Kelsen, S., Aksoy, M., Cornwell, W.D., Rogers, T.J., and Criner, G.J. (2015). Chronic bronchitis and current smoking are associated with more goblet

cells in moderate to severe COPD and smokers without airflow obstruction. PLoS One *10*, e0116108.

Knabe, L., Fort, A., Chanez, P., and Bourdin, A. (2015). Club cells and CC16: another "smoking gun"? (With potential bullets against COPD). The European respiratory journal *45*, 1519-1520.

Knight, D.A., and Holgate, S.T. (2003). The airway epithelium: structural and functional properties in health and disease. Respirology (Carlton, Vic) *8*, 432-446.

Knowles, M.R., and Boucher, R.C. (2002). Mucus clearance as a primary innate defense mechanism for mammalian airways. The Journal of clinical investigation *109*, 571-577.

Koch, S., Capaldo, C.T., Hilgarth, R.S., Fournier, B., Parkos, C.A., and Nusrat, A. (2013). Protein kinase CK2 is a critical regulator of epithelial homeostasis in chronic intestinal inflammation. Mucosal immunology *6*, 136-145.

Koval, M. (2013). Claudin heterogeneity and control of lung tight junctions. Annual review of physiology *75*, 551-567.

Kreft, M.E., Jerman, U.D., Lasic, E., Hevir-Kene, N., Rizner, T.L., Peternel, L., and Kristan, K. (2015). The characterization of the human cell line Calu-3 under different culture conditions and its use as an optimized in vitro model to investigate bronchial epithelial function. European journal of pharmaceutical sciences : official journal of the European Federation for Pharmaceutical Sciences *69*, 1-9.

Lam, H.C., Cloonan, S.M., Bhashyam, A.R., Haspel, J.A., Singh, A., Sathirapongsasuti, J.F., Cervo, M., Yao, H., Chung, A.L., Mizumura, K.*, et al.* (2013). Histone deacetylase 6-mediated selective autophagy regulates COPD-associated cilia dysfunction. The Journal of clinical investigation *123*, 5212-5230.

Lams, B.E., Sousa, A.R., Rees, P.J., and Lee, T.H. (1998). Immunopathology of the small-airway submucosa in smokers with and without chronic obstructive pulmonary disease. American journal of respiratory and critical care medicine *158*, 1518-1523.

Laniado-Laborin, R. (2009). Smoking and chronic obstructive pulmonary disease (COPD). Parallel epidemics of the 21 century. International journal of environmental research and public health *6*, 209-224.

Laucho-Contreras, M.E., Polverino, F., Gupta, K., Taylor, K.L., Kelly, E., Pinto-Plata, V., Divo, M., Ashfaq, N., Petersen, H., Stripp, B.*, et al.* (2015). Protective role for club cell secretory protein-16 (CC16) in the development of COPD. The European respiratory journal *45*, 1544-1556.

Lee, C.H., Hung, H.W., Hung, P.H., and Shieh, Y.S. (2010). Epidermal growth factor receptor regulates beta-catenin location, stability, and transcriptional activity in oral cancer. Molecular cancer *9*, 64.

Lee, P.H., Hong, J., and Jang, A.S. (2020). N-acetylcysteine decreases airway inflammation and responsiveness in asthma by modulating claudin 18 expression. Korean J Intern Med.

Lee, S.I., and Kang, K.S. (2019). N-acetylcysteine modulates lipopolysaccharide-induced intestinal dysfunction. Scientific reports *9*, 1004.

Lemmon, M.A. (2009). Ligand-induced ErbB receptor dimerization. Experimental cell research *315*, 638-648.

Leopold, P.L., O'Mahony, M.J., Lian, X.J., Tilley, A.E., Harvey, B.G., and Crystal, R.G. (2009). Smoking is associated with shortened airway cilia. PLoS One *4*, e8157.

Leung, J.M., Tiew, P.Y., Mac Aogain, M., Budden, K.F., Yong, V.F., Thomas, S.S., Pethe, K., Hansbro, P.M., and Chotirmall, S.H. (2017). The role of acute and chronic respiratory colonization and infections in the pathogenesis of COPD. Respirology (Carlton, Vic) *22*, 634-650.

Liu, W., Volpe, M.A., Zscheppang, K., Nielsen, H.C., and Dammann, C.E. (2009). ErbB4 regulates surfactant synthesis and proliferation in adult rat pulmonary epithelial cells. Experimental lung research *35*, 29-47.

Liu, Y., and Di, Y.P. (2012). Effects of second hand smoke on airway secretion and mucociliary clearance. Frontiers in physiology *3*, 342.

Lomas, D.A. (2016). Does Protease-Antiprotease Imbalance Explain Chronic Obstructive Pulmonary Disease? Annals of the American Thoracic Society *13 Suppl 2*, S130-137.

Lomas, D.A., Silverman, E.K., Edwards, L.D., Miller, B.E., Coxson, H.O., and Tal-Singer, R. (2008). Evaluation of serum CC-16 as a biomarker for COPD in the ECLIPSE cohort. Thorax *63*, 1058-1063.

Lozano, R., Naghavi, M., Foreman, K., Lim, S., Shibuya, K., Aboyans, V., Abraham, J., Adair, T., Aggarwal, R., Ahn, S.Y.*, et al.* (2012). Global and regional mortality from 235 causes of death for 20 age groups in 1990 and 2010: a systematic analysis for the Global Burden of Disease Study 2010. Lancet (London, England) *380*, 2095-2128.

Lumsden, A.B., McLean, A., and Lamb, D. (1984). Goblet and Clara cells of human distal airways: evidence for smoking induced changes in their numbers. Thorax *39*, 844-849.

Lynch, T.J., Bell, D.W., Sordella, R., Gurubhagavatula, S., Okimoto, R.A., Brannigan, B.W., Harris, P.L., Haserlat, S.M., Supko, J.G., Haluska, F.G.*, et al.* (2004). Activating mutations in the epidermal growth factor receptor underlying responsiveness of non-small-cell lung cancer to gefitinib. The New England journal of medicine *350*, 2129-2139.

MacNee, W. (2005). Oxidants and COPD. Current drug targets Inflammation and allergy *4*, 627-641.

Malerba, M., Foci, V., Patrucco, F., Pochetti, P., Nardin, M., Pelaia, C., and Radaeli, A. (2019). Single Inhaler LABA/LAMA for COPD. Frontiers in pharmacology *10*.

Mathers, C.D., and Loncar, D. (2006). Projections of global mortality and burden of disease from 2002 to 2030. PLoS medicine *3*, e442.

Messier, E.M., Bahmed, K., Tuder, R.M., Chu, H.W., Bowler, R.P., and Kosmider, B. (2013). Trolox contributes to Nrf2-mediated protection of human and murine primary alveolar type II cells from injury by cigarette smoke. Cell death & disease *4*, e573.

Meste, O., Brau, F., and Guyon, A. (2015). Robust estimation of the motile cilia beating frequency. Medical & biological engineering & computing *53*, 1025-1035.

Miettinen, P.J., Warburton, D., Bu, D., Zhao, J.S., Berger, J.E., Minoo, P., Koivisto, T., Allen, L., Dobbs, L., Werb, Z.*, et al.* (1997). Impaired lung branching morphogenesis in the absence of functional EGF receptor. Developmental biology *186*, 224-236.

Milara, J., Armengot, M., Banuls, P., Tenor, H., Beume, R., Artigues, E., and Cortijo, J. (2012). Roflumilast N-oxide, a PDE4 inhibitor, improves cilia motility and ciliated human bronchial epithelial cells compromised by cigarette smoke in vitro. British journal of pharmacology *166*, 2243-2262.

Milara, J., Peiro, T., Serrano, A., Artigues, E., Aparicio, J., Tenor, H., Sanz, C., and Cortijo, J. (2015). Simvastatin Increases the Ability of Roflumilast N-oxide to Inhibit Cigarette Smoke-Induced Epithelial to Mesenchymal Transition in Well-differentiated Human Bronchial Epithelial Cells in vitro. Copd *12*, 320-331.

Milara, J., Peiro, T., Serrano, A., and Cortijo, J. (2013). Epithelial to mesenchymal transition is increased in patients with COPD and induced by cigarette smoke. Thorax *68*, 410-420.

Milara, J., Peiro, T., Serrano, A., Guijarro, R., Zaragoza, C., Tenor, H., and Cortijo, J. (2014). Roflumilast N-oxide inhibits bronchial epithelial to mesenchymal transition induced by cigarette smoke in smokers with COPD. Pulm Pharmacol Ther *28*, 138-148.

Miller, K.P., and Ramos, K.S. (2001). Impact of cellular metabolism on the biological effects of benzo[a]pyrene and related hydrocarbons. Drug metabolism reviews *33*, 1-35.

Mio, T., Romberger, D.J., Thompson, A.B., Robbins, R.A., Heires, A., and Rennard, S.I. (1997). Cigarette smoke induces interleukin-8 release from human bronchial epithelial cells. American journal of respiratory and critical care medicine *155*, 1770-1776.

Mirza, S., Clay, R.D., Koslow, M.A., and Scanlon, P.D. (2018). COPD Guidelines: A Review of the 2018 GOLD Report. Mayo Clinic proceedings *93*, 1488-1502.

Mok, T.S., Wu, Y.L., Thongprasert, S., Yang, C.H., Chu, D.T., Saijo, N., Sunpaweravong, P., Han, B., Margono, B., Ichinose, Y.*, et al.* (2009). Gefitinib or carboplatin-paclitaxel in pulmonary adenocarcinoma. The New England journal of medicine *361*, 947-957.

Moldvay, J., Jackel, M., Paska, C., Soltesz, I., Schaff, Z., and Kiss, A. (2007). Distinct claudin expression profile in histologic subtypes of lung cancer. Lung cancer (Amsterdam, Netherlands) *57*, 159-167.

Montuschi, P., and Ciabattoni, G. (2015). Bronchodilating drugs for chronic obstructive pulmonary disease: current status and future trends. Journal of medicinal chemistry *58*, 4131-4164.

Morenz, K., Biller, H., Wolfram, F., Leonhadt, S., Rüter, D., Glaab, T., Uhlig, S., and Hohlfeld, J.M. (2012). Detection of air trapping in chronic obstructive pulmonary disease by low frequency ultrasound. BMC pulmonary medicine *12*, 8.

Morrison, D., Rahman, I., Lannan, S., and MacNee, W. (1999). Epithelial permeability, inflammation, and oxidant stress in the air spaces of smokers. American journal of respiratory and critical care medicine *159*, 473-479.

Munakata, S., Ishimori, K., Kitamura, N., Ishikawa, S., Takanami, Y., and Ito, S. (2018). Oxidative stress responses in human bronchial epithelial cells exposed to cigarette smoke and vapor from tobacco- and nicotine-containing products. Regulatory toxicology and pharmacology : RTP *99*, 122-128.

Nagai, K., Betsuyaku, T., Suzuki, M., Nasuhara, Y., Kaga, K., Kondo, S., and Nishimura, M. (2008). Dual oxidase 1 and 2 expression in airway epithelium of smokers and patients with mild/moderate chronic obstructive pulmonary disease. Antioxidants & redox signaling *10*, 705-714.

Nebert, D.W., Roe, A.L., Dieter, M.Z., Solis, W.A., Yang, Y., and Dalton, T.P. (2000). Role of the aromatic hydrocarbon receptor and [Ah] gene battery in the oxidative stress response, cell cycle control, and apoptosis. Biochemical pharmacology *59*, 65-85.

Niimi, T., Nagashima, K., Ward, J.M., Minoo, P., Zimonjic, D.B., Popescu, N.C., and Kimura, S. (2001). claudin-18, a novel downstream target gene for the T/EBP/NKX2.1 homeodomain transcription factor, encodes lung- and stomach-specific isoforms through alternative splicing. Molecular and cellular biology *21*, 7380-7390.

Norina, S.B., Ageev, V.G., and Rastopov, S.F. (1998). Motility and ciliary beating frequency detection of cells and invertebrates for environmental biomonitoring, Vol 3196 (SPIE).

Nusrat, A., Brown, G.T., Tom, J., Drake, A., Bui, T.T., Quan, C., and Mrsny, R.J. (2005). Multiple protein interactions involving proposed extracellular loop domains of the tight junction protein occludin. Molecular biology of the cell *16*, 1725-1734.

O'Donnell, R.A., Richter, A., Ward, J., Angco, G., Mehta, A., Rousseau, K., Swallow, D.M., Holgate, S.T., Djukanovic, R., Davies, D.E.*, et al.* (2004). Expression of ErbB receptors and mucins in the airways of long term current smokers. Thorax *59*, 1032-1040.

Office of the Surgeon General, and Office on Smoking Health (2004). Reports of the Surgeon General. In The Health Consequences of Smoking: A Report of the Surgeon General (Atlanta (GA): Centers for Disease Control and Prevention (US)).

Papi, A., Casoni, G., Caramori, G., Guzzinati, I., Boschetto, P., Ravenna, F., Calia, N., Petruzzelli, S., Corbetta, L., Cavallesco, G.*, et al.* (2004). COPD increases the risk of squamous histological subtype in smokers who develop non-small cell lung carcinoma. Thorax *59*, 679-681.

Parameswaran, G.I., Sethi, S., and Murphy, T.F. (2011). Effects of bacterial infection on airway antimicrobial peptides and proteins in COPD. Chest *140*, 611-617.

Park, H.Y., Churg, A., Wright, J.L., Li, Y., Tam, S., Man, S.F., Tashkin, D., Wise, R.A., Connett, J.E., and Sin, D.D. (2013). Club cell protein 16 and disease progression in chronic

obstructive pulmonary disease. American journal of respiratory and critical care medicine *188*, 1413-1419.

Patel, N.V., Acarregui, M.J., Snyder, J.M., Klein, J.M., Sliwkowski, M.X., and Kern, J.A. (2000). Neuregulin-1 and human epidermal growth factor receptors 2 and 3 play a role in human lung development in vitro. American journal of respiratory cell and molecular biology *22*, 432-440.

Paul, I., Bhattacharya, S., Chatterjee, A., and Ghosh, M.K. (2013). Current Understanding on EGFR and Wnt/β-Catenin Signaling in Glioma and Their Possible Crosstalk. Genes & cancer *4*, 427-446.

Perfetti, T., Coleman, W.M., and Smith, W.S. (1998). Determination of Mainstream and Sidestream Cigarette Smoke Components for Cigarettes of Different Tobacco Types and a Set of Reference Cigarettes. Beitrage zur Tabakforschung International/ Contributions to Tobacco Research *18*, 95-113.

Perng, D.W., Chang, T.M., Wang, J.Y., Lee, C.C., Lu, S.H., Shyue, S.K., Lee, T.S., and Kou, Y.R. (2013). Inflammatory role of AMP-activated protein kinase signaling in an experimental model of toxic smoke inhalation injury. Critical care medicine *41*, 120-132.

Perotin, J.M., Adam, D., Vella-Boucaud, J., Delepine, G., Sandu, S., Jonvel, A.C., Prevost, A., Berthiot, G., Pison, C., Lebargy, F.*, et al.* (2014). Delay of airway epithelial wound repair in COPD is associated with airflow obstruction severity. Respiratory research *15*, 151.

Peters, E.J., Morice, R., Benner, S.E., Lippman, S., Lukeman, J., Lee, J.S., Ro, J.Y., and Hong, W.K. (1993). Squamous metaplasia of the bronchial mucosa and its relationship to smoking. Chest *103*, 1429-1432.

Pezzulo, A.A., Starner, T.D., Scheetz, T.E., Traver, G.L., Tilley, A.E., Harvey, B.G., Crystal, R.G., McCray, P.B., Jr., and Zabner, J. (2011). The air-liquid interface and use of primary cell cultures are important to recapitulate the transcriptional profile of in vivo airway epithelia. American journal of physiology Lung cellular and molecular physiology *300*, L25-31.

Pierrou, S., Broberg, P., O'Donnell, R.A., Pawlowski, K., Virtala, R., Lindqvist, E., Richter, A., Wilson, S.J., Angco, G., Moller, S.*, et al.* (2007). Expression of genes involved in oxidative stress responses in airway epithelial cells of smokers with chronic obstructive pulmonary disease. American journal of respiratory and critical care medicine *175*, 577-586.

Pohl, C., Hermanns, M.I., Uboldi, C., Bock, M., Fuchs, S., Dei-Anang, J., Mayer, E., Kehe, K., Kummer, W., and Kirkpatrick, C.J. (2009). Barrier functions and paracellular integrity in human cell culture models of the proximal respiratory unit. European journal of pharmaceutics and biopharmaceutics : official journal of Arbeitsgemeinschaft fur Pharmazeutische Verfahrenstechnik eV *72*, 339-349.

Polosukhin, V.V., Cates, J.M., Lawson, W.E., Zaynagetdinov, R., Milstone, A.P., Massion, P.P., Ocak, S., Ware, L.B., Lee, J.W., Bowler, R.P.*, et al.* (2011). Bronchial secretory immunoglobulin a deficiency correlates with airway inflammation and progression of chronic obstructive pulmonary disease. American journal of respiratory and critical care medicine *184*, 317-327.

Polosukhin, V.V., Richmond, B.W., Du, R.H., Cates, J.M., Wu, P., Nian, H., Massion, P.P., Ware, L.B., Lee, J.W., Kononov, A.V., *et al.* (2017). Secretory IgA Deficiency in Individual Small Airways Is Associated with Persistent Inflammation and Remodeling. American journal of respiratory and critical care medicine *195*, 1010-1021.

Porth, C. (2011). Essentials of Pathophysiology: Concepts of Altered Health States (Wolters Kluwer/Lippincott Williams & Wilkins).

Puchelle, E., de Bentzmann, S., and Zahm, J.M. (1995). Physical and functional properties of airway secretions in cystic fibrosis--therapeutic approaches. Respiration; international review of thoracic diseases *62 Suppl 1*, 2-12.

Puchelle, E., Zahm, J.M., Tournier, J.M., and Coraux, C. (2006). Airway epithelial repair, regeneration, and remodeling after injury in chronic obstructive pulmonary disease. Proceedings of the American Thoracic Society *3*, 726-733.

Raherison, C., and Girodet, P.-O. (2009). Epidemiology of COPD. European Respiratory Review *18*, 213-221.

Rahman, I. (2005). Oxidative stress in pathogenesis of chronic obstructive pulmonary disease: cellular and molecular mechanisms. Cell biochemistry and biophysics *43*, 167-188.

Rahman, I., and MacNee, W. (1996). Role of oxidants/antioxidants in smoking-induced lung diseases. Free radical biology & medicine *21*, 669-681.

Rahman, I., and MacNee, W. (1999). Lung glutathione and oxidative stress: implications in cigarette smoke-induced airway disease. The American journal of physiology *277*, L1067-1088.

Randall, M.J., Spiess, P.C., Hristova, M., Hondal, R.J., and van der Vliet, A. (2013). Acrolein-induced activation of mitogen-activated protein kinase signaling is mediated by alkylation of thioredoxin reductase and thioredoxin 1. Redox biology *1*, 265-275.

Randell, S.H., and Boucher, R.C. (2006). Effective mucus clearance is essential for respiratory health. American journal of respiratory cell and molecular biology *35*, 20-28.

Rennard, S.I. (2003). Pathogenesis of COPD. Clinical cornerstone *5*, 11-16.

Rigden, H.M., Alias, A., Havelock, T., O'Donnell, R., Djukanovic, R., Davies, D.E., and Wilson, S.J. (2016). Squamous Metaplasia Is Increased in the Bronchial Epithelium of Smokers with Chronic Obstructive Pulmonary Disease. PLoS One *11*, e0156009.

Ritchie, M.E., Phipson, B., Wu, D., Hu, Y., Law, C.W., Shi, W., and Smyth, G.K. (2015). limma powers differential expression analyses for RNA-sequencing and microarray studies. Nucleic acids research *43*, e47.

Ritter, D., Bitsch, A., Elend, M., Schuchardt, S., Hansen, T., Brodbeck, C., Knebel, J., Fuchs, A., Gronewold, C., and Fautz, R. (2018). Development and Evaluation of an In Vitro Test System for Toxicity Screening of Aerosols Released from Consumer Products and First Application to Aerosols from a Hair Straightening Process. Applied In Vitro Toxicology *4*, 180-192.

Ritter, D., and Knebel, J. (2014). Investigations of the Biological Effects of Airborne and Inhalable Substances by Cell-Based In Vitro Methods: Fundamental Improvements to the ALI Concept. Advances in Toxicology *2014*, 11.

Rock, J.R., Randell, S.H., and Hogan, B.L. (2010). Airway basal stem cells: a perspective on their roles in epithelial homeostasis and remodeling. Disease models & mechanisms *3*, 545-556.

Rodgman, A., and Perfetti, T.A. (2008). The Chemical Components of Tobacco and Tobacco Smoke (CRC Press).

Rogers, D.F. (2003). The airway goblet cell. The international journal of biochemistry & cell biology *35*, 1-6.

Rokicki, W., Rokicki, M., Wojtacha, J., and Dzeljijli, A. (2016). The role and importance of club cells (Clara cells) in the pathogenesis of some respiratory diseases. Kardiochirurgia i torakochirurgia polska = Polish journal of cardio-thoracic surgery *13*, 26-30.

Rose, M.C., Nickola, T.J., and Voynow, J.A. (2001). Airway mucus obstruction: mucin glycoproteins, MUC gene regulation and goblet cell hyperplasia. American journal of respiratory cell and molecular biology *25*, 533-537.

Rose, M.C., and Voynow, J.A. (2006). Respiratory tract mucin genes and mucin glycoproteins in health and disease. Physiological reviews *86*, 245-278.

Saetta, M., Di Stefano, A., Turato, G., Facchini, F.M., Corbino, L., Mapp, C.E., Maestrelli, P., Ciaccia, A., and Fabbri, L.M. (1998). CD8+ T-lymphocytes in peripheral airways of smokers with chronic obstructive pulmonary disease. American journal of respiratory and critical care medicine *157*, 822-826.

Saetta, M., Turato, G., Baraldo, S., Zanin, A., Braccioni, F., Mapp, C.E., Maestrelli, P., Cavallesco, G., Papi, A., and Fabbri, L.M. (2000). Goblet cell hyperplasia and epithelial inflammation in peripheral airways of smokers with both symptoms of chronic bronchitis and chronic airflow limitation. American journal of respiratory and critical care medicine *161*, 1016-1021.

Saetta, M., Turato, G., Facchini, F.M., Corbino, L., Lucchini, R.E., Casoni, G., Maestrelli, P., Mapp, C.E., Ciaccia, A., and Fabbri, L.M. (1997). Inflammatory cells in the bronchial glands of smokers with chronic bronchitis. American journal of respiratory and critical care medicine *156*, 1633-1639.

Sahin, U., Weskamp, G., Kelly, K., Zhou, H.M., Higashiyama, S., Peschon, J., Hartmann, D., Saftig, P., and Blobel, C.P. (2004). Distinct roles for ADAM10 and ADAM17 in ectodomain shedding of six EGFR ligands. The Journal of cell biology *164*, 769-779.

Sajadimajd, S., and Khazaei, M. (2018). Oxidative Stress and Cancer: The Role of Nrf2. Current cancer drug targets *18*, 538-557.

Schamberger, A.C., Mise, N., Jia, J., Genoyer, E., Yildirim, A.O., Meiners, S., and Eickelberg, O. (2014). Cigarette smoke-induced disruption of bronchial epithelial tight junctions is prevented by transforming growth factor-beta. American journal of respiratory cell and molecular biology *50*, 1040-1052.

Schamberger, A.C., Staab-Weijnitz, C.A., Mise-Racek, N., and Eickelberg, O. (2015). Cigarette smoke alters primary human bronchial epithelial cell differentiation at the air-liquid interface. Scientific reports *5*, 8163.

Schlingmann, B., Molina, S.A., and Koval, M. (2015). Claudins: Gatekeepers of lung epithelial function. Seminars in cell & developmental biology *42*, 47-57.

Schmid, A., Baumlin, N., Ivonnet, P., Dennis, J.S., Campos, M., Krick, S., and Salathe, M. (2015). Roflumilast partially reverses smoke-induced mucociliary dysfunction. Respiratory research *16*, 135.

Schruf, E., Schroeder, V., Le, H.Q., Schönberger, T., Raedel, D., Stewart, E.L., Fundel-Clemens, K., Bluhmki, T., Weigle, S., Schuler, M.*, et al.* (2020). Recapitulating idiopathic pulmonary fibrosis related alveolar epithelial dysfunction in a human iPSC-derived air-liquid interface model. FASEB journal : official publication of the Federation of American Societies for Experimental Biology.

Sethi, S. (2000). Bacterial infection and the pathogenesis of COPD. Chest *117*, 286s-291s.

Shahdoust, M., Hajizadeh, E., Mozdarani, H., and Chehrei, A. (2013). Finding genes discriminating smokers from non-smokers by applying a growing self-organizing clustering method to large airway epithelium cell microarray data. Asian Pacific journal of cancer prevention : APJCP *14*, 111-116.

Shavelle, R.M., Paculdo, D.R., Kush, S.J., Mannino, D.M., and Strauss, D.J. (2009). Life expectancy and years of life lost in chronic obstructive pulmonary disease: findings from the NHANES III Follow-up Study. International journal of chronic obstructive pulmonary disease *4*, 137-148.

Shaykhiev, R., and Crystal, R.G. (2014a). Basal cell origins of smoking-induced airway epithelial disorders. Cell cycle (Georgetown, Tex) *13*, 341-342.

Shaykhiev, R., and Crystal, R.G. (2014b). Early events in the pathogenesis of chronic obstructive pulmonary disease. Smoking-induced reprogramming of airway epithelial basal progenitor cells. Annals of the American Thoracic Society *11 Suppl 5*, S252-258.

Shaykhiev, R., Otaki, F., Bonsu, P., Dang, D.T., Teater, M., Strulovici-Barel, Y., Salit, J., Harvey, B.G., and Crystal, R.G. (2011). Cigarette smoking reprograms apical junctional complex molecular architecture in the human airway epithelium in vivo. Cellular and molecular life sciences : CMLS *68*, 877-892.

Shaykhiev, R., Zuo, W.L., Chao, I., Fukui, T., Witover, B., Brekman, A., and Crystal, R.G. (2013). EGF shifts human airway basal cell fate toward a smoking-associated airway epithelial phenotype. Proceedings of the National Academy of Sciences of the United States of America *110*, 12102-12107.

Sheehan, J.K., Kesimer, M., and Pickles, R. (2006). Innate immunity and mucus structure and function. Novartis Foundation symposium *279*, 155-166; discussion 167-159, 216-159.

Shijubo, N., Itoh, Y., Yamaguchi, T., Shibuya, Y., Morita, Y., Hirasawa, M., Okutani, R., Kawai, T., and Abe, S. (1997). Serum and BAL Clara cell 10 kDa protein (CC10) levels and

CC10-positive bronchiolar cells are decreased in smokers. The European respiratory journal *10*, 1108-1114.

Shin, K., Fogg, V.C., and Margolis, B. (2006). Tight junctions and cell polarity. Annual review of cell and developmental biology *22*, 207-235.

Siafakas, N.M., Vermeire, P., Pride, N.B., Paoletti, P., Gibson, J., Howard, P., Yernault, J.C., Decramer, M., Higenbottam, T., Postma, D.S.*, et al.* (1995). Optimal assessment and management of chronic obstructive pulmonary disease (COPD). The European Respiratory Society Task Force. The European respiratory journal *8*, 1398-1420.

Singh, A., Rangasamy, T., Thimmulappa, R.K., Lee, H., Osburn, W.O., Brigelius-Flohe, R., Kensler, T.W., Yamamoto, M., and Biswal, S. (2006). Glutathione peroxidase 2, the major cigarette smoke-inducible isoform of GPX in lungs, is regulated by Nrf2. American journal of respiratory cell and molecular biology *35*, 639-650.

Singh, D. (2017). Small Airway Disease in Patients with Chronic Obstructive Pulmonary Disease. Tuberculosis and respiratory diseases *80*, 317-324.

Singhera, G., Yan, R., Dorscheid, D., Sin, D., and Pieper, M. (2017). Olodaterol and anti-inflammatory effects on differentiated air-liquid interface cultures of airway epithelial cells. European Respiratory Journal *50*, PA1000.

Smith, C.M., Djakow, J., Free, R.C., Djakow, P., Lonnen, R., Williams, G., Pohunek, P., Hirst, R.A., Easton, A.J., Andrew, P.W.*, et al.* (2012). ciliaFA: a research tool for automated, high-throughput measurement of ciliary beat frequency using freely available software. Cilia *1*, 14.

Soini, Y. (2011). Claudins in lung diseases. Respiratory research *12*, 70.

Sollner, J.F., Leparc, G., Hildebrandt, T., Klein, H., Thomas, L., Stupka, E., and Simon, E. (2017). An RNA-Seq atlas of gene expression in mouse and rat normal tissues. Scientific data *4*, 170185.

Spina, D. (1998). Epithelium smooth muscle regulation and interactions. American journal of respiratory and critical care medicine *158*, S141-145.

Stedman, R.L. (1968). The chemical composition of tobacco and tobacco smoke. Chem Rev *68*, 153-207.

Stockley, R.A. (2001). Proteases and antiproteases. Novartis Foundation symposium *234*, 189-199; discussion 199-204.

Suissa, S., Patenaude, V., Lapi, F., and Ernst, P. (2013). Inhaled corticosteroids in COPD and the risk of serious pneumonia. Thorax *68*, 1029-1036.

Sweerus, K., Lachowicz-Scroggins, M., Gordon, E., LaFemina, M., Huang, X., Parikh, M., Kanegai, C., Fahy, J.V., and Frank, J.A. (2017). Claudin-18 deficiency is associated with airway epithelial barrier dysfunction and asthma. The Journal of allergy and clinical immunology *139*, 72-81.e71.

Taylor, M., Carr, T., Oke, O., Jaunky, T., Breheny, D., Lowe, F., and Gaca, M. (2016). E-cigarette aerosols induce lower oxidative stress in vitro when compared to tobacco smoke. Toxicology mechanisms and methods *26*, 465-476.

Thorley, A.J., and Tetley, T.D. (2007). Pulmonary epithelium, cigarette smoke, and chronic obstructive pulmonary disease. International journal of chronic obstructive pulmonary disease *2*, 409-428.

Thornton, D.J., Rousseau, K., and McGuckin, M.A. (2008). Structure and function of the polymeric mucins in airways mucus. Annual review of physiology *70*, 459-486.

Tilley, A.E., O'Connor, T.P., Hackett, N.R., Strulovici-Barel, Y., Salit, J., Amoroso, N., Zhou, X.K., Raman, T., Omberg, L., Clark, A.*, et al.* (2011). Biologic Phenotyping of the Human Small Airway Epithelial Response to Cigarette Smoking. PLOS ONE *6*, e22798.

U.S. Department of Health and Human Services, Centers for Disease Control and Prevention, National Center for Chronic Disease Prevention and Health Promotion, and Office on Smoking and Health (2010). How Tobacco Smoke Causes Disease: The Biology and Behavioral Basis for Smoking-Attributable Disease: A Report of the Surgeon General, Vol 7 (Atlanta (GA): Centers for Disease Control and Prevention (US)).

Vallath, S., Hynds, R.E., Succony, L., Janes, S.M., and Giangreco, A. (2014). Targeting EGFR signalling in chronic lung disease: therapeutic challenges and opportunities. The European respiratory journal *44*, 513-522.

Van Itallie, C.M., and Anderson, J.M. (2006). Claudins and epithelial paracellular transport. Annual review of physiology *68*, 403-429.

Vergauwen, H., Tambuyzer, B., Jennes, K., Degroote, J., Wang, W., De Smet, S., Michiels, J., and Van Ginneken, C. (2015). Trolox and ascorbic acid reduce direct and indirect oxidative stress in the IPEC-J2 cells, an in vitro model for the porcine gastrointestinal tract. PLoS One *10*, e0120485.

Vermeer, P.D., Einwalter, L.A., Moninger, T.O., Rokhlina, T., Kern, J.A., Zabner, J., and Welsh, M.J. (2003). Segregation of receptor and ligand regulates activation of epithelial growth factor receptor. Nature *422*, 322-326.

Vinhas, R., Cortes, L., Cardoso, I., Mendes, V.M., Manadas, B., Todo-Bom, A., Pires, E., and Verissimo, P. (2011). Pollen proteases compromise the airway epithelial barrier through degradation of transmembrane adhesion proteins and lung bioactive peptides. Allergy *66*, 1088-1098.

Vogelmeier, C.F., Criner, G.J., Martinez, F.J., Anzueto, A., Barnes, P.J., Bourbeau, J., Celli, B.R., Chen, R., Decramer, M., Fabbri, L.M.*, et al.* (2017). Global Strategy for the Diagnosis, Management, and Prevention of Chronic Obstructive Lung Disease 2017 Report. GOLD Executive Summary. American journal of respiratory and critical care medicine *195*, 557-582.

Wang, G., Lou, H.H., Salit, J., Leopold, P.L., Driscoll, S., Schymeinsky, J., Quast, K., Visvanathan, S., Fine, J.S., Thomas, M.J.*, et al.* (2019). Characterization of an immortalized human small airway basal stem/progenitor cell line with airway region-specific differentiation capacity. Respiratory research *20*, 196.

Weng, M.S., Chang, J.H., Hung, W.Y., Yang, Y.C., and Chien, M.H. (2018). The interplay of reactive oxygen species and the epidermal growth factor receptor in tumor progression and drug resistance. Journal of experimental & clinical cancer research : CR *37*, 61.

Wex, E., Kollak, I., Duechs, M.J., Naline, E., Wollin, L., and Devillier, P. (2015). The long-acting β2 -adrenoceptor agonist olodaterol attenuates pulmonary inflammation. British journal of pharmacology *172*, 3537-3547.

Whitsett, J.A. (2018). Airway Epithelial Differentiation and Mucociliary Clearance. Annals of the American Thoracic Society *15*, S143-s148.

Wickstrom, C., Davies, J.R., Eriksen, G.V., Veerman, E.C., and Carlstedt, I. (1998). MUC5B is a major gel-forming, oligomeric mucin from human salivary gland, respiratory tract and endocervix: identification of glycoforms and C-terminal cleavage. The Biochemical journal *334 (Pt 3)*, 685-693.

Wilson, K.J., Gilmore, J.L., Foley, J., Lemmon, M.A., and Riese, D.J., 2nd (2009). Functional selectivity of EGF family peptide growth factors: implications for cancer. Pharmacology & therapeutics *122*, 1-8.

Wollin, L., and Pieper, M.P. (2010). Tiotropium bromide exerts anti-inflammatory activity in a cigarette smoke mouse model of COPD. Pulm Pharmacol Ther *23*, 345-354.

Woodruff, P.G., Wolff, M., Hohlfeld, J.M., Krug, N., Dransfield, M.T., Sutherland, E.R., Criner, G.J., Kim, V., Prasse, A., Nivens, M.C.*, et al.* (2010). Safety and efficacy of an inhaled epidermal growth factor receptor inhibitor (BIBW 2948 BS) in chronic obstructive pulmonary disease. American journal of respiratory and critical care medicine *181*, 438-445.

Wright, N.A. (1984). The biology of epithelial cell populations / Nicholas Wright and Malcolm Alison (Oxford [Oxfordshire] : New York: Clarendon Press ; Oxford University Press).

Xiao, C., Puddicombe, S.M., Field, S., Haywood, J., Broughton-Head, V., Puxeddu, I., Haitchi, H.M., Vernon-Wilson, E., Sammut, D., Bedke, N.*, et al.* (2011). Defective epithelial barrier function in asthma. The Journal of allergy and clinical immunology *128*, 549-556.e541-512.

Yaghi, A., and Dolovich, M.B. (2016). Airway Epithelial Cell Cilia and Obstructive Lung Disease. Cells *5*.

Yaghi, A., Zaman, A., Cox, G., and Dolovich, M.B. (2012). Ciliary beating is depressed in nasal cilia from chronic obstructive pulmonary disease subjects. Respiratory medicine *106*, 1139-1147.

Yang, J., Zuo, W.L., Fukui, T., Chao, I., Gomi, K., Lee, B., Staudt, M.R., Kaner, R.J., Strulovici-Barel, Y., Salit, J.*, et al.* (2017). Smoking-Dependent Distal-to-Proximal Repatterning of the Adult Human Small Airway Epithelium. American journal of respiratory and critical care medicine *196*, 340-352.

Yarden, Y., and Sliwkowski, M.X. (2001). Untangling the ErbB signalling network. Nature reviews Molecular cell biology *2*, 127-137.

Yi, G., Liang, M., Li, M., Fang, X., Liu, J., Lai, Y., Chen, J., Yao, W., Feng, X., Hu*, et al.* (2018). A large lung gene expression study identifying IL1B as a novel player in airway inflammation in COPD airway epithelial cells. Inflammation research : official journal of the European Histamine Research Society [et al].

Yoshida, T., and Tuder, R.M. (2007). Pathobiology of cigarette smoke-induced chronic obstructive pulmonary disease. Physiological reviews *87*, 1047-1082.

Yu, X., Ng, C.P., Habacher, H., and Roy, S. (2008). Foxj1 transcription factors are master regulators of the motile ciliogenic program. Nature genetics *40*, 1445-1453.

Yun, J.H., Morrow, J., Owen, C.A., Qiu, W., Glass, K., Lao, T., Jiang, Z., Perrella, M.A., Silverman, E.K., Zhou, X.*, et al.* (2017). Transcriptomic Analysis of Lung Tissue from Cigarette Smoke-Induced Emphysema Murine Models and Human Chronic Obstructive Pulmonary Disease Show Shared and Distinct Pathways. American journal of respiratory cell and molecular biology *57*, 47-58.

Zhang, H., Berezov, A., Wang, Q., Zhang, G., Drebin, J., Murali, R., and Greene, M.I. (2007). ErbB receptors: from oncogenes to targeted cancer therapies. The Journal of clinical investigation *117*, 2051-2058.

Zhao, H., Yu, H., Martin, T.A., Teng, X., and Jiang, W.G. (2016). The role of JAM-B in cancer and cancer metastasis (Review). Oncology reports *36*, 3-9.

Zou, W., Zou, Y., Zhao, Z., Li, B., and Ran, P. (2013). Nicotine-induced epithelial-mesenchymal transition via Wnt/β-catenin signaling in human airway epithelial cells. American journal of physiology Lung cellular and molecular physiology *304*, L199-209.

Zscheppang, K., Dork, T., Schmiedl, A., Jones, F.E., and Dammann, C.E. (2011). Neuregulin receptor ErbB4 functions as a transcriptional cofactor for the expression of surfactant protein B in the fetal lung. American journal of respiratory cell and molecular biology *45*, 761-767.

Zuo, W.L., Shenoy, S.A., Li, S., O'Beirne, S.L., Strulovici-Barel, Y., Leopold, P.L., Wang, G., Staudt, M.R., Walters, M.S., Mason, C.*, et al.* (2018). Ontogeny and Biology of Human Small Airway Epithelial Club Cells. American journal of respiratory and critical care medicine *198*, 1375-1388.

Supplementary Information

Table 7: Human Tight Junctions RT² Profiler PCR Array. Log fold changes (logFC) of genes encoding proteins that form impermeable barriers between epithelial cells to regulate polarity, proliferation, and differentiation in cigarette smoke (CS) exposed small airway epithelial cell (SAEC) air-liquid interface (ALI) cultures compared to air controls. Experiments were performed with cultures form healthy donors (HC) and chronic obstructive pulmonary disease (COPD) patients.

	HC (CS vs. Air)		COPD (CS vs. Air)	
	logFC	adj. P value	logFC	adj. P value
CLDN11	-2,1661	0,0166	-3,0974	0,0002
IGSF5	-1,9782	0,1002	-2,2130	0,0344
CTNNA3	-1,8454	0,1199	-2,3815	0,0035
CLDN19	-1,3481	0,0695	-1,7988	0,0105
JAM3	-1,1617	0,0069	-1,1257	0,0049
CLDN18	-0,7914	0,3075	-1,7390	0,0246
PARD6B	-0,6225	0,0000	-0,5529	0,0000
CLDN9	-0,5277	0,0281	-0,3659	0,1541
MAGI2	-0,4808	0,0224	-0,4950	0,0190
CLDN16	-0,3635	0,2215	-0,4371	0,1422
ICAM1	-0,3555	0,6270	0,0574	0,9402
MPDZ	-0,3378	0,0710	-0,4602	0,0108
CRB1	-0,2847	0,6107	-0,7673	0,1697
ICAM2	-0,2499	0,4099	-0,7210	0,0140
MAGI1	-0,2176	0,0616	-0,2240	0,0445
GNAI1	-0,2127	0,3343	-0,1551	0,4289
CGN	-0,1998	0,3584	-0,2041	0,2772
CLDN8	-0,1681	0,8202	-0,4748	0,4962
PTEN	-0,1606	0,3190	-0,1559	0,2682
MLLT4	-0,1559	0,4303	-0,2937	0,0839
PARD3	-0,1527	0,3361	-0,1405	0,3141
SYMPK	-0,1432	0,2066	-0,0958	0,3483
CLDN3	-0,1222	0,6771	-0,6267	0,0183
ASH1L	-0,1178	0,1638	-0,0970	0,2040
SPTB	-0,1076	0,8779	-0,3034	0,5139
TJP3	-0,1004	0,6315	-0,2157	0,2061
INADL	-0,0954	0,6647	-0,0455	0,8248
TJAP1	-0,0744	0,5706	-0,0679	0,5495
CLDN1	-0,0545	0,8352	0,2571	0,1995
MPP5	-0,0534	0,6516	0,0140	0,9042
CLDN15	-0,0447	0,9261	0,0207	0,9582
OCLN	-0,0432	0,7624	0,0825	0,4748
F11R	-0,0175	0,9393	0,0151	0,9416
PRKCZ	-0,0117	0,9464	-0,0511	0,7053
CTNNB1	0,0038	0,9826	0,1421	0,2240
TJP1	0,0361	0,8014	0,1249	0,2598
VAPA	0,0454	0,8306	0,0404	0,8275
PRKCI	0,0550	0,7737	0,0348	0,8414
SMURF1	0,0705	0,5245	0,2184	0,0243
ARHGEF2	0,0732	0,6498	0,0893	0,5104
CSNK2A1	0,0877	0,5675	0,2047	0,1158
YBX3	0,0904	0,4969	0,0037	0,9793
MPP6	0,0918	0,5492	-0,0215	0,8885
CLDN4	0,0943	0,7033	0,1477	0,4642
CSNK2A2	0,1293	0,2049	0,2124	0,0244
SPTAN1	0,1301	0,3432	0,0921	0,4481
ACTN1	0,1327	0,5388	0,0771	0,7000
CDC42	0,1467	0,3580	0,2339	0,0948
ACTN4	0,1514	0,3066	0,0640	0,6422
AMOTL1	0,1675	0,4953	0,0560	0,8126
CASK	0,1811	0,2829	0,3183	0,0365
RAC1	0,1825	0,1256	0,2226	0,0451
LLGL2	0,1846	0,2209	-0,0544	0,7125
EPB41	0,2018	0,0876	0,2300	0,0383
MARK2	0,2358	0,0427	0,2638	0,0191
ILK	0,2400	0,0920	0,2623	0,0504
TJP2	0,2415	0,0567	0,2348	0,0501
CLDN12	0,2428	0,1436	0,3874	0,0140
CD99	0,2559	0,5134	0,3037	0,3724
CSNK2B	0,2716	0,0117	0,2882	0,0068
CDK4	0,2984	0,0761	0,2064	0,1814
RHOA	0,3267	0,0419	0,3292	0,0321
CRB3	0,3413	0,0876	0,3248	0,0869
LLGL1	0,3736	0,0386	0,2319	0,1697
CTTN	0,4501	0,0001	0,4437	0,0001
CLDN7	0,4764	0,0017	0,5301	0,0006
PARD6A	0,5342	0,0949	0,3826	0,2282
CTNNA1	0,6103	0,0002	0,5493	0,0008
TIAM1	0,7858	0,0001	0,5018	0,0064
HCLS1	1,0767	0,0001	1,1095	0,0001
CLDN14	1,4714	0,3581	0,2731	0,8478
CLDN10	2,8334	0,0000	2,4739	0,0000

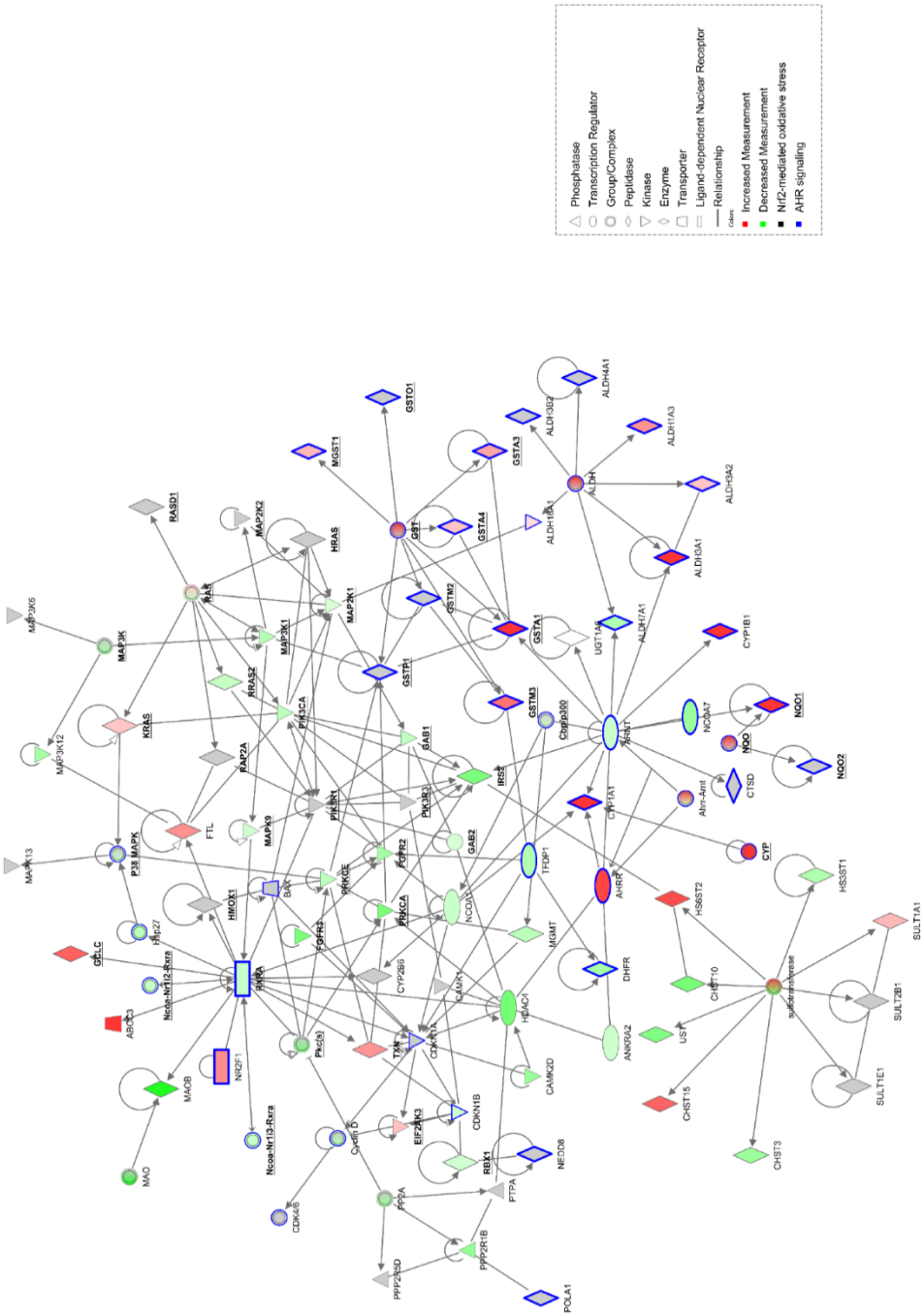

Figure 48: Cigarette smoke induces xenobiotic metabolism in the air-liquid interface (ALI) culture as well as in smoking individuals. Network representation focusing on related transcripts (according to Ingenuity Pathway Analysis) that are annotated as being involved in xenobiotic metabolism and are either de-regulated in small airway epithelial cell (SAEC) ALI cultures (*in vitro* model) or in SAEC from human smokers (*in vivo* data from epithelial brushes). Coloring indicates the deregulation in SAEC from human smokers (red color = up-regulation; green = down-regulation; grey = de-regulation in SAEC ALI cultures only). Bold and underlined transcripts are associated with Nuclear factor erythroid 2-related factor 2 (Nrf2)-mediated oxidative stress; transcripts associated with aryl hydrocarbon receptor (AHR) signaling are highlighted in blue. The network was generated using IPA (QIAGEN Inc., https://www.qiagenbioinformatics.com/products/ingenuity-pathway-analysis). (Gindele et al., 2020)

Table 8: Deregulated Canonical Pathways in cigarette smoke (CS)-exposed small airway epithelial cell (SAEC) air-liquid interface (ALI) cultures according to Ingenuity Pathways Analysis (Gindele et al., 2020)

Ingenuity Canonical Pathways	-log(p-value)	Ratio
NRF2-mediated Oxidative Stress Response	7,95	0,14
Estrogen Biosynthesis	4,77	0,22
Xenobiotic Metabolism Signaling	4,05	0,09
Bupropion Degradation	3,58	0,24
Pentose Phosphate Pathway	3,46	0,40
RAR Activation	3,44	0,09
γ-glutamyl Cycle	3,28	0,36
Protein Kinase A Signaling	3,26	0,07
Nicotine Degradation II	3,16	0,14
Acetone Degradation I (to Methylglyoxal)	3,12	0,20
LPS/IL-1 Mediated Inhibition of RXR Function	3,08	0,08
Aryl Hydrocarbon Receptor Signaling	3,00	0,10
Acute Phase Response Signaling	2,92	0,09
Retinoate Biosynthesis I	2,90	0,18
Hepatic Fibrosis Signaling Pathway	2,79	0,07
STAT3 Pathway	2,76	0,10
Vitamin-C Transport	2,60	0,25
Methylglyoxal Degradation III	2,40	0,22
Glutathione Biosynthesis	2,39	0,67
Nicotine Degradation III	2,32	0,13
Melatonin Signaling	2,26	0,11
Iron homeostasis signaling pathway	2,26	0,09
cAMP-mediated signaling	2,24	0,07
GPCR-Mediated Integration of Enteroendocrine Signaling Exemplified by an L Cell	2,23	0,11
Glutathione-mediated Detoxification	2,20	0,16
Antioxidant Action of Vitamin C	2,10	0,09
Pentose Phosphate Pathway (Oxidative Branch)	2,10	0,50
Pregnenolone Biosynthesis	1,94	0,23
Glutathione Redox Reactions I	1,94	0,17
Complement System	1,93	0,14
Tyrosine Degradation I	1,89	0,40
Osteoarthritis Pathway	1,86	0,07
Colanic Acid Building Blocks Biosynthesis	1,85	0,21
Role of Macrophages. Fibroblasts and Endothelial Cells in Rheumatoid Arthritis	1,84	0,06
G-Protein Coupled Receptor Signaling	1,83	0,07
Ovarian Cancer Signaling	1,80	0,08
Aldosterone Signaling in Epithelial Cells	1,79	0,08
Histidine Degradation VI	1,77	0,20
Cardiac Hypertrophy Signaling (Enhanced)	1,76	0,06
ERK5 Signaling	1,74	0,10
Pentose Phosphate Pathway (Non-oxidative Branch)	1,72	0,33
Sperm Motility	1,67	0,07
Ubiquinol-10 Biosynthesis (Eukaryotic)	1,62	0,18
Histamine Degradation	1,62	0,18
Melatonin Degradation I	1,61	0,10
TNFR2 Signaling	1,61	0,13
Thioredoxin Pathway	1,59	0,29
Autophagy	1,58	0,10
Wnt/Ca+ pathway	1,55	0,10
Agranulocyte Adhesion and Diapedesis	1,53	0,07
Colorectal Cancer Metastasis Signaling	1,53	0,06
Ethanol Degradation II	1,51	0,13
p53 Signaling	1,51	0,08
Oxidative Ethanol Degradation III	1,49	0,16
Chondroitin Sulfate Biosynthesis (Late Stages)	1,48	0,10
Superoxide Radicals Degradation	1,47	0,25
PXR/RXR Activation	1,46	0,09
Superpathway of Melatonin Degradation	1,46	0,09
Leukocyte Extravasation Signaling	1,45	0,07
The Visual Cycle	1,43	0,15
MIF-mediated Glucocorticoid Regulation	1,43	0,12
Role of JAK2 in Hormone-like Cytokine Signaling	1,43	0,12
Xanthine and Xanthosine Salvage	1,43	1,00
Adenine and Adenosine Salvage VI	1,43	1,00
UDP-N-acetyl-D-galactosamine Biosynthesis I	1,43	1,00
Granulocyte Adhesion and Diapedesis	1,42	0,07
NF-κB Signaling	1,42	0,07
TR/RXR Activation	1,42	0,08
TNFR1 Signaling	1,41	0,10
Cardiac β-adrenergic Signaling	1,40	0,07
TWEAK Signaling	1,39	0,11
Noradrenaline and Adrenaline Degradation	1,39	0,11
Maturity Onset Diabetes of Young (MODY) Signaling	1,37	0,14
UDP-N-acetyl-D-galactosamine Biosynthesis II	1,37	0,22
Corticotropin Releasing Hormone Signaling	1,33	0,07
Hepatic Fibrosis / Hepatic Stellate Cell Activation	1,32	0,06
Pancreatic Adenocarcinoma Signaling	1,28	0,07
Ethanol Degradation IV	1,27	0,13
p70S6K Signaling	1,27	0,07
Death Receptor Signaling	1,26	0,08
Glioma Signaling	1,26	0,07
Caveolar-mediated Endocytosis Signaling	1,25	0,08
Relaxin Signaling	1,25	0,07
Type I Diabetes Mellitus Signaling	1,24	0,07
Inhibition of Matrix Metalloproteases	1,24	0,10
Chondroitin Sulfate Biosynthesis	1,23	0,09
Leptin Signaling in Obesity	1,23	0,08
GNRH Signaling	1,21	0,06
Wnt/β-catenin Signaling	1,21	0,06
PI3K/AKT Signaling	1,19	0,06
Tryptophan Degradation X (Mammalian. via Tryptamine)	1,18	0,12
Toll-like Receptor Signaling	1,18	0,08
Dermatan Sulfate Biosynthesis	1,15	0,08
Gap Junction Signaling	1,15	0,06
Role of Osteoblasts. Osteoclasts and Chondrocytes in Rheumatoid Arthritis	1,14	0,06

Ingenuity Canonical Pathways	-log(p-value)	Ratio
Gluconeogenesis I	1,14	0,12
Guanosine Nucleotides Degradation III	1,14	0,17
Guanine and Guanosine Salvage I	1,13	0,50
L-DOPA Degradation	1,13	0,50
Alanine Degradation III	1,13	0,50
Alanine Biosynthesis II	1,13	0,50
Sulfate Activation for Sulfonation	1,13	0,50
Adenine and Adenosine Salvage I	1,13	0,50
GDP-L-fucose Biosynthesis I (from GDP-D-mannose)	1,13	0,50
Glutamate Dependent Acid Resistance	1,13	0,50
Oncostatin M Signaling	1,12	0,09
tRNA Splicing	1,12	0,09
Apelin Cardiomyocyte Signaling Pathway	1,10	0,07
Role of IL-17A in Psoriasis	1,08	0,15
Urate Biosynthesis/Inosine 5'-phosphate Degradation	1,08	0,15
NAD Phosphorylation and Dephosphorylation	1,08	0,15
Bile Acid Biosynthesis. Neutral Pathway	1,08	0,15
Neuropathic Pain Signaling In Dorsal Horn Neurons	1,07	0,07
Hepatic Cholestasis	1,06	0,06
Apelin Adipocyte Signaling Pathway	1,06	0,07
IL-17A Signaling in Airway Cells	1,04	0,08
Glioblastoma Multiforme Signaling	1,03	0,06
Dermatan Sulfate Biosynthesis (Late Stages)	1,03	0,09
PFKFB4 Signaling Pathway	1,03	0,09
HER-2 Signaling in Breast Cancer	1,02	0,07
Dopamine Degradation	1,00	0,10
PDGF Signaling	0,98	0,07
P2Y Purigenic Receptor Signaling Pathway	0,98	0,06
Choline Biosynthesis III	0,97	0,13
Adenosine Nucleotides Degradation II	0,97	0,13
Uracil Degradation II (Reductive)	0,97	0,33
NADH Repair	0,97	0,33
Tetrahydrobiopterin Biosynthesis I	0,97	0,33
Thymine Degradation	0,97	0,33
Tetrahydrobiopterin Biosynthesis II	0,97	0,33
S-adenosyl-L-methionine Biosynthesis	0,97	0,33
Tyrosine Biosynthesis IV	0,97	0,33
Gαs Signaling	0,97	0,07
Role of NFAT in Cardiac Hypertrophy	0,96	0,06
Regulation of the Epithelial-Mesenchymal Transition Pathway	0,96	0,06
RANK Signaling in Osteoclasts	0,95	0,07
Adrenomedullin signaling pathway	0,91	0,06
Circadian Rhythm Signaling	0,90	0,09
3-phosphoinositide Degradation	0,90	0,06
GPCR-Mediated Nutrient Sensing in Enteroendocrine Cells	0,89	0,06
D-myo-inositol-5-phosphate Metabolism	0,89	0,06
D-myo-inositol (1.4.5)-trisphosphate Degradation	0,88	0,12
CD27 Signaling in Lymphocytes	0,86	0,08
Non-Small Cell Lung Cancer Signaling	0,86	0,07
Arsenate Detoxification I (Glutaredoxin)	0,85	0,25
α-tocopherol Degradation	0,85	0,25
Glutathione Redox Reactions II	0,85	0,25
Proline Biosynthesis I	0,85	0,25
Phenylalanine Degradation I (Aerobic)	0,85	0,25
Acetate Conversion to Acetyl-CoA	0,85	0,25
Purine Nucleotides Degradation II (Aerobic)	0,84	0,11
PI3K Signaling in B Lymphocytes	0,83	0,06
EGF Signaling	0,82	0,07
Interferon Signaling	0,82	0,08
Insulin Receptor Signaling	0,82	0,06
ATM Signaling	0,80	0,06
Bladder Cancer Signaling	0,80	0,06
Hereditary Breast Cancer Signaling	0,80	0,06
D-myo-inositol (1.4.5.6)-Tetrakisphosphate Biosynthesis	0,80	0,06
D-myo-inositol (3.4.5.6)-tetrakisphosphate Biosynthesis	0,80	0,06
Macropinocytosis Signaling	0,80	0,07
Unfolded protein response	0,80	0,07
B Cell Receptor Signaling	0,80	0,05
Thrombin Signaling	0,80	0,05
Role of NANOG in Mammalian Embryonic Stem Cell Pluripotency	0,80	0,06
Notch Signaling	0,79	0,08
Type II Diabetes Mellitus Signaling	0,78	0,06
Apoptosis Signaling	0,78	0,06
IL-15 Production	0,77	0,06
Fatty Acid α-oxidation	0,76	0,10
Protein Citrullination	0,76	0,20
Tetrahydrofolate Salvage from 5.10-methenyltetrahydrofolate	0,76	0,20
Serine Biosynthesis	0,76	0,20
Tetrapyrrole Biosynthesis II	0,76	0,20
Lysine Degradation II	0,76	0,20
Myo-inositol Biosynthesis	0,76	0,20
Lysine Degradation V	0,76	0,20
Galactose Degradation I (Leloir Pathway)	0,76	0,20
Glutamate Degradation III (via 4-aminobutyrate)	0,76	0,20
April Mediated Signaling	0,75	0,08
RhoA Signaling	0,75	0,06
Tight Junction Signaling	0,74	0,05
Huntington's Disease Signaling	0,74	0,05
Putrescine Degradation III	0,73	0,10
Prolactin Signaling	0,73	0,06
Clathrin-mediated Endocytosis Signaling	0,72	0,05
Phagosome Formation	0,72	0,06
NF-κB Activation by Viruses	0,71	0,06
FXR/RXR Activation	0,71	0,06
Induction of Apoptosis by HIV1	0,71	0,07
PTEN Signaling	0,71	0,06
IGF-1 Signaling	0,71	0,06
Glucocorticoid Receptor Signaling	0,71	0,05
B Cell Activating Factor Signaling	0,70	0,07
Mechanisms of Viral Exit from Host Cells	0,70	0,07

Ingenuity Canonical Pathways	-log(p-value)	Ratio
Triacylglycerol Biosynthesis	0,70	0,07
Proline Biosynthesis II (from Arginine)	0,69	0,17
Chondroitin and Dermatan Biosynthesis	0,69	0,17
Arginine Degradation VI (Arginase 2 Pathway)	0,69	0,17
UDP-N-acetyl-D-glucosamine Biosynthesis II	0,69	0,17
Adenine and Adenosine Salvage III	0,69	0,17
Glycogen Biosynthesis II (from UDP-D-Glucose)	0,69	0,17
GDP-mannose Biosynthesis	0,69	0,17
Superpathway of Inositol Phosphate Compounds	0,68	0,05
Phagosome Maturation	0,68	0,05
MIF Regulation of Innate Immunity	0,68	0,07
Intrinsic Prothrombin Activation Pathway	0,68	0,07
Retinol Biosynthesis	0,68	0,07
FGF Signaling	0,68	0,06
Synaptic Long Term Potentiation	0,68	0,05
Thrombopoietin Signaling	0,68	0,06
Phospholipases	0,68	0,06
Superpathway of D-myo-inositol (1.4.5)-trisphosphate Metabolism	0,67	0,09
IL-4 Signaling	0,67	0,06
Opioid Signaling Pathway	0,66	0,05
IL-8 Signaling	0,66	0,05
Cellular Effects of Sildenafil (Viagra)	0,65	0,05
Pyridoxal 5'-phosphate Salvage Pathway	0,64	0,06
IL-23 Signaling Pathway	0,64	0,07
Superpathway of Serine and Glycine Biosynthesis I	0,63	0,14
Phosphatidylcholine Biosynthesis I	0,63	0,14
Purine Ribonucleosides Degradation to Ribose-1-phosphate	0,63	0,14
HGF Signaling	0,62	0,05
iNOS Signaling	0,62	0,07
IL-17A Signaling in Gastric Cells	0,62	0,08
Role of JAK family kinases in IL-6-type Cytokine Signaling	0,62	0,08
Role of Oct4 in Mammalian Embryonic Stem Cell Pluripotency	0,61	0,07
eNOS Signaling	0,61	0,05
Dendritic Cell Maturation	0,60	0,05
NAD Salvage Pathway II	0,59	0,08
Glycolysis I	0,59	0,08
IL-1 Signaling	0,59	0,05
Th17 Activation Pathway	0,59	0,05
SPINK1 General Cancer Pathway	0,59	0,06
Apelin Endothelial Signaling Pathway	0,58	0,05
Histidine Degradation III	0,58	0,13
Salvage Pathways of Pyrimidine Deoxyribonucleotides	0,58	0,13
Dopamine-DARPP32 Feedback in cAMP Signaling	0,57	0,05
Neuroprotective Role of THOP1 in Alzheimer's Disease	0,57	0,05
Endothelin-1 Signaling	0,56	0,05
Production of Nitric Oxide and Reactive Oxygen Species in Macrophages	0,56	0,05
3-phosphoinositide Biosynthesis	0,56	0,05
Growth Hormone Signaling	0,56	0,06
Small Cell Lung Cancer Signaling	0,56	0,06
Sphingosine-1-phosphate Signaling	0,56	0,05
Role of Tissue Factor in Cancer	0,56	0,05
Heparan Sulfate Biosynthesis (Late Stages)	0,56	0,06
Cell Cycle: G2/M DNA Damage Checkpoint Regulation	0,55	0,06
Renin-Angiotensin Signaling	0,55	0,05
Synaptogenesis Signaling Pathway	0,55	0,04
PPARα/RXRα Activation	0,55	0,05
α-Adrenergic Signaling	0,55	0,05
Basal Cell Carcinoma Signaling	0,55	0,06
GABA Receptor Signaling	0,55	0,05
Amyloid Processing	0,54	0,06
GP6 Signaling Pathway	0,54	0,05
Sucrose Degradation V (Mammalian)	0,54	0,11
Heme Biosynthesis II	0,54	0,11
Folate Transformations I	0,54	0,11
Neuregulin Signaling	0,54	0,05
Sonic Hedgehog Signaling	0,53	0,07
UVC-Induced MAPK Signaling	0,52	0,06
Salvage Pathways of Pyrimidine Ribonucleotides	0,52	0,05
Molecular Mechanisms of Cancer	0,52	0,04
Estrogen-Dependent Breast Cancer Signaling	0,52	0,05
Glioma Invasiveness Signaling	0,52	0,05
Hypoxia Signaling in the Cardiovascular System	0,52	0,05
UVA-Induced MAPK Signaling	0,51	0,05
G Beta Gamma Signaling	0,51	0,05
UVB-Induced MAPK Signaling	0,51	0,06
Nitric Oxide Signaling in the Cardiovascular System	0,50	0,05
Embryonic Stem Cell Differentiation into Cardiac Lineages	0,50	0,10
Prostanoid Biosynthesis	0,50	0,10
Erythropoietin Signaling	0,50	0,05
G Protein Signaling Mediated by Tubby	0,49	0,06
Dopamine Receptor Signaling	0,49	0,05
Role of IL-17A in Arthritis	0,48	0,06
VDR/RXR Activation	0,47	0,05
Heparan Sulfate Biosynthesis	0,47	0,05
Neuroinflammation Signaling Pathway	0,47	0,04
Mouse Embryonic Stem Cell Pluripotency	0,46	0,05
Sumoylation Pathway	0,46	0,05
Epithelial Adherens Junction Signaling	0,46	0,05
Role of BRCA1 in DNA Damage Response	0,45	0,05
White Adipose Tissue Browning Pathway	0,45	0,05
Gustation Pathway	0,45	0,05
T Cell Receptor Signaling	0,45	0,05
CNTF Signaling	0,44	0,05
LPS-stimulated MAPK Signaling	0,43	0,05
PEDF Signaling	0,43	0,05
MSP-RON Signaling Pathway	0,43	0,05
Virus Entry via Endocytic Pathways	0,43	0,05
CREB Signaling in Neurons	0,43	0,04
Coagulation System	0,42	0,06
CDK5 Signaling	0,42	0,05

Ingenuity Canonical Pathways	-log(p-value)	Ratio
Adipogenesis pathway	0,41	0,04
Semaphorin Signaling in Neurons	0,41	0,05
Assembly of RNA Polymerase III Complex	0,41	0,08
Sertoli Cell-Sertoli Cell Junction Signaling	0,41	0,04
Oleate Biosynthesis II (Animals)	0,41	0,08
Leukotriene Biosynthesis	0,41	0,08
PCP pathway	0,41	0,05
AMPK Signaling	0,40	0,04
Cell Cycle Regulation by BTG Family Proteins	0,39	0,05
Cardiac Hypertrophy Signaling	0,38	0,04
Synaptic Long Term Depression	0,38	0,04
Tec Kinase Signaling	0,38	0,04
Regulation of IL-2 Expression in Activated and Anergic T Lymphocytes	0,37	0,04
Endocannabinoid Developing Neuron Pathway	0,36	0,04
Androgen Biosynthesis	0,36	0,07
CD40 Signaling	0,35	0,05
Myc Mediated Apoptosis Signaling	0,35	0,05
Fc Epsilon RI Signaling	0,35	0,04
Protein Ubiquitination Pathway	0,35	0,04
Endocannabinoid Cancer Inhibition Pathway	0,35	0,04
Calcium-induced T Lymphocyte Apoptosis	0,34	0,05
Eicosanoid Signaling	0,34	0,05
p38 MAPK Signaling	0,34	0,04
Axonal Guidance Signaling	0,34	0,04
Role of PKR in Interferon Induction and Antiviral Response	0,34	0,05
Granzyme B Signaling	0,34	0,06
Extrinsic Prothrombin Activation Pathway	0,34	0,06
Glutaryl-CoA Degradation	0,34	0,06
Pyrimidine Ribonucleotides Interconversion	0,34	0,05
Parkinson's Signaling	0,34	0,06
Systemic Lupus Erythematosus In B Cell Signaling Pathway	0,34	0,04
Serotonin Degradation	0,34	0,04
Cell Cycle: G1/S Checkpoint Regulation	0,34	0,04
Factors Promoting Cardiogenesis in Vertebrates	0,33	0,04
Cholecystokinin/Gastrin-mediated Signaling	0,33	0,04
Melanocyte Development and Pigmentation Signaling	0,33	0,04
Role of IL-17F in Allergic Inflammatory Airway Diseases	0,33	0,05
ErbB Signaling	0,33	0,04
LXR/RXR Activation	0,32	0,04
Dermatan Sulfate Degradation (Metazoa)	0,32	0,06
IL-10 Signaling	0,32	0,04
Role of JAK1 and JAK3 in γc Cytokine Signaling	0,32	0,04
Pyrimidine Ribonucleotides De Novo Biosynthesis	0,32	0,05
Serotonin Receptor Signaling	0,32	0,05
1D-myo-inositol Hexakisphosphate Biosynthesis II (Mammalian)	0,30	0,06
D-myo-inositol (1.3.4)-trisphosphate Biosynthesis	0,30	0,06
FAT10 Signaling Pathway	0,30	0,06
CCR3 Signaling in Eosinophils	0,30	0,04
Ephrin B Signaling	0,29	0,04
Calcium Signaling	0,29	0,04
VEGF Signaling	0,29	0,04
Atherosclerosis Signaling	0,29	0,04
RhoGDI Signaling	0,29	0,04
GADD45 Signaling	0,29	0,05
DNA damage-induced 14-3-3σ Signaling	0,29	0,05
14-3-3-mediated Signaling	0,28	0,04
T Helper Cell Differentiation	0,28	0,04
Role of Pattern Recognition Receptors in Recognition of Bacteria and Viruses	0,28	0,04
Endocannabinoid Neuronal Synapse Pathway	0,28	0,04
nNOS Signaling in Neurons	0,28	0,04
CDP-diacylglycerol Biosynthesis I	0,27	0,05
Inflammasome pathway	0,27	0,05
SAPK/JNK Signaling	0,27	0,04
GDNF Family Ligand-Receptor Interactions	0,26	0,04
Neurotrophin/TRK Signaling	0,26	0,04
PPAR Signaling	0,26	0,04
HOTAIR Regulatory Pathway	0,26	0,04
Role of Wnt/GSK-3β Signaling in the Pathogenesis of Influenza	0,25	0,04
IL-7 Signaling Pathway	0,25	0,04
Phosphatidylglycerol Biosynthesis II (Non-plastidic)	0,25	0,05
Methionine Degradation I (to Homocysteine)	0,25	0,05
IL-3 Signaling	0,24	0,04
Role of Lipids/Lipid Rafts in the Pathogenesis of Influenza	0,23	0,04
Differential Regulation of Cytokine Production in Intestinal Epithelial Cells by IL-17A and IL-17F	0,23	0,04
Tryptophan Degradation III (Eukaryotic)	0,23	0,04
Apelin Cardiac Fibroblast Signaling Pathway	0,23	0,04
Lymphotoxin β Receptor Signaling	0,23	0,04
Role of JAK1. JAK2 and TYK2 in Interferon Signaling	0,22	0,04
Cysteine Biosynthesis III (mammalia)	0,22	0,04
D-myo-inositol (1.4.5)-Trisphosphate Biosynthesis	0,21	0,04
Lipid Antigen Presentation by CD1	0,20	0,04
Antiproliferative Role of TOB in T Cell Signaling	0,20	0,04
Estrogen-mediated S-phase Entry	0,20	0,04
Natural Killer Cell Signaling	0,00	0,03
Amyotrophic Lateral Sclerosis Signaling	0,00	0,03
Actin Cytoskeleton Signaling	0,00	0,03
Mitochondrial Dysfunction	0,00	0,03
Ceramide Signaling	0,00	0,02
Regulation of Actin-based Motility by Rho	0,00	0,03
Activation of IRF by Cytosolic Pattern Recognition Receptors	0,00	0,02
Fcγ Receptor-mediated Phagocytosis in Macrophages and Monocytes	0,00	0,03
IL-12 Signaling and Production in Macrophages	0,00	0,03
Role of RIG1-like Receptors in Antiviral Innate Immunity	0,00	0,02
TREM1 Signaling	0,00	0,03
Role of NFAT in Regulation of the Immune Response	0,00	0,02
CCR5 Signaling in Macrophages	0,00	0,03
Cytotoxic T Lymphocyte-mediated Apoptosis of Target Cells	0,00	0,03
IL-17 Signaling	0,00	0,03
fMLP Signaling in Neutrophils	0,00	0,03
CXCR4 Signaling	0,00	0,04

Ingenuity Canonical Pathways	-log(p-value)	Ratio
4-1BB Signaling in T Lymphocytes	0,00	0,03
CTLA4 Signaling in Cytotoxic T Lymphocytes	0,00	0,02
IL-9 Signaling	0,00	0,03
CD28 Signaling in T Helper Cells	0,00	0,03
IL-15 Signaling	0,00	0,01
Role of Cytokines in Mediating Communication between Immune Cells	0,00	0,02
Reelin Signaling in Neurons	0,00	0,03
HIF1α Signaling	0,00	0,03
Angiopoietin Signaling	0,00	0,01
Agrin Interactions at Neuromuscular Junction	0,00	0,03
Docosahexaenoic Acid (DHA) Signaling	0,00	0,03
iCOS-iCOSL Signaling in T Helper Cells	0,00	0,02
Mitotic Roles of Polo-Like Kinase	0,00	0,02
HMGB1 Signaling	0,00	0,02
Role of CHK Proteins in Cell Cycle Checkpoint Control	0,00	0,02
FLT3 Signaling in Hematopoietic Progenitor Cells	0,00	0,01
Human Embryonic Stem Cell Pluripotency	0,00	0,04
Antiproliferative Role of Somatostatin Receptor 2	0,00	0,03
Androgen Signaling	0,00	0,03
Germ Cell-Sertoli Cell Junction Signaling	0,00	0,03
Melanoma Signaling	0,00	0,02
Prostate Cancer Signaling	0,00	0,03
Renal Cell Carcinoma Signaling	0,00	0,04
Acute Myeloid Leukemia Signaling	0,00	0,01
Thyroid Cancer Signaling	0,00	0,02
Graft-versus-Host Disease Signaling	0,00	0,02
Chronic Myeloid Leukemia Signaling	0,00	0,03
Gα12/13 Signaling	0,00	0,03
mTOR Signaling	0,00	0,03
Communication between Innate and Adaptive Immune Cells	0,00	0,02
Crosstalk between Dendritic Cells and Natural Killer Cells	0,00	0,03
Systemic Lupus Erythematosus Signaling	0,00	0,01
Cdc42 Signaling	0,00	0,01
ILK Signaling	0,00	0,04
FAK Signaling	0,00	0,02
EIF2 Signaling	0,00	0,01
Retinoic acid Mediated Apoptosis Signaling	0,00	0,02
PAK Signaling	0,00	0,02
Rac Signaling	0,00	0,04
Phospholipase C Signaling	0,00	0,04
Altered T Cell and B Cell Signaling in Rheumatoid Arthritis	0,00	0,02
Breast Cancer Regulation by Stathmin1	0,00	0,04
Nur77 Signaling in T Lymphocytes	0,00	0,03
PKCθ Signaling in T Lymphocytes	0,00	0,03
Role of MAPK Signaling in the Pathogenesis of Influenza	0,00	0,04
Role of PI3K/AKT Signaling in the Pathogenesis of Influenza	0,00	0,03
Role of Hypercytokinemia/hyperchemokinemia in the Pathogenesis of Influenza	0,00	0,02
OX40 Signaling Pathway	0,00	0,03
Inhibition of Angiogenesis by TSP1	0,00	0,03
Cyclins and Cell Cycle Regulation	0,00	0,04
Cell Cycle Control of Chromosomal Replication	0,00	0,04
Assembly of RNA Polymerase II Complex	0,00	0,02
IL-17A Signaling in Fibroblasts	0,00	0,03
Actin Nucleation by ARP-WASP Complex	0,00	0,01
NGF Signaling	0,00	0,04
Paxillin Signaling	0,00	0,01
Signaling by Rho Family GTPases	0,00	0,03
Telomerase Signaling	0,00	0,03
Transcriptional Regulatory Network in Embryonic Stem Cells	0,00	0,04
nNOS Signaling in Skeletal Muscle Cells	0,00	0,02
VEGF Family Ligand-Receptor Interactions	0,00	0,04
ErbB4 Signaling	0,00	0,03
Netrin Signaling	0,00	0,02
Triacylglycerol Degradation	0,00	0,02
tRNA Charging	0,00	0,03
Stearate Biosynthesis I (Animals)	0,00	0,02
Superpathway of Methionine Degradation	0,00	0,03
Gαi Signaling	0,00	0,03
Gαq Signaling	0,00	0,03
Regulation of Cellular Mechanics by Calpain Protease	0,00	0,03
Remodeling of Epithelial Adherens Junctions	0,00	0,01
Role of p14/p19ARF in Tumor Suppression	0,00	0,03
HIPPO signaling	0,00	0,04
Estrogen Receptor Signaling	0,00	0,04
ERK/MAPK Signaling	0,00	0,04
JAK/Stat Signaling	0,00	0,04
Phototransduction Pathway	0,00	0,02
Chemokine Signaling	0,00	0,04
Integrin Signaling	0,00	0,03
Glutamate Receptor Signaling	0,00	0,02
TGF-β Signaling	0,00	0,02
IL-6 Signaling	0,00	0,03
BMP signaling pathway	0,00	0,01
PD-1. PD-L1 cancer immunotherapy pathway	0,00	0,01
Cancer Drug Resistance By Drug Efflux	0,00	0,02
Th1 and Th2 Activation Pathway	0,00	0,03
Th1 Pathway	0,00	0,02
Th2 Pathway	0,00	0,03
Sirtuin Signaling Pathway	0,00	0,03
SPINK1 Pancreatic Cancer Pathway	0,00	0,03
NER Pathway	0,00	0,01
Apelin Pancreas Signaling Pathway	0,00	0,02
BAG2 Signaling Pathway	0,00	0,02
FAT10 Cancer Signaling Pathway	0,00	0,02
T Cell Exhaustion Signaling Pathway	0,00	0,02
Systemic Lupus Erythematosus In T Cell Signaling Pathway	0,00	0,02
Senescence Pathway	0,00	0,03
Inhibition of ARE-Mediated mRNA Degradation Pathway	0,00	0,02
GM-CSF Signaling	0,00	0,03
Ephrin Receptor Signaling	0,00	0,03

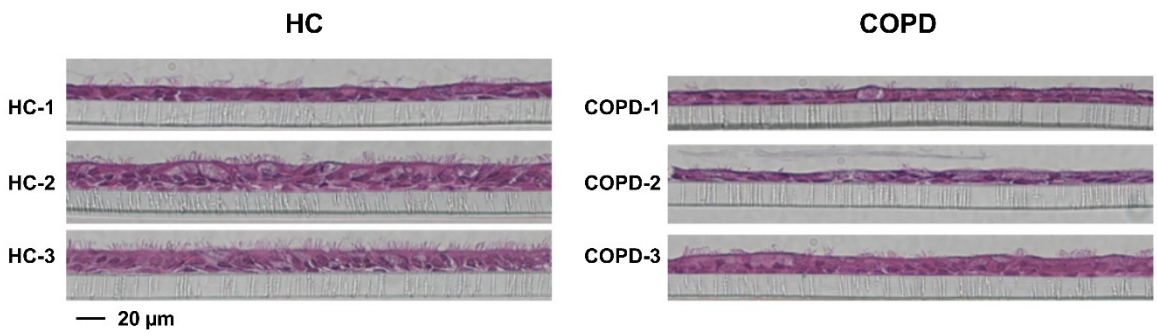

Figure 49: Hematoxylin & Eosin (H&E) stainings of small airway epithelial cell (SAEC) air-liquid interface (ALI) cultures from healthy donors (HC, n=3) and chronic obstructive pulmonary disease (COPD) patients (n=3). Cells were differentiated under ALI conditions for 28 days. (Gindele et al., 2020)

Table 9: RNA sequencing expression raw data. Reads per kilo base per million (RPKM) mapped reads of specific genes. Donors A, B and C are healthy controls; Donors D, E and F are chronic obstructive pulmonary disease (COPD) patients. Cultures were intermittently exposed to cigarette smoke (CS) or air during differentiation. (Gindele et al., 2020)

GeneID	GeneName	A_CS_1	A_CS_2	A_CS_3	A_air_1	A_air_2	A_air_3
ENSG00000013297	*CLDN11*	0,1	0,179	0,471	0,585	1,33	0,78
ENSG00000026508	*CD44*	78,417	93,959	103,296	61,997	54,429	55,892
ENSG00000066405	*CLDN18*	1,449	0,481	1,022	2,169	2,443	1,982
ENSG00000073282	*TP63*	18,583	24,627	22,859	23,864	24,136	21,594
ENSG00000122735	*DNAI1*	53,531	47,938	67,92	77,331	88,665	80,837
ENSG00000129654	*FOXJ1*	180,114	279,427	248,849	253,06	262,111	301,227
ENSG00000134873	*CLDN10*	130,776	119,742	90,868	22,286	23,061	23,079
ENSG00000149021	*SCGB1A1*	4937,77	7616,98	9798,84	18120,6	18099,1	17792,9
ENSG00000161055	*SCGB3A1*	1380,72	2819,5	2837,54	7300,1	6783,72	6317
ENSG00000163207	*IVL*	0,968	0,201	0,46	0,26	0,285	0,245
ENSG00000166086	*JAM3*	0,994	1,04	0,86	1,92	1,759	1,708
ENSG00000171401	*KRT13*	48,022	32,714	27,929	4,85	4,29	4,435
ENSG00000175793	*SFN*	110,66	80,472	62,463	32,125	36,519	31,356
ENSG00000181458	*TMEM45A*	75,635	76,526	101,41	105,662	139,898	138,834
ENSG00000181885	*CLDN7*	280,623	223,618	190,915	169,997	173,639	165,412
ENSG00000185499	*MUC1*	934,919	1157,05	1004,56	613,795	662,972	632,618
ENSG00000186081	*KRT5*	652,247	1043,56	776,853	439,411	382,089	352,922
ENSG00000186847	*KRT14*	3,286	2,866	1,84	0,283	0,117	0,137
ENSG00000197446	*CYP2F1*	41,644	78,646	99,199	201,36	219	215,447
ENSG00000205420	*KRT6A*	53,444	73,843	63,95	19,461	18,745	15,379
ENSG00000215182	*MUC5AC*	47,333	119,974	128,157	47,793	56,31	52,171

GeneID	GeneName	B_CS_1	B_CS_2	B_CS_3	B_air_1	B_air_2	B_air_3
ENSG00000013297	*CLDN11*	0,077	0,13	0,11	0,557	0,306	0,407
ENSG00000026508	*CD44*	73,956	117,293	105,629	47,865	46,442	41,458
ENSG00000066405	*CLDN18*	0,746	1,114	0,522	1,149	4,376	0,56
ENSG00000073282	*TP63*	21,403	23,892	24,352	24,989	24,684	25,617
ENSG00000122735	*DNAI1*	45,944	66,349	59,877	62,725	105,407	49,242
ENSG00000129654	*FOXJ1*	265,717	257,803	279,483	268,056	277,216	300,74
ENSG00000134873	*CLDN10*	162,359	119,177	99,145	17,311	15,377	15,926
ENSG00000149021	*SCGB1A1*	3247,7	5669,24	7256,57	19621,6	18995,3	23949,4
ENSG00000161055	*SCGB3A1*	1177,76	1781,08	3208,28	8385,71	7908,54	10660,7
ENSG00000163207	*IVL*	0,335	0,216	0,098	0,197	0,134	0,096
ENSG00000166086	*JAM3*	0,387	0,625	0,695	1,573	1,45	1,601
ENSG00000171401	*KRT13*	74,881	50,578	66,908	4,542	4,626	3,883
ENSG00000175793	*SFN*	127,023	80,682	91,903	33,635	28,086	30,478
ENSG00000181458	*TMEM45A*	17,639	20,324	22,589	48,134	49,094	53,806
ENSG00000181885	*CLDN7*	329,075	210,047	227,46	189,047	175,311	172,371
ENSG00000185499	*MUC1*	985,461	879,159	971,688	474,859	447,988	434,019
ENSG00000186081	*KRT5*	1194,01	1590,61	1757,38	572,443	442,707	513,33
ENSG00000186847	*KRT14*	5,992	2,548	2,443	0,117	0,193	0,214
ENSG00000197446	*CYP2F1*	24,569	52,347	59,596	217,748	242,12	281,455
ENSG00000205420	*KRT6A*	105,683	94,887	103,565	22,535	15,489	18,13
ENSG00000215182	*MUC5AC*	244,972	465,214	608,863	154,216	137,202	185,147

GeneID	GeneName	C_CS_1	C_CS_2	C_CS_3	C_air_1	C_air_2	C_air_3
ENSG00000013297	*CLDN11*	0,311	0,993	0,341	1,741	1,374	2,172
ENSG00000026508	*CD44*	56,871	63,754	145,492	32,115	37,925	28,812
ENSG00000066405	*CLDN18*	2,269	1,647	0,425	0,708	1,233	3,315
ENSG00000073282	*TP63*	14,629	18,263	33,591	14,864	15,403	12,607
ENSG00000122735	*DNAI1*	96,863	98,792	60,01	66,782	79,022	129,021
ENSG00000129654	*FOXJ1*	315,25	350,784	252,448	332,381	313,295	340,247
ENSG00000134873	*CLDN10*	103,532	57,186	78,737	10,313	11,254	10,025
ENSG00000149021	*SCGB1A1*	6172,71	7826,02	9526,48	15331	14316,8	14375,3
ENSG00000161055	*SCGB3A1*	3994,63	6563,41	5276,15	8994,12	8348,22	10493,2
ENSG00000163207	*IVL*	0,428	0,219	0,329	0,146	0,227	0,196
ENSG00000166086	*JAM3*	0,375	0,709	0,33	1,009	1,76	1,6
ENSG00000171401	*KRT13*	19,459	17,314	48,781	4,984	5,679	6,089
ENSG00000175793	*SFN*	70,035	65,606	135,712	27,759	29,062	26,265
ENSG00000181458	*TMEM45A*	77,563	59,296	101,688	100,506	100,288	80,572
ENSG00000181885	*CLDN7*	278,808	274,367	267,066	191,526	202,879	207,665
ENSG00000185499	*MUC1*	1150,12	1103,55	1179,79	576,687	603,982	581,514
ENSG00000186081	*KRT5*	435,212	733,9	1346,5	232,691	259,967	216,444
ENSG00000186847	*KRT14*	0,48	0,751	2,065	0,041	0,091	0
ENSG00000197446	*CYP2F1*	48,196	65,788	75,509	148,511	149,544	148,347
ENSG00000205420	*KRT6A*	30,74	42,287	113,208	11,447	13,882	9,522
ENSG00000215182	*MUC5AC*	85,875	181,1	207,506	37,325	44,329	46,598

GeneID	GeneName	D_CS_1	D_CS_2	D_CS_3	D_air_1	D_air_2	D_air_3
ENSG00000013297	*CLDN11*	0,267	0,064	0,2	2,593	2,524	5,203
ENSG00000026508	*CD44*	82,687	109,338	94,929	63,134	60,714	72,346
ENSG00000066405	*CLDN18*	0,172	0,124	0,171	0,953	0,968	0,558
ENSG00000073282	*TP63*	40,874	39,608	37,594	44,277	42,155	44,236
ENSG00000122735	*DNAI1*	20,901	35,273	39,876	45,555	49,88	39,251
ENSG00000129654	*FOXJ1*	147,221	233,938	228,201	219,906	251,987	260,996
ENSG00000134873	*CLDN10*	124,088	135,772	73,049	17,398	16,272	17,052
ENSG00000149021	*SCGB1A1*	6709,46	12110,9	15012,2	33465,6	31154,6	33597,6
ENSG00000161055	*SCGB3A1*	3019,51	4991,38	8699,69	12167,9	13102,8	17325,1
ENSG00000163207	*IVL*	0,717	0,16	0,199	0,1	0,244	0,17
ENSG00000166086	*JAM3*	0,312	0,317	0,638	1,235	1,242	0,873
ENSG00000171401	*KRT13*	156,513	44,914	69,038	11,155	11,12	15,16
ENSG00000175793	*SFN*	203,352	86,419	106,022	46,249	47,647	53,99
ENSG00000181458	*TMEM45A*	51,176	66,971	58,11	117,258	122,613	113,964
ENSG00000181885	*CLDN7*	369,033	233,797	245,941	188,933	189,248	196,17
ENSG00000185499	*MUC1*	1345,08	1504,53	1395,09	645,117	663,239	690,175
ENSG00000186081	*KRT5*	1471,3	1605,62	1800,81	680,228	637,973	766,243
ENSG00000186847	*KRT14*	7,38	0,993	1,636	0,108	0,166	0,251
ENSG00000197446	*CYP2F1*	32,992	76,144	85,824	304,773	299,998	337,144
ENSG00000205420	*KRT6A*	82,954	66,919	69,703	22,947	18,979	25,037
ENSG00000215182	*MUC5AC*	131,25	289,051	310,727	82,443	84,088	95,704

GeneID	GeneName	E_CS_1	E_CS_2	E_CS_3	E_air_1	E_air_2	E_air_3
ENSG00000013297	*CLDN11*	0,405	0,085	1,04	2,326	1,554	2,508
ENSG00000026508	*CD44*	288,389	213,773	257,546	158,95	117,151	154,856
ENSG00000066405	*CLDN18*	0,235	1,553	2,947	4,232	6,329	6,276
ENSG00000073282	*TP63*	43,255	34,757	27,566	23,913	21,838	25,268
ENSG00000122735	*DNAI1*	4,074	53,63	67,123	103,511	130,937	128,151
ENSG00000129654	*FOXJ1*	7,529	138,188	59,408	143,126	169,764	146,914
ENSG00000134873	*CLDN10*	84,907	262,151	200,015	42,224	40,99	38,093
ENSG00000149021	*SCGB1A1*	2195,49	6319,56	5902,81	14068,8	15942,9	12779,1
ENSG00000161055	*SCGB3A1*	117,837	924,293	466,847	2167,88	3250,95	2197,35
ENSG00000163207	*IVL*	4,38	0,632	1,111	1,149	0,399	1,506
ENSG00000166086	*JAM3*	0,364	0,634	0,729	1,424	1,258	1,593
ENSG00000171401	*KRT13*	12,801	54,332	3,25	37,949	36,676	34,879
ENSG00000175793	*SFN*	277,687	177,518	124,591	76,522	60,411	74,494
ENSG00000181458	*TMEM45A*	66,999	111,862	155,658	171,067	125,049	136,264
ENSG00000181885	*CLDN7*	345,084	272,939	216,653	206,285	193,751	202,448
ENSG00000185499	*MUC1*	488,677	1121,16	850,894	769,923	723,345	724,505
ENSG00000186081	*KRT5*	1003,6	1311,9	597,805	632,051	601,5	608,341
ENSG00000186847	*KRT14*	2,77	5,216	0,543	0,104	0,185	0,381
ENSG00000197446	*CYP2F1*	0,807	54,489	33,124	164,827	207,422	157,519
ENSG00000205420	*KRT6A*	169,377	251,469	112,003	40,32	47,885	43,144
ENSG00000215182	*MUC5AC*	77,905	1340,1	833,531	224,477	289,928	250,647

GeneID	GeneName	F_CS_1	F_CS_2	F_CS_3	F_air_1	F_air_2	F_air_3
ENSG00000013297	*CLDN11*	0,358	0,287	0,384	0,669	0,989	1,088
ENSG00000026508	*CD44*	65,419	74,553	80,935	64,436	57,335	87,046
ENSG00000066405	*CLDN18*	0,676	1,05	2,128	1,364	2,069	1,192
ENSG00000073282	*TP63*	31,765	27,696	27,177	37,206	42,134	35,378
ENSG00000122735	*DNAI1*	43,311	69,23	94,968	61,07	77,784	65,834
ENSG00000129654	*FOXJ1*	255,459	219,722	236,517	201,643	206,877	273,567
ENSG00000134873	*CLDN10*	70,597	41,287	33,505	11,326	9,009	13,037
ENSG00000149021	*SCGB1A1*	5592,49	13448,5	13833,8	23705,6	24258,1	21949,6
ENSG00000161055	*SCGB3A1*	2095,86	4180,31	5470,54	9081,79	11025,5	10059,5
ENSG00000163207	*IVL*	0,134	0,081	0,101	0,113	0,129	0,286
ENSG00000166086	*JAM3*	1,374	2,247	2,417	3,023	4,406	4,392
ENSG00000171401	*KRT13*	39,035	10,966	12,204	6,334	4,454	8,083
ENSG00000175793	*SFN*	112,143	47,547	44,403	36,813	33,006	44,799
ENSG00000181458	*TMEM45A*	39,018	79,072	65,844	123,525	106,223	122,69
ENSG00000181885	*CLDN7*	273,858	198,627	197,939	165,371	155,57	206,079
ENSG00000185499	*MUC1*	1027,46	904,383	717,171	564,355	498,851	594,853
ENSG00000186081	*KRT5*	1055,27	724,231	709,018	637,164	596,073	651,141
ENSG00000186847	*KRT14*	1,693	0,498	0,427	0,085	0,109	0,133
ENSG00000197446	*CYP2F1*	46,09	119,09	148,36	258,134	301,633	292,871
ENSG00000205420	*KRT6A*	39,26	17,508	20,644	10,021	9,081	22,458
ENSG00000215182	*MUC5AC*	46,522	64,57	61,007	10,93	8,332	23,218

Assessment of the normality assumption – Figure 19

1. Visuals assessment of the conditional and marginal studentized residuals with quantile-quantile plots (QQ plots).
   - Approximately, the residuals should follow a normal distribution.
   - Empirical quantiles of the residuals are compared with the theoretical quantiles from a normal distribution. If the normality assumption is satisfied, the plot of the normal quantiles versus the empirical quantiles forms a straight line.

2. Assessment of the conditional and marginal studentized residuals with the Shapiro-Wilk test.
   - The hypothesis '*The data follows a normal distribution'* is tested against the alternative '*The data does not follow a normal distribution'*.
   - The test statistic is based on the QQ plots.
   - If the hypothesis cannot be rejected, this means that the data doesn't contradict the assumption of a normal distribution. But this does not mean that it was shown that the data is normally distributed. (Reasons: small sample size (low power), data (nearly) normally distributed).
   - If the hypothesis is rejected and the alternative is accepted one can conclude that the data does not originate from a normal distribution.

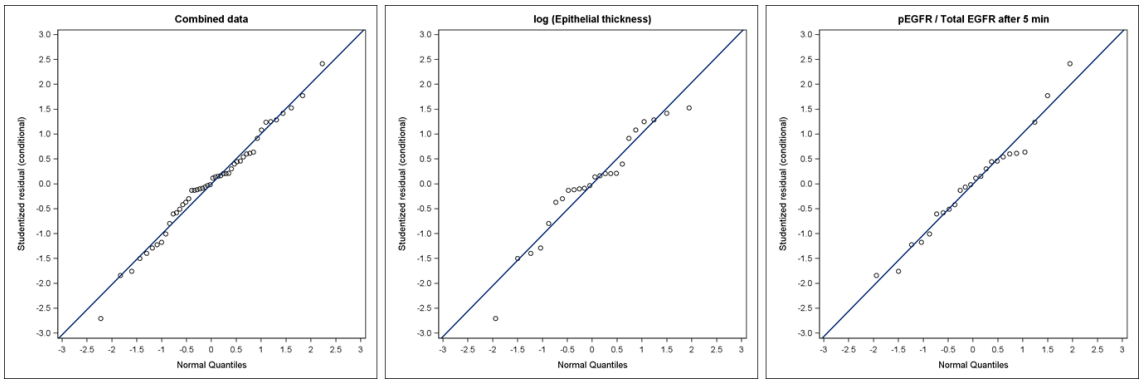

Figure 50: Conditional residuals: QQ plot, combined and by parameter

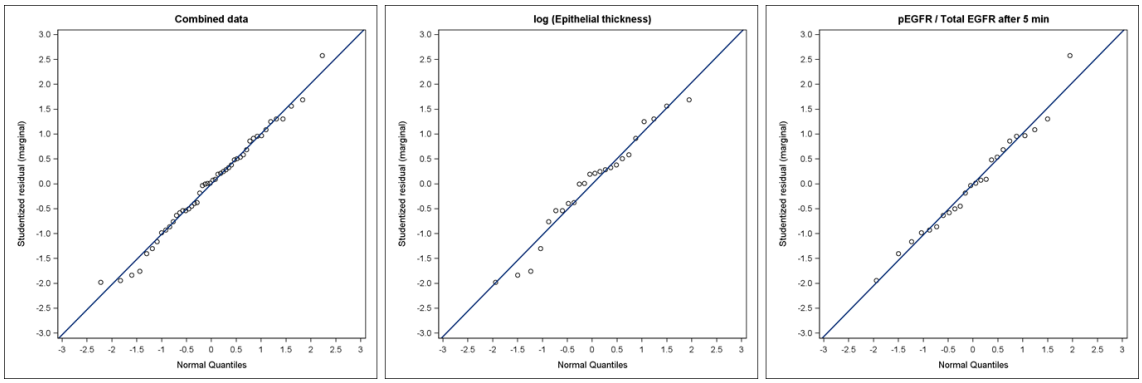

Figure 51: Marginal residuals: QQ plot, combined and by parameter

QQ-Plots as well as p-values of the Shapiro-Wilk test do not indicate severe deviations from the assumption that the data follows a normal distribution.

Table 9: Checking the normality assumption of the linear model. p-values of Shapiro-Wilk test.

	Conditional studentized residual	Marginal studentized residual
Combined data	0.8249	0.8929
log (Epithelial thickness)	0.1405	0.3615
pEGFR /Total EGFR after 5 min	0.7484	0.8997

Assessment of normality assumption - Figures 21-23

1. Visuals assessment of the conditional and marginal studentized residuals with quantile-quantile plots (QQ plots).
   - Approximately, the residuals should follow a normal distribution.
   - Empirical quantiles of the residuals are compared with the theoretical quantiles from a normal distribution. If the normality assumption is satisfied, the plot of the normal quantiles versus the empirical quantiles forms a straight line.

2. Assessment of the conditional and marginal studentized residuals with the Shapiro-Wilk test.
   - The hypothesis '*The data follows a normal distribution'* is tested against the alternative '*The data does not follow a normal distribution'*.
   - The test statistic is based on the QQ plots.
   - If the hypothesis cannot be rejected, this means that the data doesn't contradict the assumption of a normal distribution. But this does not mean that it was shown that the data is normally distributed. (Reasons: small sample size (low power), data (nearly) normally distributed).
   - If the hypothesis is rejected and the alternative is accepted one can conclude that the data does not originate from a normal distribution.

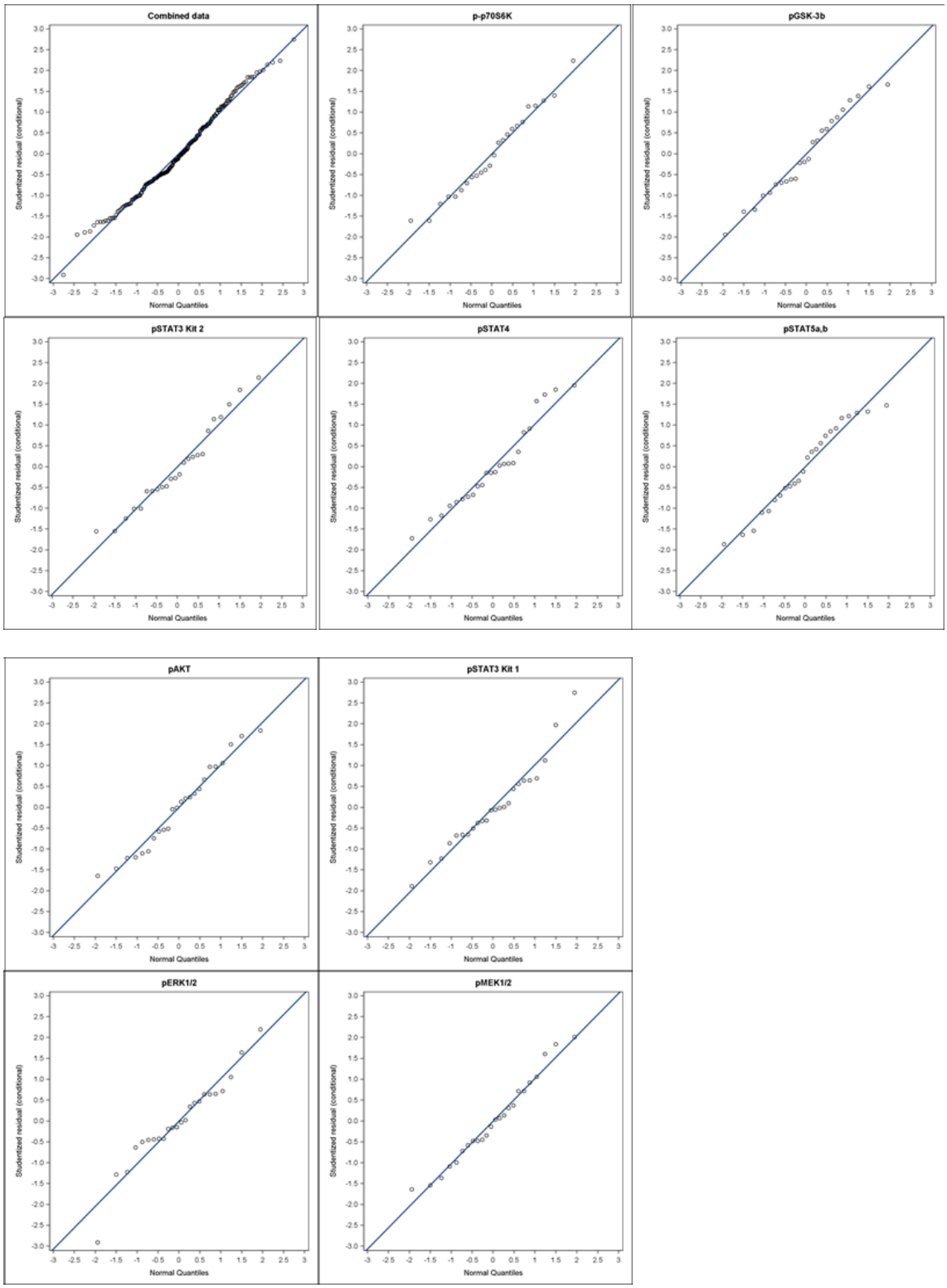

Figure 52: Conditional residuals: QQ plot, combined and by parameter

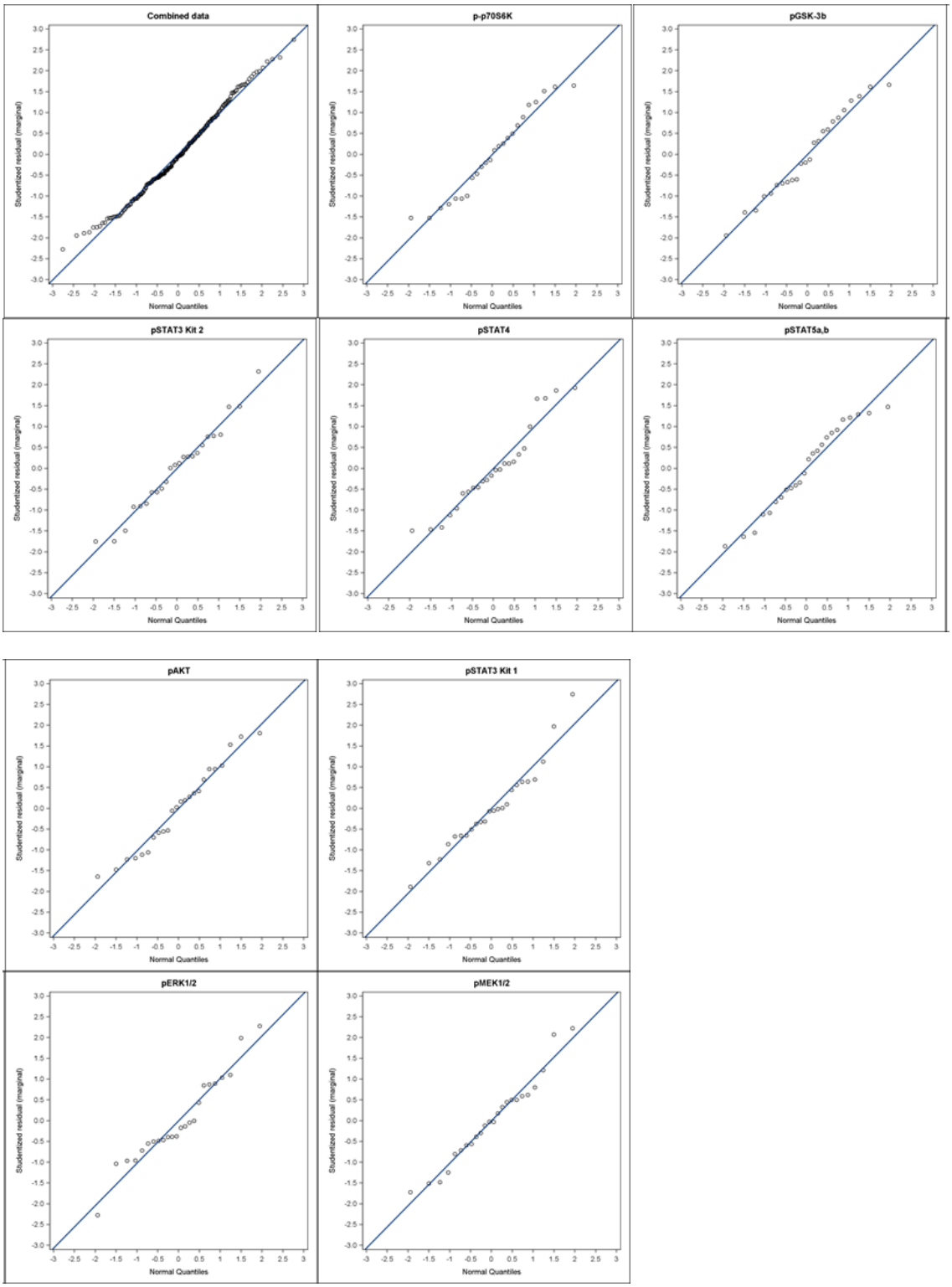

Figure 53: Marginal residuals: QQ plot, combined and by parameter

QQ-Plots as well as p-values of the Shapiro-Wilk test do not indicate severe deviations from the assumption that the data follows a normal distribution.

Table 10: Checking the normality assumption of the linear model. p-values of Shapiro-Wilk test.

		Conditional studentized residual	Marginal studentized residual
Combined		0.1497	0.1249
p-p70S6K		0.6773	0.2223
pGSK-3b		0.5334	0.5334
pAKT		0.4981	0.4501
pSTAT3	Kit 1	0.3048	0.3048
pSTAT3	Kit 2	0.3730	0.8186
pSTAT4		0.1543	0.0945
pSTAT5a,b		0.2387	0.2387
pERK1/2		0.2293	0.2297
pMEK1/2		0.6626	0.5837

Assessment of normality assumption - Figures 40, 42-45 and 47

1. Visuals assessment of the conditional and marginal studentized residuals with quantile-quantile plots (QQ plots).
   - Approximately, the residuals should follow a normal distribution.
   - Empirical quantiles of the residuals are compared with the theoretical quantiles from a normal distribution. If the normality assumption is satisfied, the plot of the normal quantiles versus the empirical quantiles forms a straight line.

2. Assessment of the conditional and marginal studentized residuals with the Shapiro-Wilk test.
   - The hypothesis '*The data follows a normal distribution'* is tested against the alternative '*The data does not follow a normal distribution'*.
   - The test statistic is based on the QQ plots.
   - If the hypothesis cannot be rejected, this means that the data doesn't contradict the assumption of a normal distribution. But this does not mean that it was shown that the data is normally distributed. (Reasons: small sample size (low power), data (nearly) normally distributed).
   - If the hypothesis is rejected and the alternative is accepted one can conclude that the data does not originate from a normal distribution.

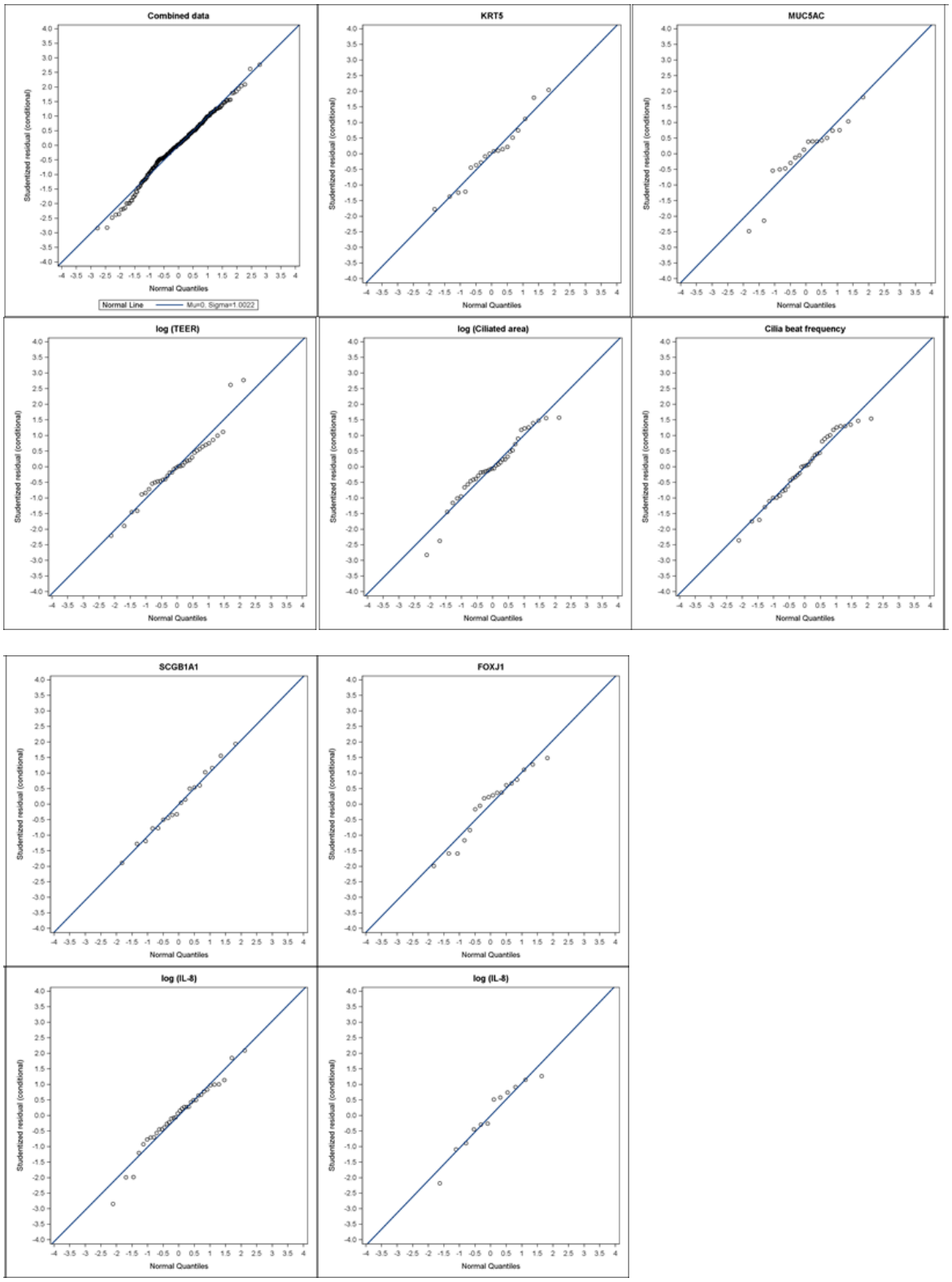

Figure 54: Conditional residuals: QQ plot, combined and by parameter

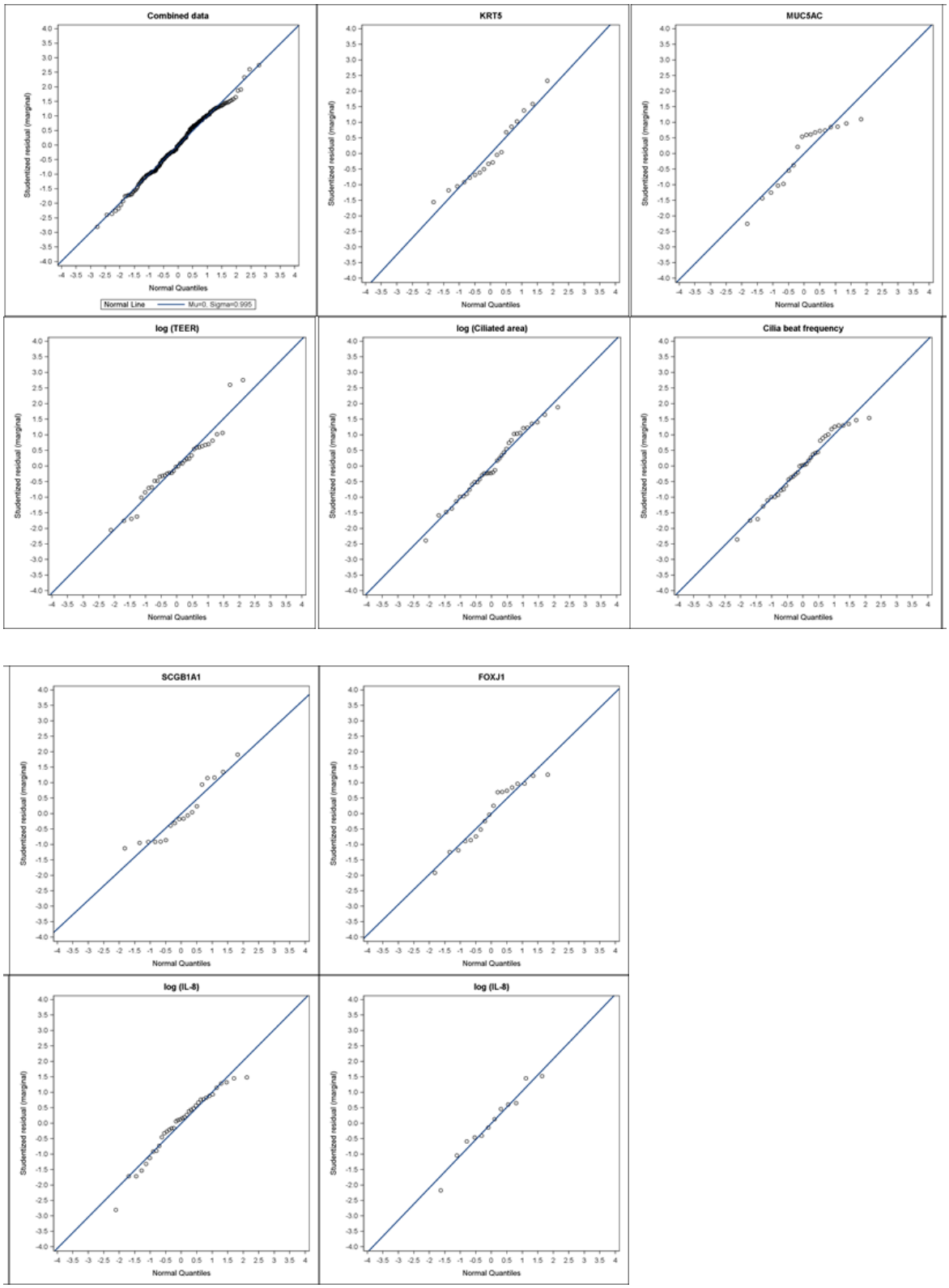

Figure 55: Marginal residuals: QQ plot, combined and by parameter

QQ-Plots as well as p-values of the Shapiro-Wilk test do not indicate severe deviations from the assumption that the data follows a normal distribution, even though some deviations can be seen.

		Conditional studentized residual	Marginal studentized residual
All figures	Combined data	0.1311	0.4027
Figure 40	KRT5	0.6389	0.3080
	MUC5AC	0.0566	0.0145
	SCGB1A1	0.9852	0.0609
	FOXJ1	0.1738	0.1567
Figures 42-45	log (TEER)	0.0829	0.0666
	log (Ciliated area)	0.0837	0.7275
	Cilia beat frequency	0.3152	0.3152
	log (IL-8)	0.3243	0.1387
Figure 47	log (IL-8)	0.4276	0.8430

Acknowledgement

The acknowledgement was removed from the published dissertation for reasons of data protection.

The acknowledgement was removed from the published dissertation for reasons of data protection.

Curriculum Vitae

The curriculum vitae was removed from the published dissertation for reasons of data protection.

The curriculum vitae was removed from the published dissertation for reasons of data protection.